UNIVERSITY OF WEST BOHEMIA

FACULTY OF APPLIED SCIENCES

Flexible hard coatings prepared by magnetron sputtering

Ing. Martin Jaroš

A thesis submitted for the degree of Doctor of Philosophy
in the field of Plasma Physics and Physics of thin films

Supervisor: prof. Ing. Jindřich Musil, DrSc.

Department of Physics

Pilsen 2018

ZÁPADOČESKÁ UNIVERZITA V PLZNI

FAKULTA APLIKOVANÝCH VĚD

Tvrdé flexibilní povlaky připravené magnetronovým naprašováním

Ing. Martin Jaroš

Disertační práce
k získání akademického titulu doktor
v oboru Fyzika plazmatu a tenkých vrstev

Školitel: prof. Ing. Jindřich Musil, DrSc.

Katedra Fyziky

Plzeň 2018

Preface

I hereby declare that for writing the thesis I was using duly cited literature and scientific articles published during my Ph.D. studies. The thesis is submitted in a form of six scientific publications.

The contribution of the author to the publications:

- Active participation in the design of the experiments.
- Carried out all the deposition, together with all the necessary measurements of the depositions and plasma characteristics.
- Measurements of the film thickness, mechanical and electrical properties.
- Active participation in the interpretation of the results.
- Active participation in writing the papers.

The results included in the thesis were obtained during my Ph.D. study at the Department of Physics and NTIS, European Centre of Excellence, University of West Bohemia, since September 2014. The research was financially supported by the projects SGS – 2013 – 045 (2013 – 2015): New thin-film materials and plasma deposition systems, and SGS – 2016 – 056 (2016 – 2018): New nanostructured thin-film materials formed by plasma technologies.

Pilsen 2. 11. 2018 ……………………………………… Ing. Martin Jaroš

Included Papers

Paper I

J. Musil, **M. Jaroš**, R. Čerstvý, S. Haviar:
"Evolution of microstructure and macrostress in sputtered hard Ti(Al,V)N films with increasing energy delivered during their growth by bombarding ions"
J. Vac. Sci. Technol. A. 35 (2017) 020601.

Paper II

M. Jaroš, J. Musil, R. Čerstvý, S. Haviar:
"Effect of energy on structure, microstructure and mechanical properties of hard Ti(Al,V)N_x films prepared by magnetron sputtering"
Surf. Coat. Technol. 332 (2017) 190–197.

Paper III

J. Musil, **M. Jaroš**:
"Plasma and floating potentials in magnetron discharges"
J. Vac. Sci. Technol. A. 35 (2017) 060605.

Paper IV

M. Jaroš, J. Musil, R. Čerstvý, S. Haviar:
"Effect of energy on macrostress in Ti(Al,V)N films prepared by magnetron sputtering"
Vacuum 158 (2018) 52-59

Paper V

M. Jaroš, J. Musil, S. Haviar:
"Interrelationships among macrostress, microstructure and mechanical behavior of sputtered hard Ti(Al,V)N films"
Material Letters 235 (2019) 92.

Paper VI

J. Musil, **M. Jaroš**, Š. Kos, R. Čerstvý, S. Haviar:
"Hard TiN_2 dinitride films prepared by magnetron sputtering"
J. Vac. Sci. Technol. A 36, (2018) 040602.

Acknowledgments

Firstly I would like to express my sincere gratitude to my supervisor Prof. Ing. Jindřich Musil, DrSc. for his patience, motivation, and immense knowledge. Without his guidance, this work would not be possible.

Also, many thanks for the Head of the Department of Physics Prof. RNDr. Jaroslav Vlček, CSc. for his great support during all my study. Last but not least, I would like to thank all the staff and Ph.D. students of the Department of Physics for the friendly atmosphere, professionalism and a lot of help during my 4 years here.

Table of Content

1. Introduction 8
   1.1. Energy delivered to growing film 8
      1.1.1. Effect of the momentum of bombarding particles 10
      1.1.2. Effect of the fluxes of bombarding particles 12

2. Aims of the Ph.D. thesis 18

3. Evolution of microstructure and macrostress in sputtered hard Ti(Al,V)N films with increasing energy delivered during their growth by bombarding ions 19
   3.1. Introduction 20
   3.2. Experiment 21
   3.3. Results and discussion 22
   3.4. Conclusions 25

4. Effect of energy on structure, microstructure and mechanical properties of hard $Ti(Al,V)N_x$ 28
   4.1. Introduction 29
   4.2. Experimental 30
   4.3. Results and discussion 31
      4.3.1. Energy delivered by bombarding ions 31
      4.3.2. Energy $\mathcal{E}_{fn}$ delivered by fast neutrals and controlled by the total sputtering gas pressure p_T 36
      4.3.3. Interrelationships between energies $\mathcal{E}_{bi}$ and $\mathcal{E}_{fn}$, preferred crystallographic orientation and resistance to cracking of $Ti(Al,V)N_x$ films 38
   4.4. Conclusions 40

5. PLASMA AND FLOATING POTENTIALS IN MAGNETRON DISCHARGES 44
   5.1. Introduction 45
   5.2. Experimental details 46
   5.3. Results and discussion 47
      5.3.1. Elimination of the effect of chamber walls on properties of sputtered films 49
   5.4. Conclusions 51

6. Effect of energy on macrostress in Ti(Al,V)N films prepared by magnetron sputtering 53
6.1. Introduction 54
6.2. Experimental 55
6.3. Results and discussion 56
6.3.1. Macrostress reduction by pulsed bipolar substrate bias U_{ps} 56
6.3.2. Macrostress reduction by overshoots in pulsed sputtering 59
6.3.3. Control of macrostress in films sputtered at high repetition frequencies of pulses 62
6.4. Conclusions 64

7. Interrelationships among macrostress, microstructure and mechanical behavior of sputtered hard Ti(Al,V)N films 68
7.1. Introduction 69
7.2. Experimental 69
7.3. Results and discussion 69
7.4. Conclusions 74

8. Hard TiN_2 dinitride films prepared by magnetron sputtering 77
8.1. Introduction 78
8.2. Principle of sputtering of $TMN_{x>1}$ nitride films 78
8.3. Experimental 79
8.4. Results and discussion 79
8.5. Conclusions 82

9. Main obtained results 84

10. List of publications of the author 85

Abstract 87

Resumé 88

1. Introduction

The properties of thin films can be controlled by various number of parameters during the deposition, such as the power P of the magnetron discharge, the film thickness h, the substrate temperature T_s, the substrate bias U_s, the substrate ion current density i_s, the flux of ions ν_i incident on the substrate, the deposition rate a_D of the film, magnetic field arrangement the substrate-to-target distance d_{s-t}, the total pressure $p_T = p_{Ar} + p_{RG}$ of sputtering gas mixture, the partial pressure of the argon p_{Ar} and the reactive gas p_{RG}, etc.. There is a huge number of papers devoted to the investigation of the relationships between the deposition parameters of film and its functional properties, for instance, see Ref. [1 - 20].

The problem with this approach lies in the fact that the correct combination of preselected deposition parameters necessary to form films with wanted properties is unknown. Therefore different approaches should be used. The main parameter which really controls the film properties is ***the energy $\mathcal{E}$*** and therefore, the correlations between the properties of the film and the energy are of key importance [21 - 25]. Different combinations of deposition parameters result in different energy $\mathcal{E}$ delivered to the growing film. It means that at first, correlations between the film properties and the energy $\mathcal{E}$ should be found and then, based on this knowledge the necessary deposition parameters which ensure the formation of the films with prescribed properties should be determined.

This thesis investigates the effect of the energy $\mathcal{E}$ on the preferred crystallographic orientation (texture) of grains in sputtered films, their microstructure, physical and mechanical properties, stoichiometry and their resistance to cracking in detail. For this investigation, the sputter deposited Ti(Al,V)N and $TiN_{x>1}$ thin films were selected.

Great attention is devoted also to (i) the control of the structure, microstructure, resistance to cracking and the macrostress σ of film by the energy $\mathcal{E}$ delivered to the film during its growth in the DC and pulsed magnetron discharges, (ii) the energy $\mathcal{E}$ delivered to the film held at different substrate biases U_s, (iii) the energy $\mathcal{E}$ delivered to the film at different plasma potentials and (iv) the energy $\mathcal{E}$ delivered to the film by fast neutrals.

1.1. Energy delivered to growing film

The energy $\mathcal{E}$ delivered to the growing film has a crucial effect on its structure, microstructure, elemental and phase composition, and physical properties [21 - 25]. The energy $\mathcal{E}$ can be delivered by (i) the substrate heating $\mathcal{E}_{sh}$, (ii) the conversion of the kinetic energy of particles $\mathcal{E}_p$, i.e. by the energy of bombarding ions ($\mathcal{E}_{bi}$) and/or fast neutrals ($\mathcal{E}_{fn}$) incident on the surface of growing film, (iii) the heat evolved during the formation of the compound $\mathcal{E}_{ch}$ (the energy released in exothermic chemical reactions), (iv) the heating from the sputtered magnetron target $\mathcal{E}_{mt}$ which almost always is not perfectly cooled, and (v) the radiation from the plasma $\mathcal{E}_{rad}$. The total energy $\mathcal{E}_T$ delivered to the growing film can be expressed by the following formula [26].

$$\mathcal{E}_T = \mathcal{E}_{sh}(T_s, t_d) + \mathcal{E}_p(U_s, i_s, a_D, p_T, t_d) + \mathcal{E}_{ch}(T_s, t_d) + \mathcal{E}_{mt}(W_d, t_d, d_{s-t}) + \mathcal{E}_{rad}(t_d) \quad (1.1)$$

Where T_s is the substrate temperature, t_d is the time of the film deposition, U_s is the substrate bias, i_s is the substrate ion current density, a_D is the deposition rate of film, $p_T = p_{Ar} + p_{RG}$ is the total pressure of the sputtering gas mixture, p_{Ar} and p_{RG} are the partial pressures of argon and reactive gas (RG), respectively, $W_d = (U_d \times I_d)/S$ is the magnetron target power density, I_d, and U_d are the magnetron current and voltage, respectively, S is the whole area of

magnetron target and $d_{s\text{-}t}$ is the substrate-to-target distance. The energy delivered to the growing film by incident particles $\mathcal{E}_p$ is composed of two terms

$$\mathcal{E}_p = \mathcal{E}_{bi} + \mathcal{E}_{fn} \quad (1.2)$$

From Fig. 1.1 follows that $\mathcal{E}_{fn}$ can play a significant role in low pressure sputtering. The energy of fast neutrals $\mathcal{E}_{fn}$ increases with decreasing p_T due to prolongation of main-free path λ and therefore reduction of collision between atoms. For the atmosphere with N_2 dominating applies [27]:

$$\lambda \approx {}^{0.4}/_{p_T} \quad (1.3)$$

However in the case of the conventional sputtering process the number of collision increase and $\mathcal{E}_{fn} \rightarrow 0$, therefore $\mathcal{E}_{bi}$ plays the dominant role.

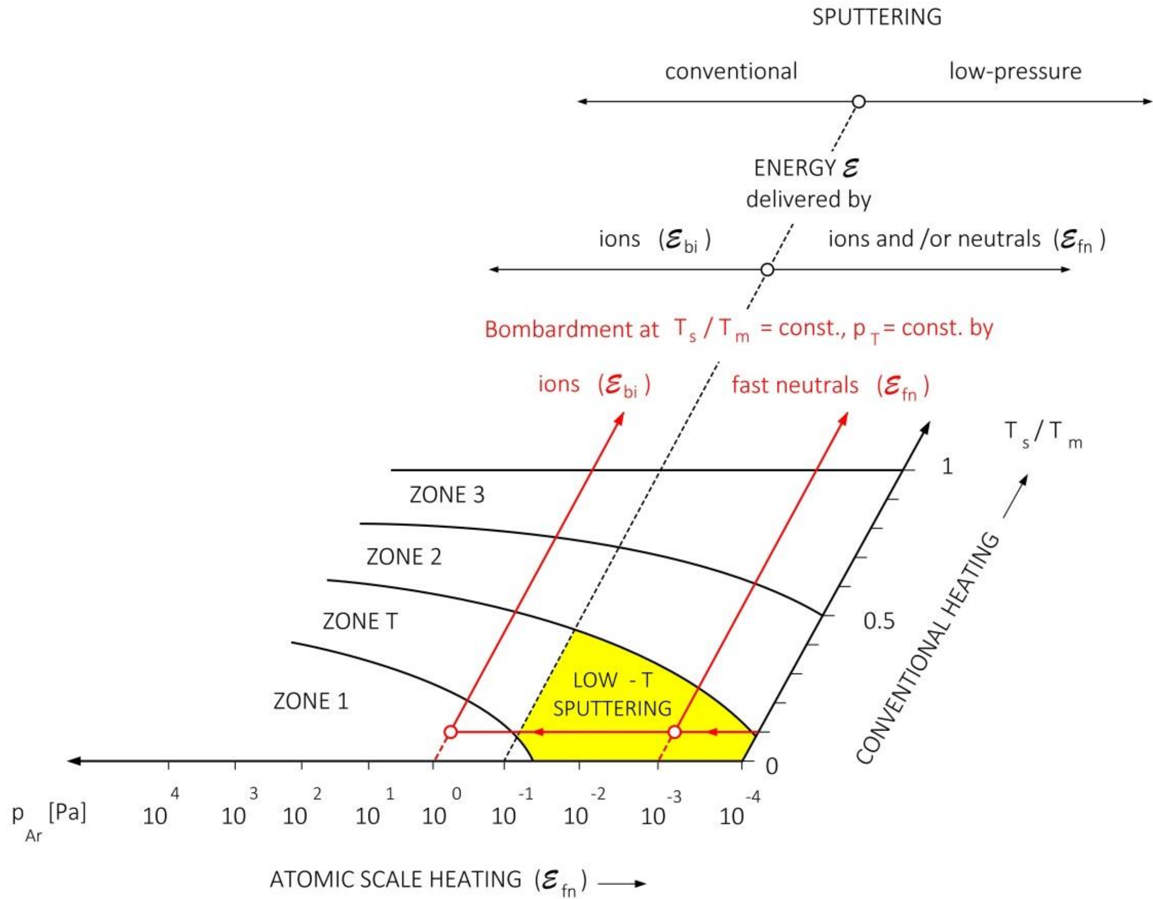

Figure 1.1 Schematic illustration of two dimensional (2D) Thornton's SZM showing the evolution of the film microstructure as functions of conventional heating (T_s/T_m) and atomic scale heating (p_{Ar}, $\mathcal{E}_{fn}$) and controlled by the energy $\mathcal{E}_{bi}$ by bombarding ions at high p_{Ar} or only by the energy $\mathcal{E}_{fn}$ of fast neutrals at low pressures ≤ 0.1 Pa.

This means that in a collision discharge the energy $\mathcal{E}_p$ can be expressed in the following form [27, 28]:

$$\mathcal{E}_p\,[\mathrm{J/cm^3}] = \mathcal{E}_{bi} = \mathcal{E}_i(\nu_i/\nu_{ca}) \quad (1.4)$$

where $\mathcal{E}_i$ is the energy of the one ion, ν_i and ν_{ca} is the flux of ions and condensing atoms, respectively.

In a collision plasma discharge the energy $\mathcal{E}_{bi}$ delivered per a volume unit of the deposited film can be expressed in the following form [27, 28]:

$$\mathcal{E}_{bi}\,[\mathrm{J/cm^3}] \approx \frac{(U_p - U_s) \times i_s}{a_D} \cdot N_{i,max} \quad (1.5)$$

Where U_p is plasma potential, a_D is deposition rate, i_s is current density and $N_{i,max}$ is a probability of an ion arriving at the substrate with the maximum energy. For a collision discharge, $N_{i,max}$ can be calculated as $N_{i,max}=\exp\left(^{-L}/_{\lambda}\right)$. Where the sheath thickness L was determined by Cthe hild-Langmuir equation for a collisionless sheath [29].

For typical DC magnetron deposition parameters ($U_d \approx 500$ V, $I_d \approx 0.5$ A, $p_T \approx 1$ Pa) applies that the $N_{i,max} \sim 1$, furthermore the $|U_s| >> |U_p|$, therefore the eq. (1.5) can be additionally simplified to

$$\mathcal{E}_{bi}\,[\mathrm{J/cm^3}] \approx \frac{U_s \times i_s}{a_D} \quad (1.6)$$

Despite the fact that Eq. (1.6) is very simplified it is very useful. Usability of Eq. (1.6) is further enhanced due to easily measured values of U_s, i_s and a_D.

Control of the energy $\mathcal{E}_p$ delivered into the film can be principally divided into two categories (i) control of the momentum of bombarding particles or (ii) control of the fluxes of bombarding particles.

1.1.1. Effect of the momentum of bombarding particles

There are many ways how to control the momentum of bombarding particles. In this section, three principles are outlined. Increasing the momentum of individual bombarding particles can be achieved by: (i) decreasing the total pressure, (ii) increasing negative substrate bias and (iii) increasing the plasma potential. The principle of increasing the particle momentum by decreasing the total pressure is based on the reduction of a number of collisions (see Eq. (1.3) and Figure 1). In the case of bombarding ions, the negative substrate bias can be used to control the $\mathcal{E}_{bi}$, see Eq. (1.6).

By increasing the momentum of individual bombarding particles, the properties of sputter deposited film, such as mechanical, size of grains and their crystallographic orientation, microstructure, macrostress can be controlled. Example of such control of the microstructure by $\mathcal{E}_p = f(p_T)$ from Ref. [30] can be seen in Fig. 1.2 (a). In Fig. 1.2 (b) the control of macrostress and microstructure by $\mathcal{E}_{bi} = f(U_s)$ can be seen (from Ref. [26, 31]).

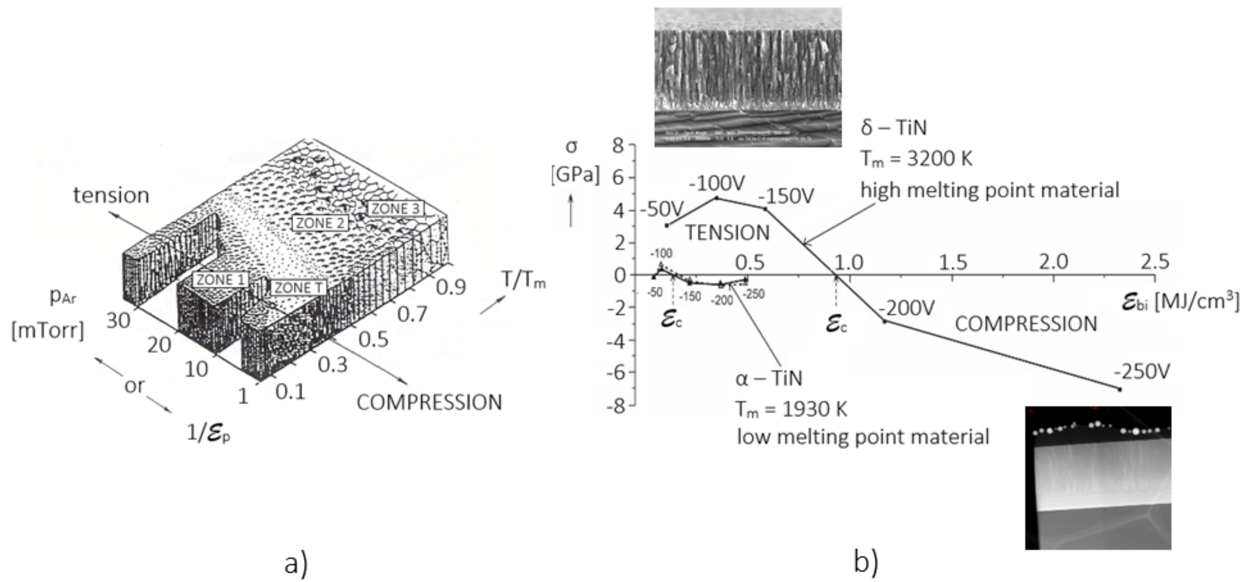

Figure 1.2 (a) Structural zone model (SZM) of sputtered metallic films developed by J. A. Thornton. Adapted after Ref. [30] and (b) Macrostress σ in sputtered α - Ti (N) and δ - $TiN_x \approx 1$ films as a function of energy $\mathcal{E}_{bi}$ at $p_T = p_{Ar} + p_{N2} = 5$ Pa and $T_s = 350$ ℃, i.e. at $T_s/T_m = 0.32$ and 0.19 for the α - Ti(N) film and the δ - $TiN_x \approx 1$film , respectively. Adapted from Ref. [26, 31].

Additional control of the momentum of bombarding ions can be achieved by control of the plasma potential U_p (see Eq. (1.5)) by using magnetron voltage oscillations, an example of such oscillations see Fig. 1.3. The positive magnetron voltage during the deposition results in the increment of the plasma potential, and therefore the momentum of bombarding ions is increased. It is important to emphasize that the magnetron voltage oscillations are not properties of the plasma itself but rather a consequence of a relationship between properties (induction, capacity, resistance) of the whole deposition system: (i) power sources, (ii) plasma sources and (iii) plasma. For more detail, investigation of the magnetron voltage oscillations see Ref. [32 - 37]. The number of high energetic ions (50 – 195 eV) created by magnetron voltage oscillation is not negligible. From Ref. [36] follows, that the flux of high energetic ions can be up to 1/3 of the total flux of bombarding ions, see Fig. 1.4.

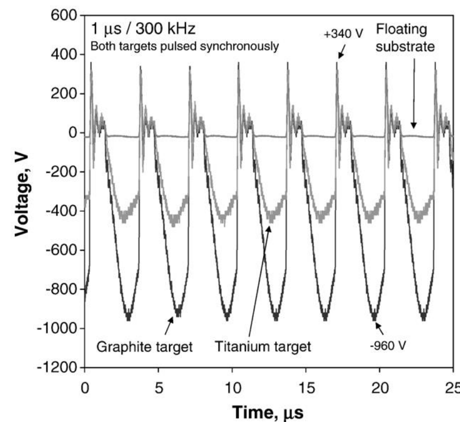

Figure 1.3 Example of voltage waveforms for synchronous pulsing of graphite and titanium targets at 1 µs/ 300 kHz. The positive overshoots for graphite and titanium are +340 and +320 V, respectively Adapted from Ref. [35].

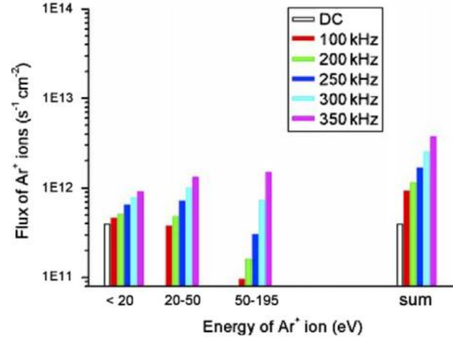

Figure 1.4 Flux of the Ar^+ ions in three energy ranges as well as the sum at different p-DC frequencies (substrate grounded). Adapted from Ref. [36].

1.1.2. Effect of the fluxes of bombarding particles

The fluxes of the bombarding particles ν_i and ν_{ca} (which are difficult to determine) can be represented by i_s and a_D, which can be easily measured. From this follows that $\mathcal{E}_{bi}$ can be increased by increasing i_s at constant a_D or by diseasing a_D at a constant i_s. There are many attempts to densify the plasma and therefore increase the ratio i_s/a_D by increasing i_s. In this section, three principles are outlined. Increasing the flux of bombarding particles can be achieved by (i) use of HiPiMS, (ii) addition of hot cathode, (iii) tuning the magnetic field.

Using HiPiMS for plasma creation brings many benefits to the deposition process. One of this benefits is a creation of denser plasma. This can be seen in Fig. 1.5. Plasma discharge created by HiPiMS using I_{da} = 50 A at p_{Ar} = 1 Pa results in plasma electron density of ≈2 × 10^{18} m^{-3}, which is ≈ 70 times denser than plasma created using I_{da} = 5 A [38]. For more information about the benefits of using HiPiMS see for example Ref. [38 - 42]

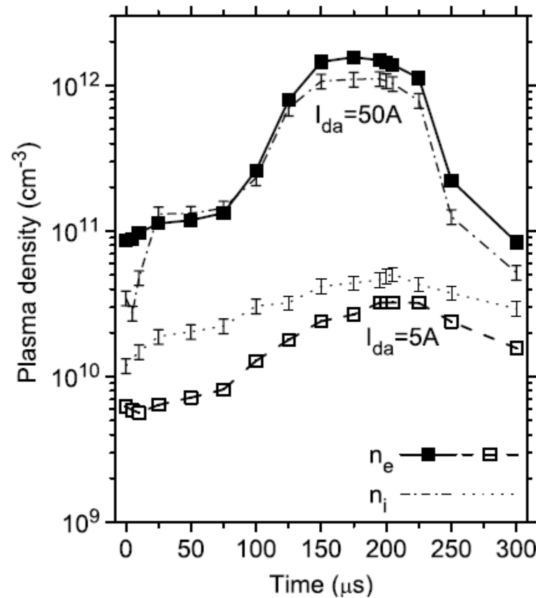

Figure 1.5 Time evolution of the electron density n_e, and ion density n_i, at average pulse current I_{da} = 5 and 50 A. Adapted from Ref. [38].

Another attempt to increase the plasma density lies in the use of hot cathode. By controlling the filament cathode current I_p the plasma potential and electron density at low p_{Ar} = 0.3 Pa can be tailored, see Fig. 1.6. From this figure follows that by increasing the filament cathode current I_p from 0 to 50 A the plasma density and plasma potential increases from 2.6×10^{16} to 4.5×10^{16} m^{-3} and 3.8 to 5.6 V respectively. For additional information about the use of hot cathode, see Ref. [43 - 45].

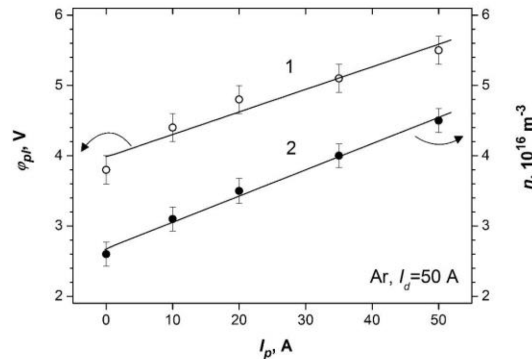

Figure 1.6 Plasma potential and density as a function of the filament cathode current I_p. *Adapted from Ref. [43].*

Ion flux can be also modified by a magnetic field. Direct measurement of ion current density as a function of the coil current can be seen in Fig. 1.7. From this figure follows that by introducing the coil current I_{coil} = 35 A the ion current density is significantly increased up to i_s = 3.4 mA/cm^2. For more information about how the magnetic field controls the properties of plasma discharge and therefore properties of sputter deposited films see Ref. [46 - 50].

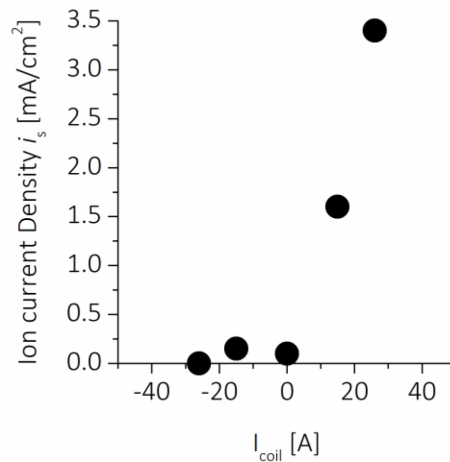

Figure 1.7 Ion current density as a function of the coil current. Adapted from Ref. [46].

Very important is also the effect of deposition rate a_D, particularly in a reactive magnetron sputtering when the deposition rate a_D decreases with increasing partial pressure of reactive gas p_{RG} at the same discharge current I_d of the magnetron discharge, see Fig. 1.8. This figure shows the evolution of the deposition rate a_D of magnetron sputtered Ti(Fe)N_x films and the energy delivered to them during their growth as a function of partial pressure of nitrogen p_{N2} at three values of the magnetron current I_d. From this figure, it is clearly seen that in the formation of the

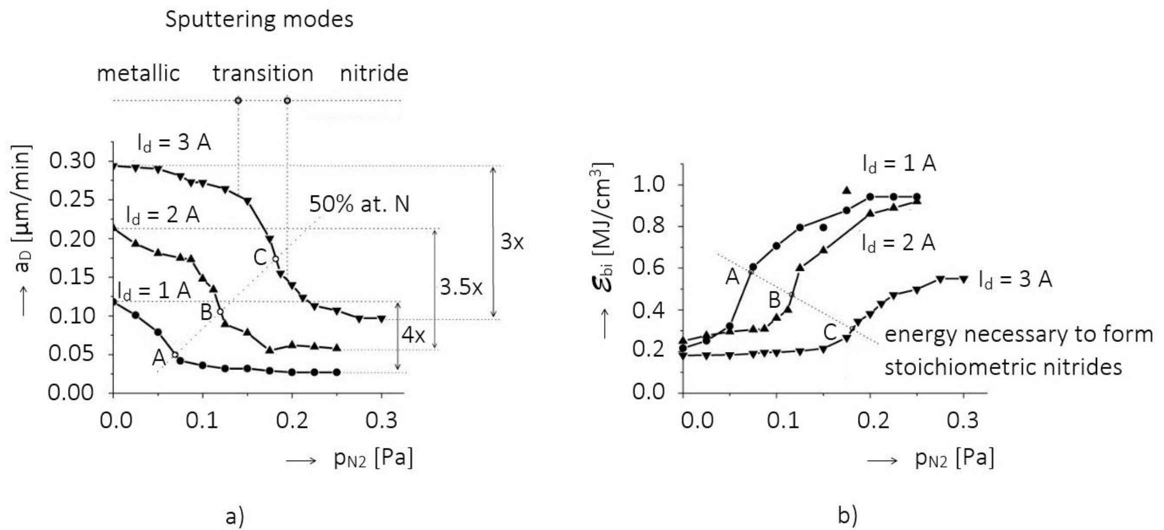

Figure 1.8 (a) Deposition rate a_D of Ti(Fe)N_x films and (b) energy $\mathcal{E}_{bi}$ delivered to them during their growth by bombarding ions as a function of partial pressure of nitrogen p_{N2}. The films were sputtered using a DC magnetron equipped with a TiFe (90/10 at.%) alloy target of 100 mm in diameter at (i) I_d = 1 A, i_s = 0.5 mA/cm^2, (ii) I_d = 2 A, i_s = 1 mA/cm^2, (iii) I_d = 3 A, i_s = 1 mA/cm^2, and U_s = -100 V, T_s = 300 ℃, d_{s-t} = 60 mm and $p_T = p_{Ar} + p_{N2}$ = 0.5 Pa. Adapted from Ref. [28].

stoichiometric and over-stoichiometric Ti(Fe)$N_{x \geq 1}$ nitride films a greater energy $\mathcal{E}_{bi}$ is delivered in the films during its growth compared with that delivered to the sub-stoichiometric Ti(Fe)$N_{x < 1}$ films; here x = N/(Ti + Fe). It is a very important fact because the magnitude of the energy $\mathcal{E}_{bi}$ decides also on the structure, microstructure of the growing film and the macrostress σ generated in it during its growth. For more information see Ref [28]

References

[1] A. Raveh, L. Martinu, S.C. Gujrathi, J.E. Klemberg-Sapieha, M.R. Wertheimer: Structure – property relationships in dual-frequency plasma deposited hard a-C:H films, Surf. Coat. Technol. 53 (1992), 275-282.

[2] A.J. Perry, A. Inspector: Process and property relationships in hard coatings made by plasma- and ion-assisted methods, Surf. Coat. Technol. 52 (1992), 261-267.

[3] F. Sanchette, T.H. Loi, A. Billard, C. Frantz: Structure-properties relationship of metastable Al-Cr and Al-Ti alloys deposited by rf magnetron sputtering: role of nitrogen, Surf. Coat. Technol. 74-75 (1995), 903-909.

[4] M. Oden, C. Ericksson, G. Hakansson, H. Ljungcrantz: Microstructure and mechanical behaviour of arc-evaporated Cr-N coatings, Surf. Coat. Technol. 114 (1999), 39-51.

[5] F. Lapostolle, A. Billard, J. von Stebut: Structure/mechanical properties relationship of titanium-oxygen coatings reactively sputter – deposited, Surf. Coat. Technol. 135 (2000), 1-7.

[6] L. Karlsson, L. Hultman, M.P. Johansson, J.-E. Sundgren, H. Ljungcrantz: Growth, microstructure, and mechanical properties of arc evaporated $TiC_{1-x}N_{1-x}$ ($0 \leq x \leq 1$) films, , Surf. Coat. Technol. 126 (2000), 1-14.

[7] S. Carvalho, L. Rebouta, A. Cavaleiro, L.A. Rocha, J. Comes, E. Alves: Microstructure and mechanical properties of nanocomposite (Ti,Si,Al)N coatings, Thin Solid Films 398-399 (2001), 391-396.

[8] J. Almer, M.Oden, G.Hakansson: Microstructure, stress and mechanical properties of arc-evaporated Cr-C-N coatings, Thin Solid Films 385 (2001), 190-197.

[9] J. Musil, H. Zeman, F. Kunc, H. Poláková: Relationships between hardness, Young´s modulus and elastic recovery in hard nanocomposite coatings, Surf. Coat.Technol. 154(2002), 304-313.

[10] J. Musil, H. Zeman, J. Kasl: Relationship between structure and mechanical properties in hard Al-Si-Cu-N films prepared by magnetron sputtering, Thin Solid Films 413 (2002), 121-130.

[11] H. Watanabe, Y. Sato, C. Nie, A. Ando, S. Ohtani, N. Iwamoto: The mechanical properties and microstructure of Ti-Si-N nanocomposite films by ion plating, Surf. Coat. Technol. 169-170 (2003), 452-455.

[12] H.S. Barshilia, A. Jain, K.S. Rajam: Structure, hardness and thermal stability of nanolayered TiN/CrN multilayer coatings, Vacuum 72 (2003), 241-248.

[13] P. Jedrzejowski, J.E. Klemberg-Sapieha, L. Martinu: Relationship between the mechanical properties and the microstructure of nanocomposite TiN/$SiN_{1.3}$ coatings prepared by low-temperature PECVD, Thin Solid Films 426 (2003), 150-159.

[14] S.D. Ekpe, F.J. Jimenez, D.J. Field, M.J. Davis, S.K. Dew: Effect of magnetic field strength on deposition rate and energy flux in a dc magnetron sputtering system, J.Vac.Sci.Technol. A 27(6) (2009) 1275- 1280.

[15] C.S. Sandu, N. Cusnir, D. Oezer, R. Sanjines, J. Patscheider: Influence of bias voltage on the microstructure and physical properties of magnetron sputtered Zr-Si-N nanocomposite films, Surf. Coat. Technol. 204 (2009), 969-972.

[16] F. Cai, X. Huang, Q. Yang, R. Wei, D. Nagy: Microstructure and tribological properties of CrN and CrSiCN coatings, Surf. Coat. Technol. 205 (2010), 182-188.

[17] X.C. Zhang, C.J. Liu, F.Z. Xuan, Z.D. Wang, S.T. Tu: Effect of residual stresses on the strength and fracture energy of the brittle film: Multiple cracking analysis, Computational Materials Science, 50 (2010), 246-252.

[18] C.Q. Chen, Y.T. Pei, J.T.M. DeHosson: Effect of size on the mechanical response of metallic glasses investigated through in situ TEM bending and compression experiments, Acta Materialia 58 (2010), 189-200.

[19] E. Silva, M.R. de Figueiredo, R. Franz, R.E. Galindo, C. Palacio, A. Espinosa, S. Calderon, S. Carvalho: Structure-property relations in ZrCN coatings for tribological applications, Surf. Coat. Technol. 205 (2010), 2134-2141.

[20] D. Depla, B.R. Braeckman: Quantitative correlations between intrinsic stress and microstructure of thin films, Thin Solid Films 604 (2016), 90-93

[21] J. Musil: Sputtering systems with enhanced ionization for ion plating of hard wear resistant coatings, Proc. of the 1st Meeting on the Ion Engineering Society of Japan (IESJ-92), Tokyo, Japan, 1992, pp. 295-304.

[22] H. Poláková, J. Musil, J. Vlček, J. Alaart, C. Mitterer: Structure- hardness relations in sputtered Ti-Al-V-N films, Thin Solid Films 444 (2003), 189-198.

[23] J. Musil, H. Poláková, J. Šůna, and J. Vlček: Effect of ion bombardment on properties of hard reactively sputtered single-phase films, Surf.Coat.Technol. 177-178 (2004), 289-298.

[24] J. Musil, and J. Šůna: The role of energy in formation of sputtered nanocomposite films, Materials Science Forum 502 (2005), 291-296.

[25] J. Musil, J. Šícha, D. Heřman, R. Čerstvý: Role of energy in low-temperature high-rate formation of hydrophilic TiO2 thin films using pulsed magnetron sputtering, J. Vac. Sci. Technol. A 25(4) (2007), 666-674.

[26] J. Musil: Physical and mechanical properties of hard nanocomposite films prepared by reactive magnetron sputtering, Chapter 10 in *Nanostructured Coatings,* J.T.M. DeHosson and A. Cavaleiro (Eds.) New York, Springer Science + Business Media, LCC, 2006, pp. 407-463.

[27] J. Vlček, K. Rusňák, V. Hájek and L. Martinů (1999). Reactive magnetron sputtering of CNx films: Ion bombardment effects and process characterization using optical emission spectroscopy. J.Appl.Phys. 86: 3646-3654

[28] J. Musil, J. Vlček, P. Baroch: Magnetron discharges for thin films plasma processing, Chapter 3 in „*Materials Surface Processing by Directed Energy Techniques*, Y.Pauleau (Ed.), 2006, Elsevier Science Publisher B.V., Oxford, UK, pp. 67-106.

[29] Lieberman, M. A., and Lichtenberg, A.J. (1994). Principles of Plasma Discharges and Materials Processing,Wiley Interscience, New York.

[30] J.A. Thornton: (i) Recent developments in sputtering – Magnetron sputtering, Metal Finishing 77(5) (1979), 83-87 and (ii) High rate thick films growth, Ann. Rev. Mater. Sci. 7 (1977), 239-260.

[31] J. Musil, V. Poulek, V. Valvoda, R. Kužel Jr., H.A. Jehn, M.E. Baumgartner: Relation of deposition conditions of Ti-N films prepared by dc magnetron sputtering to their microstructure and macrostress, Surf.Coat.Technol. 60 (1993), 484-488.

[32] P. J. Kelly, J. Hisek, Y. Zhou, R. D. Pilkington and R. D. Arnell: ADVANCED COATINGS THROUGH PULSED MAGNETRON SPUTTERING, Surface Engineering 20(3) (2004).

[33] J. Lin, J.J. Moore, B. Mishra, W.D. Sproul, J.A. Rees: Examination of the pulsing phenomena in pulsed-closed field unbalanced magnetron sputtering (P-CFUBMS) of Cr–Al–N thin films, Surface & Coatings Technology 201 (2007), 4640–4652

[34] J. O'Brien, P.J. Kelly: Characterization studies of the pulsed dual cathode magnetron sputtering process for oxide films, Surface and Coatings Technology 142-144 (2001) 621-627

[35] J.M. Anton, B. Mishra, J.J. Moore, J.A. Rees, W.D. Sproul: Investigation of processing parameters for pulsed closed-field unbalanced magnetron co-sputtered TiC–C thin films, Surface & Coatings Technology 201 (2006) 4131–4135

[36] Y.T. Pei, C.Q. Chen, K.P. Shaha, J.Th.M. De Hosson, J.W. Bradley, S.A. Voronin, M. Čada: Microstructural control of TiC/a-C nanocomposite coatings with pulsed magnetron sputtering, Acta Materialia 56 (2008) 696‑709

[37] J.W. Bradley, H. Backer, P.J. Kelly, R.D. Arnell: Time-resolved Langmuir probe measurements at the substrate position in a pulsed mid-frequency DC magnetron plasma, Surface and Coatings Technology 135 _2001.

[38] A.D. Pajdarová, J. Vlček, P. Kudláček, J. Lukáš: Electron energy distributions and plasma parameters in high-power pulsed magnetron sputtering discharges, Plasma Sources Sci. Technol. 18 (2009) 025008.

[39] P.A. Cormier, A. Balhamri, A.L. Thomann, R. Dussart, N. Semmar: Measuring the energy flux at the substrate position during magnetron sputter deposition processes, J. Appl. Phys. 113 (2013) 013305.

[40] P Poolcharuansin, J W Bradley: Short- and long-term plasma phenomena in a HiPIMS discharge, Plasma Sources Sci. Technol. 19 (2010) 025010.

[41] V. Stranak, A.P. Herrendorf, S. Drache, M. Cada, Z. Hubicka, R. Bogdanowicz, M. Tichy, R. Hippler: Plasma diagnostics of low pressure high power impulse magnetron sputtering assisted by electron cyclotron wave resonance plasma, Journal of Applied Physics 112, (2012) 093305.

[42] A. Mishra, P. J. Kelly, J. W. Bradley: The evolution of the plasma potential in a HiPIMS discharge and its relationship to deposition rate, Plasma Sources Sci. Technol. 19 (2010) 045014.

[43] O.V. Krysina, N.N. Koval, I.V. Lopatin, V.V. Shugurov, S.S. Kovalsky: Generation of low-temperature plasma by low-pressure arcs for synthesis of nitride coatings, Journal of Physics: Conference Series 669 (2016) 012032.

[44] N.N. Koval, Yu.F. Ivanov, I.V. Lopatin, Yu.H. Akhmadeev, V.V. Shugurov, O.V. Krysina, V.V. Denisov: Generation of Low-Temperature Gas Discharge Plasma in Large Vacuum Volumes for Plasma Chemical Processes, Russian Journal of General Chemistry, 85 (2015) 1326

[45] Yu.H. Akhmadeev, S.V. Grigoriev, N.N. Koval, P.M. Schanin: Plasma sources based on a low-pressure arc discharge, Laser and Particle Beams, 21 (2003) 249.

[46] M. Trant, M. Fischer, K. Thorwarth, S. Gauter, J. Patscheider, H.J. Hug: Tunable ion flux density and its impact on AlN thin films deposited in a confocal DC magnetron sputtering system, Surface & Coatings Technology 348 (2018) 159

[47] F. Adibi, I. Petrov, J. E. Greene, L. Hultman, and J.E. Sundgren: Effects of high flux low energy (20–100 eV) ion irradiation during deposition on the microstructure and preferred orientation of Ti0.5Al0.5N alloys grown by ultrahigh vacuum reactive magnetron sputtering, J. Appl. Phys. 73 (1993) 8580.

[48] C.S. Shin, D. Gall, Y.W. Kim, N. Hellgren, I. Petrov, J.E. Greene: Development of preferred orientation in polycrystalline NaCl-structure δ-TaN layers grown by reactive magnetron sputtering: Role of low-energy ion surface interactions, J. Appl. Phys. 92 (2002) 9.

[49] L. Hultman, J.E. Sundgren, J.E. Greene, D.B. Bergstrom, I. Petrov: Highflux low energy (20 eV) N+2 ion irradiation during TiN deposition by reactive magnetron sputtering: Effects on microstructure and preferred orientation, J. Appl. Phys. 78, (1995) 5395

[50] J.S. Chun, I. Petrov, J.E. Greene: Dense fully 111-textured TiN diffusion barriers: Enhanced lifetime through microstructure control during layer growth, Journal of Applied Physics 86 (1999) 3633

2. Aims of the Ph.D. thesis

The subject of the Ph.D. thesis is the preparation of metal nitride films with multifunctional properties and an enhanced resistance to cracking by magnetron sputtering and the investigation of the interrelationships between the deposition parameters, energy $\mathcal{E}$ delivered into the film and the film properties.

The aims of the Ph.D. thesis are the following:

1. To investigate the effect of energy $\mathcal{E}$ delivered into the growing Ti(Al,V)N nitride films on their properties, such as (i) texture, (ii) microstructure, (iii) mechanical properties, (iv) macrostress and (v) resistance to cracking.

2. To investigate the effect of plasma and floating potential on energy $\mathcal{E}$ delivered into the growing film and on reproducibility of sputter deposited films.

3. To create hard overstoichiometric $TiN_{x>1}$ dinitride thin films using magnetron sputtering and to determine the discharge properties under which such films can be sputter deposited.

Paper I

3. Evolution of microstructure and macrostress in sputtered hard Ti(Al,V)N films with increasing energy delivered during their growth by bombarding ions

Jindřich Musil, **Martin Jaroš**, Radomír Čerstvý, Stanislav Haviar
J. Vac. Sci. Technol. A 35, 020601 (2017)

Abstract

This letter reports on the effect of the energy $\mathcal{E}_{bi}$, delivered to the sputtered Ti(Al,V)N film by bombarding ions, on its microstructure, macrostress σ, mechanical properties, and resistance to cracking. The films were deposited by reactive magnetron sputtering. Interrelationships between these parameters were investigated in detail. It was shown that (1) the increase of the energy $\mathcal{E}_{bi}$ makes it possible to convert (i) the film microstructure from columnar to dense, non-columnar, (ii) the macrostress σ from tensile ($\sigma > 0$) to compressive ($\sigma < 0$), (iii) the brittle hard film with low ratio $H/E^* < 0.1$ and low elastic recovery $W_e < 60\%$ to the flexible hard film with high ratio $H/E^* \geq 0.1$ and high elastic recovery $W_e \geq 60\%$, (2) the flexible hard Ti(Al,V)N films with high ratio $H/E^* \geq 0.1$, high elastic recovery $W_e \geq 60\%$ and compressive macrostress can be formed not only in the Transition Zone (Zone *T* in which the films exhibit a dense, voids-free microstructure) of the Thornton's structural zone model (SZM) but also in Zone *1* in which the films exhibit a columnar microstructure and (3) the line corresponding to the films with zero macrostress ($\sigma = 0$) in the SZM lies in Zone *1* corresponding to the columnar microstructure; here *H* is the film hardness and $E^* = E(1 - \nu^2)$ is the effective Young's modulus, *E* is Young's modulus and ν is the Poisson's ratio.

3.1. Introduction

Recently, the hard nanocomposite films with enhanced hardness and unique properties, for instance, the films with high-temperature stability and oxidation resistance considerably higher than 1000 °C, high erosion resistance, high electrical conductivity, high optical transparency, etc. have been developed [1-35]. The detailed investigation of correlations between the physical and mechanical properties of these films have shown that it is also possible to create flexible films which are simultaneously hard and resistant to cracking [36-44]. Such films exhibit a high ratio of the hardness H and the effective Young's modulus E^* ($H/E^* \geq 0.1$), high elastic recovery $W_e \geq 60\%$, compressive macrostress ($\sigma < 0$) and a dense voids-free microstructure; here $E^* = E/(1 - \nu^2)$, *E* is Young's modulus and ν is the Poisson's ratio [28, 45, 46]. These properties of flexible hard films can be achieved by optimization of the deposition parameters used in sputtering. In this article, it is demonstrated that these parameters are well controlled by the energy $\mathcal{E}_{bi}$ delivered to the growing film by bombarding ions. It is shown that the Ti(Al,V)N films exhibit (i) a columnar microstructure and low resistance to cracking when sputtered at low energy $\mathcal{E}_{bi}$ and (ii) a dense, voids-free microstructure and an enhanced resistance to cracking when sputtered at high energy $\mathcal{E}_{bi}$. In the simplest case of a collision-less, fully ionized plasma the energy $\mathcal{E}_{bi}$ can be expressed in the following form [28, 45-47]

$$\mathcal{E}_{bi}\ [\mathrm{J/cm^3}] = (U_s - U_p) \times i_s/a_D \approx U_s \times i_s/a_D \tag{3.1}$$

Eq. (3.1) clearly shows two important facts. The energy $\mathcal{E}_{bi}$ delivered to the growing film by bombarding ions (1) can be easily calculated from measured deposition parameters (U_s, i_s) and the film deposition rate $a_D = h/t_d$ calculated from the measured film thickness *h* and the deposition time t_d and (2) strongly depends not only on U_s and i_s but also on a_D. The second fact is of extraordinary importance in (i) the reactive sputtering of compounds and (ii) the high-rate sputtering of films because the energy $\mathcal{E}_{bi}$ delivered to the growing film deceases with increasing a_D.

The main aim of this letter is to report on results of the detailed investigation of the correlations between the microstructure, structure, macrostress σ and resistance against cracking of the Ti(Al,V)N film sputtered as a function of the energy $\mathcal{E}_{bi}$ delivered to it by bombarding ions during its growth.

3.2. Experiment

The $Ti(Al,V)N_x$ films were sputter deposited in a mixture of Ar + N_2 sputtering gases using a DC dual magnetron with closed magnetic field equipped with a TiAlV (6 at.% Al, 4 at.% V) alloy target of diameter ∅ = 50 mm. Magnetrons were tilted to the normal of the substrate surface at the angle of 20°. The films were sputtered on Si(111) and Mo substrates at the discharge current I_d = 0.5 A, target power density $W_t = I_d U_d / S \approx 10$ W/cm^2, substrate temperature T_s = 500°C, substrate bias U_s ranging from 0 to -100 V, substrate-to-target distance d_{s-t} = 60 mm, partial pressure of nitrogen p_{N2} = 0.8 Pa and total pressure of sputtering gas $p_T = p_{Ar} + p_{N2}$ = 1 Pa; here U_d is discharge voltage and S is the area of the target. The $Ti(Al,V)N_x$ films sputtered under these conditions are crystalline and almost stoichiometric (x = N/(Ti + Al + V) ≈ 1, see Fig. 3.1.

The film thickness h and the macrostress σ were measured by a DEKTAK 8 Stylus Profiler, Veeco. The film structure was characterized by an XRD spectrometer PANalytical X'Pert PRO in the Bragg-Brentano configuration using CuKα radiation (λ = 0.154187 nm). The mechanical properties were determined from load vs. displacement curves measured by a Fisherscope H 100VP with a Vickers diamond indenter at load L = 20 mN at $d/h < 0.1$; here d is the diamond impression in the film at L = 20 mN. The resistance of the Ti(Al,V)N film to cracking was assessed by the indentation test in which the diamond indenter was impressed in the film at high load L = 1N; for more details see the paper [46].

3.3. Results and discussion

The interrelationships between the mechanical properties (H, E^*, W_e, H/E^*) of the Ti(Al,V)N film, its macrostress σ, microstructure, resistance to cracking and the energy $\mathcal{E}_{bi}$ delivered to the growing film by bombarding ions were investigated in detail. These interrelationships are schematically illustrated in Fig. 3.2.

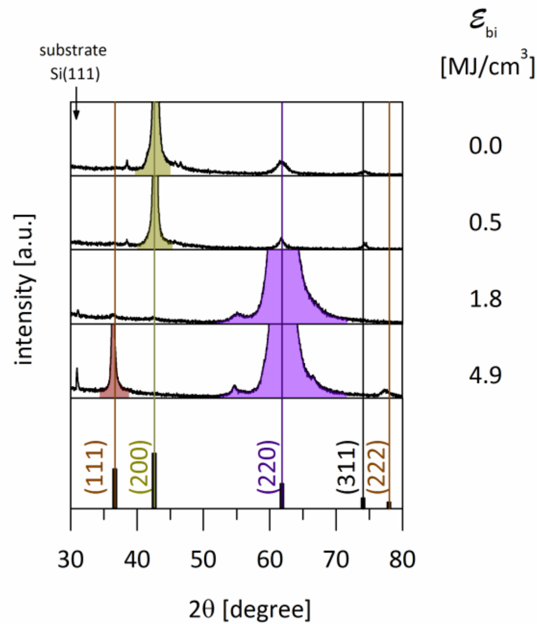

Figure 3.1 Evolution of XRD patterns of Ti(Al,V)N films with increasing energy $\mathcal{E}_{bi}$ delivered to them during their growth by bombarding ions. Deposition parameters: I_d = 0.5 A, T_s = 500 ℃, W_t ≈ 10 W/cm^2, p_{N2} = 0.8 Pa, $p_T = p_{Ar} + p_{N2}$ = 1 Pa and U_s ranging from 0 to -100 V. Physical and mechanical properties of these films are given in Table 3.1.

Fig. 3.2 displays the evolution of the microstructure, mechanical properties and the TEM cross-sectional images of the Ti(Al,V)N film with increasing energy $\mathcal{E}_{bi}$. Fig. 3.3 displays the evolution of the surface morphology of the Ti(Al,V)N films after the indentation at high load L = 1 N with increasing energy $\mathcal{E}_{bi}$. Fig. 3.4 shows the transition of the films with a columnar microstructure to the films with a dense, voids-free microstructure with increasing energy $\mathcal{E}_{bi}$. The physical and mechanical properties of these films are given in Table 3.1.

Main conclusions which can be drawn from Figs. 3.2 and 3.3 and Table 3.1 are the following

1. The density of the Ti(Al,V)N film microstructure and the macrostress σ both increase with increasing energy $\mathcal{E}_{bi}$. The microstructure gradually changes from columnar with voids (Fig. 3.2a) to a dense, voids-free microstructure without columns (Fig. 3.2d). The increase of the energy $\mathcal{E}_{bi}$ results in an increased mobility of the condensing atoms at the surface of the growing film, the microstructure densification and a transition from films with a columnar microstructure to films with a dense, voids-free microstructure.

2. The Ti(Al,V)N films with a columnar microstructure can exhibit not only tensile macrostress ($\sigma > 0$) but also compressive macrostress ($\sigma < 0$). The compressive macrostress arises when the columns are in strong contact.

3. The Ti(Al,V)N films with a columnar microstructure and a weak contact between columns (the low compressive macrostress $|\sigma| \rightarrow 0$), however, exhibit low resistance to cracking, see the cracks on the photo in Fig. 3.3b. Responsible for the cracking of this films are: (1) the columnar microstructure, (2) the low ratio $H/E^* < 0.1$, (3) the low compressive macrostress $|\sigma| \leq 0.5$ GPa and (4) the low elastic recovery $W_e \approx 60\%$, see Table 3.1.

4. The Ti(Al,V)N films with a dense microstructure (the very densely packed columns (Fig. 3.2c) and the featureless microstructure without columns corresponding to zone *T* of Thornton's Structural zone model (SZM) [48,49] (Fig. 3.2d)) exhibit enhanced resistance to cracking. These films are characterized by (1) a dense voids-free microstructure, (2) the high ratio $H/E^* > 0.1$, (3) the high compressive macrostress $|\sigma| \geq 0.5$ GPa and (4) the high elastic recovery $W_e \geq 70\%$.

5. The highest energy of 4.9 MJ/cm^3 cannot be considered as the optimal energy because the Ti(Al,V)N film sputtered at $\mathcal{E}_{bi}$ = 4.9 MJ/cm^3 already exhibits too high compressive macrostress σ = -5.5 GPa, which may result in the film delamination from the substrate when the film is too thick. The films with high ratio $H/E^* > 0.1$, high elastic recovery $W_e > 60\%$, a dense, voids-free microstructure and a lower compressive macrostress (σ = -2.5 GPa) are good flexible, hard films with enhanced resistance to cracking.

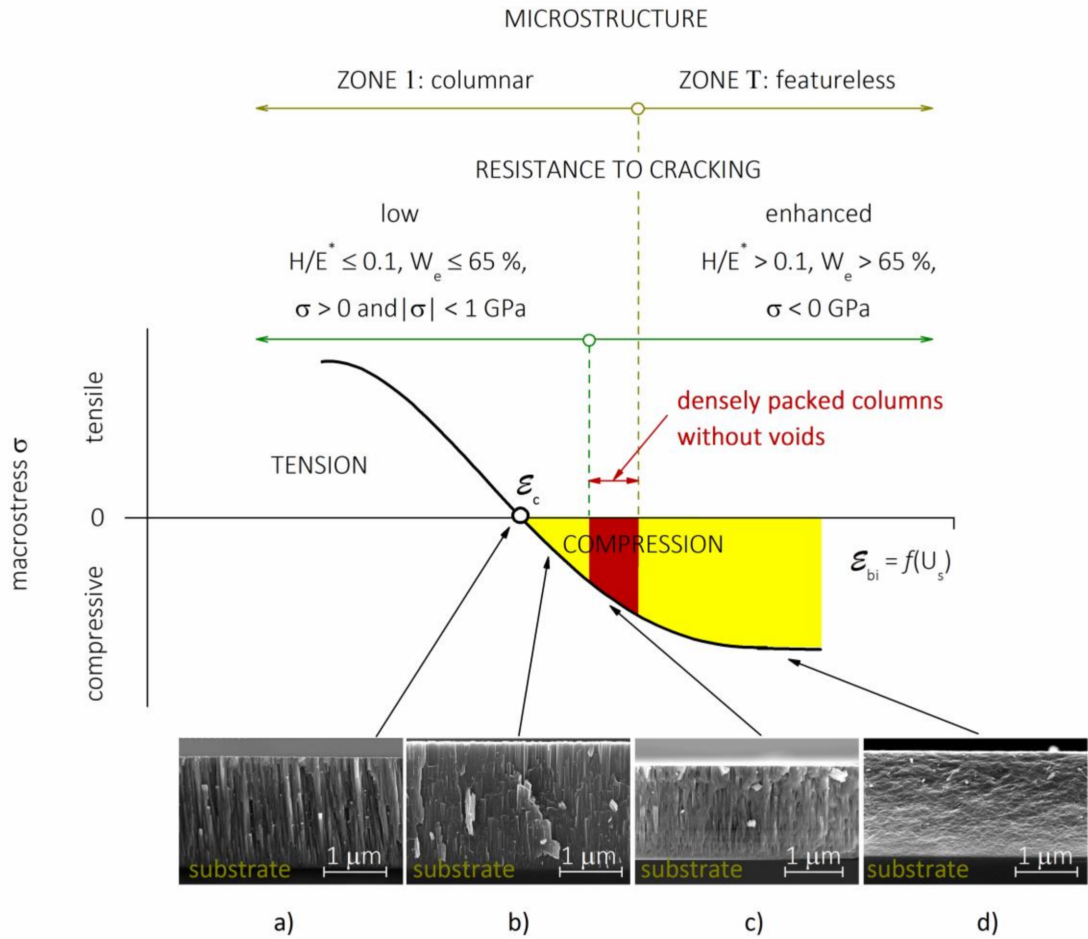

Figure 3.2 Schematic illustration of the interrelationships between the microstructure, mechanical properties, macrostress σ of the Ti(Al,V)N film, its resistance to cracking and the energy $\mathcal{E}_{bi}$ delivered to the growing film by bombarding ions in the DC reactive magnetron sputtering. (a) The film No. 1, (b) the film No. 2, (c) the film No. 3 and (d) the film No. 4, see Table 3.1.

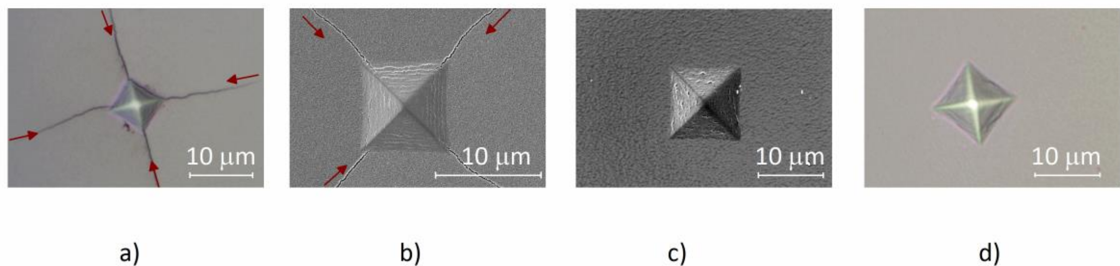

Figure 3.3 The evolution of the microstructure, the surface morphology with the diamond indenter impression at load L = 1 N and the macrostress σ of the Ti(Al,V)N film with increasing energy $\mathcal{E}_{bi}$. (a) $\mathcal{E}_{bi}$ = 0 MJ/cm^3, σ = 0 GPa, (b) $\mathcal{E}_{bi}$ = 0.5 MJ/cm^3, σ = - 0.4 GPa, (c) $\mathcal{E}_{bi}$ = 1.8 MJ/cm^3, σ = - 2.5 GPa, (d) $\mathcal{E}_{bi}$ = 4.9 MJ/cm^3, σ = - 5.5 GPa.

Table 3.1 Physical and mechanical properties of Ti(Al,V)N_x films sputtered by the DC magnetron at I_d = 0.5 A, W_t ≈ 10 W/cm^2, T_s = 500 ℃, d_{s-t} = 60 mm, p_{N2} = 0.8 Pa, p_T = 1 Pa as a function of the substrate bias U_s.

Film	$\mathcal{E}_{bi}$	U_s	i_s	a_D	h	H	E^*	W_e	H/E^*	σ	Microstructure
No.	[MJ/cm^3]	[V]	[mA/cm^2]	[nm/min]	[nm]	[GPa]	[GPa]	[%]		[GPa]	
1	0	0	0	12.8	1700	25.2	260	64	0.097	≈ 0.0	Columnar with woids
2	0.5	-20	0.7	16.7	2000	24.7	268	62	0.092	-0.4	Columnar with woids
3	1.8	-50	0.9	16.2	2100	32.6	275	76	0.119	-2.5	Columnar, voids-free
4	4.9	-100	1.1	13.7	1400	30.1	240	79	0.125	-5.5	Dense, voids-free

In Fig. 3.2 $\mathcal{E}_c$ denotes the critical energy $\mathcal{E}_{bi}$ at which the sputtered films exhibit zero macrostress (σ = 0). The critical energy $\mathcal{E}_c$ depends on the elemental composition of the film and the ratio T_s/T_m; here T_s is the substrate temperature and T_m is the melting temperature of the film's material [28, 45]. The films sputtered at low energies ($\mathcal{E}_{bi} < \mathcal{E}_c$) exhibit tensile stress (σ > 0) and the films sputtered at high energies ($\mathcal{E}_{bi} > \mathcal{E}_c$) exhibit compressive stress (σ < 0). Our experiments show that the line σ = f (p_{Ar}) corresponding to the films with zero macrostress (σ = 0) in the Thornton's Structural Zone Model SZM [48, 49] lies in Zone *1*, see the red curve in Fig. 3.4.

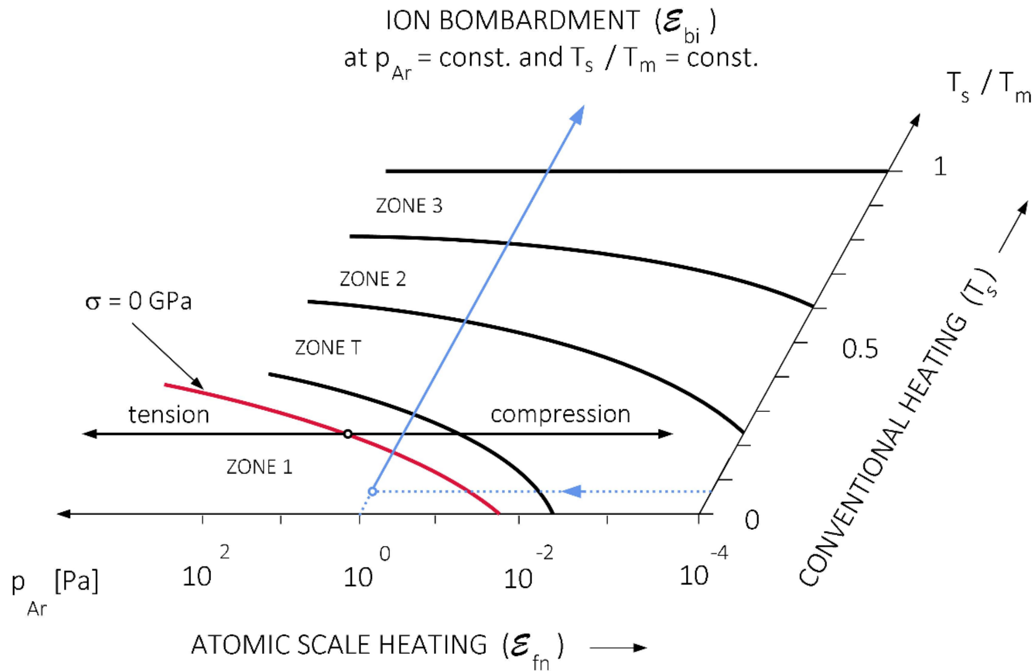

Figure 3.4 Schematic illustration of two dimensional (2D) Thornton´s structural zone model (SZM) showing that the line corresponding to the films with zero macrostress (σ = 0) lies in zone 1. $\mathcal{E}_{fn}$ and $\mathcal{E}_{bi}$ denote the energy delivered to the growing film by fast neutral particles, i.e. by bombarding and condensing fast atoms, and bombarding ions, respectively.

It means that the films with a columnar structure can exhibit also compressive stress (σ < 0). In the case when the value of the compressive macrostress (σ < 0) is low the film with a columnar microstructure easily cracks. This fact was confirmed also in the paper of Y.T.Pei et al [50] in which the cracking of the TiC/a-C:H films with a columnar

microstructure sputtered at a quite high negative substrate bias U_s = -100 V is reported. In the case when the value of the compressive macrostress is sufficiently high the films with a columnar microstructure exhibit strongly enhanced resistance to cracking. The blue straight line in Fig. 3.4 shows the evolution of the film microstructure from columnar to dense, voids-free with increasing ion bombardment ($\mathcal{E}_{bi}$) at constant values of Ar pressure p_{Ar} and T_s/T_m ratio.

3.4. Conclusions

In summary we can conclude that (1) The flexible hard Ti(Al,V)N films with enhanced resistance to cracking can be formed when the energy $\mathcal{E}_{bi}$ delivered to them during their growth is greater than the critical energy $\mathcal{E}_c$, (2) The critical energy $\mathcal{E}_c$ depends on the elemental composition of the film and the ratio T_s/T_m, (3) The flexible hard Ti(Al,V)N films exhibit high ratio $H/E^* \geq 0.1$, high elastic recovery $W_e > 70\%$, compressive macrostress ($\sigma < 0$) and dense, voids-free microstructure, (4) The flexible hard films with columnar voids-free microstructure can be also formed when these films exhibit the compressive macrostress ($\sigma < 0$), (5) The formation of flexible hard Ti(Al,V)N films can be efficiently controlled by the energy $\mathcal{E}_{bi}$ delivered to them during their growth by bombarding ions and (6) The line $\sigma = f(p)$ corresponding to the films with zero macrostress ($\sigma = 0$) lies in Zone *1* of the Thornton's SZM in which films with columnar microstructure are created. All these conclusions are of general validity and were confirmed already in nine different material coating systems [36-44]. Obtained results deepen the present state of the knowledge in the field and represent a huge application potential.

Acknowledgments

This work was supported by the Czech Science Foundation under Project No. GA16-18183S.

References

[1] H. Gleiter: Nanocrystaline materials, Progress in Materials Science 33 (1989) 223.

[2] S. Veprek, S. Reiprich: A concept for design of novel superhard coatings, Thin Solid Films 268 (1995) 64.

[3] H. Gleiter: Nanostructured materials: state of art and perspectives, Nanostructured Materials 6 (1996) 3.

[4] S. Yip: Nanocrystals: The strongest size, Nature 391 (1998) 532.

[5] A. A. Voevodin, J. S. Zabinski: Superhard, functionally gradient, nanolayered and nanocomposite diamond-like carbon coatings for wear protection, Diamond and Related Materials 7 (1998) 463.

[6] J. Musil: Hard and superhard nanocomposite coatings, Surf.Coat.Technol. 125 (2000) 322.

[7] H. Gleiter: Nanostructured materials: basic concepts and microstructure, Acta Mater. 48 (2000) 1.

[8] A. Leyland, A. Matthews: On the significance of the H/E ratio in wear control: a nanocomposite coating approach to optimised tribological behaviour, Wear 246 (2000) 1.

[9] L. Hultman: Thermal stability of nitride thin films, Vacuum 57 (2000) 1.

[10] R. Hauert, J. Patscheider: From Alloying to Nanocomposites—Improved Performance of Hard Coatings, Adv. Eng. Mater. 2 (2000) 247.

[11] S. Veprek: Handbook of Ceramic Hard Materials, edited by R. Riedel (WILEY-VCH, Weinheim, 2000), pp. 104-139.

[12] H. Gleiter: Tuning the electronic structure of solids by means of nanometer-sized microstructures, Scripta Mater. 44 (2001) 1161.

[13] R. A. Andrievskii: Thermal stability of nanomaterials, Russian Chemical Reviews 71 (2002) 853.

[14] J. Patscheider: Nanocomposite Hard Coatings for Wear Protection, MRS Bulletin 28 (2003) 180.

[15] S. Zhang, D. Sun, Y. Fu, H. Du: Recent advances of superhard nanocomposite coatings: a review, Surf. Coat. Technol. 167 (2003) 113.

[16] R. A. Andrievski: Nanomaterials based on high-melting carbides, nitrides and borides, Russian Chemical Reviews, 74 (2005) 1061.

[17] S. Zhang, D. Sun, Y. Fu H. Du: Toughening of hard nanostructural thin films: a critical review, Surf. Coat. Technol. 198 (2005) 2.

[18] J. Musil: Nanostructured Coatings, edited by J. T. M. De Hosson and A. Cavaleiro (Springer Science + Business Media, LCC, New York, 2006), pp. 407-463.

[19] L. Hultman, C. Mitterer: Nanostructured Coatings, edited by J. T. M. De Hosson and A. Cavaleiro (Springer Science + Business Media, LCC, New York, 2006), pp. 464-510.

[20] P. H. Mayrhofer, C. Mitterer, L.Hultman: Microstructural design of hard coatings, Progress in Materials Science 51 (2006) 1032.

[21] C. Lu, Y. W. Mai, Y. G. Shen: Recent advances on understanding the origin of superhardness in nanocomposite coatings: A critical review, J. Mater. Sci. 41 (2006) 937.

[22] C. S. Sandu, F. Medjani, R. Sanjines: OPTICAL AND ELECTRICAL PROPERTIES OF SPUTTERED Zr-Si-N THIN FILMS: FROM SOLID SOLUTION TO NANOCOMPOSITE, Rev. Adv. Mater. Sci. 15 (2007) 173.

[23] J. Musil, M. Jirout: Toughness of hard nanostructured ceramic thin films, Surf. Coat. Technol. 201 (2007) 5148.

[24] A. Raveh, I. Zukerman, R. Shneck, R. Avni, I. Fried: Thermal stability of nanostructured superhard coatings: A review, Surf. Coat. Technol. 201 (2007) 6136.

[25] Y. H. Lu, Y. G. Shen: Nanostructure transition: From solid solution Ti(N,C) to nanocomposite nc-Ti(N,C)/a-(C,CNx), Appl. Phys. Lett. 90 (2007) 221913.

[26] S. Zhang, H. L. Wang, S. E. Ong, D. Sun, X. L. Bui: Hard yet Tough Nanocomposite Coatings – Present Status and Future Trends, Plasma Process. Polym. 4 (2007) 219.

[27] J. Musil, J. Vlček, P. Zeman: Hard amorphous nanocomposite coatings with oxidation resistance above 1000°C, Advances in Applied Ceramics 107 (2008) 148.

[28] J. Musil: Hard nanocomposite coatings: Thermal stability, oxidation resistance and toughness, Surf.Coat.Technol. 207 (2012) 50.

[29] S.Veprek: Recent search for new superhard materials: Go nano!, J.Vac.Sci.Technol. A 31 (2013) 050822.

[30] J. Musil, P. Zeman, P. Baroch: Hard Nanocomposite Coatings, Comprehensive Materials Processing, edited by D. Cameron (Elsevier, 2014), pp. 325-353.

[31] J. Kohout, J. Vlček, J. Houška, P. Mareš, R. Čerstvý, P. Zeman, M. Zhang, J. Jiang, E. I. Meletis, Š. Zuzjaková: Hard multifunctional Hf–B–Si–C films prepared by pulsed magnetron sputtering, Surf. Coat. Technol. 257 (2014) 301.

[32] P. Zeman, Š. Zuzjaková, P. Mareš, R. Čerstvý, M. Zhang, J. Jiang, E. I. Meletis, J. Vlček: Superior high-temperature oxidation resistance of magnetron sputtered Hf–B–Si–C–N film, Ceramics International 42 (2016) 4853.

[33] J. Vlček, A. Belosludstsev, J. Rezek, J. Houška, J. Čapek, R. Čerstvý, S. Haviar: High-rate reactive high-power impulse magnetron sputtering of hard and optically transparent HfO2 films, Surf. Coat. Technol. 290 (2016) 58.

[34] H. Frager, B. M. Howe, G. Greczynski, J. Jensen, A. B. Mei, J. Lu, L. Hultman, J. E. Greene, I. Petrov: Novel hard, tough HfAlSiN multilayers, defined by alternating Si bond structure, deposited using modulated high-flux, low-energy ion irradiation of the growing film, J. Vac. Sci. Technol. A 33 (2015) 05E103.

35 S. Ali, B. Paul, R. Magnusson, G. Greczynski, E. Broitman, B. Jonson, P. Eklund, J. Birch: Novel transparent MgSiON thin films with high hardness and refractive index, Vacuum 131 (2016) 1.

[36] J. Musil, J. Sklenka, R. Čerstvý: Transparent Zr–Al–O oxide coatings with enhanced resistance to cracking, Surf. Coat. Technol. 206 (2012) 2105.

[37] J. Musil, R. Jílek, M. Meissner, T. Tolg, R. Čerstvý: Two-phase single layer Al-O-N nanocomposite films with enhanced resistance to cracking, Surf. Coat. Technol. 206 (2012) 4230.

[38] J. Musil, R. Jílek, R. Čerstvý: Flexible Ti-Ni-N thin films prepared by magnetron sputtering, Journal of Materials Science and Engineering. A 4 (2014) 27.

[39] J. Musil, J. Blažek, K. Fajfrlík, R. Čerstvý: Flexible antibacterial Al–Cu–N films, Surf. Coat. Technol. 264 (2015) 114.

[40] J. Musil, M. Zítek, K. Fajfrlík, R. Čerstvý: Flexible antibacterial Zr-Cu-N thin films resistant to cracking, J. Vac. Sci. Technol. A 34 (2016) 021508.

[41] J. Musil, J. Sklenka, R. Čerstvý: Protection of brittle film against cracking, Appl. Surf. Sci. 370 (2016) 306.

[42] J. Musil, S. Zenkin, S. Kos, R. Čerstvý, S. Haviar: Flexible hydrophobic ZrN nitride films, Vacuum 131 (2016) 34.

[43] J. Musil, D. Javdošňák, R. Čerstvý, S. Haviar, G. Remnev, V. Uglov: Effect of energy on the formation of flexible hard Al-Si-N films prepared by magnetron sputtering, Vacuum 133 (2016) 43.

[44] J. Musil, G. Remnev, L. Legostaev, V. Uglov, A. Lebedynskiy, A. Lauk, J. Procházka, S. Haviar, E. Smolyanskiy: Flexible hard Al-Si-N films for high temperature operation, Surf. Coat. Technol. 307 (2016) 1112.

[45] J. Musil: Flexible hard nanocomposite coatings RSC Advances 5 (2015) 60482.

[46] J. Musil: Thin films and Coatings: Toughening and Toughening Characterization, edited by S .Zhang (CRC Press, USA, 2015), pp. 377-463.

[47] J. Musil, J. Šícha, D. Heřman, R. Čerstvý: Role of energy in low-temperature high-rate formation of hydrophilic TiO2 thin films using pulsed magnetron sputtering, J. Vac. Sci. Technol. A 25 (2007) 666.

[48] J. A. Thornton: HIGH RATE THICK FILM GROWTH, Ann. Rev. Mater. Sci. 7 (1977) 239.

[49] J. A. Thornton: Recent developments in sputtering – magnetron sputtering, Metal. Finish. 77 (1979) 660.

[50] Y. T. Pei, D. Galvan, J. Th. M. De Hosson: Nanostructure and properties of TiC/a-C:H composite coatings, Acta Mater. 53 (2005) 4505.

Paper II

4. Effect of energy on structure, microstructure and mechanical properties of hard $Ti(Al,V)N_x$

M. Jaroš, J. Musil, R. Čerstvý, S. Haviar
Surf. Coat. Technol. 332 (2017) 190–197

Abstract

The article reports on the effect of the energy $\mathcal{E}$ delivered to the growing film by bombarding ions $\mathcal{E}_{bi}$ and/or fast neutrals $\mathcal{E}_{fn}$ on its physical (structure, microstructure) and mechanical properties, and resistance to cracking. The effect of the energy $\mathcal{E} = \mathcal{E}_{bi} + \mathcal{E}_{fn}$ on the film properties is demonstrated on the $Ti(Al,V)N_x$ films deposited by reactive magnetron sputtering. The films were sputtered on Si(111) and Mo substrates in a mixture $Ar+N_2$ gases by a dual magnetron with closed magnetic field and equipped with TiAlV (6 at.% Al, 4 at.% V) alloy targets. It was shown that (1) The energy $\mathcal{E} = \mathcal{E}_{bi} + \mathcal{E}_{fn}$ is a key parameter controlling the physical and mechanical properties, and the resistance of cracking of sputtered $Ti(Al,V)N_x$ films, (2) The structure of $Ti(Al,V)N_x$ films varies from TiN(200) to TiN(220) with increasing energy $\mathcal{E}$, (3) The $Ti(Al,V)N_x$ films with high ratio $H/E^* \geq 0.1$, high elastic recovery $W_e \geq 60\%$ and dense voids-free microstructure exhibit an enhanced resistance to cracking and can be produced only in the case when a sufficient energy $\mathcal{E}$ is delivered to the growing film either by bombarding ions $\mathcal{E}_{bi}$ or by bombarding fast neutrals $\mathcal{E}_{fn}$ and (4) The energy $\mathcal{E}_{fn}$ makes it possible to sputter crystalline films on dielectric substrates held on a floating potential $U_s = U_{fl}$.

4.1. Introduction

It is well known that properties of thin films are determined by their elemental and phase composition (crystalline phase, an amorphous phase or a mixture of crystalline and amorphous phase), structure (size of grains and their crystallographic orientation), and microstructure (porous/columnar, dense/voids-free). Up to now, the properties of the thin film are controlled by different deposition parameters, such as the power P of the magnetron discharge, the film thickness h, the substrate temperature T_s, the substrate bias U_s, the substrate ion current density i_s, the flux of ions ν_i incident on the substrate, the deposition rate a_D of film, the substrate-to-target distance $d_{s\text{-}t}$, the total pressure $p_T = p_{Ar} + p_{RG}$ of sputtering gas mixture, the partial pressure of the argon p_{Ar} and the reactive gas p_{RG}, etc., used in its formation. There are a huge number of papers devoted to the investigation of the relationships between the deposition parameters of the film and its structure, microstructure, phase, and elemental composition, macrostress, physical and functional properties, for instance, see Ref. [1-23]. A set (combination) of many deposition parameters must be always selected in sputtering of the film. The problem in this approach is the fact that a correct combination of the deposition parameters necessary to form the film with prescribed properties is unknown. Different combinations of deposition parameters result in different energy $\mathcal{E}$ delivered to the growing film what is difficult to predict. It means that the main parameter which really controls the film properties is the energy $\mathcal{E}$ and thereby the correlations between the properties of the film and the energy $\mathcal{E}$ are of a key importance [24-39]. Therefore, an opposite approach in the development of new films should be used. At first, correlations between the film properties and the energy $\mathcal{E}$ should be found. Then, based on this knowledge the necessary deposition parameters which ensure the formation of the films with prescribed properties should be determined.

In the simplest case of a collision-less, fully ionized plasma the energy $\mathcal{E}_{bi}$ can be expressed in the following form [29, 39]

$$\mathcal{E}_{bi}\ [\mathrm{J/cm^3}] = (U_p - U_s) \times i_s/a_D \qquad \text{at } U_p > U_s \tag{4.1}$$

Here, U_p is the plasma potential, U_s is the substrate bias, i_s is the substrate ion current density and a_D is the deposition rate of film. Under the assumption that $|U_p| << |U_s|$, which is well fulfilled in many experiments, Eq. (4.1) can be simplified in the following simple form

$$\mathcal{E}_{bi}\ [J/cm^3] \approx |U_s| \times i_s/a_D \tag{4.2}$$

Eq. (4.2) clearly shows two important facts. The energy $\mathcal{E}_{bi}$ delivered to the growing film by bombarding ions (1) can be easily calculated from the measured deposition parameters (U_s, i_s) and the film deposition rate $a_D = h/t_d$ calculated from the measured film thickness h and the deposition time t_d and (2) strongly depends not only on U_s and i_s but also on a_D. The second fact is of an extraordinary importance in (i) the reactive sputtering of compounds and (ii) the high-rate sputtering of the film because the energy $\mathcal{E}_{bi}$ delivered to the growing film deceases with increasing a_D.

This article investigates the effect of the energy $\mathcal{E}$ delivered to the growing $Ti(Al,V)N_x$ film on its preferred crystallographic orientation (texture) of grains, microstructure, physical and mechanical properties, and resistance to cracking in detail. A great attention is devoted also to (i) the control of the structure and microstructure of film by the energy $\mathcal{E}$ delivered to the film during its growth in the DC and pulsed magnetron discharges, (ii) the energy $\mathcal{E}$ delivered to the film held at different substrate biases U_s and (iii) the energy $\mathcal{E}$ delivered to the film by fast neutrals.

4.2. Experimental

The $Ti(Al,V)N_x$ thin films were sputter deposited in a mixture of Ar + N_2 sputtering gases using a dual magnetron with closed magnetic field equipped with TiAlV (6 at.% Al, 4 at.% V) alloy targets of diameter $\varnothing$ = 50 mm. The targets were attached to the cathode bodies of the dual magnetron using pure Ti fixing rings. The magnetrons were supplied by an Advanced Energy Pinnacle Plus+ 5/5kW power supply operated either in DC or pulse mode. The magnetrons were tilted to the vertical axis at the angle 20°; for more details see Ref. [40]. The $Ti(Al,V)N_x$ films were deposited on Si(111) and Mo substrates at low power density $W_t = I_d \times U_d /S \leq 20\ W/cm^2$. The Si plates 20 × 20 × 0.52 mm^3 were used for the X-ray diffraction and the Si strips 30 x 5 x 0.64 mm^3 were used for the measurement of the film macrostress. The Mo substrates (80 × 15 × 0.20 mm^3) were used for the assessment of the film resistance to cracking in bending. A pre-deposition etching of the substrates was performed in the pulsed discharge (burning between the substrate and the shutter) at the voltage U_{et} = 400 V, current I_{et} = 0.5 A, repetition frequency f_{et} = 100 kHz, τ = 0.5, substrate temperature T_s = 500°C and substrate-to-target distance $d_{s\text{-}t}$ = 60 mm in argon at pressure p_{Ar} = 1 Pa for 5 min; the index "et" denotes the ion etching. A pre-deposition cleaning of the magnetron targets was performed in DC mode of sputtering with a closed target at the magnetron voltage U_d = 400 V and current I_d = 0.5 A, target power density W_d = 10 W/cm^2 in argon at pressure p_{Ar} = 1 Pa for 3 min. The film thickness h was measured by a stylus profilometer DEKTAK 8. The macrostress σ was evaluated from the bending of Si plate using the Stoney's formula [41]. The film structure was characterized using an XRD diffractometer PANalytical X Pert PRO in the Bragg-Brentano configuration with CuKα radiation. The elemental composition of the $Ti(Al,V)N_x$ films on the Si substrate was analyzed in a scanning electron microscope (SU-70, Hitachi) operated at a primary electron energy of 15 keV using energy dispersive spectroscopy (EDS, UltraDry, Thermo Scientific) and wave dispersive spectroscopy (WDS, Magnaray, Thermo Scientific). Pure metal standards were used for the determination of Ti, Al and V concentrations. The nitrogen concentration was calculated from a difference between the results obtained by the WDS and the EDS measurements using a ZrN standard. This approach was chosen due to the strong overlapping of titanium and nitrogen X-Ray peaks. Mechanical properties of sputtered films were determined from load vs. displacement curves measured by a microhardness tester Fisherscope H100 with Vickers diamond indenter at a load 20 mN. The resistance of the $Ti(Al,V)N_x$ films to cracking was determined using the indentation test at high loads L ranging from 0.25 to 1 N determining the critical load L_{cr} when cracks in the film occur and by the bending test. The Mo strip coated with the sputtered film was bent around a fixed cylinder of different radius r. By decreasing the radius r a strain induced in the film was increased. The critical strain ε_{cr} at which cracks in the film occur was measured. The critical strain ε_{cr} was calculated from the following formula [39]

$$\varepsilon_{cr} \approx h_{Mo}/2r \quad (4.3)$$

Here, h_{Mo} is the thickness of Mo strip.

4.3. Results and discussion

In this article presents the results of a detailed investigation of the effect of the energy $\mathcal{E} = \mathcal{E}_{bi} + \mathcal{E}_{fn}$ on the preferred crystallographic orientation, mechanical properties and resistance to cracking of sputtered films. The energy $\mathcal{E}_{bi}$ delivered into a growing film by bombarding ions in the simplest form of fully ionized collisionless plasma can be calculated from Eq. (4.2). All necessary quantities - the substrate bias U_s, the substrate ion current density i_s and the film deposition rate a_D - can be measured and the energy $\mathcal{E}_{bi}$ delivered to the sputtered films can be easily determined. However, the same value of the energy $\mathcal{E}_{bi}$ can be obtained either at high values of U_s and low values of i_s or at low values of U_s and high values of i_s and in both cases at the same value of a_D. Therefore, different combinations of U_s, i_s and a_D result in different growth and properties of the sputtered films. The energy $\mathcal{E}_{fn}$ delivered to the film by fast neutrals can be tuned by the total sputtering gas pressure p_T. The energy $\mathcal{E}_{fn}$ increases with decreasing p_T due to prolongation of the main-free path λ and reduction of $\mathcal{E}_{fn}$ in collisions. Therefore, a lower energy $\mathcal{E}_{fn}$ is delivered into the growing film at a higher pressure p_T compared with that delivered at a lower pressure p_T.

4.3.1 Energy delivered by bombarding ions

4.3.1.1 Energy $\mathcal{E}_{bi}$ controlled by the substrate bias U_s

The evolution of the structure and mechanical properties of the $Ti(Al,V)N_x$ film sputtered in DC magnetron discharge with increasing energy $\mathcal{E}_{bi}$, delivered to growing film by bombarding ions, and controlled by the substrate bias U_s are displayed in Figs. 4.1 and 4.2. From Fig. 4.1 it is seen that the preferred crystallographic orientation of the $Ti(Al,V)N_x$ films strongly depends on the value of the energy $\mathcal{E}_{bi}$. The $Ti(Al,V)N_x$ films with the dominant TiN(200) reflection are sputtered at low values of energy $\mathcal{E}_{bi} \leq 1.1$ MJ/cm^3. The intensity of the TiN(200) reflection decreases with increasing $\mathcal{E}_{bi}$. The dominant TiN(220) reflection occurs at $\mathcal{E}_{bi} = 1.6$ MJ/cm^3 and coexists with the TiN(200) reflection. The TiN(200) reflection is almost fully converted to TiN(111) and TiN(220) reflections approximately at $\mathcal{E}_{bi} = 2.4$ MJ/cm^3. The $Ti(Al,V)N_x$ films sputtered at higher energies $\mathcal{E}_{bi} \geq 2.4$ MJ/cm^3 are composed of TiN(220) and TiN(111) grains.

The stoichiometry x = N/(Ti+Al+V) of the $Ti(Al,V)N_x$ film increases with increasing energy $\mathcal{E}_{bi}$ from x = 1.04 at $\mathcal{E}_{bi} = 0.1$ MJ/cm^3 to x = 1.17 at $\mathcal{E}_{bi} = 4.8$ MJ/cm^3, see Fig. 4.1 and Table 4.1, where also its main physical and mechanical properties are given. From Table 1 it is seen that while the substrate ion current density i_s increases, the deposition rate a_D of the film decreases with increasing negative substrate bias U_s. It is the reason why the energy $\mathcal{E}_{bi}$ increases with increasing negative substrate bias U_s. The hardness H increases with increasing $\mathcal{E}_{bi}$ from 22 GPa at $\mathcal{E}_{bi} = 0.1$ MJ/cm^3 to 32 GPa at $\mathcal{E}_{bi} = 1.9$ MJ/cm^3 and then slightly decreases to 30 GPa at $\mathcal{E}_{bi} = 4.8$ MJ/cm^3. The effective Young's modulus E^* also increases with increasing $\mathcal{E}_{bi}$ from 262 GPa at $\mathcal{E}_{bi} = 0.1$ MJ/cm^3 to 275 GPa at $\mathcal{E}_{bi} = 1.9$ MJ/cm^3 but then, compared with the hardness H, more strongly decreases to 240 GPa at $\mathcal{E}_{bi} = 4.8$ MJ/cm^3. The $Ti(Al,V)N_x$ films sputtered at $\mathcal{E}_{bi} \geq 1.7$ MJ/cm^3 exhibit a high ratio $H/E^* > 0.1$ and a high elastic recovery $W_e > 70\%$ and thereby also an enhanced resistance to cracking; for more details see Refs. [42 - 50].

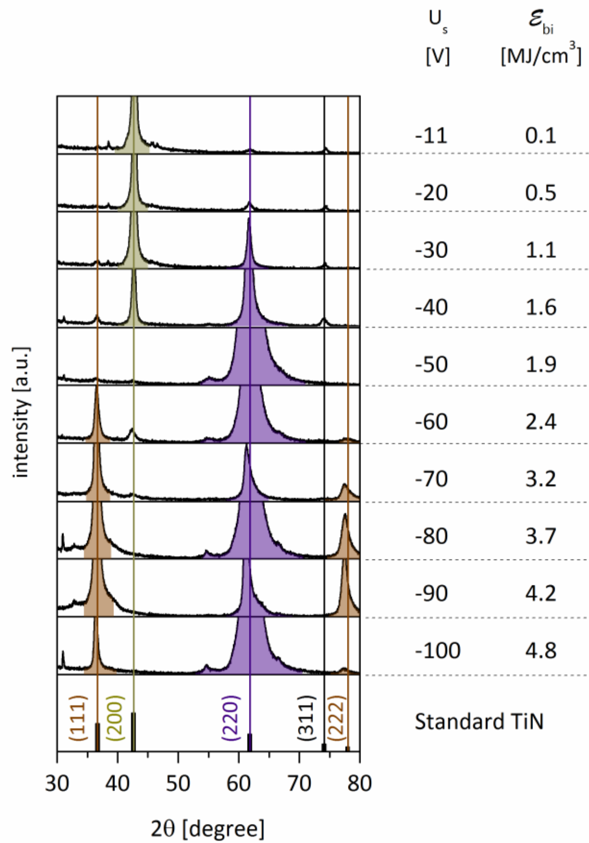

Figure 4.1 XRD patterns from Ti(Al,V)N_x films DC sputtered on Si(111) substrate at I_d = 0.5 A, $W_t \approx$ 10 W/cm², T_s = 500 °C, d_{s-t} = 60 mm, $p_T = p_{Ar} + p_{N2}$ = 0.2 + 0.8 = 1 Pa as a function $\mathcal{E}_{bi}$ as a function of negative substrate bias U_s.

The evolution of the mechanical properties of the Ti(Al,V)N_x film sputtered in DC magnetron discharge with increasing energy $\mathcal{E}_{bi}$ is displayed in Fig. 4.2 and Table 4.1, and the following issues can be drawn:

- The energy $\mathcal{E}_{bi}$ delivered to the growing film increases with increasing negative substrate bias U_s at constant values of (i) the low discharge current I_d = 0.5 A and (ii) the high partial pressure of nitrogen p_{N2} = 0.8 Pa.
- The Ti(Al,V)N_x films sputtered at low energies $\mathcal{E}_{bi} \leq$ 1.7 MJ/cm³ exhibit low ratio $H/E^* < 0.1$, low elastic recovery $W_e \leq 60\%$ and a strong TiN(200) texture. These films sputtered at low substrate biases $|U_s| \leq 50$ V are brittle and easily crack.
- The Ti(Al,V)N_x films sputtered at high substrate biases $|U_s| > 50$ V and therefore high energies $\mathcal{E}_{bi} >$ 1.7 MJ/cm³ exhibit high ratio $H/E^* \geq 0.1$, high elastic recovery $W_e > 60\%$ and no TiN(200) texture. These films exhibit an enhanced resistance to cracking.
- The Ti(Al,V)N_x films sputtered at the highest energies $\mathcal{E}_{bi} \geq$ 3.7 MJ/cm³ exhibit the highest resistance to cracking.
- The absence or small amount of the TiN(200) grains in Ti(Al,V)N_x film can be used as an indicator that the Ti(Al,V)N_x film with enhanced mechanical properties is formed.
- The compressive macrostress ($\sigma < 0$) generated in sputtered Ti(Al,V)N_x films strongly increases with increasing substrate bias U_s up to -5.5 GPa at U_s = -100 V.

The high compressive macrostress σ in the sputtered $Ti(Al,V)N_x$ film strongly decreases its adhesion to the substrate and very often the film delaminates from it. Therefore, it is needed to deliver in the growing film the energy $\mathcal{E}_{bi}$ necessary to form flexible hard films with enhanced resistance to cracking at lower negative substrate biases U_s.

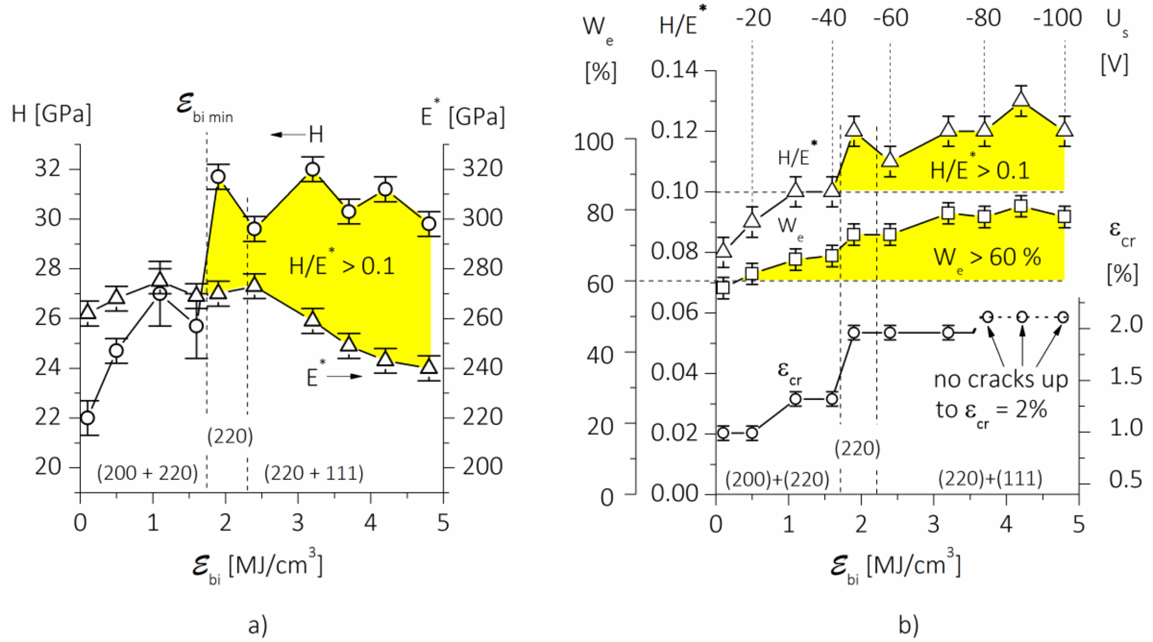

Figure 4.2 The evolution of (a) hardness H, effective Young's modulus E^* and TiN texture and (b) elastic recovery W_e, H/E^* ratio, critical strain ε_{cr} to failure and TiN texture of the sputtered $Ti(Al,V)N_x$ films as a function of the energy $\mathcal{E}_{bi}$ as a function of negative substrate bias U_s.

Table 4.1 Physical and mechanical properties of $Ti(Al,V)N_x$ films sputtered by DC dual magnetron at I_d = 0.5 A, $W_t = U_d \times I_d/S$ = 10 W/cm², T_s = 500 °C, d_{s-t} = 60 mm and $p_T = p_{Ar} + p_{N2}$ = 0.2 + 0.8 = 1 Pa on Si (111) controlled by the substrate bias U_s; here x = N/(Ti + Al +V) is the film stoichiometry and S is the area of the sputtered target.

											Cracks in	
											bending	indent.
U_s	i_s	$\mathcal{E}_{bi}$	x	h	a_D	H	E^*	W_e	H/E^*	σ	ε_{cr}	L_{cr}
[V]	[mA/cm²]	[MJ/cm³]		[nm]	[nm/min]	[GPa]	[GPa]	[%]		[GPa]	[%]	[N]
-11	0.24	0.1	1.04	2200	18.3	22	262	58	0.08	-0.4	1.0	0.25
-20	0.74	0.5	1.04	2000	16.7	25	268	62	0.09	-0.4	1.0	0.25
-30	0.93	1.1	0.99	1900	14.6	27	275	66	0.10	-1.0	1.3	0.25
-40	0.96	1.6	1.03	2000	14.3	26	269	67	0.10	-2.4	1.3	0.25
-50	0.91	1.9	1.07	1900	14.6	32	275	76	0.12	-3.1	2.0	> 1
-60	0.96	2.4	1.05	2000	14.3	30	273	73	0.11	-1.5	2.0	> 1
-70	1.01	3.2	1.11	1600	13.3	32	259	79	0.12	-2.9	2.0	> 1
-80	1.04	3.7	1.15	1600	13.3	30	249	78	0.12	-1.9	> 2.0	> 1
-90	1.07	4.2	1.10	1500	13.6	31	243	81	0.13	-4.0	> 2.0	> 1
-100	1.10	4.8	1.17	1400	13.7	30	240	78	0.12	-5.5	> 2.0	> 1

4.3.1.2 Energy $\mathcal{E}_{bi}$ controlled by the substrate ion current density i_s

In this section properties of the Ti(Al,V)N_x films sputtered at a low substrate bias U_s = -40 V in a DC and pulsed magnetron discharges are reported. The evolution of the structure and mechanical properties of the Ti(Al,V)N_x film with increasing energy $\mathcal{E}_{bi}$, delivered to the growing film by bombarding ions and controlled by the substrate ion current density i_s are displayed in Figs. 4.3 and 4.4, respectively. The substrate ion current density i_s extracted to the substrate from the DC magnetron discharge was increased by increasing the discharge current I_d, i.e. by intensification of the magnetron discharge, what results in the creation of a dense plasma. Higher values of the substrate ion current I_s at U_s = -40 V can be extracted from a dense plasma only. However, the increase of the current I_d also results in the increase of the film deposition rate a_D and thereby also in the simultaneous decrease of the energy $\mathcal{E}_{bi}$ delivered to the film during its growth by bombarding ions, see Table 4.2.

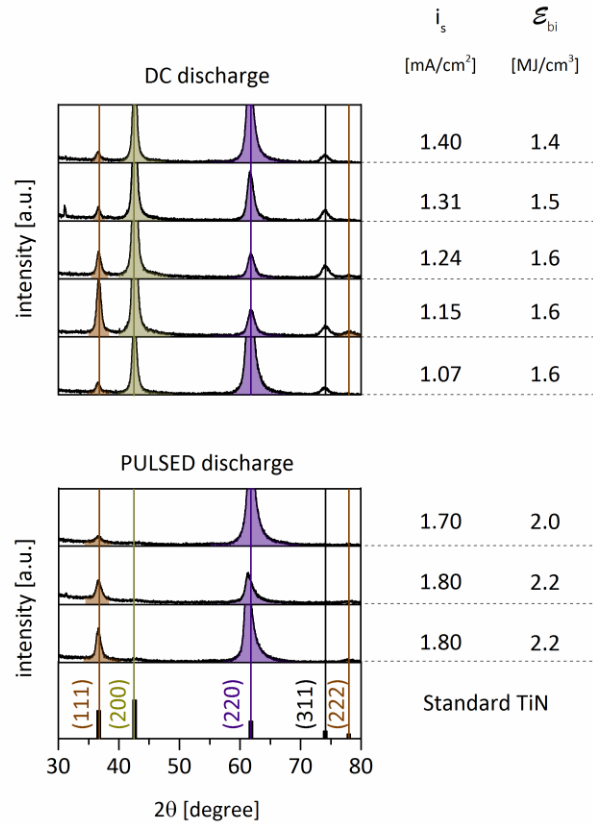

Figure 4.3 XRD patterns from Ti(Al,V)N_x films on the Si(111) substrate sputtered at T_s = 500 ℃, d_{s-t} =60 mm, p_T = 1 Pa, p_{N2} = 0.8 Pa using (i) DC deposition at $W_t \leq 16.5$ W/cm^2, U_s =-40V, (ii) pulse deposition at f_r = 100 kHz, τ = 0.5, W_t = 16.3 W/cm^2, U_s = -20V as a function E_{bi} controlled by substrate ion current density.

In order to increase the ion current density i_s the DC magnetron discharge was replaced by the pulsed bipolar dual magnetron discharge. A higher value of the ion current density i_s was extracted from denser plasma at low substrate biases $U_s \leq |20\ \text{V}|$. At low substrate biases $U_s \leq |20\ \text{V}|$ the plasma potential U_p increased to + 23 V due to the positive value of the magnetron voltage during the pulse-off time. The positive plasma potential of + 23 V and the negative substrate bias of – 20 V results in the sheath potential U_{sh} = |43 V|, from which the energy $\mathcal{E}_{bi}$ is calculated from

Eq. (4.1). From denser plasma higher ion currents I_s to the substrate were extracted and higher ion current density $i_s \geq 1.7$ mA/cm^2 were achieved. Therefore, the Ti(Al,V)N_x films deposited in the pulsed discharge generated by the pulsed bipolar dual magnetron exhibit high ratio $H/E^* \geq 0.12$, high elastic recovery $W_e \geq 73\%$ and are characterized by a strong TiN(220) texture, see Fig. 4.3. These films are slightly over-stoichiometric and its stoichiometry x = N/(Ti+Al+V) ranges from 1.00 to 1.09, see Table 4.2. The evolution of the mechanical properties of these films with increasing energy $\mathcal{E}_{bi}$ is displayed in Fig. 4.4.

From Figs. 4.3 and 4.4 and Table 4.2 the following issues can be drawn:

- The energy $\mathcal{E}_{bi}$ delivered to the growing film prepared in the DC magnetron discharge decreases with increasing discharge current I_d due to increasing of the film deposition rate a_D and decreasing the energy $\mathcal{E}_{bi}$. All films are formed at low energy $\mathcal{E}_{bi} < 1.7$ MJ/cm^3. They are polycrystalline, almost stoichiometric (x = N/(Ti+Al+V) ≈ 1) and exhibit strong TiN(200) texture and columnar microstructure which is responsible for a low resistance to cracking despite quite a high ratio $H/E^* \approx 0.1$ and high elastic recovery $W_e > 60\%$.
- All Ti(Al,V)N_x films prepared in the pulsed bipolar dual magnetron discharge are deposited at high ion current density $i_s \geq 1.7$ mA/cm^2. They are also polycrystalline and almost stoichiometric (x = N/(Ti+Al+V) ≈ 1) but exhibit no TiN(200) texture, high ratio $H/E^* \geq 0.12$, high elastic recovery $W_e > 60\%$, and no TiN(200) reflection. These films exhibit an enhanced resistance to cracking in the indentation test ($L_{cr} \geq 1$ N) but a lower resistance to cracking in the bending test.
- This experiment also confirms the conclusion already given in the section 4.3.1.1 that the polycrystalline Ti(Al,V)N_x films with the TiN(200) are brittle, i.e. they exhibit a low resistance to cracking, on the contrary, the films with TiN(220) texture are strong and tough and exhibit the enhanced resistance to cracking.
- The thick (1000 to 2000 nm) Ti(Al,V)N_x films sputtered at low negative substrate biases $|U_s| \leq 50$ V and energies $\mathcal{E}_{bi}$ ranging from 1.6 to 2.2 MJ/cm^3 exhibit low compressive macrostresses ($|\sigma| \leq 2$ GPa).

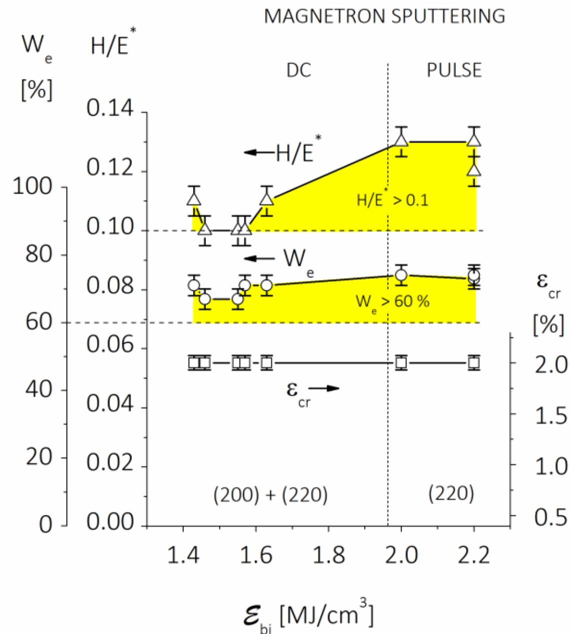

Figure 4.4 H/E^* ratio, elastic recovery W_e, and critical strain ε_{cr} in Ti(Al,V)N_x films reactively sputtered on Si(111) and Mo substrate in (i) the DC discharge at W_t ranging from 11.4 to 16.5 W/cm^2, U_s = -40V, and (ii) the pulsed bipolar dual magnetron discharge at W_t = 16.3 W/cm^2, U_s = -15 and -20 V, f_r = 100 kHz, and T_s =500 ℃, d_{s-t} =60 mm, $p_T = p_{Ar} + p_{N2}$ = 0.2 + 0.8 = 1 Pa as a function $\mathcal{E}_{bi}$ as a function substrate ion current density i_s.

Table 4.2 Physical and mechanical properties of Ti(Al,V)N_x films sputtered on the Si(111) and Mo substrates at d_{S-T} = 60 mm, T_s =500 °C, $p_T = p_{Ar} + p_{N2}$ = 0.2 + 0.8 = 1 Pa by (i) DC dual magnetron discharge at U_s = -40 V, U_p ≈ + 3 V, (ii) pulsed bipolar dual magnetron discharge at f_r = 100 kHz, τ = 0.5, I_{da} = 1.6V, U_p ≈ + 23 V. The substrate ion current density i_s was controlled by the discharge current I_d.

												Cracks in	
DC dual magnetron deposition												bending	indenataion
I_d	W_t	i_s	$\mathcal{E}_{bi}$	x	h	a_D	H	E^*	W_e	H/E^*	σ	ε_{cr}	L_{cr}
[A]	[W/cm²]	[mA/cm²]	[MJ/cm³]		[nm]	[nm/min]	[GPa]	[GPa]	[%]		[GPa]	[%]	[N]
0.55	11.4	1.07	1.6	1.03	1900	15.8	29.0	272	71	0.11	-1.8	2.0	0.25
0.60	12.6	1.15	1.6	1.09	2000	17.5	28.1	274	70	0.10	-1.4	2.0	0.25
0.65	13.8	1.24	1.6	1.02	2100	19.1	26.7	272	67	0.10	-1.3	2.0	0.25
0.70	15.2	1.31	1.5	1.05	2200	21.6	26.9	278	67	0.10	-1.4	2.0	0.25
0.75	16.5	1.40	1.4	1.05	2200	23.4	29.9	283	71	0.11	-1.8	2.0	0.25
Pulsed dual bipolar magnetron deposition													
U_s	W_t	i_s	$\mathcal{E}_{bi}$	x	h	a_D	H	E^*	W_e	H/E^*	σ	ε_{cr}	L_{cr}
[V]	[W/cm²]	[mA/cm²]	[MJ/cm³]		[nm]	[nm/min]	[GPa]	[GPa]	[%]		[GPa]	[%]	[N]
-15	16.3	1.7	2.0	1.09	1.0	20.0	24.0	190	74	0.13	-1.7	2.0	1
-20	16.3	1.8	2.2	1.03	1.3	21.7	24.3	194	73	0.13	-1.4	2.0	> 1
-20	16.3	1.8	2.2	1.00	2.5	21.7	28.5	235	74	0.12	-1.4	2.0	> 1

4.3.2 Energy $\mathcal{E}_{fn}$ delivered by fast neutrals and controlled by the total sputtering gas pressure p_T

The energy $\mathcal{E}$ delivered to the growing film can be delivered not only by bombarding ions ($\mathcal{E}_{bi}$) but also by bombarding fast neutrals ($\mathcal{E}_{fn}$) at low sputtering gas pressures $p_T = p_{Ar} + p_{N2} < 1$ Pa. This fact is demonstrated by sputtering of the Ti(Al,V)N_x films held at the floating potential ($U_s = U_{fl}$) as a function of the total sputtering gas pressure p_T. The Ti(Al,V)N_x films were sputtered by pulsed dual magnetron operated in a bipolar mode at the repetition frequency of pulses f_r = 200 kHz, τ = 0.5, I_{dp} = 1.2 A, U_{da} ≈ 220 V, $U_s = U_{fl}$, T_s= 500°C, d_{s-t} =60 mm, p_{N2}/p_T = 0.8. As the substrates are held at the floating potential $U_s = U_{fl}$ both the substrate ion current density i_s and the energy $\mathcal{E}_{bi}$ are very low, almost zero. It means that in this case the energy $\mathcal{E}$ is delivered to the growing film is delivered mainly by fast neutrals ($\mathcal{E}_{fn}$), i.e. $\mathcal{E} \approx \mathcal{E}_{fn}$. The energy of fast neutrals $\mathcal{E}_{fn}$ increases with decreasing p_T due to the prolongation of the mean free path λ between particles and therefore a reduction of collisions between atoms. It means that a lower energy $\mathcal{E}_{fn}$ is delivered to the growing film at higher pressures p_T compared with $\mathcal{E}_{fn}$ delivered to it at lower pressures p_T. The evolution of the structure of the Ti(Al,V)N_x films sputtered under these conditions is displayed in Fig. 4.5. These films are crystalline and slightly over-stoichiometric (x = N/(Ti + Al + V) ≈ from 1.06 to 1.25. Physical and mechanical properties of sputtered Ti(Al,V)N_x films are summarized in Table 4.3.

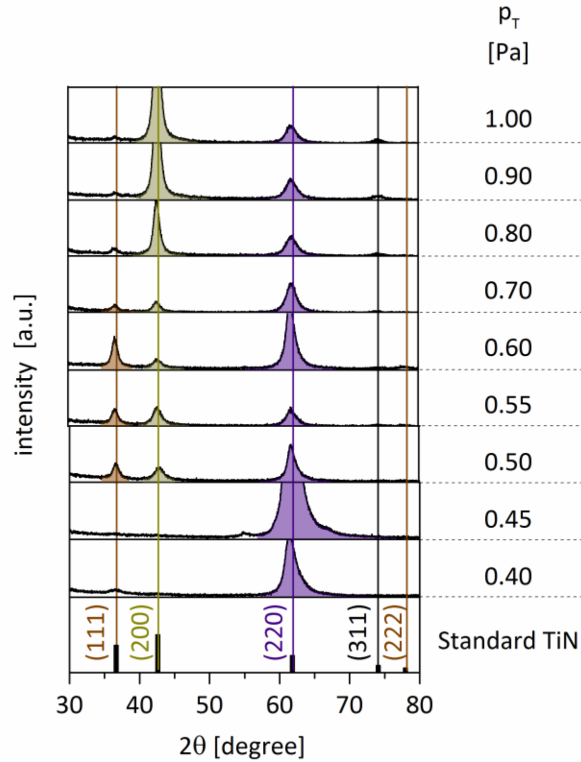

Figure 4.5 Evolution of XRD patterns from Ti(Al,V)N_x film sputtered by pulsed bipolar dual magnetron on Si(111) substrate at f_r = 200 kHz, I_d = 1.2 A, W_t ≈ 13 W/cm², U_s = U_{fl}, T_s = 500 °C, $d_{s\text{-}t}$ = 60 mm with decreasing total sputtering gas pressure p_T.

Table 4.3 Physical and mechanical properties of Ti(Al,V)N_x films sputtered by pulsed bipolar dual magnetron at f_r = 200 kHz, I_d = 1.2 A, W_t = 13 W/cm², U_s = U_{fl}, T_s = 500 °C, $d_{s\text{-}t}$ = 60 mm, p_{N2} = 0.8 Pa on Si(111) and Mo substrate controlled by the magnetron sputtering gas pressure $p_T = p_{Ar} + p_{N2}$; $W_t = U_d \times I_d/S$; S is the area of sputtered target and x = N/(Ti + Al +V) is the film stoichiometry.

									Cracks in	
									bending	indentation
p_T	h	x	a_D	H	E^*	W_e	H/E^*	σ	ε_{cr}	L_{cr}
[Pa]	[nm]		[nm/min]	[GPa]	[GPa]	[%]		[GPa]	[%]	[N]
0.40	800		6.7	21.8	173	75	0.13	-2.0	> 2.0	0.5*
0.45	1100	1.23	7.3	31.0	225	82	0.14	-2.2	2.0	0.5*
0.50	1300	1.24	8.3	25.5	209	76	0.12	-1.7	2.0	> 1
0.55	1400	1.25	8.7	25.4	214	75	0.12	-1.9	2.0	> 1
0.60	1800	1.17	12.0	27.6	238	75	0.12	-1.4	2.0	> 1
0.70	1600	1.11	11.4	24.9	245	70	0.10	-1.3	1.3	> 1
0.80	2000	1.06	15.3	18.1	179	63	0.10	-0.7	1.0	0.25
0.90	1800	1.10	15.0	23.2	237	68	0.10	-0.6	1.0	0.25
1.00	1900	1.10	15.8	23.8	240	68	0.10	-0.6	1.3	0.25

* The indentation load L_{cr} is low due to delamination of the film from the substrate not due to the film cracking

This experiment demonstrate the indirect but clear effect of the energy $\mathcal{E}_{fn}$ on the physical and mechanical properties of Ti(Al,V)N_x films sputtered at low (0.4 Pa) and high (1 Pa) total sputtering gas pressure p_T and partial pressure of nitrogen p_{N2} = 0.8 p_T on substrate held at floating potential (U_s = U_{fl}). From Fig. 4.5 and Table 4.3 the following issues can be drawn:

- The structure of Ti(Al,V)N_x films varies from the dominant TiN(200) to the dominant TiN(220) texture with decreasing total sputtering gas pressure p_T. It is indirect evidence that the energy $\mathcal{E}_{fn}$ increases with decreasing p_T as expected.
- The ratio H/E^*, elastic recovery W_e and compressive macrostress ($\sigma < 0$) increase with decreasing p_T. Also, these facts indicate that the energy $\mathcal{E}_{fn}$ increases with decreasing p_T.
- The Ti(Al,V)N_x films are over-stoichiometric (x = [N/(Ti+Al+V)] $\geq$ 1) films and their stoichiometry x increases with decreasing p_T probably due to the domination of nitrogen N absorption on the film surface over its resputtering from the film surface when the film deposition rate a_D decreases with decreasing p_T.
- The microstructure of the Ti(Al,V)N_x films converts from columnar to dense, voids-free non-columnar microstructure with decreasing p_T, see Fig. 4.6.
- The resistance of Ti(Al,V)N_x films against cracking improves with decreasing p_T, see Table 4.3.
- All these findings show that the energy $\mathcal{E}_{fn}$ can fully substitute the energy $\mathcal{E}_{bi}$ in the formation of flexible hard coatings. This fact opens a new way to form flexible hard nanocrystalline films on electrically insulating substrates.

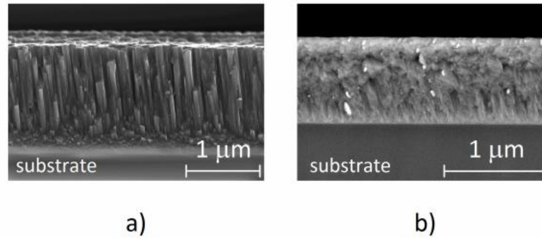

Figure 4.6 SEM images of the microstructure of Ti(Al,V)N_x film sputtered by pulsed bipolar dual magnetron on Si(111) substrate at f_r = 200 kHz, I_d = 1.2 A, $W_t \approx$ 13 W/cm^2, U_s = U_{fl}, T_s = 500 °C, d_{s-t} = 60 mm, p_{N2} = 0.8 Pa and (a) p_T = 1 Pa and (b) p_T = 0.4 Pa.

In summary, it can be concluded that the microstructure of the films deposited on the substrate held at the floating potential U_s = U_{fl} can be densified by the bombardment the fast neutrals when the film is sputtered at low values of the sputtering gas pressures $p_T < 0.7$ Pa. Moreover, it is possible to sputter defect-free electrically insulating films because there is no accumulation of a charge on the surface of the growing film. These are the main advantages of the sputtering of the films held at the floating potential U_s = U_{fl} at low sputtering gas pressures ($p_T < 0.7$ Pa).

4.3.3 Interrelationships between energies $\mathcal{E}_{bi}$ and $\mathcal{E}_{fn}$, preferred crystallographic orientation and resistance to cracking of Ti(Al,V)N_x films

Main results of our investigation are summarized in Fig. 4.7. This figure clearly illustrates main interrelationships between the $\mathcal{E}_{bi}$ controlled by ion bombardment (U_s, i_s) and the energy of fast neutrals $\mathcal{E}_{fn}$ controlled by the total pressure of sputtering gas p_T, the preferred orientation and the resistance to cracking of the Ti(Al,V)N_x film. The low and enhanced resistance to cracking is characterized by the diamond indenter load L_{cr} at which the tested film cracks, see Fig. 4.8. In Fig. 4.8 the morphology of two Ti(Al,V)N films after loading by the diamond indenter at the same high

load L = 1 N are compared: (a) the brittle hard Ti(Al,V)N film with low H/E^* = 0.9, low W_e = 58% sputtered at low energy $\mathcal{E}_{bi}$ = 0.5 MJ/cm^3 and (b) the flexible hard Ti(Al,V)N film with high H/E^* = 0.12, high W_e =78% sputtered at high energy $\mathcal{E}_{bi}$ = 4.8 MJ/cm^3. This figure clearly shows that while the brittle hard film sputtered at low energy cracks, the flexible hard film exhibit no cracks under the same load L = 1N.

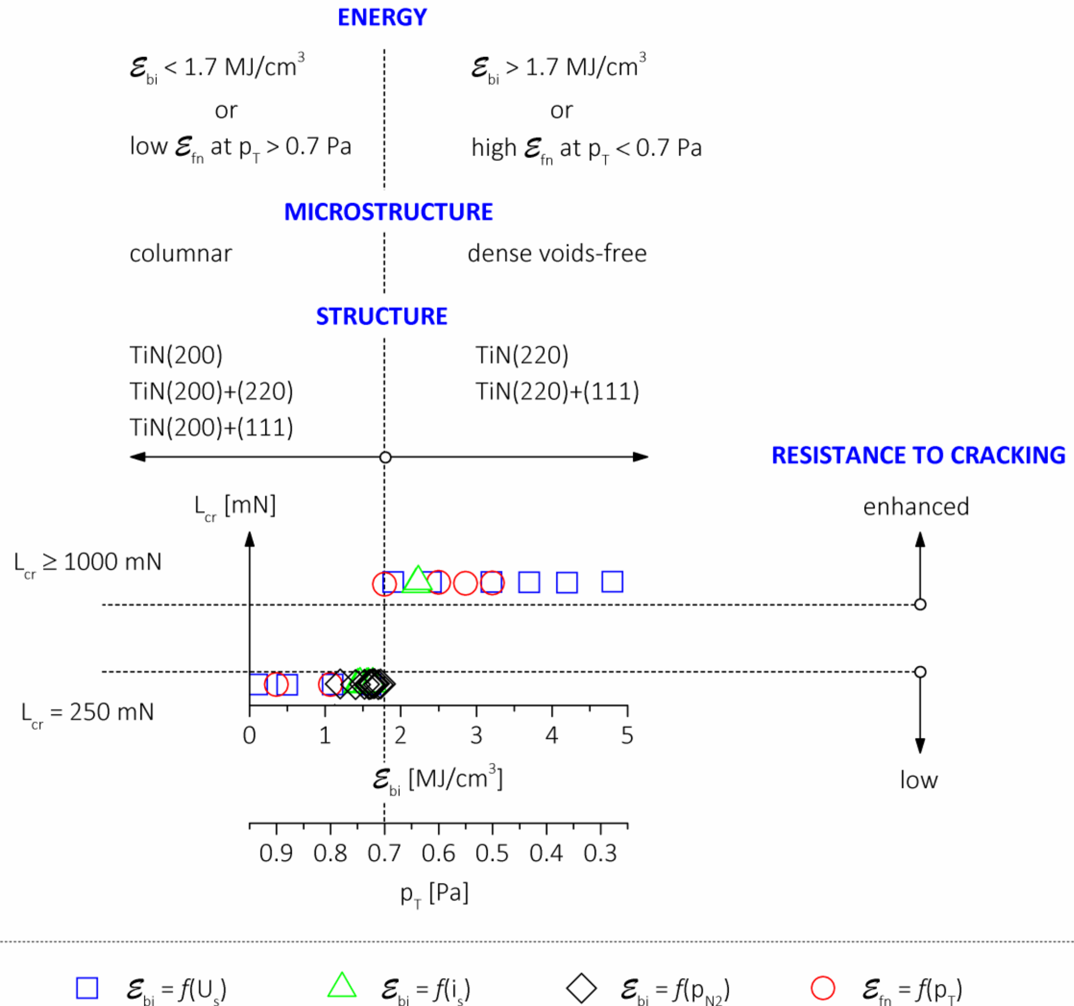

Figure 4.7 Schematic illustration of interrelationships between the energy $\mathcal{E}_{bi}$ and $\mathcal{E}_{fn}$, and the structure, microstructure and resistance to cracking of the Ti(Al,V)N_x film.

Three main issues following from Fig. 4.7 are:

- The Ti(Al,V)N_x films sputtered at low energies $\mathcal{E}_{bi}$ < 1.7 MJ/cm^3 or under low bombardment by fast neutrals $\mathcal{E}_{fn}$ at high sputtering gas pressures p_T > 0.7 Pa containing TiN(200) grains exhibit columnar microstructure and low resistance to cracking.
- The Ti(Al,V)N_x films sputtered at high energies $\mathcal{E}_{bi}$ ≥ 1.7 MJ/cm^3 or under high bombardment by fast neutrals $\mathcal{E}_{fn}$ at low sputtering gas pressures p_T ≤ 0.7 Pa containing no or low amount of TiN(200) grains exhibit dense, voids-free non-columnar microstructure and enhanced resistance to cracking.
- The energy $\mathcal{E}_{bi}$ delivered to the growing film can be fully substituted by the energy of fast neutrals $\mathcal{E}_{fn}$ in the formation of the film with the same properties.

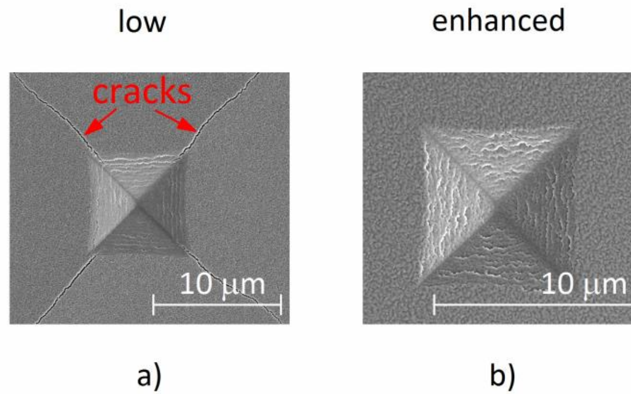

Figure 4.8. Comparison of the surface morphology of (a) brittle hard Ti(Al,V)N_x films sputtered at low energy $\mathcal{E}_{bi}$ = 0.5 MJ/cm^3 exhibit stoichiometry x = 1.04 and (b) flexible hard Ti(Al,V)N_x film sputtered at high energy $\mathcal{E}_{bi}$ = 4.8 MJ/cm^3 exhibit stoichiometry x = 1.17.

4.4. Conclusions

The article reports on a detailed investigation of the interrelationships between the energy $\mathcal{E}_{bi}$ and $\mathcal{E}_{fn}$ delivered to the Ti(Al,V)N_x film by bombarding ions and fast neutrals, respectively, and its structure, microstructure, mechanical properties, and resistance to cracking. Main issues of this study can be summarized as follows:

- The texture of Ti(Al,V)N_x film varies from TiN(200) to TiN(220) with increasing energy $\mathcal{E}_{bi}$ or $\mathcal{E}_{fn}$.
- The Ti(Al,V)N_x films sputtered at low energies $\mathcal{E}_{bi} < 1.7$ MJ/cm^3 and high sputtering gas pressures $p_T > 0.7$ Pa are characterized by the TiN(200) reflection and low resistance to cracking. On the other hand, the Ti(Al,V)N_x films sputtered at high energies $\mathcal{E}_{bi} \geq 1.7$ MJ/cm^3 and low pressures $p_T < 0.7$ Pa exhibit no TiN(200) reflection but an enhanced resistance to cracking. It indicates that the absence of the TiN (200) reflection in XRD pattern can be used as an indicator that the Ti(Al,V)N_x film with enhanced resistance to cracking is formed.
- The Ti(Al,V)N_x film with high ratio $H/E^* \geq 0.1$, high elastic recovery $W_e \geq 60\%$, dense, voids-free non-columnar microstructure and compressive macrostress ($\sigma < 0$) exhibit an enhanced resistance to cracking.
- In sputtering of the Ti(Al,V)N_x film with enhanced resistance to cracking the energy $\mathcal{E}_{bi}$ can be fully substituted by the energy $\mathcal{E}_{fn}$. This finding is of a general validity. Moreover, the use of the energy $\mathcal{E}_{fn}$ in the deposition of films makes it possible to sputter nanocrystalline and crystalline films on electrically insulating substrates without their heating and arcing on their surfaces.
- The energy $\mathcal{E}$ is a key parameter controlling the physical and mechanical properties of sputtered films including their resistance to cracking and enabling their production in a reproducible way.

Acknowledgments

This work was supported by the project LO1506 of the Czech Ministry of Education, Youth and Sports under the program NPU I.

References

[1] F.Lapostolle, A.Billard, J. von Stebut: Structure/mechanical properties relationship of titanium-oxygen coatings reactively sputter – deposited, Surf. Coat. Technol. 135 (2000), 1-7.

[2] L.Karlsson, L.Hultman, M.P.Johansson, J.-E.Sundgren, H.Ljungcrantz: Growth, microstructure, and mechanical properties of arc evaporated TiC1-xN1-x (0 ≤ x ≤ 1) films, Surf. Coat. Technol. 126 (2000), 1-14.

[3] J.Ding, Y.Meng, S.Wen: Mechanical properties and fracture toughness of multilayer hard coatings using nanoindentation, Thin Solid Films 371 (2000), 178-182.

[4] W.J.Meng, R.C.Tittsworth, L.E.Rehn: Mechanical properties and microstructure of TiC/amorphous hydrocarbon nanocomposite coatings, Thin Solid Films 377-376 (2000), 222-232.

[5] M.Oden, J.Almer, G.Hakansson, M.Olsson: Microstructure-property relationships in arc-evaporated Cr-N coatings, Thin Solid Films 377-376 (2000), 407-412.

[6] J.Patscheider, T.Zehnder, M.Diserens: Structure-performance relations in nanocomposite coatings, Surf. Coat. Technol. 146 (2001), 201 – 208.

[7] T.Mae, M.Nose, M.Zhou, T.Nagae, K.Shimamura: The effect of Si addition on the structure and mechanical properties of ZrN thin films deposited by an rf reactive sputtering method, Surf. Coat. Technol. 142-144 (2001), 954-958.

[8] S.Carvalho, L.Rebouta, A.Cavaleiro, L.A.Rocha, J.Comes, E.Alves: Microstructure and mechanical properties of nanocomposite (Ti,Si,Al)N coatings, Thin Solid Films 398-399 (2001), 391-396.

[9] J.Almer, M.Oden, G.Hakansson: Microstructure, stress and mechanical properties of arc-evaporated Cr-C-N coatings, Thin Solid Films 385 (2001), 190-197.

[10] J.Musil, H.Zeman, F.Kunc, H.Poláková: Relationships between hardness, Young´s modulus and elastic recovery in hard nanocomposite coatings, Surf. Coat.Technol. 154(2002), 304-313.

[11] J.Musil, H.Zeman, J.Kasl: Relationship between structure and mechanical properties in hard Al-Si-Cu-N films prepared by magnetron sputtering, Thin Solid Films 413 (2002), 121-130.

[12] H.Watanabe, Y.Sato, C.Nie, A.Ando, S.Ohtani, N.Iwamoto: The mechanical properties and microstructure of Ti-Si-N nanocomposite films by ion plating, Surf. Coat. Technol. 169-170 (2003), 452-455.

[13] H.S.Barshilia, A.Jain, K.S.Rajam: Structure, hardness and thermal stability of nanolayered TiN/CrN multilayer coatings, Vacuum 72 (2003), 241-248.

[14] P.Jedrzejowski, J.E.Klemberg-Sapieha, L.Martinu: Relationship between the mechanical properties and the microstructure of nanocomposite TiN/SiN1.3 coatings prepared by low temperature PECVD, Thin Solid Films 426 (2003), 150-159.

[15] Y.T.Pei, D.Galvan, J.Th.M. De Hosson: Nanostructure and properties of TiC/a-C:H composite coatings, Acta Materialia 53 (2005), 4505-4521.

[16] J.Soldán, J.Musil: Structure and mechanical properties of DC magnetron sputtered TiC/Cu films, Vacuum 81 (2006), 531-538.

[17] J.Lin, B.Mishra, J.J.Moore, W.D.Sproul: Microstructure, mechanical and tribological properties of Cr1-xAlxN films deposited by pulsed-closed field unbalanced magnetron sputtering (P-CFUBMS), Surf. Coat. Technol. 201 (2006), 4329-4334.

[18] M.Audronis, A,Leyland, P.J.Kelly, A.Matthews: The effect of pulsed magnetron sputtering on the structure and mechanical properties of CrB2 coatings, Surf. Coat. Technol. 201 (2006), 3970-3976.

[19] C.H.Lai, M.H.Tsai, S.J.Lin, J.W.Yeh: Influence of substrate temperature and mechanical properties of multi-element (AlCrTaTiZr)N coatings, Surf. Coat. Technol. 201 (2007), 6993-6998.

[20] A.Pelisson, M.Parlinska-Wojtan, H.J.Hug, J.Patscheider: Microstructure and mechanical properties of Al-Si-N transparent hard coatings deposited by magnetron sputtering, Surf. Coat. Technol. 202 (2007), 884-889.

[21] J.Soldán, J.Neidhardt, B.Satory, R.Kaindl, R.Cerstvy, P.H.Mayrhofer, R.Tessadri, P.Polcik, M.Lechthaler, C.Mitterer: Structure-property relations of arc-evaporated Al-Cr-Si-N coatings, Surf. Coat. Technol. 202 (2008), 3555-3562.

[22] K.Polychronopoulou, C.Rebholtz, M.a.Baker, L.Theodorou, N.G.Demas, S.J.Hinder, A.A.Polycarpou, C.C.Doumanidis, K.Bobel: Nanostructure, mechanical and tribological properties of reactive magnetron sputtered TiCx coatings, Diamond and Related Materials 17 (2008), 2054-2061.

[23] J.H.Huang, Z.E.Tsai, G.P.Yu: Mechanical properties and corrosion resistance of nanocrystalline ZrNxOy coatings on AlSL 304 stainless steel by ion plating, Surf. Coat. Technol. 202 (2008), 4992-5000.

[24] J.Musil: Sputtering systems with enhanced ionization for ion plating of hard wear resistant coatings, Proc. of the 1st Meeting on the Ion Engineering Society of Japan (IESJ-92), Tokyo, Japan, 1992, pp. 295-304.

[25] H.Poláková, J.Musil, J.Vlček, J.Alaart, C.Mitterer: Structure- hardness relations in sputtered Ti-Al-V-N films, Thin Solid Films 444 (2003), 189-198.

[26] J.Musil, H.Poláková, J.Šůna, J.Vlček: Effect of ion bombardment on properties of hard reactively sputtered single-phase films, Surf.Coat.Technol. 177-178 (2004), 289-298.

[27] J.Musil, J.Šůna: The role of energy in formation of sputtered nanocomposite films, Materials Science Forum 502 (2005), 291-296.

[28] J.Musil, J.Šícha, D.Heřman, R.Čerstvý: Role of energy in low-temperature high-rate formation of hydrophilic TiO2 thin films using pulsed magnetron sputtering, J. Vac. Sci. Technol. A 25(4) (2007), 666-674.

[29] J.Musil: Flexible hard nanocomposite coatings, RSC Advances 5 (2015), 60482-60495.

[30] J.Musil, J.Vlček, P.Baroch: Magnetron discharges for thin films plasma processing, Chapter 3 in „Materials Surface Processing by Directed Energy Techniques, Y.Pauleau (Ed.), 2006, Elsevier Science Publisher B.V., Oxford, UK, pp. 67-106.

[31] J.A.Thornton: (i) Recent developments in sputtering – Magnetron sputtering, Metal Finishing 77(5) (1979), 83-87 and (ii) High rate thick films growth, Ann. Rev. Mater. Sci. 7 (1977), 239-260.

[32] J.Musil: Physical and mechanical properties of hard nanocomposite films prepared by reactive magnetron sputtering, Chapter 10 in Nanostructured Coatings, J.T.M. DeHosson and A. Cavaleiro (Eds.) New York, Springer Science + Business Media, LCC, 2006, pp. 407-463.

[33] J.Musil, V.Poulek, V.Valvoda, R.Kužel Jr., H.A.Jehn, M.E.Baumgartner: Relation of deposition conditions of Ti-N films prepared by dc magnetron sputtering to their microstructure and macrostress, Surf.Coat.Technol. 60 (1993), 484-488.

[34] B.A.Movchan, A.V.Demchishin: Study of the structure and properties of thick vacuum condensates of nickel, titanium, tungsten, aluminum oxide and zirconium oxide, Phys. Met. Metallogr. 28 (1969), 83-90.

[35] P.Pokorný, J.Musil, P.Fitl, M.Novotný, J.Lančok, J.Bulíř: Contamination of magnetron sputtered metallic films by oxygen from residual atmosphere in deposition chamber, Plasma Processes and Polymers 12 (2015), 416-421.

[36] J.Musil: Low-pressure magnetron sputtering, Vacuum 50(3-4) (1998), 363-372.

[37] J.Musil: Hard and superhard nanocomposite coatings, Surf.Coat.Technol. 125 (2000), 322-330.

[38] J.Musil: Hard nanocomposite coatings: Thermal stability, oxidation resistance and toughness, Surf.Coat.Technol. 207 (2012), 50-65.

[39] J.Musil: Advanced hard nanocomposite coatings with enhanced toughness and resistance to cracking, Chapter 7 in Thin Films and Coatings: Toughening and Toughening Characterization, S.Zhang (Editor) CRC Press, USA, 2015, pp. 377-463.

[40] J.Musil, P.Baroch: Discharge in dual magnetron sputtering system, IEEE Transactions on Plasma Science 33(20 (2005), 338-339.

[41] G.G.Stoney: The transition of metallic films deposited by electrolysis, Proc. R. Soc. London, Ser. A82 (1909), 172-175.

[42] J. Musil, J. Sklenka, R. Čerstvý: Transparent Zr-Al-O oxide coatings with enhanced resistance to cracking, Surf. Coat. Technol. 206 (2012), 2105-2109.

[43] J. Musil, R. Jílek, M. Meissner, T. Tolg, R. Čerstvý: Two-phase single layer Al-O-N nanocomposite films with enhanced resistance to cracking, Surf.Coat.Technol. 206 (2012), 4230-4234.

[44] J. Musil, R. Jílek, R. Čerstvý: Flexible Ti-Ni-N thin films prepared by magnetron sputtering, J. Mater. Sci. Technol. A 4(2) (2014), 27-33.

[45] J. Musil, J. Blažek, K. Fajfrlík, R. Čerstvý: Flexible antibacterial Al-Cu-N films, Surf. Coat. Technol. 264, (2015) 114-120.

[46] J. Musil, M. Zítek, K. Fajfrlík, R. Čerstvý: Flexible antibacterial Zr-Cu-N thin films resistant to cracking, J. Vac Sci. Technol. A 34 (2016), 021508-1 to -7.

[47] J. Musil, J. Sklenka, R. Čerstvý: Protection of brittle film against cracking, Appl. Surf. Sci. 370, 306 (2016), 306-311.

[48] J. Musil, S. Zenkin, S. Kos, R. Čerstvý, S. Haviar: Flexible hydrophobic ZrN nitride films, Vacuum (2016), 131 (2016), 34-38.

[49] J. Musil, D. Javdošňák, R. Čerstvý, S. Haviar, G. Remnev, V. Uglov: Effect of energy on formation of flexible Al-Si-N films prepared by magnetron sputtering, Vacuum 133 (2016), 43-45.

[50] J. Musil, G. Remnev, L. Legostaev, V. Uglov, A. Lebedynskiy, A. Lauk, J. Procházka, S. Haviar. E. Smolyanskiy: Flexible hard Al-Si-N films for high temperature operation, Surf. Coat. Technol., 307 (2016), 1112-1118.

Paper III

5. PLASMA AND FLOATING POTENTIALS IN MAGNETRON DISCHARGES

J. Musil, **M. Jaroš**
J. Vac. Sci. Technol. A. 35 (2017) 060605

Abstract

This letter reports on great differences in values of the plasma U_p and floating U_{fl} potentials in sputtering discharges generated by single and dual magnetrons. It is shown that (i) the differences of U_p and U_{fl} result in strongly different properties of films sputtered by single and dual magnetrons at the same power delivered to the magnetron discharge, (ii) in the DC single and dual magnetron discharges the values of U_p and U_{fl} strongly depend on the electric conductivity of the surface of the grounded deposition chamber, and (iii) the Pulsed dual magnetron with closed magnetic B field is only one sputtering system which enables to sputter the films with fully reproducible properties.

5.1. Introduction

It is well known that the energy $\mathcal{E}_{bi}$ delivered into the sputtered film by bombarding ions decides on its physical and mechanical properties such as its structure, microstructure, hardness H, effective Young's modulus E^*, elastic recovery W_e, ratio H/E^*, macrostress σ, etc. In the simplest case of 100% ionized and collisionless discharge, the energy $\mathcal{E}_{bi}$ is determined by the following formula [1, 2]

$$\mathcal{E}_{bi}\ [\mathrm{J/cm^3}] = (U_p - U_s) \times i_s/a_D \qquad \text{at } U_p > U_s \qquad (5.1)$$

Here, U_p is the plasma potential, U_s is the substrate bias, i_s is the substrate ion current density and a_D is the deposition rate of the film. Eq. (5.1) shows that the effect of U_p on $\mathcal{E}_{bi}$ can be very small in the case when $|U_p| << |U_s|$ but, on the contrary, U_p can strongly influence $\mathcal{E}_{bi}$ in the case when $|U_p| \approx |U_s|$. The plasma potential U_p strongly depends on the deposition parameters used in the magnetron sputtering, the mode (type) of the magnetron operation (the direct current (DC), pulsed, high-power pulsed magnetron (HPPMS) sputtering) [3 - 9], the geometrical arrangement of the sputtering device [10], the target power density $W_t = U_d \times I_d/S$ [11], the sputtering gas pressure p [6, 11], and the state of the surface of the deposition chamber (electrically conductive, semiconducting, electrically insulating); here U_d and I_d is the voltage and current of the magnetron discharge, and S is the area of the sputtered target. These facts are the main reason why the properties of films sputtered under the same deposition conditions can strongly differ and in many cases cannot be formed in a reproducible way. No investigation of this problem was performed so far. Up to now, main attention was concentrated mainly on the measurement of the degree of ionization of sputtering gas, electron and ion energy distribution functions (EEDFs and IEDFs) [12] and species generated in the magnetron discharges in reactive sputtering and in the presence of different kinds of the inert and reactive sputtering gases and their mixtures.

This article shows great differences in the values of the plasma potential U_p and the floating potential U_{fl} in the magnetron discharge generated by (i) the DC single and DC dual magnetron and (ii) the Pulsed dual magnetron operating at the same deposition conditions. Besides, it is shown that the electric conductivity of the surface of walls of the deposition chamber strongly influences U_p and U_{fl} in a reactive magnetron sputtering of films. The way how these changes of U_p and U_{fl} can be fully eliminated is shown.

5.2. Experimental details

The plasma potential U_p and the floating potential U_{fl} in the magnetron discharge was measured in a cylindrical deposition chamber (the diameter $\varnothing$ = 600 mm, the height h = 600 mm) equipped successively with three sputtering systems: (1) DC single magnetron, (2) DC dual magnetron and (3) Pulsed dual magnetron, see Fig. 5.1. All magnetrons

were the same and were equipped with Ti (6Al 4V) alloy targets made of a VT6 titanium alloy containing 6 at.% Al and 4 at.% V. Both DC and Pulsed dual magnetron systems have a closed magnetic field B between magnetrons, see Figs. 1b and 1c. The sputtering discharges were generated at the same power $P_{DC} = P_{1\,DC} + P_{2\,DC} = P_{1\,p} + P_{2\,p} = 500$ W and the same sputtering gas pressure $p = p_{Ar} + p_{N2} = 0.2 + 0.8 = 1$ Pa; here indexes 1DC and 2DC, and 1p and 2p denote the powers delivered to the magnetron 1 and 2 by two DC power supplies (Advanced Energy Pinnacle Plus+ 5/5 kW operated in a DC mode), and by a Pulsed the pulsed power supply (Advanced Energy Pinnacle Plus+ 5/5 kW operated in bipolar mode with asynchronous pulses), respectively, see Fig. 5.2, p_{Ar} and p_{N2} are partial pressures of argon and nitrogen, respectively. More details on the discharge of the dual magnetron with closed and open (mirror) magnetic field B are given in Ref. [13].

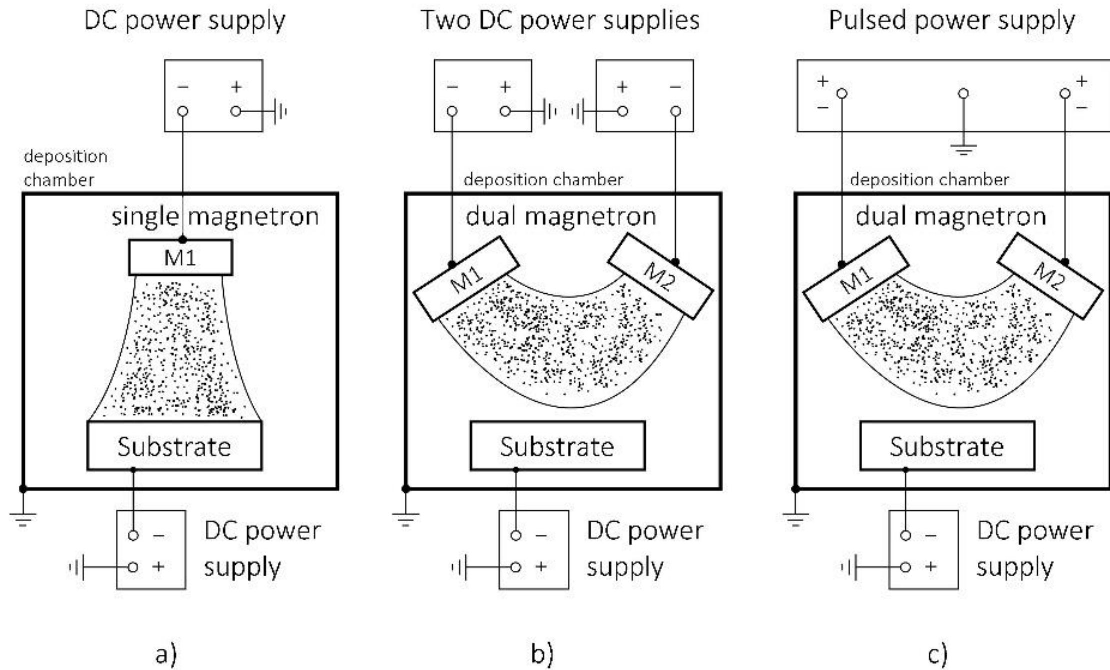

Figure 5.1 Schematic illustration of the discharge generated by (a) DC single magnetron, (b) DC dual magnetron and (c) Pulsed dual magnetron and the electrical connection of power supplies.

The voltage on the magnetron 1 and the magnetron 2 in the DC dual magnetron system and in the pulsed dual magnetron system is shown in Fig. 5.2. Fig. 5.2b shows that during the pulse-off time the magnetron voltage is slightly positive. It enables to remove the positive charge accumulated on the target when electrically insulating films are sputtered, to avoid arcing on the target surface and to form defect-free films [14]. The Ti(Al,V)N films were reactively sputtered on 15330 steel substrates placed at the substrate temperature $T_s = 500°C$, the substrate-to-target distance $d_{s-t} = 60$ mm and the total sputtering gas pressure $p_T = p_{Ar} + p_{N2} = 0.2$ Pa $+ 0.8$ Pa $= 1$ Pa; here p_{Ar} and p_{N2} is the partial pressure of argon and nitrogen, respectively. All measurements of the plasma potential U_p and the floating potential U_{fl} were carried out in the discharge generated at an unheated substrate. The change of the electrical conductivity of the surface of the deposition chamber from electrically conductive to non-conductive (electrically insulating) was carried out by a pulsed reactive sputtering of TiO_2 films from the Ti(Al,V) targets of the dual magnetron at the total pressure $p_T = p_{Ar} + p_{O2} = 0.5 + 0.5 = 1$ Pa and the pulsed averaged power $P_{da} = 1000$ W.

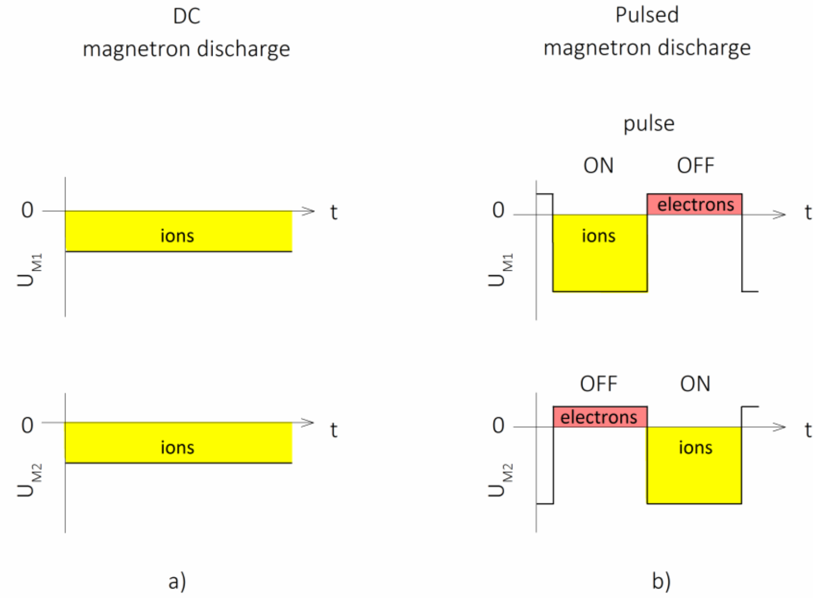

Figure 5.2 Schematic illustration of the voltage on the magnetron 1 and the magnetron 2 at (a) the DC dual magnetron and (b) the Pulsed bipolar dual magnetron operated with asynchronous pulses.

5.3. Results and discussion

In this section two problems were investigated in detail: (1) Differences in the plasma potential U_p and the floating potential U_{fl} in the DC and pulsed magnetron discharges and (2) The elimination of the effect of the electrical conductivity of the surface of the deposition chamber on properties of sputtered films and the finding of the magnetron sputtering system which enables to sputter films with fully reproducible properties.

The plasma potential U_p and the floating potential U_{fl} were determined from Volt-Ampere (V-A) characteristics measured at the substrate. Our experiments show that the V-A characteristics at the substrate measured in the discharge generated by the DC single magnetron (Fig. 5.1a) and by the DC dual magnetron (Fig. 5.1b) are identical. Therefore, the V-A characteristics measured at the substrate immersed in the DC dual magnetron discharge and in the Pulsed bipolar dual magnetron discharge are compared only, see Fig. 5.3.

Fig. 5.3 shows strong differences in the values of U_p and U_s in the DC and Pulsed bipolar dual magnetron discharges generated at the same power P = 500 W. Main results of this experiment are the following:

- The single magnetrons (Fig. 5.1a) and the dual magnetrons with the closed magnetic field (Fig. 5.1b) powered by the DC power have always the ground outside the magnetron discharge, i.e. outside the chamber walls. On the contrary, the pulsed dual magnetrons with closed magnetic field operated with asynchronous pulses (Fig. 5.1c) have the ground inside the magnetron discharge.
- In discharges of the DC single and DC dual magnetrons, the floating potential U_{fl} is negative. Therefore, the films sputtered in discharges generated by the DC single and dual magnetrons can be bombarded by electrons also at negative substrate biases $|U_s| < |U_{fl}|$. On the contrary, the films sputtered in discharges generated by the pulsed dual magnetrons with closed B field can be bombarded by ions also at positive substrate biases if $U_{fl} \geq U_s \geq 0$. It is the main reason why properties of the films sputtered under the same deposition conditions on the grounded substrate by the DC and Pulsed dual magnetrons strongly differ, see and Fig. 5.3 and Table 5.1.

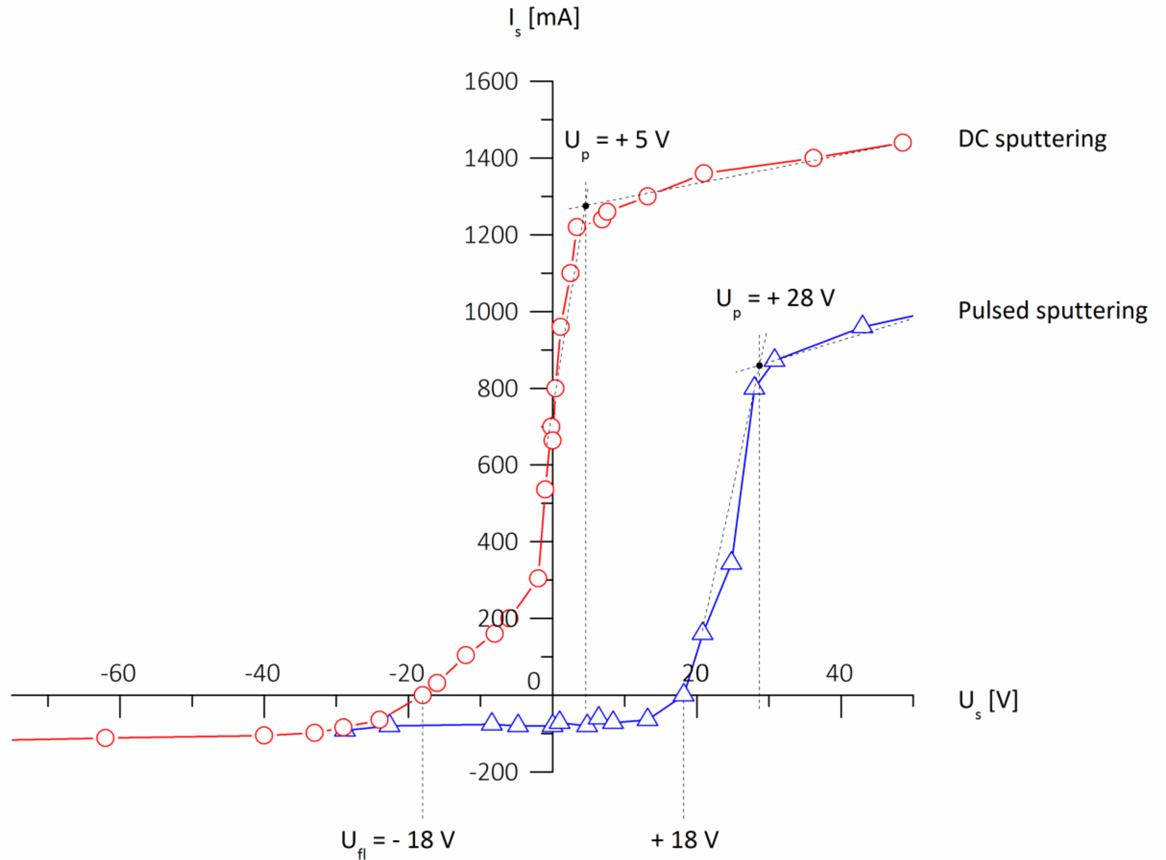

Figure 5.3 V-A characteristics measured on the substrate immersed in the dual magnetron discharge powered by (a) DC power $P_{1\,DC} = P_{2\,DC} = 250$ W and (b) Pulsed power with asynchronous pulses with $P_{1p} = P_{2p} = 500$ W, repetition frequency $f_r = 1/T = 100$ kHz and duty cycle $\tau/T = 0.5$; here indexes 1 DC and 2 DC and 1p and 2p denote the powers delivered to the magnetron 1 and 2 by the two DC power supplies and the Pulsed power supply, respectively.

Fig. 5.4 displays XRD patterns from the Ti(Al,V)N films reactively sputtered on the grounded substrate ($U_s = 0$ V) by the DC and Pulsed bipolar dual magnetron at the same deposition conditions: $W_{t\,DC} = 12.8$ W/cm^2, $W_{tp} = 25.6$ W/cm^2, $T_s = 500°$C, $d_{s\text{-}t} = 60$ mm and $p_T = p_{Ar} + p_{N2} = 0.2 + 0.8 = 1$ Pa; here $W_{t\,DC}$ and $W_{t\,p}$ is the target power density of one magnetron in the DC dual magnetron and in the Pulsed bipolar dual magnetron, respectively. The structures of both films strongly differ. While the DC sputtered film is polycrystalline, the pulsed sputtered exhibit a strong TiN (111) structure. These strong changes of the film structure result also in strong differences of the mechanical properties of the films sputtered by the DC and Pulsed dual magnetron, respectively, see Table 5.1. The film deposited by DC dual magnetron sputtering exhibits lower values of the hardness H, the elastic recovery W_e and the low ratio $H/E^* \leq 0.1$ compared with those of the film deposited by Pulsed dual magnetron sputtering. Moreover, the pulsed sputtered film exhibits an enhanced resistance to cracking due to the high ratio $H/E^* = 0.1$ [2, 15]. This experiment clearly shows how important it is to know the floating U_{fl} and plasma U_p potential on the substrate and inside magnetron discharge, respectively, during deposition of the film.

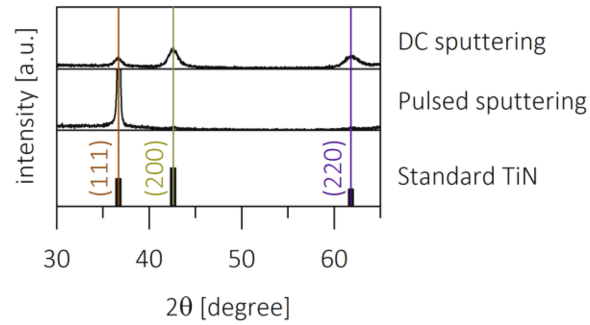

Figure 5.4 XRD patterns of the Ti(Al,V)N films sputtered on the grounded substrate (U_s = 0 V) by DC and Pulsed dual magnetron powered at the same deposition conditions: $W_{t\,DC} \approx W_{tp}$ = 12.8 W/cm², T_s = 500 ℃, $d_{s\text{-}t}$ = 60 mm and $p_T = p_{Ar} + p_{N2}$ = 0.2 + 0.8 = 1 Pa.

Table 5.1 Deposition conditions, energy $\mathcal{E}$ delivered in growing Ti(Al,V)N films sputtered on the grounded substrate (U_s = 0) by DC and Pulsed bipolar dual magnetron at the same deposition conditions: $W_{t\,DC} \approx W_{tp}$ = 12.8 W/cm², T_s = 500 ℃, $d_{s\text{-}t}$ = 60 mm and $p_T = p_{Ar} + p_{N2}$ = 0.2 + 0.8 = 1 Pa, and mechanical properties of sputtered films.

Sputtering	U_s [V]	I_s	i_s [mA/cm²]	$\mathcal{E}_{bi}$ [MJ/cm³]	$\mathcal{E}_{el}$ [MJ/cm³]	h [nm]	a_D [nm/min]	H [GPa]	E^* [GPa]	W_e [%]	H/E^*	σ [GPa]
DC	0	electrons	10.60	--	3.4	1700	18.9	16.1	195	58	0.08	0.3
Pulsed	0	ions	1.12	1	--	1400	15.6	23.5	224	67	0.10	-1.2

5.3.1 Elimination of the effect of chamber walls on properties of sputtered films

The place of the ground of the electrical connection of power supplies used for the generation of the magnetron discharge – outside discharge (the chamber walls) or inside discharge (the sputtered target of magnetron) – strongly influences V-A characteristics on the substrate, see Fig. 5.5. When the ground is outside discharge the V-A characteristics depend on the electrical conductivity of the chamber walls, see Fig. 5.5a. The negative floating potential U_{fl} on the substrate increases with decreasing electrical conductivity of the chamber walls. These changes of U_{fl} are caused by the walls contamination by (i) the oxygen and nitrogen during opening of the deposition chamber to the air for the de-loading of coated parts (samples) and its loading by non-coated ones and particularly (ii) the condensing of different reactive species created during the reactive magnetron sputtering of films. The contamination of the surface of the grounded deposition chamber is the main reason why the sputtering of the films with fully reproducible properties is a very serious problem.

This problem can be fully avoided in the case when the ground is inside the magnetron discharge, see Fig. 5.5b. In this case, the V-A characteristics do not depend on the electric conductivity of the surface of the chamber walls. It means that the Pulsed sputtering by the dual magnetron with closed B field is the best sputtering system enabling deposition of films with fully reproducible properties.

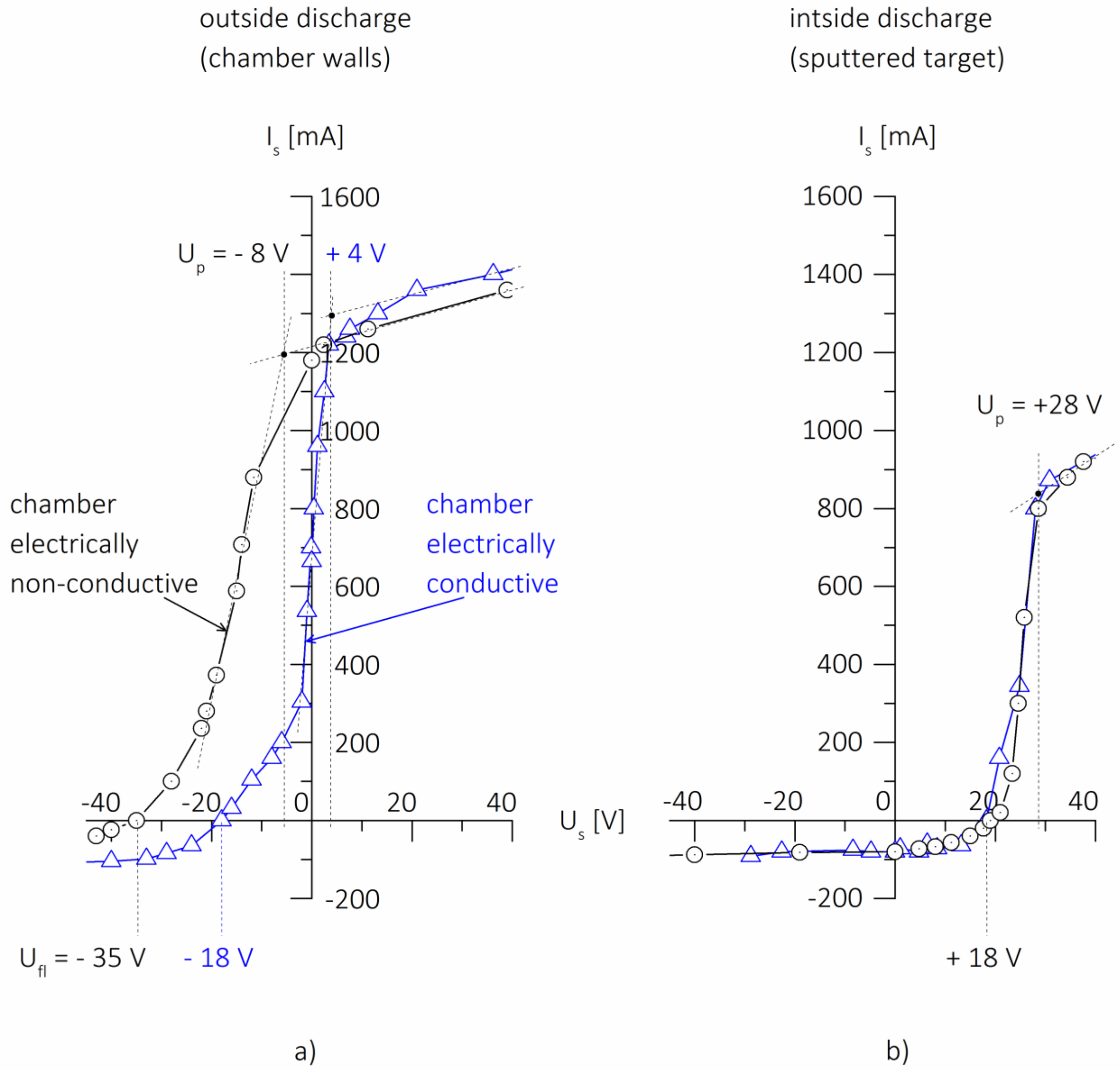

Figure 5.5 V-A characteristics measured on the substrate immersed in the dual magnetron discharge powered by (a) DC power and (b) Pulsed power with asynchronous pulses in the deposition chamber whose walls are electrically conductive (triangles) and non-conductive (circles).

5.4. Conclusions

Results of the reported investigation are very important for both the deepening of the present state of knowledge in the field of reactive magnetron sputtering of thin films and the design of new advanced sputtering systems which enable to sputter the films with fully reproducible properties. Main results can be summarized as follows:

1. Properties of the films sputtered by the single and dual magnetrons at the same power *P* delivered to the magnetron discharge and other constant deposition conditions (U_s, T_s, $d_{s\text{-}t}$, p) differ due to different values of the plasma potential U_p and the floating potential U_{fl} what results in a different energy $\mathcal{E}_{bi} = (U_p - U_s) \times i_s/a_D$ delivered to the growing film by bombarding ions
2. The values of U_p and U_s strongly depend on the electrical connection of the power supply the magnetron. For the single and DC dual magnetron, the ground is outside discharge. In contrast, for the Pulsed dual magnetron with a closed magnetic field, the ground is inside the discharge.
3. The properties of the films sputtered on the grounded substrate by the single and DC dual magnetrons at the same power P and other constant deposition conditions strongly differ from those sputtered by the pulsed dual magnetrons with the closed magnetic field. It is due to the fact that while in the single and DC dual magnetron discharge electrons flow on the grounded substrate, in the pulsed dual magnetron with the closed magnetic field on the contrary ions flow on the grounded substrate. It results in a great difference in the energy $\mathcal{E}$ delivered to the growing film.
4. In discharges of the single magnetrons and the DC dual magnetrons powered by two grounded power supplies the values of U_p and U_s depend on the state of the surface of the chamber walls (electrically conductive or non-conductive) and the formation of reactively sputtered films is very difficult. On the other hand, in pulsed discharges of the dual magnetrons with a closed magnetic field in which the ground is inserted inside the discharge the values of U_p and U_{fl} do not depend on the state of deposition chamber walls. It means that the Pulsed dual magnetron ensures a long-term reactive sputtering of the films with fully reproducible properties without any effect of varying contamination of the deposition chamber walls.

Acknowledgment

This work was supported by the project LO1506 of the Czech Ministry of Education, Youth and Sports under the program NPU I. The authors thank to R. Čerstvý for the XRD patterns of the Ti(Al,V)N films.

References

[1] J. Musil, J. Šícha, D. Heřman and R. Čerstvý: Role of energy in low-temperature high-rate formation of hydrophilic TiO2 thin films using pulsed magnetron sputtering, J. Vac. Sci. Technol. A 25(4) (2007) 666-674/

[2] J. Musil: Hard nanocomposite coatings: Thermal stability, oxidation resistance and toughness, Surf. Coat. Technol. 207 (2012), 50-65.

[3] J. W. Bradley, H. Bäcker, P. J. Kelly and R. D. Arnell: Time-resolved Langmuir probe measurements at the substrate position in a pulsed mid-frequency DC magnetron plasma, Surf. Coat. Technol. 135 (2001) 221-228.

[4] C. Muratore, J. J. Moore and J. A. Rees: Electrostatic quadrupole plasma mass spectrometer and Langmuir probe measurements of mid-frequency pulsed DC magnetron discharges, Surf. Coat. Technol. 163 (2003) 12-18

[5] H. Bäcker, P. S. Henderson, J. W. Bradley and P. J. Kelly: Time-resolved investigation of plasma parameters during deposition of Ti and TiO_2 thin films, Surf. Coat. Technol. 174 (2003) 909-913.

[6] J. Vlček, A. D. Pajdarová and J. Musil: Pulsed dc Magnetron Discharges and their Utilization on Plasma Surface Engieneering, Contrib. Plasma Phys. 44 (2004) 426-436.

[7] F. Richter, Th. Welyel, Th. Dunger and H. Kupfer: Time-resolved characterization of pulsed magnetron discharges using Langmuir probes, Surf. Coat. Technol. 188 (2004) 384-391.

[8] A. Mishra, P. J. Kelly and J. W. Bradley: The evolution of the plasma potential in a HiPIMS discharge and its relationship to deposition rate, Plasma Sources Sci. Technol. 19 (2010) 045014.

[9] B. B. Sahu, J. G. Han, J. B. Kim, M. Kumar, S. Jin and M. Hori: Study of Plasma Properties for the Low-Temperature Deposition of Highly Conductive Aluminum Doped ZnO Film Using ICP Assisted DC Magnetron Sputtering, Plasma Process and Polymers 13 (2016) 134-146.

[10] J. W. Bradley, H. Bäcker, P. J. Kelly and R. D. Arnell: Space and time resolved Langmuir probe measurements in a 100 kHz pulsed rectangular magnetron system, Surf. Coat. Technol. 142 (2001) 337-341.

[11] L. Sirghi, T. Aoki and Y. Hatanaka: Diagnostics of the radio frequency magnetron discharge plasma used for TiO2 thin sputtering deposition, Surf. Coat. Technol. 187 (2004) 358-363.

[12] A. D. Pajdarová, J. Vlček, P. Kudláček and J. Lukáš: Electron energy distributions and plasma parameters in high-power pulsed magnetron sputtering discharges, Plasma Sources Science and Technology, 18 (2009) 025008.

[13] J. Musil and P. Baroch: Discharge in dual magnetron sputtering system, IEEE Trans. Plasma Sci., 2005, 33(2) (2005) 338-339.

[14] W. D. Sproul, D. J. Christie and D.C. Carter: Control of reactive sputtering processes, Thin Solid Films 491 (2005) 1-17.

[15] J. Musil: Flexible hard nanocomposite coatings, RSC Advances 5 (2015) 60482-60495.

Paper IV

6. Effect of energy on macrostress in Ti(Al,V)N films prepared by magnetron sputtering

M. Jaroš, J. Musil, R. Čerstvý, S. Haviar
Vacuum 158 (2018) 52-59

Abstract

The article reports on the effect of the energy $\mathcal{E}$ delivered into the growing film on its macrostress, microstructure, mechanical properties and resistance to cracking of Ti(Al,V)N films. The Ti(Al,V)N films were deposited on Si(111) and Mo substrates by magnetron sputtering in a mixture Ar+N_2 gases using a dual magnetron with closed magnetic field and equipped with TiAlV (6 at.% Al, 4 at.% V) alloy targets. It is shown that the compressive macrostress σ in sputtered films can be reduced either by the pulsed bipolar bias voltage U_{sp} with alternating negative and positive pulses or the electron and ion bombardment during overshoots in the pulsed magnetron sputtering. All sputtered films with high ratio $H/E^* \geq 0.1$, compressive macrostress ($\sigma < 0$), and non-columnar microstructure exhibit an enhanced resistance to cracking; here H is the hardness and E^* is the effective Young's modulus. The high compressive macrostress in the film is not the necessary condition for the formation of the films with an enhanced resistance to cracking.

6.1. Introduction

There is a huge number of papers devoted to the investigation of relationships between the deposition parameters of the film and its structure [1-12], microstructure [8-26], phase and elemental composition [2-5, 15-20], macrostress [4-9, 18-25], physical and functional properties [1-31]. Despite these facts, it is very difficult to sputter in different deposition chambers with different magnetrons, and different power supplies (DC, pulsed) the films with reproducible properties. It is due to the fact that different combinations of deposition parameters, different magnetrons (single, dual, etc.) and different arrangement of substrate holders (stationary, rotating) result in different energies $\mathcal{E}$ delivered into the growing film. It means that the main parameter controlling the properties of the film is the energy $\mathcal{E}$ [32-42]. Therefore, the knowledge of correlations between the energy $\mathcal{E}$ and the film properties is very important.

In the deposition of films using an ion plating process, i.e. in the case when the substrate on which the film is deposited is held on a negative substrate bias U_s, the most important is the energy $\mathcal{E}_{bi}$ delivered to the film during its growth by bombarded ions. In the simplest case of a collision-less, fully ionized plasma the energy $\mathcal{E}_{bi}$ can be expressed in the following form [42]

$$\mathcal{E}_{bi}\ [\mathrm{J/cm^3}] = |U_p - U_s| \times i_s/a_D \quad (6.1)$$

Here, U_p is the plasma potential, U_s is the substrate bias, i_s is the substrate ion current density and a_D is the deposition rate of the film. Under the assumption that $|U_p| << |U_s|$, which is well fulfilled in many experiments, Eq. (6.1) can be simplified in the following simple form

$$\mathcal{E}_{bi}\ [\mathrm{J/cm^3}] \approx |U_s| \times i_s/a_D \quad (6.2)$$

Eq. (6.2) shows that the energy $\mathcal{E}_{bi}$ delivered to the growing film by bombarding ions can be easily calculated from measured deposition parameters (U_s, i_s) and the film deposition rate $a_D = h/t_d$ calculated from the measured film thickness h and the deposition time t_d.

Recently, it was demonstrated that the Ti(Al,V)N films with enhanced resistance to cracking are created at high energies $\mathcal{E}_{bi} > 1.7$ MJ/cm^3 [43]. However, the intensive ion bombardment generates high compressive stresses (up to - 3 GPa to - 5 GPa) in sputtered films [44]. Such films easily delaminate from the substrate and crack. Therefore, it is necessary to decrease the compressive macrostress σ but simultaneously to deliver to the film sufficiently high

energy $\mathcal{E}_{bi}$ necessary to sputter the film with dense, non-columnar microstructure exhibiting no delamination from the substrate and an enhanced resistance to cracking.

The solution of this quite difficult task is the subject of this article. It is shown that the films with an enhanced resistance to cracking and a low compressive macrostress $|\sigma| \leq 1$ GPa can be formed in the case when σ generated in the sputtered film is relaxed by bombardment of electrons during its growth. Two methods are described in detail: (1) the DC sputtering with pulsed bipolar bias with alternating negative and positive pulses and (2) the pulsed sputtering with electron bombardment of the film during overshoots at the end of each pulse. Both methods efficiently reduce the compressive macrosrostress ($\sigma < 0$) in sputtered films. It was demonstrated in sputtering of the Ti(Al,V)N nitride films.

6.2. Experimental

The Ti(Al,V)N nitride films were reactively sputter deposited on Si(111) and Mo substrates at substrate temperature T_s = 500°C and substrate-to-target distance $d_{s\text{-}t}$ = 60 mm by a dual magnetron with closed magnetic field equipped with TiAlV (6 at.% Al, 4 at.% V) alloy targets of diameter ∅ = 50 mm in a mixture of Ar + N2 sputtering gases. The magnetrons were tilted at angle 20° to the vertical axis [45] and supplied by an Advanced Energy Pinnacle Plus+ 5/5kW power supply operated either in the DC or pulse mode. The Ti(Al,V)N films deposited by a dual magnetron powered by DC power were sputtered at I_d = 1 A results in $W_t = I_d U_d / S \approx 16$ W/cm^2, and the substrate held either at constant negative bias U_s or at pulsed bipolar positive/negative bias. The Ti(Al,V)N films deposited by a dual magnetron powered by pulsed power were sputtered at the repetition frequency of pulses f_r ranging from 100 kHz to 350 kHz, τ/T = 0.5 and I_d ranging from 1.6 to 2 A resulting in the target power density $W_t = I_{dp} U_{dp} / S < 16$ W/cm^2 and the substrate bias held at the floating potential U_{fl} or at the constant negative bias; here I_{dp} and U_{dp} is the discharge current and voltage during pulse-on time, respectively, and S is the total area of the sputtered target. All Ti(Al,V)N_x films were sputtered in the nitrogen-rich atmosphere at p_{N2}/p_T = 0.8. The films sputtered under these conditions were almost stoichiometric (x = N/(Ti+Al+V) ≈ 1) and their stoichiometry x varied in a very narrow range from 0.98 to 1.09 only. The Si plates (20 x 20 x 0.64 mm^3) were used for of X-ray diffraction patterns and the Si strips (30 x 5 x 0.64 mm^3) were used for the measurement of the macrostress σ in the sputtered films. The Mo substrates (80 x 15 x 0.20 mm^3) coated by sputtered films were used for the assessment of the film resistance to cracking in bending. A pre-deposition etching of substrates was performed in the pulsed discharge (generated between the substrate and the shutter) at the voltage U = 400 V, current I = 0.5 A, repetition frequency f_r = 100 kHz, τ/T = 0.5, substrate temperature T_s = 500°C and shutter-to-target distance $d_{s\text{-}t}$ = 60 mm in argon at pressure p_{Ar} = 1 Pa for 5 min. A pre-deposition cleaning of the magnetron targets was performed in DC mode of sputtering at the magnetron voltage U_d = 400 V and current I_d = 0.5 A, target power density $W_t \approx 10$ W/cm^2 in argon at pressure p_{Ar} = 1 Pa for 3 min.

The film thickness h was measured by a stylus profilometer DEKTAK 8. The macrostress σ was evaluated from the bending of Si plate using the Stoney's formula [46]. The film structure was characterized by X-ray diffraction using an XRD diffractometer PANalytical X Pert PRO in the Bragg-Brentano configuration with CuKα radiation. The elemental composition of the Ti(Al,V)N films deposited on Si substrates was analyzed by a scanning electron microscope (SU-70, Hitachi) operated at a primary electron energy of 15 keV using both the energy dispersive spectroscopy (EDS, UltraDry, Thermo Scientific) and the wave dispersive spectroscopy (WDS, Magnaray, Thermo Scientific). Pure metal standards for the determination of Ti, Al and V concentrations in the film were used. The nitrogen concentration was calculated as the difference to 100 wt. %. The Ti(Al,V)$N_{x\approx1}$ films exhibit stochiometry x = N/(Ti+Al+V) ranging from 0.98 to 1.09. Mechanical properties of sputtered films were determined from load vs. displacement curves measured by a microhardness tester Fisherscope H100 with Vickers diamond indenter at a load of 20 mN. The resistance of the

Ti(Al,V)N films to cracking was determined by (i) the indentation test at high loads L_{cr} (critical load when cracks occur) ranging from 0.25 to 1 N and (ii) the bending test; more details are given in [42, 47, 48]. The Mo strip coated with the sputtered film was bent around a fixed cylinder of different radius r. The strain induced in the film by bending was increased by decreasing of the radius r of fixed cylinder. The critical strain ε_{cr} at which cracks in the film occur was measured. The critical strain ε_{cr} was calculated from the following formula [42]

$$\varepsilon_{cr} \approx h_{Mo}/2r \qquad (6.3)$$

Here, h_{Mo} is the thickness of the Mo strip.

6.3. Results and discussion

In this section, two ways of sputtering of the low-stress Ti(Al,V)N films with enhanced resistance to cracking are described in detail. Both methods of a reduction of the macrostress σ in sputtered films are based on an electron heating of the film material during its growth controlled by the energy $\mathcal{E}_{bi}$ delivered into the growing film by bombarding ions. This section consists of three subsections: (1) The macrostress reduction controlled by pulsed bipolar substrate bias U_{sp}, (2) The macrostress reduction controlled by overshoots in pulsed sputtering and (3) Correlations between the energy $\mathcal{E}_{bi}$, the macrostress σ in film, its microstructure, and resistance to cracking.

6.3.1. Macrostress reduction by pulsed bipolar substrate bias U_{ps}

The principle of a reduction of the macrostress σ in the sputtered film at a pulsed substrate bias U_{sp} is based on alternating of the ion and the electron bombardment of the film during its growth, see Fig. 6.1. The alternating ion and electron bombardment of the growing film is realized by alternating negative and positive pulses. The microstructure of growing film is densified during the negative pulse of the substrate bias U_{sp} by ion bombardment. Simultaneously, the compressive macrostress ($\sigma < 0$) is generated in the film and its magnitude increases with increasing voltage of the negative pulse. On the other hand, the macrostress σ, generated in the film during the ion bombardment, is relaxed by the electron current which thermally anneals the growing film during the positive pulse of the pulsed substrate bias U_{sp}. It means that the films sputtered at DC substrate bias $U_{s\ DC}$ will always exhibit a higher compressive macrostress ($\sigma < 0$) compared with the films sputtered at a pulsed bipolar substrate bias U_{sp}.

The relaxing of the compressive macrostress ($\sigma < 0$) in the sputtered film by the electron bombardment was confirmed by sputtering of the Ti(Al,V)N films under the same deposition conditions at DC and pulsed bipolar bias. Results of this experiment are summarized in Table 6.1. From Table 6.1 the following important issues can be drawn

1. The film sputter deposited at DC negative bias U_s, i.e. at the ion bombardment of the growing film only, exhibits the high compressive macrostress (σ = - 4 GPa) compared with the film sputter deposited at the pulsed bias U_{sp} with alternating negative and positive pulses (σ = - 0.8 GPa).
2. The energy $\mathcal{E}_{bi}$ delivered to the film growing at pulsed bipolar bias U_{sp} is lower (1.6 MJ/cm^3) than the energy delivered to the film growing at DC bias $U_{s\ DC}$ (3.7 MJ/cm^3). This is a reason why the film sputter deposited at a pulsed bias U_{sp} exhibits the X-ray amorphous structure and the film sputter deposited at DC bias $U_{s\ DC}$ is the crystalline with a dominant TiN (220) texture, see Fig. 6.2.

3. The electron bombardment of the growing film, however, results not only in the strong decrease of the compressive macrostress σ but also in decrease of its hardness H, elastic recovery W_e, H/E^* ratio and the low resistance to cracking, see Table 6.1.

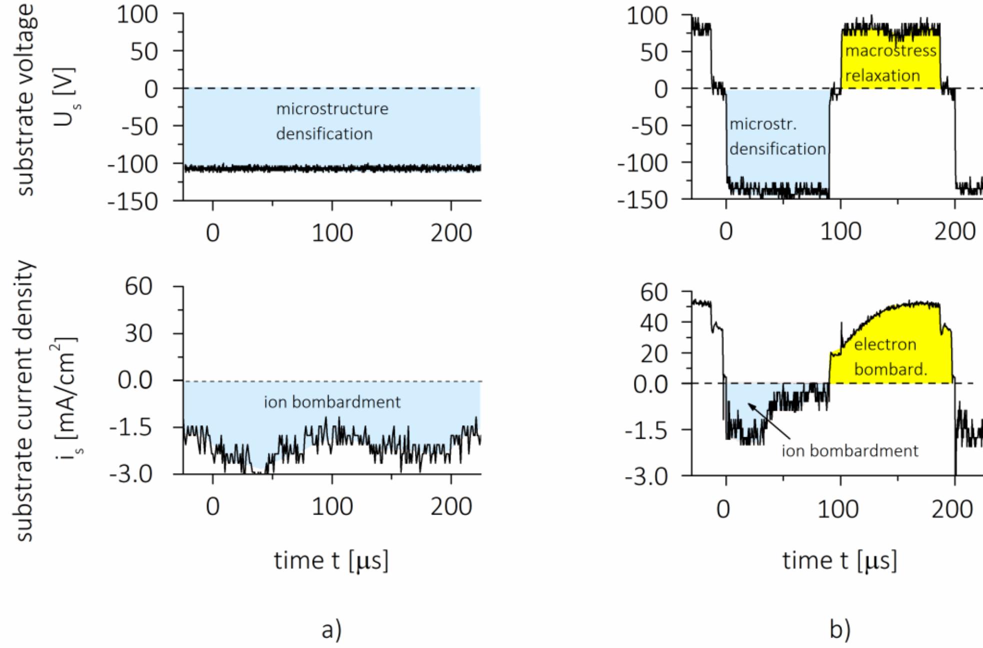

Figure 6.1 Comparison of DC and pulsed substrate bias used in deposition of Ti(Al,V)N films by DC dual magnetron discharge generated at I_d = 1 A, T_s = 500°C, d_{s-t} = 60 mm, $p_T = p_{Ar} + p_{N2}$ = 0.8 + 0.2 = 1 Pa. (a) Continuous ion bombardment and (b) alternating ion/electron bombardment of the growing Ti(Al,V)N film by ions and electrons produced by DC bias (U_s = - 100 V) and pulsed bias (U_{sp} = - 130/+70V, f_r = 5 kHz), respectively. Here, U_{sp} is the pulsed substrate bias U_{sp} and i_{sp} is the pulsed substrate current density.

Table 6.1 Physical and mechanical properties and compressive macrostress (σ < 0) in the Ti(Al,V)N films sputtered by DC dual magnetron operated at I_d = 1 A, T_s = 500°C, d_{s-t} = 60 mm, $p_T = p_{Ar} + p_{N2}$ = 0.2 + 0.8 = 1 Pa on the substrate held at (i) DC substrate bias voltage $U_{s\,DC}$ and (ii) pulsed substrate bias voltage U_{sp} voltage with repetition frequency of pulses f_r = 5 kHz. The bending test was performed on the films sputtered on the Mo strip and the indentation test on the films sputtered on the Si substrates

bias	f_r	U_{sp}	i_s	h	a_D	τ_e/τ_i	$\mathcal{E}_{bip}$	σ	H	E^*	W_e	H/E^*	ε_{cr}	L_{cr}	structure	texture
voltage	[kHz]	[V]	[mA/cm^2]	[nm]	[nm/min]		[MJ/cm^3]	[GPa]	[GPa]	[GPa]	[%]		[%]	[N]		
DC	0	-40	1	2100	36	0	1.6	-1.7	28.4	282	70	0.10	---	0.25	crystaline	(200)+(220)
DC	0	-100	1.8	1100	37.5	0	3.7	-4.0	30.7	220	81	0.14	>2.0	>1	crystaline	(220)
pulsed	5	-100/70	0.9	1000	33	1.3	1.6	-0.8	19.1	175	68	0.11	1.3	0.75	XRA	

$\mathcal{E}_{bip}$ is the average energy of ions during the negative pulse of pulsed substrate bias U_{sp}, and XRA is X-ray amorphous

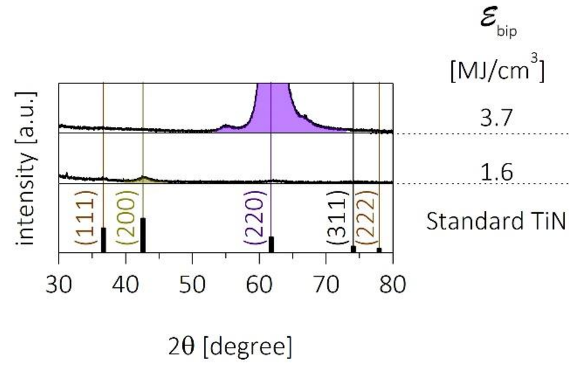

Figure 6.2 Comparison of the structure of the Ti(Al,V)N film sputter deposited at (i) DC substrate bias $U_{s\ DC}$ = -100 V and a high energy $\mathcal{E}_{bi}$ = 3.7 MJ/cm^3 and (ii) the pulsed substrate bias U_{sp} and a low energy $\mathcal{E}_{bip}$ = 1.6 MJ/cm^3.

The electron bombardment of the growing film is the reason why the macrostress σ generated in the film sputter deposited at the pulsed substrate bias U_{sp} with alternating negative and positive pulses is considerably lower than that in the film sputter deposited at the DC negative substrate bias voltage U_s. The length of the negative pulse τ_i and the length of the positive pulse τ_e can be different. It means that the efficiency of a relaxing of macrostress σ in the film can be controlled by the ratio τ_e/τ_i. The possibility to control the macrostress σ in sputtered films by the ratio τ_e/τ_i was also demonstrated in sputtering the Ti(Al,V)N films at pulsed bipolar substrate bias U_{sp}. Results of this experiment are summarized in Table 6.2.

Table 6.2 Physical and mechanical properties and compressive macrostress (σ < 0) in the Ti(Al,V)N films sputtered by DC dual magnetron operated at I_d = 1 A, T_s = 500°C, d_{s-t} = 60 mm, $p_T = p_{Ar} + p_{N2}$ = 0.2 + 0.8 = 1 Pa on the substrate held at pulsed bipolar substrate bias U_{sp} with two repetition frequencies f_r of alternating negative and positive pulses. The bending test was performed on the films sputtered on the Mo strip and the indentation test on the films sputtered on the Si substrates.

f_r	U_{sp}	h	i_{sp}	a_D	τ_e/τ_i	$\mathcal{E}_{bip}$	σ	H	E^*	W_e	H/E^*	ε_{cr}	L_{cr}	texture
[kHz]	[V]	[nm]	[mA/cm^2]	[nm/min]		[MJ/cm^3]	[GPa]	[GPa]	[GPa]	[%]		[%]	[N]	
High electron bombardment														
25	-130/+110	1500	1.3	45	3.2	2.3	-1.7	29.5	260	73	0.11	>2	>1	-220
25	-130/+110	2600	1.3	45	3.2	2.4	-1.9	28	270	70	0.1	>2	>1	-220
Low electron bombardment														
5	-130/+70	1300	1.3	33	1.3	3.1	-2.1	28.2	211	79	0.13	delam	>1	-220
5	-130/+70	2100	1.3	31	1.3	3.3	-2.4	33.5	246	82	0.14	delam	>1	-220
$\mathcal{E}_{bip}$ is the average energy of ions during the negative pulse of pulsed substrate bias U_{sp}														
"delam" denotes that the films delaminates from Mo strips during bending														

The Table 6.2 shows the properties of the Ti(Al,V)N films sputtered at pulsed substrate bias U_s with two repetition frequencies f_r of alternating negative and positive pulses of different lengths and the same value of the negative substrate voltage U_{sp} = -130 V and two values of the positive substrate voltage (f_r = 5 kHz with U_s = -130/+70 V, τ_e/τ_I =1.3 (low electron bombardment), and f_r = 25 kHz with U_s = -130/+130 V, τ_e/τ_i = 3.2 (high electron bombardment)); here τ_e and τ_i is the length of positive and negative pulse, respectively. This selection of parameters of the pulsed bipolar bias U_{sp} makes it possible to investigate the effect of the electron bombardment on mechanical properties of the film, its macrostress σ and resistance to cracking. From the Table 6.2 it is seen that (1) the Ti(Al,V)N

film sputtered under high electron bombardment (U_{sp+} = +110 V) and the ion energy $\mathcal{E}_{bi}$ = 2.4 MJ/cm^3 exhibit high hardness H = 28 GPa, high ratio H/E^* = 0.10, high elastic recovery W_e = 70%, low compressive macrostress σ = - 1.9 GPa and enhanced resistance to cracking ($\varepsilon_{cr} > 2$ and $L_{cr} > 1$ N) and (2) the Ti(Al,V)N film sputtered under lower electron bombardment (U_{sp+} = +70 V) and the higher ion energy $\mathcal{E}_{bi}$ = 3.1 MJ/cm^3 exhibit higher values H, H/E^*, W_e, $|\sigma| > 2$ GPa and also an enhanced resistance to cracking in compression ($L_{cr} > 1$ N) but this film already delaminates from Mo strip due too high compressive macrostress $|\sigma| > 2$ GPa. This experiment clearly demonstrates that properties of the sputtered film can be well controlled by an optimized bombardment with ions and electrons during its growth.

6.3.2. Macrostress reduction by overshoots in pulsed sputtering

The control of the energy of bombarding ions $\mathcal{E}_{bi}$ by the pulsed sputtering of the film is based on the utilization of strong discharge oscillations connected with transient pulse phenomena after the pulse off. Experiments demonstrating this fact were performed in the pulsed dual magnetron (DM) discharge. The DM was supplied by the pulse asymmetric bipolar Advanced Energy Pinnacle Plus+ 5kW power supply unit (PSU) with the reverse positive pulse (10% of the negative voltage). Each magnetron is alternatively sputtered (pulse-on) or discharged (pulse-off) with the repetition frequency $f_r = 1/T_r$. The schematic illustration of the PSU supplying the DM composed of two independent asymmetric bipolar units is shown in Fig. 6.3. The PSU symmetry point can be either floating (the DM is floating PSU – DMF) or connected to the grounded chamber (the DM is grounded PSU – DMG). In our experiment the PSU - DMG was used.

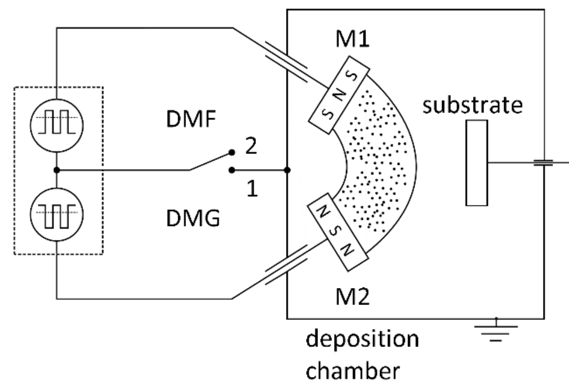

Figure 6.3 Schematic illustration of the asymmetric bipolar Advanced Energy Pinnacle Plus+ 5 kW pulsed power supply (PSU). The abbreviations DMG and DMF denote that the PSU symmetry point is grounded (the position 1) and floating, i.e. disconnected from the grounded deposition chamber, (the position 2).

The oscillations generated in the pulsed bipolar DM discharge are illustrated in Fig. 6.4. This figure shows the time evolution of the voltage U_{d1} on the magnetron 1 (M1) and U_{d2} on the magnetron 2 (M2) of the dual magnetron with a closed magnetic field B [45]. The pulsed bipolar DM discharge was generated at three repetition frequencies (a) 100 kHz, (b) 200 kHz and (c) 350 kHz. The oscillations superposed on the DC substrate bias U_{sp} are clearly seen.

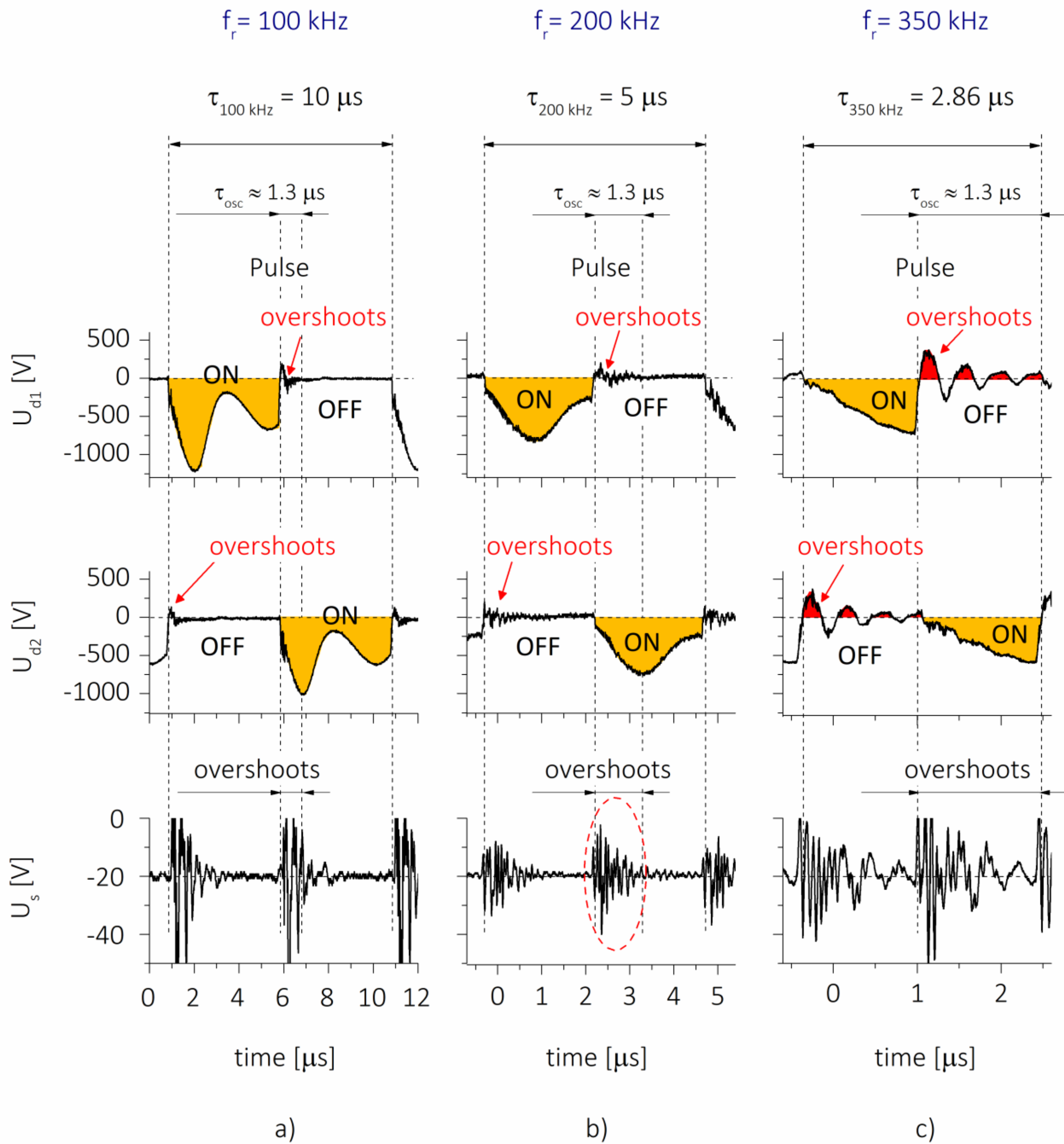

Figure 6.4 Time waveforms of the voltage U_{d1} and U_{d2} on the magnetron 1 and the magnetron 2, respectively, of the dual magnetron (DMG) operated in pulsed bipolar mode at $I_d = I_{d1} + I_{d2} = 1.6$ A, $T_s = 500°C$, $d_{s\text{-}t} = 60$ mm, $p_T = p_{Ar} + p_{N2} = 0.2 + 0.8 = 1$ Pa and three repetition frequencies (a) 100 kHz, (b) 200 kHz and (c) 350 kHz, and the DC substrate bias $U_{s\,DC} = -20$V.

The principle of the control of the macrostress σ in the growing film during pulsed sputtering is based on the control of the ion bombardment of the film during its growth. Splashes of oscillations (called as the packets or the overshoots) superposed on the substrate potential U_s play a key role in the control of the film macrostress σ, see Fig. 6.4. These splashes are generated after the switching off of pulses. Therefore, the magnitude of σ in the sputtered film depends on the total number of splashes N_{spls} generated during the whole time of the film deposition. The number N_{spls} of

splashes increases with increasing repetition frequency f_r of pulses. Fig. 6.4 shows that (1) the magnetron voltage U_d sinusoidally changes during the pulse-on time τ_{on}, (2) the length of sinusoid decreases with increasing f_r from ~T_r at f_r = 100 kHz to ~T_r/4 at $f_r \approx$ 350 kHz, and (3) the splashes of oscillations, strongly attenuating with increasing time, are created not only on the voltage waveform of the discharge voltage U_d(t) but also on the waveform of the DC negative substrate bias $U_{s\ DC}$; the splashes of oscillations are denoted by dotted ellipses in Fig. 6.4b, (4) the duration of the splashes of oscillations is $\tau_{osc} \approx$ 1.3 µs is practically constant and does not depend on the repetition frequency of pulses f_r and (5) the number of splashes of oscillations N_{spls} increases with increasing f_r.

During oscillations of the substrate bias U_{sp}, the growing film is exposed to a strong ion bombardment. It is due to a strong increase of U_{sp} during negative half periods of oscillations. This strong ion bombardment results in an increase of macrostress σ generated in the film. Therefore, a reduction of the macrostress σ in the sputtered film can be achieved by a reduction of the number N_{spls} of splashes of the oscillations. It can be achieved by decreasing of the repetition frequency f_r of sputtering pulses. This fact was confirmed experimentally by sputtering of the Ti(Al,V)N films on the Si(111) substrates held on the floating potential U_s = U_{fl} under the same deposition conditions at two repetition frequencies of pulses f_r = 200 kHz and 350 kHz. The film sputter deposited at f_r = 200 kHz, i.e. under a lower ion bombardment, exhibits not only the low macrostress (σ = - 0.6 GPa) as expected but also the columnar microstructure because the ion bombardment was already weak and insufficient to create the film with dense voids-free microstructure, see Table 6.3 and Fig. 6.5. More information about overshoots and its effect on plasma and coating properties can be found in Refs. [49- 57].

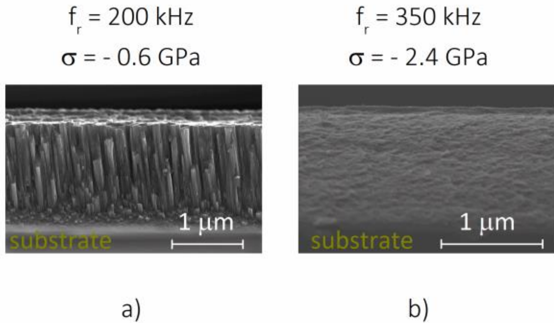

Figure 6.5 Microstructure of the Ti(Al,V)N films with (a) low and (b) high compressive macrostress (σ < 0) sputtered on Si(111) substrates by pulsed DM at two repetition frequencies f_r = 200 kHz and f_r = 350 kHz, respectively, and W_d = 12 W/cm^2, U_s = U_{fl}, T_s = 500°C, d_{s-t} = 60 mm, p_T = p_{Ar} + p_{N2} = 0.2 + 0.8 = 1 Pa.

Table 6.3 Physical and mechanical properties of the Ti(Al,V)N films sputtered by pulsed dual magnetron at W_d = 12 W/cm^2, T_s = 500°C, d_{s-t} = 60 mm, p_T = p_{Ar} + p_{N2} = 0.2 + 0.8 = 1 Pa, floating potential U_s = U_{fl} at two repetition frequencies f_r = 200 kHz and 350 kHz.

f_r	h	a_D	$\mathcal{E}_{bi}$	σ	H	E^*	W_e	H/E^*	ε_{cr}	L_{cr}	micostructure
[kHz]	[nm]	[nm/min]	[MJ/cm^3]	[GPa]	[GPa]	[GPa]	[%]		[%]	[N]	
200	1900	15.8	---	-0.6	23.8	240	68	0.1	1.3	0.25	columnar
350	1300	4.6	---	-2.4	21.4	173	76	0.12	>2	>1	dense

This experiment shows that a pulsed magnetron sputtering is an efficient way which allows controlling the macrostress σ of the film held even at a floating potential $U_s = U_{fl}$ a and its microstructure by selection of repetition frequency of pulses. This finding is of a great application potential, particularly for sputtering of dielectric films or deposition of films on dielectric substrates, for instance, on the glass, etc. Both, the films with a porous columnar microstructure or flexible hard protective films with dense, voids-free microstructure can be created on substrates held at a floating potential $U_s = U_{fl}$.

6.3.3. Control of macrostress in films sputtered at high repetition frequencies of pulses

Fig. 6.6 shows V-A discharge characteristics of a pulsed magnetron discharge used for sputtering of the Ti(Al,V)N films at f_r = 350 kHz and different values of the DC substrate bias $U_{s\,DC}$ ranging from negative (-60 V) to positive (+40 V) including grounded and floating substrates, i.e. $U_{s\,DC} = 0$ and $U_{s\,DC} = U_{fl}$ ranging from +15 to ~ +150 V. From Fig. 6.6a it is seen that the main source of the ion energy $\mathcal{E}_{bi}$ during the film deposition are positive half-periods of overshoot oscillations when the sheath voltage is positive, i.e. $U_{sh} \approx U_{dp} - U_s > 0$ and superposed on the negative DC substrate voltage $U_{s\,DC} < 0$. All films sputtered at $U_{s\,DC} < 0$ and f_r = 350 kHz exhibit similar properties, see Table 6.4. On the other hand, the compressive macrostress ($\sigma < 0$) generated in these films by bombarding ions is relaxed to low values $\sigma \approx$ - 0.3 GPa by bombarding electrons during negative half-periods of the oscillations when the substrate current density $I_s \approx 0$ and the sheat voltage is negative, i.e. $U_{sh} = U_{dp} - U_s < 0$. This decrease of compressive macrostress results in a decrease of the hardness to $H \approx 9$ GPa. From Figs. 6.6b to 6.6c it is seen that also films sputtered at grounded, floating and positively biased substrates are bombarded by ions. This fact is demonstrated by the positive peaks of the sheat voltage corresponding to positive half-periods of overshoot oscillations. In the case of a floating substrate potential (Fig. 6.6c) the ion bombardment cannot be measured since fluxes of electrons and ions incident on the substrate are the same and the substrate current I_s = 0 mA/cm^2. On the contrary, at a positive substrate bias, the electron bombardment of sputtered film dominates over an ion bombardment, see Fig.6.6d.

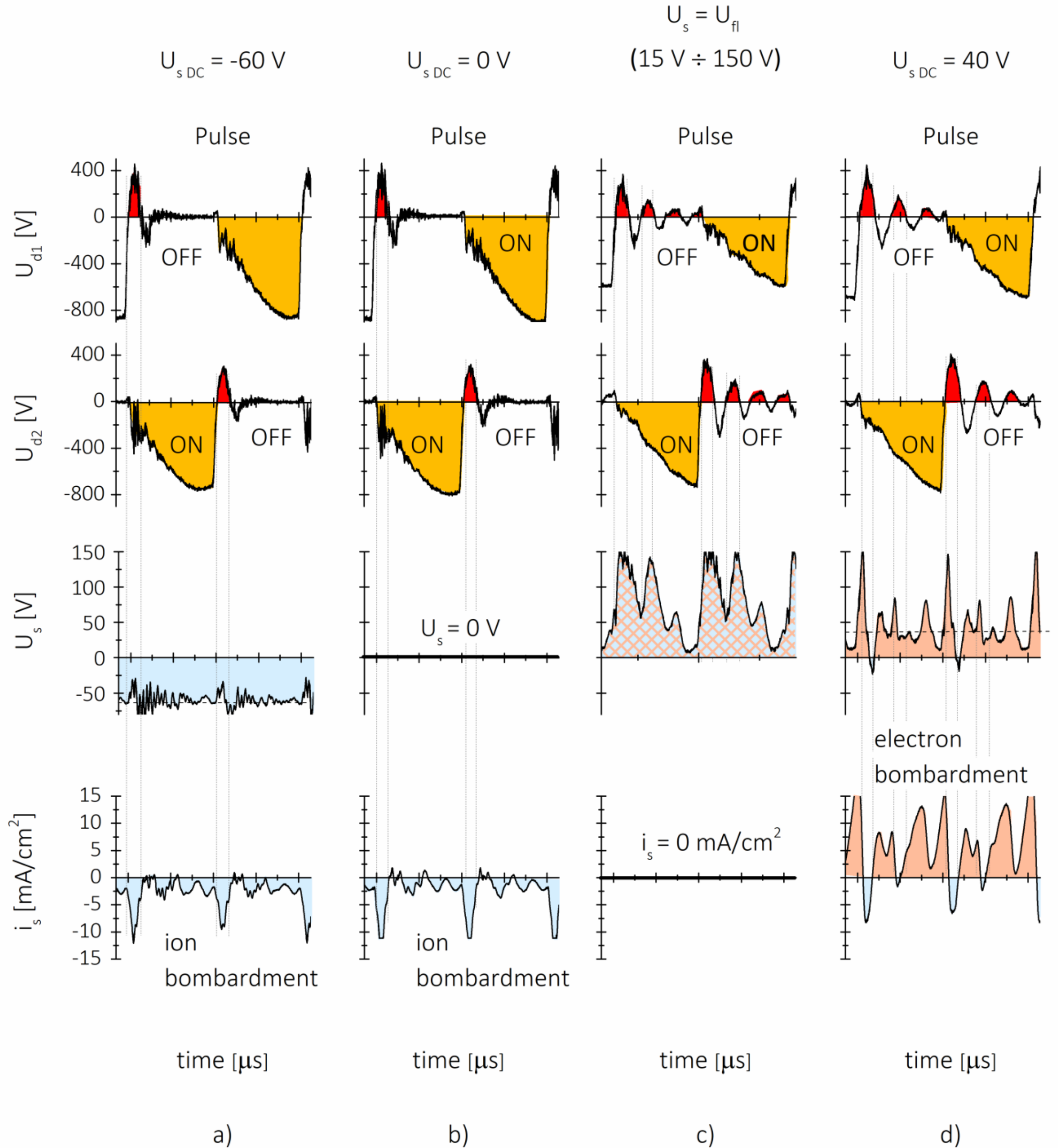

Figure 6.6 Time evolution of voltage U_{d1} and U_{d2} on the magnetron M_1 and M_2 of dual magnetron, voltage U_s on the substrate and current density on the substrate in pulsed dual magnetron discharge generated at W_d = 12 W/cm², T_s = 500°C, $d_{s\text{-}t}$ =60 mm, $p_T = p_{Ar} + p_{N2}$ = 0.2 + 0.8 = 1 Pa, f_r = 350 kHz and the substrate biased at a) $U_{s\,DC}$ = -60 V, b) grounded U_s = 0 V, c) floating $U_s = U_{fl}$ = 15 ~ 150 V and d) $U_{s\,DC}$ = +40 V.

Physical and mechanical properties of $Ti(Al,V)N_x$ films sputtered by pulsed dual magnetron at f_r = 350 kHz at different values of negative DC substrate bias $U_{s\,DC}$ were investigated in detail, see Table 6.4. The energy $\mathcal{E}_{bi}$ increases and the film deposition rate a_D decreases with increasing negative $U_{s\,DC}$. On the other hand, values of H, E^*, H/E^* ratio, W_e and σ are low of about 10 GPa, 140 GPa, 0.07, 45 % and - 0.3 GPa, respectively. These films are brittle and easily crack. For more detail see Ref. [47].

Table 6.4 Mechanical properties, compressive macrostress (σ < 0) and resistance to cracking of the Ti(Al,V)N films sputtered by pulsed DC dual magnetron, operated in bipolar mode at I_d = 2 A, is ranging from 2.2 to 2.4 mA/cm² T_s = 500°C, d_{s-t} = 60 mm, $p_T = p_{Ar} + p_{N2}$ = 0.2 + 0.8 = 1 Pa and f_r = 350 kHz on Si(111) substrates, as a function of negative DC substrate bias $U_{s\,DC}$.

$U_{s\,DC}$	h	a_D	$\mathcal{E}_{bi}$	σ	H	E^*	W_e	H/E^*	ε_{cr}	L_{cr}	TiN
[V]	[nm]	[nm/min]	[MJ/cm³]	[GPa]	[GPa]	[GPa]	[%]		[%]	[N]	structure
-60	1100	18	7.5	-0.3	8.3	141	40	0.06	2	0.25	220
-80	1000	16.7	11.1	-0.2	10.4	139	49	0.07	2	0.25	220
-100	800	13.3	17.7	-0.4	9.4	143	44	0.07	2	0.25	220
-100	1000	11.1	21.2	-0.4	9.7	142	46	0.07	2	0.25	220

6.4. Conclusions

The article reports on a detailed investigation of the effect of the energy $\mathcal{E}_{bi}$ delivered into the Ti(Al,V)N film by bombarding ions on its macrostress, microstructure, mechanical properties and resistance to cracking. Main conclusions of this study can be summarized as follows:

1. The compressive macrostress σ in sputter deposited Ti(Al,V)N films can be reduced by (i) the pulsed bipolar bias voltage U_{sp} with alternating negative and positive pulses and/or (ii) the alternating ion and electron bombardment of the growing film during overshoots generated in a pulsed magnetron sputtering discharge.
2. The Ti(Al,V)N films with enhanced resistance to cracking are formed only in the case when the energy $\mathcal{E}$ delivered during their growth is sufficiently high ($\mathcal{E}_{bi}$ > 1.7 MJ/cm³). These films exhibit (i) a dense, voids-free microstructure, (ii) a high ratio $H/E^* \geq 0.1$, (iii) a high elastic recovery $W_e \geq 60\%$ and (iv) an enhanced resistance to cracking.
3. A reduction of compressive macrostress (σ< 0) down to about σ ≈ - 0.4 GPa results in a reduction of the film hardness and its resistance to cracking.
4. Our investigations clearly demonstrate the compressive macrostress (σ < 0) generated in the sputtered film can be effectively controlled by alternating ion and electron bombardment already during its growth.

Acknowledgments

This work was supported by the project LO1506 of the Czech Ministry of Education, Youth and Sports under the program NPU I.

References

[1] F.Lapostolle, A.Billard, J. von Stebut: Structure/mechanical properties relationship of titanium-oxygen coatings reactively sputter – deposited, Surf. Coat. Technol. 135 (2000), 1-7.

[2] L.Karlsson, L.Hultman, M.P.Johansson, J.-E.Sundgren, H.Ljungcrantz: Growth, microstructure, and mechanical properties of arc evaporated $TiC_{1-x}N_{1-x}$ ($0 \leq x \leq 1$) films, Surf. Coat. Technol. 126 (2000), 1-14.

[3] J.Ding, Y.Meng, S.Wen: Mechanical properties and fracture toughness of multilayer hard coatings using nanoindentation, Thin Solid Films 371 (2000), 178-182.

[4] W.J.Meng, R.C.Tittsworth, L.E.Rehn: Mechanical properties and microstructure of TiC/amorphous hydrocarbon nanocomposite coatings, Thin Solid Films 377-376 (2000), 222-232.

[5] M.Oden, J.Almer, G.Hakansson, M.Olsson: Microstructure-property relationships in arc-evaporated Cr-N coatings, Thin Solid Films 377-376 (2000), 407-412.

[6] J.Patscheider, T.Zehnder, M.Diserens: Structure-performance relations in nanocomposite coatings, Surf. Coat. Technol. 146 (2001), 201 – 208.

[7] T.Mae, M.Nose, M.Zhou, T.Nagae, K.Shimamura: The effect of Si addition on the structure and mechanical properties of ZrN thin films deposited by an rf reactive sputtering method, Surf. Coat. Technol. 142-144 (2001), 954-958.

[8] S.Carvalho, L.Rebouta, A.Cavaleiro, L.A.Rocha, J.Comes, E.Alves: Microstructure and mechanical properties of nanocomposite (Ti,Si,Al)N coatings, Thin Solid Films 398-399 (2001), 391-396.

[9] J.Almer, M.Oden, G.Hakansson: Microstructure, stress and mechanical properties of arc-evaporated Cr-C-N coatings, Thin Solid Films 385 (2001), 190-197.

[10] J.Musil, H.Zeman, F.Kunc, H.Poláková: Relationships between hardness, Young´s modulus and elastic recovery in hard nanocomposite coatings, Surf. Coat.Technol. 154(2002), 304-313.

[11] J.Musil, H.Zeman, J.Kasl: Relationship between structure and mechanical properties in hard Al-Si-Cu-N films prepared by magnetron sputtering, Thin Solid Films 413 (2002), 121-130.

[12] H.Watanabe, Y.Sato, C.Nie, A.Ando, S.Ohtani, N.Iwamoto: The mechanical properties and microstructure of Ti-Si-N nanocomposite films by ion plating, Surf. Coat. Technol. 169-170 (2003), 452-455.

[13] H.S.Barshilia, A.Jain, K.S.Rajam: Structure, hardness and thermal stability of nanolayered TiN/CrN multilayer coatings, Vacuum 72 (2003), 241-248.

[14] P.Jedrzejowski, J.E.Klemberg-Sapieha, L.Martinu: Relationship between the mechanical properties and the microstructure of nanocomposite TiN/$SiN_{1.3}$ coatings prepared by low temperature PECVD, Thin Solid Films 426 (2003), 150-159.

[15] Y.T.Pei, D.Galvan, J.Th.M. De Hosson: Nanostructure and properties of TiC/a-C:H composite coatings, Acta Materialia 53 (2005), 4505-4521.

[16] J.Soldán, J.Musil: Structure and mechanical properties of DC magnetron sputtered TiC/Cu films, Vacuum 81 (2006), 531-538.

[17] J.Lin, B.Mishra, J.J.Moore, W.D.Sproul: Microstructure, mechanical and tribological properties of Cr1-xAlxN films deposited by pulsed-closed field unbalanced magnetron sputtering (P-CFUBMS), Surf. Coat. Technol. 201 (2006), 4329-4334.

[18] M.Audronis, A,Leyland, P.J.Kelly, A.Matthews: The effect of pulsed magnetron sputtering on the structure and mechanical properties of CrB2 coatings, Surf. Coat. Technol. 201 (2006), 3970-3976.

[19] C.H.Lai, M.H.Tsai, S.J.Lin, J.W.Yeh: Influence of substrate temperature and mechanical properties of multi-element (AlCrTaTiZr)N coatings, Surf. Coat. Technol. 201 (2007), 6993-6998.

[20] N.J.M. Carvalho, E. Yoestbergen, B.J. Kooi and J.Th.M. De Hooson: Stress analysis and microstructure of PVD monolayer TiN and multilayer TiN/(Ti,Al)N coatings, Thin Solid Films 429 (2003) 179.

[21] G. Liu, Y. Yang, B. Huang, X. Luo, S. Ouzang, G. Zhao, N. Jin and P. li: Effects of substrate temprityre on the structure, residual stress and nanohardness of Ti6Al4V films prepared by magnetron sputtering, Applied Surface Science 370 (2016) 53.

[22] J. Kohout, E. Bousser, T. Schmitt, R. Vernhes, O. Zabeida, J. Klemberg-Sapieha and L. Martinu: Stable reactive deposition of amorphous Al2O3 films with low residual stress and enhanced toughness using pulsed dc magnetron sputtering with very low duty cycle, Vacuum 124 (2016) 96.

[23] A.Pelisson, M.Parlinska-Wojtan, H.J.Hug, J.Patscheider: Microstructure and mechanical properties of Al-Si-N transparent hard coatings deposited by magnetron sputtering, Surf. Coat. Technol. 202 (2007), 884-889.

[24] J.Soldán, J.Neidhardt, B.Satory, R.Kaindl, R.Cerstvy, P.H.Mayrhofer, R.Tessadri, P.Polcik, M.Lechthaler, C.Mitterer: Structure-property relations of arc-evaporated Al-Cr-Si-N coatings, Surf. Coat. Technol. 202 (2008), 3555-3562.

[25] K.Polychronopoulou, C.Rebholtz, M.a.Baker, L.Theodorou, N.G.Demas, S.J.Hinder, A.A.Polycarpou, C.C.Doumanidis, K.Bobel: Nanostructure, mechanical and tribological properties of reactive magnetron sputtered TiCx coatings, Diamond and Related Materials 17 (2008), 2054-2061.

[26] J.H.Huang, Z.E.Tsai, G.P.Yu: Mechanical properties and corrosion resistance of nanocrystalline ZrNxOy coatings on AlSL 304 stainless steel by ion plating, Surf. Coat. Technol. 202 (2008), 4992-5000.

[27] J.Musil: Sputtering systems with enhanced ionization for ion plating of hard wear resistant coatings, Proc. of the 1st Meeting on the Ion Engineering Society of Japan (IESJ-92), Tokyo, Japan, 1992, pp. 295-304.

[28] H.Poláková, J.Musil, J.Vlček, J.Alaart, C.Mitterer: Structure- hardness relations in sputtered Ti-Al-V-N films, Thin Solid Films 444 (2003), 189-198.

[29] J.Musil, H.Poláková, J.Šůna, J.Vlček: Effect of ion bombardment on properties of hard reactively sputtered single-phase films, Surf.Coat.Technol. 177-178 (2004), 289-298.

[30] J.Musil, J.Šůna: The role of energy in formation of sputtered nanocomposite films, Materials Science Forum 502 (2005), 291-296.

[31] J.Musil, J.Šícha, D.Heřman, R.Čerstvý: Role of energy in low-temperature high-rate formation of hydrophilic TiO2 thin films using pulsed magnetron sputtering, J. Vac. Sci. Technol. A 25(4) (2007), 666-674.

[32] J.Musil: Flexible hard nanocomposite coatings, RSC Advances 5 (2015), 60482-60495.

[33] J.Musil, J.Vlček, P.Baroch: Magnetron discharges for thin films plasma processing, Chapter 3 in „Materials Surface Processing by Directed Energy Techniques, Y.Pauleau (Ed.), 2006, Elsevier Science Publisher B.V., Oxford, UK, pp. 67-106.

[34] J.A.Thornton: (i) Recent developments in sputtering – Magnetron sputtering, Metal Finishing 77(5) (1979), 83-87 and (ii) High rate thick films growth, Ann. Rev. Mater. Sci. 7 (1977), 239-260.

[35] J.Musil: Physical and mechanical properties of hard nanocomposite films prepared by reactive magnetron sputtering, Chapter 10 in Nanostructured Coatings, J.T.M. DeHosson and A. Cavaleiro (Eds.) New York, Springer Science + Business Media, LCC, 2006, pp. 407-463.

[36] J.Musil, V.Poulek, V.Valvoda, R.Kužel Jr., H.A.Jehn, M.E.Baumgartner: Relation of deposition conditions of Ti-N films prepared by dc magnetron sputtering to their microstructure and macrostress, Surf.Coat.Technol. 60 (1993), 484-488.

[37] B.A.Movchan, A.V.Demchishin: Study of the structure and properties of thick vacuum condensates of nickel, titanium, tungsten, aluminum oxide and zirconium oxide, Phys. Met. Metallogr. 28 (1969), 83-90.

[38] P.Pokorný, J.Musil, P.Fitl, M.Novotný, J.Lančok, J.Bulíř: Contamination of magnetron sputtered metallic films by oxygen from residual atmosphere in deposition chamber, Plasma Processes and Polymers 12 (2015), 416-421.

[39] J.Musil: Low-pressure magnetron sputtering, Vacuum 50(3-4) (1998), 363-372.

[40] J.Musil: Hard and superhard nanocomposite coatings, Surf.Coat.Technol. 125 (2000), 322-330.

[41] J.Musil: Hard nanocomposite coatings: Thermal stability, oxidation resistance and toughness, Surf.Coat.Technol. 207 (2012), 50-65.

[42] J.Musil: Advanced hard nanocomposite coatings with enhanced toughness and resistance to cracking, Chapter 7 in Thin Films and Coatings: Toughening and Toughening Characterization, S.Zhang (Editor) CRC Press, USA, 2015, pp. 377-463.

[43] M. Jaroš, J. Musil, R. Čerstvý and S. Haviar: Effect of energy on physical and mechanical properties of hard Ti(Al,V)Nx films prepared by magnetron sputtering, Surf.Coat.Technol. 332 (2017), 190-197.

[44] J. Musil,M. Jaroš, R. Čerstvý and S. Haviar: Evolution of microstructure and macrostress in sputtered hard Ti(Al,V)N films with increasing energy delivered during their growth by bombarding ions: Journal of Vacuum Science & Technology A 35(2017) 020601.

[45] J.Musil, P.Baroch: Discharge in dual magnetron sputtering system, IEEE Transactions on Plasma Science 33(20 (2005), 338-339.

[46] G.G.Stoney: The transition of metallic films deposited by electrolysis, Proc. R. Soc. London, Ser. A82 (1909), 172-175.

[47] J. Musil, J. Sklenka, R. Čerstvý: Transparent Zr-Al-O oxide coatings with enhanced resistance to cracking, Surf. Coat. Technol. 206 (2012), 2105-2109.

[48] J. Musil, J. Sklenka, R. Čerstvý: Protection of brittle film against cracking, Appl. Surf. Sci. 370, 306 (2016), 306-311.

[49] J.Šícha, O.Novák, J.Vlček, P.Kudláček: Ion flux characteristics in pulsed dual magnetron discharge used for deposition of photoactive TiO2 films, Plasma Process. Polym. 8 (2011), 191-198.

[50] J.W.Bradley, H.Bäcker, P.J.Kelly and R.D.Arnell: Space and time resolved Langmuir probe measurements in a 100 kHz pulsed rectangular magnetron system, Surf. Coat. Technol. 142 (2001) 337-341.

[51] J.Vlček, A.D.Pajdarová and J.Musil: Pulsed dc Magnetron Discharges and their Utilization on Plasma Surface Engieneering, Contrib. Plasma Phys. 44 (2004) 426-436.

[52] R.D.Armell, P.J.Kelly and J.W.Bradley: Recent developments in pulsed magnetron sputtering, Surf. Coat. Technol. 188 (2004) 158-163

[53] C.Muratore, J.J.Moore and J.A.Rees: Electrostatic quadrupole plasma mass spectrometer and Langmuir probe measurements of mid-frequency pulsed DC magnetron discharges, Surf. Coat. Technol. 163 (2003) 12-18

[54] F.Richter, Th.Welyel, Th.Dunger and H.Kupfer: time-resolved characterization of pulsed magnetron discharges using Langmuir probes, Surf. Coat. Technol. 188 (2004) 384-391.

[55] H.Bäcker, P.S.Henderson, J.W.Bradley and P.J.Kelly: Time-resolved investigation of plasma parametres during deposition of Ti and TiO2 thin films, Surf. Coat. Technol. 174 (2003) 909-913.

[56] J.Lin, J.J.Moore, B.Mishra, W.D.Sproul and J.A.Rees: Examination of the phenomena in pulsed-closed field unbalanced magnetron sputtering (P-CFUBMS) of Cr-Al-N thin films, Surf. Coat. Technol. 201 (2007) 4640-4652.

[57] J.M.Anton, B.Mishra, J.J.Moore, J.A.Rees and W.D.Sproul: Investigation of processing parameters for pulsed closed unbalanced magnetron co-sputtered TiC-C thin films, Surf. Coat. Technol. 201 (2006) 4131-4135.

Paper V

7. Interrelationships among macrostress, microstructure and mechanical behavior of sputtered hard Ti(Al,V)N films

M. Jaroš, J. Musil, S. Haviar
Material Letters 235 (2019) 92

Abstract

The article reports on the influence of a compressive macrostress σ in the Ti(Al,V)N film on its mechanical properties, structure, microstructure, and resistance to cracking. The macrostress σ controlled by the energy $\mathcal{E}_{bi}$ delivered into the growing film by bombarding ions. The Ti(Al,V)N films were sputtered by a dual magnetron with the closed magnetic field. It is shown that (1) the compressive macrostress ($\sigma < 0$) increases the hardness *H* of the film and the ratio H/E^* , (2) the film exhibits a dense, voids-free, non-columnar microstructure in the case when the energy $\mathcal{E}_{bi} \geq 3$ MJ/cm^3, (3) the enhanced resistance of the film is controlled by its mechanical properties, microstructure and macrostress σ; here E^* is the effective Young's modulus.

7.1. Introduction

A macrostress σ generated in the film prepared by an ion plating sputtering strongly influences its hardness H and structure and thereby its physical and functional properties. The stabilization of β-Ta [1] or *c*-Zr_3N_4 phase in the film [2], the superconductivity of film [3], the Curie temperature of film [4], a change of the preferred orientation of film [5-7] and the lifetime of the cutting tools coated by protective hard coatings [8-10] can be given as examples. However, so far, there is little information about the influence of σ on the hardness H of film and its resistance to cracking [11-13].

7.2. Experimental

The Ti(Al,V)N thin films were sputter deposited using a dual magnetron with closed magnetic field equipped with TiAlV (6 at.% Al, 4 at.% V) alloy targets (∅ = 50 mm) in a mixture of 20% Ar+ 80% N_2 sputtering gases at total pressure $p_T = p_{Ar} + p_{N2}$ ranging from 0.4 to 1.0 Pa. The magnetrons were powered by an Advanced Energy Pinnacle Plus+5/5 kW power supply operated either in DC or pulse mode at a low power density in the pulse of $W_{t\,DC} = W_{tp} \leq 25$ W/cm^2; here $W_{t\,DC}$ and W_{tp} is the target power density in DC discharge and during the pulse-on in the pulsed discharge. For a more detailed description of deposition conditions see Ref. [14-18] The Ti(Al,V)N films were deposited onto Si(111) substrates.

The film thickness was measured by a stylus profilometer DEKTAK 8. The macrostress σ was evaluated from the bending of Si plate using the Stoney's formula [19]. The elemental composition of the Ti(Al,V)N films on the Si substrate was analyzed in a scanning electron microscope (SU- 70, Hitachi) operated at a primary electron energy of 15 keV using energy dispersive spectroscopy (EDS, UltraDry, Thermo Scientific) and wave dispersive spectroscopy (WDS, Magnaray, Thermo Scientific). Mechanical properties of sputtered films were determined from load vs. displacement curves measured by a microhardness tester Fisherscope H100with Vickers diamond indenter at a load of 20 mN. The resistance of the Ti(Al,V)N films to cracking was assessed by a critical load L_{cr} at which cracks in the film occurred.

7.3. Results and discussion

It is well known that the hardness H, structure, microstructure of the sputtered film and the macrostress σ generated in it during its growth depend on many deposition parameters. It means that the interrelationship between the deposition parameters of the film and its properties is a multi-parameters function

Film properties = f (U_d, I_d, W_t, T_s, U_s, i_s, ν_i, ν_{ca}, d_{s-t}, h, a_D, p_0, p_{Ar}, p_{RG}, p_T, etc.) (7.1)

Here U_d is the voltage of magnetron discharge, I_d is the current of magnetron discharge, W_t is the target power density, T_s is the substrate temperature, U_s is the substrate bias, i_s is the substrate ion current density, ν_i is the flux of bombarding ions, ν_{ca} is the flux of condensing atoms, d_{s-t} is the substrate-to-target distance, a_D is the deposition rate of coating, p_0 is the base pressure in the deposition chamber before inlet of sputtering gas, p_{Ar} is the partial pressure of argon, p_{RG} is the partial pressure of a reactive gas, $p_T = p_{Ar} + p_{RG}$ is the total pressure of sputtering gas.

This fact practically excludes to find correct interrelations among H, σ, structure and microstructure of the sputtered film and its resistance to cracking because every deposition parameter has a different effect on these properties of the sputtered film. It is due to the fact that at each combination of deposition parameters you deliver a different energy $\mathcal{E}$ in the growing coating. In this case, it is excluded to sputter the film with fully reproducible properties. Therefore, the film properties must be expressed as a function of one parameter only, i.e. as a function of the energy $\mathcal{E}$

Film properties = f ($\mathcal{E}$) (7.2)

The energy $\mathcal{E}$ is a key parameter which controls the properties of the sputtered film and enables its formation with fully reproducible properties. It is a reason why the interrelations among H, σ, structure and microstructure of the sputtered film and its resistance to cracking are compared based on the energy $\mathcal{E}$. In our experiments the energy delivered into sputtered Ti(Al,V)N by bombarding ions, i.e. $\mathcal{E} = \mathcal{E}_{bi}$. The energy $\mathcal{E}_{bi}$ is calculated from measured values of substrate bias U_s, substrate ion current density i_s and the film deposition rate a_D from the formula [20]

$$\mathcal{E}_{bi} = U_s \times i_s / a_D \qquad (7.3)$$

Interrelationships among the hardness H, H/E^* ratio, microstructure, structure, and compressive macrostress σ in the Ti(Al,V)N film and its resistance to cracking are displayed in Figs. 7.1 - 7.4. The evolution of the H and H/E^* of the Ti(Al,V)N film with columnar microstructure and dense non-columnar microstructure as a function of compressive macrostress σ is displayed in Fig. 7.1. Fig. 7.1a shows that the H and the H/E^* ratio of the Ti(Al,V)N film with columnar microstructure increase from 22 to 31 GPa and 0.08 to 0.13, respectively, with increasing σ from -0.4 to -3 GPa. The same behavior exhibit also the Ti(Al,V)N films with dense, non-columnar microstructure**.** H and H/E^* ratio increase from 8 to 30 GPa and 0.06 to 0.14, respectively, with increasing σ from -0.4 to -5.5 GPa but with a smaller increase of H/E^* at σ ranging from -2 to -5.5 GPa than that in films with smaller compressive macrostress $|\sigma| < 3$ GPa.

Main results displayed in Fig. 7.1 can be briefly summarized as follows

1. The magnitude of the hardness H of the film with low compressive macrostress $|\sigma| < 3$ GPa strongly depend on its microstructure. Films with columnar microstructure exhibit higher H compared with the films with non-columnar microstructure. This difference is due to different values of $\mathcal{E}_{bi}$ used in sputtering and relaxing of σ by an electron heating of the growing film during overshoots in pulsed sputtering, see Table 7.1 and Ref. [17].
2. The hardness H of the film is a complex function of two competing parameters – the energy $\mathcal{E}_{bi}$ and enhancement or relaxing σ - which strongly influence its growth process and thus its structure, microstructure, and mechanical properties, particularly its H/E^* ratio and elastic recovery W_e, see Figs. 7.2 and 7.3 and Table 7.1. This is a reason why, for instance, the films with approx. same H exhibit different microstructure (compare the films No. 1 and No. 3) or the films with a low compressive macrostress exhibit different H, H/E, W_e, structure and microstructure (compare the films No. 1 and No. 4).

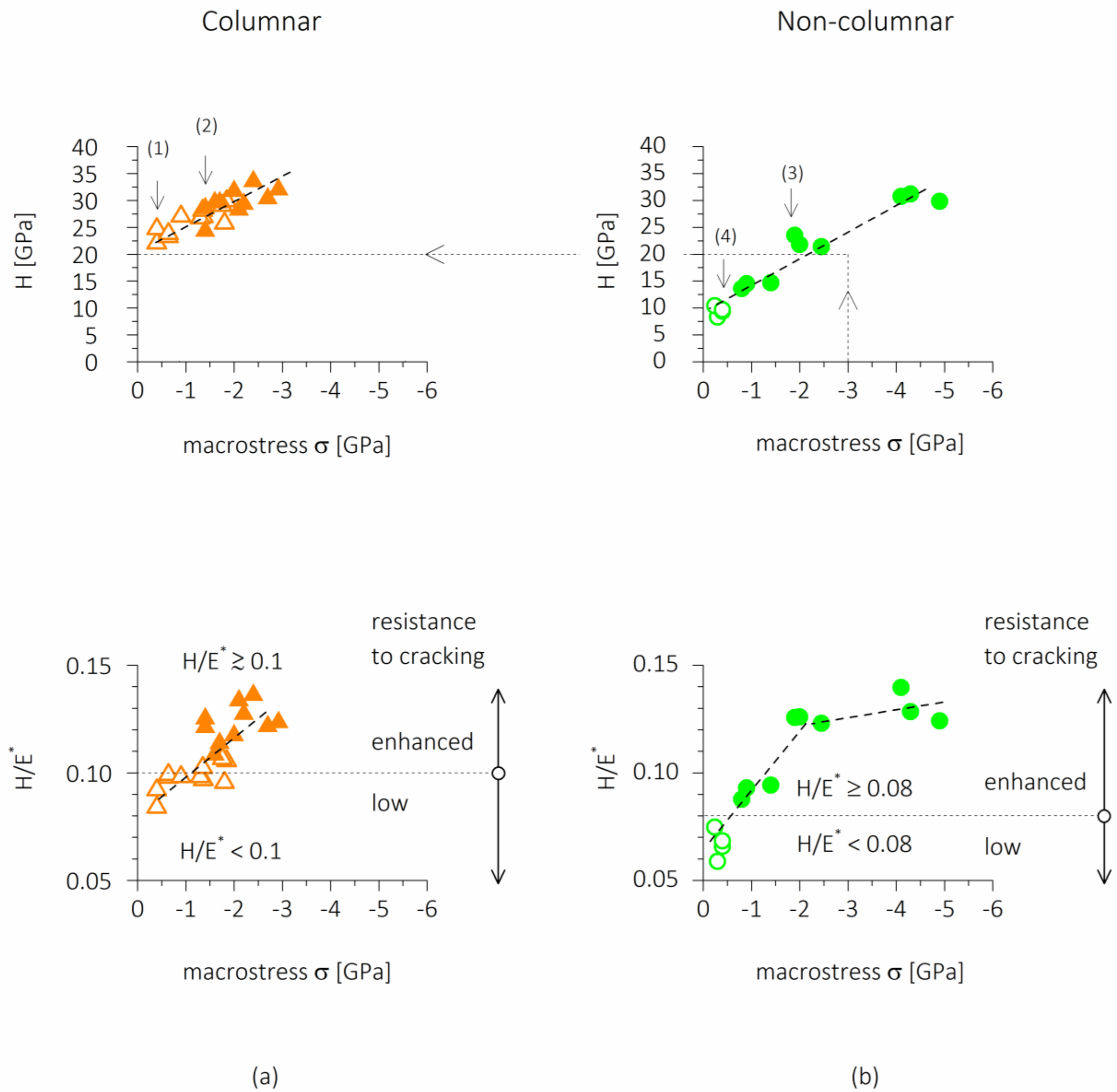

Figure 7.1 The hardness H and H/E ratio of the Ti(Al,V)N film with columnar and non-columnar microstructure as a function of compressive macrostress σ < 0. The open and full symbols denote films with low and enhanced resistance to cracking, respectively.*

The energy $\mathcal{E}_{bi}$ strongly influences also the preferred orientation of sputtered Ti(Al,V)N films, see Fig. 7.2. In this figure, the effect of $\mathcal{E}_{bi}$ on the structure of Ti(Al,V)N films deposited by DC and pulsed sputtering is illustrated. The films with numbers 1, 2, 3, 4 are given in Fig. 7.1 and their physical and mechanical properties in Table 7.1.

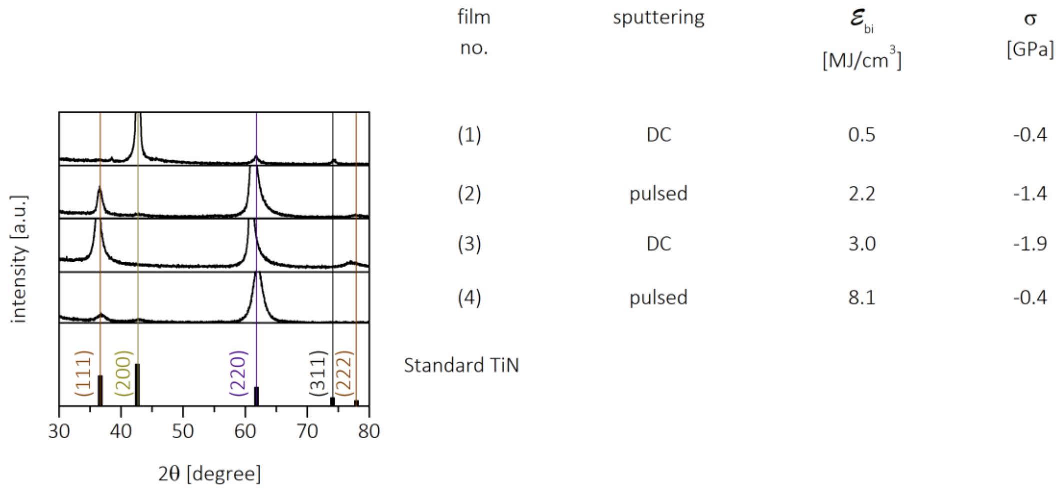

Figure 7.2 XRD patterns of the Ti(Al,V)N films with columnar microstructure (the films No.1 and 2) and with non-columnar microstructure (the films No.3 and 4). The films with numbers 1,2,3,4 are given in Fig.1 and their physical and mechanical properties in Table 1.

The microstructure of the Ti(Al,V)N film depends on the energy $\mathcal{E}_{bi}$ delivered to the growing film by bombarding ions. The energy $\mathcal{E}_{bi}$ is calculated from measured values of substrate bias U_s, substrate ion current density i_s and the film deposition rate a_D from the formula $\mathcal{E}_{bi} = U_s \times i_s/a_D$; more details are given in Ref. [20]. The films sputtered at low energies $\mathcal{E}_{bi} < 3$ MJ/cm^3 have a columnar microstructure, see Fig. 7.3a. On the contrary, the films sputtered at high energies $\mathcal{E}_{bi} \geq 3$ MJ/cm^3 have a non-columnar microstructure, see Fig. 7.3b. It is worthwhile to note that also the films with dense, voids-free non-columnar can be soft if the compressive macrostress generated under high ion bombardment at a high $\mathcal{E}_{bi}$ is simultaneously relaxed by a sufficiently high electron heating using the pulsed sputtering with overshoots or the pulsed substrate bias U_{sp} with alternating polarity of pulses [17], see the film No. 4 in Table 7.1.

The macrostress σ and the microstructure of the sputtered film strongly influence also its resistance to cracking [19]. The effect of the microstructure of the Ti(Al,V)N film with a low compressive macrostress σ = - 0.4 GPa on its resistance to cracking is illustrated in Fig. 7.4. The resistance of the film to cracking was assessed by the indentation test in which the diamond indenter was impressed into the film surface under a high load L at which the film cracks [20]. Longer cracks mean a weaker resistance to cracking. On the other hand, shorter cracks mean an enhanced resistance to cracking.

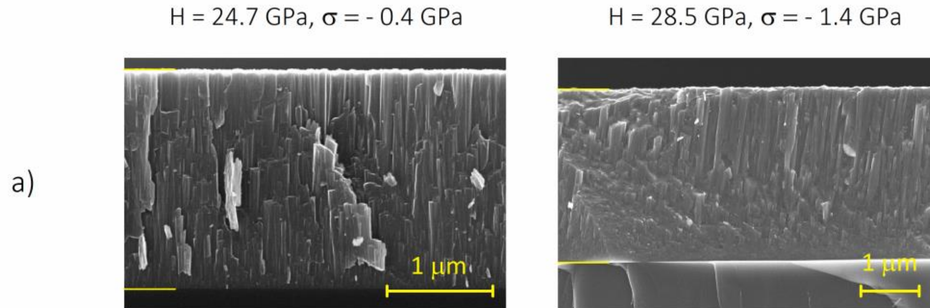

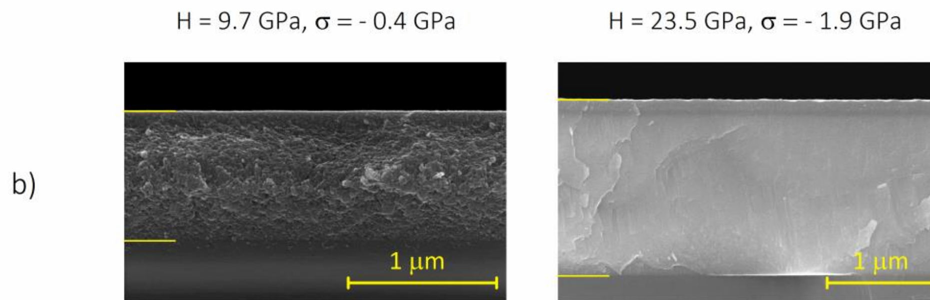

Figure 7.3 SEM images of a cross-section of the Ti(Al,V)N films with columnar microstructure (the films No. 1 and 2) and with non-columnar microstructure (the films No. 3 and 4). The films with numbers 1,2,3,4 are given in Fig. 7.1 and their physical and mechanical properties in Table 7.1.

Table 7.1 Physical and mechanical properties of four Ti(Al,V)N films denoted in Fig.1 as films No. 1, 2, 3, and 4.

Film No.	sputtering process	h [nm]	U_s [V]	i_s [mA/cm^2]	a_D [nm/min	$\mathcal{E}_{bi}$ [MJ/cm^3]	σ [GPa]	H [GPa]	E^* [GPa]	H/E^*	W_e [%]	L_{cr} [N]	microstructure
1	DC	2000	-20	0.7	17	0.5	-0.4	24.7	268	0.07	62	0.25	comulnar - voids
2	pulsed/100 kHz	2500	-20	1.8	22	2.2	-1.4	28.5	235	0.12	73	> 1	comulnar - dense
3	DC	1200	-20	1.9	15	3	-1.9	23.5	187	0.13	80	>1	non-columnar
4	pulsed/350 kHz	1000	-100*	1.5	11	8.1	-0.4	9.7	142	0.07	46	0.25	non-columnar
* pulsed discharge with strong overshoots													

Columnar microstructure

σ = - 0.4 GPa

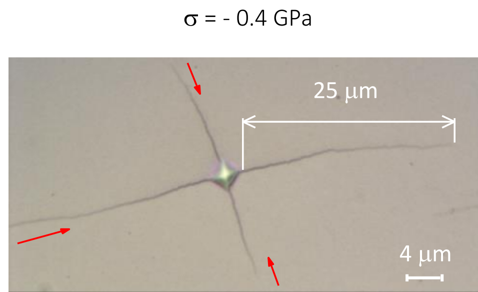

a)

Non-columnar microstructure

σ = - 0.4 GPa

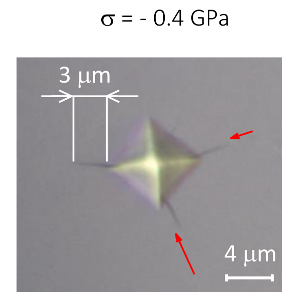

b)

Figure 7.4 LOM image of surface morphology of Ti(Al,V)N films after the indentation test. Measured Ti(Al.V)N films exhibit compressive macrostress σ = - 0.4 GPa and (a) columnar microstructure (the film No. 1) or (b) non-columnar microstructure (the film No. 4), respectively. Indentation test was carried out for load (a) L = 0.25 N or (b) L = 0.75 N, respectively.

The surface morphology of the Ti(Al,V)N film with columnar and non-columnar microstructure after indentation test at L = 0.25 N and L = 075 N is displayed in Fig. 7.4a and 7.4b, respectively. From this figure, it is seen that the film with columnar microstructure exhibits a low resistance to cracking. On the other hand, the film with non-columnar microstructure with shorter cracks even at a high load L exhibits an enhanced resistance to cracking. This experiment clearly shows that the film microstructure is a key parameter which decides on its resistance to cracking as shown in Ref. [14,15,20].

7.4. Conclusions

Main results of this investigation can be briefly summarized as follows

1. The hardness H of the film increases with increasing compressive macrostress σ.
2. The hardness H of the film is a complex function of two competing parameters: the energy $\mathcal{E}_{bi}$ and macrostress. Both parameters $\mathcal{E}_{bi}$ and σ influence the growth process of film and thereby also its structure, microstructure, and mechanical properties.
3. The compressive residual macrostress σ leads to an apparent increase in hardness H and fracture resistance of sputtered films.
4. The macrostress σ generated in the film during its growth can be simultaneously relaxed by the electron heating using either a pulsed sputtering with overshoots or a pulsed bias with pulses of alternating polarity. This way the different combination of mechanical properties of the film and its microstructure and macrostress σ can be achieved.
5. Hard films with high ratio H/E^* > 0.1, high elastic recovery W_e > 60%, dense, voids-free microstructure and compressive macrostress σ < 0 exhibit an enhanced resistance to cracking.
6. The energy $\mathcal{E}_{bi}$ is a key parameter which makes it possible to create the films with prescribed properties in the fully reproducible way.

Acknowledgments

This work was supported by the project LO1506 of the Czech Ministry of Education, Youth and Sports under program NPU I.

References

[1] K. Kondo, M. Nakabayashi, K. Kawakami, T. Chijimatsu, M. Nakaishi, M. Yamada, M. Yamabe, and K. Sugishima: Stress stabilization of βtantalum and its crystal structure, Journal of Vacuum Science & Technology A 11 (1993), 3067.

[2] M. Chhowalla, H. E. Unalan: Thin films of hard cubic Zr3N4 stabilized by stress, Nature Materials 4 (2005), 317–322.

[3] Y. Han, W.Y. Li, L. X. Cao, X.Y. Wang, B. Xu, B. R. Zhao, Y. Q. Guo, and J. L. Yang: Superconductivity in Iron Telluride Thin Films under Tensile Stress, PRL 104 (2010), 017003.

[4] G. A. Rossetti Jr., L. E. Cross, and K. Kushida: Stress induced shift of the Curie point in epitaxial PbTiO3 thin films, Applied Physics Letters 59 (1991), 2524.

[5] A.R. Shetty, A. Karimi: Texture change through film thickness and off-axis accommodation of (0 0 2) planes, Applied Surface Science 258 (2011), 1630– 1638.

[6] J.P. Zhao, Z.Y. Chen, X. Wang, Y.H. Yu, S.Q. Yang, T.S. Shi, X.H. Liu: The influence of ion energy on the structure of TiN films during filtered arc deposition, Nuclear Instruments and Methods in Physics Research B 135 (1998), 388-391.

[7] G. Abadias: Stress and preferred orientation in nitride-based PVD coatings, Surface & Coatings Technology 202 (2008), 2223–2235.

[8] G. Skordaris, K. D. Bouzakis, T. Kotsanis, P. Charalampous, E. Bouzakis, B. Breidenstein, B. Bergmann, B. Denkena: Effect of PVD film’s residual stresses on their mechanical properties, brittleness, adhesion and cutting performance of coated tools, CIRP Journal of Manufacturing Science and Technology 18 (2017), 145–151.

[9] W. Tillmann, T. Sprute, F. Hoffmann, Y. Chang, C. Tsai: Influence of bias voltage on residual stresses and tribological properties of TiAlVN-coatings at elevated temperatures, Surface & Coatings Technology 231 (2013), 122–125.

[10] O. Gonzalo, V. G. Navas, B. Coto, I. Bengoetxea, U. R. de Gopegi, M. Etxaniz: Influence of the coating residual stresses on the tool wear, Procedia Engineering 19 (2011), 106 – 111.

[11] J. Musil: Hard and superhard nanocomposite coatings, Surface and Coatings Technology 125 (2000), 322–330.

[12] S. Kataria, S.K. Srivastava, Praveen Kumar, G. Srinivas, Siju, Jakeer Khan, D.V. Sridhar Rao, Harish C. Barshilia: Nanocrystalline TiN coatings with improved toughness deposited by pulsing the nitrogen flow rate, Surface & Coatings Technology 206 (2012), 4279–4286.

[13] H. Poláková, J. Musil, J. Vlček, J. Allaart, C. Mitterer: Structure-hardness relations in sputtered Ti–Al–V–N films, Thin Solid Films 444 (2003), 189–198.

[14] J.Musil; Hard nanocomposite coatings: Thermal stability, oxidation resistance and toughness, Surf. Coat. Technol. 207 (2012), 50-65.

[15] J.Musil: Flexible hard nanocomposite coatings, RSC Advances 5 (2015), 60482-60495.

[16] M. Jaroš, J. Musil, R. Čerstvý and S. Haviar: Effect of energy on physical and mechanical properties of hard Ti(Al,V)Nx films prepared by magnetron sputtering, Surf.Coat.Technol. 332 (2017), 190-197.

[17] M. Jaroš, J. Musil, R. Čerstvý, S. Haviar: "*Effect of energy on macrostress in Ti(Al,V)N films prepared by magnetron sputtering*" under revision in journal Vacuum 2018

[18] J. Musil, Š. Kos, M. Jaroš, R. Čerstvý, S. Haviar, S. Zenkin, Z. Čiperová: "*Overstoichiometric* $TMN_{x>1}$ *transition metal nitride coatings*" Jap. J. Appl. Phys. (2018), submitted for publication

[19] G.G.Stoney: The transition of metallic films deposited by electrolysis, Proc. R. Soc. London, Ser. A82 (1909), 172-175.

[20] J.Musil: Advanced hard nanocomposite coatings with enhanced toughness and resistance to cracking, Chapter 7 in Thin Films and Coatings: Toughening and Toughening Characterization, S.Zhang (Editor) CRC Press, USA, 2015, pp. 377-463.

Paper VI

8. Hard TiN_2 dinitride films prepared by magnetron sputtering

J. Musil, **M. Jaroš**, Š. Kos, R. Čerstvý, S. Haviar

J. Vac. Sci. Technol. A 36, (2018) 040602

Abstract

This letter reports on the formation of hard TiN_2 dinitride films prepared by magnetron sputtering. TiN_2 films were reactively sputtered in an Ar +N_2 gas mixture using a pulsed dual magnetron with a closed magnetic field *B*. The principle of the formation of TiN_2 film by magnetron sputtering is briefly described. The stoichiometry x = N/Ti of the TiN_x film was controlled by deposition parameters, and its maximum value of x = 2.3 was achieved. For the first time, a possibility to form the TiN_2 dinitride films by magnetron sputtering has been demonstrated. Mechanical properties of sputtered films were investigated in detail.

Keywords: TiN_2 dinitride film, Structure, Microstructure, Mechanical properties, Magnetron sputtering

8.1. Introduction

Recently, a great attention has been devoted to the formation of nitrogen-rich $TMN_{x>1}$ transition metal nitrides with the stoichiometry x = N/TM ranging from 1 to 2 [1- 10] and also with x =4 [2]. Theoretical studies of these materials based on *ab initio* calculations show that these novel overstoichiometric nitrides should exhibit extraordinary properties such as superhardness, electrical conductivity, and optical transparency, which originate from metal-nitrogen charge transfer, the nature of the N-N bonds, and a mixture of ionic and covalent N-N bonds [11-14]. It was reported that bulk titanium dinitrides were successfully synthesized under High Pressure and High Temperature of (HPHT synthesis), i.e. using *an equilibrium process* [1, 4, 14-17]. For instance, The TiN_2 dinitride material with bulk modulus 360 - 385 GPa was synthesized from the titanium nitride flakes and N_2 gas compressed to 73 GPa and heated to 2400 K in a laser-heated diamond anvil cell [4]. Recently, it was reported that titanium dinitrides were prepared also as $TiN_{x=2}$ films at low pressures of about 0.3 Pa by the simultaneous action of a Ti evaporation by an arc evaporator and a strong ionization of N_2 gas in a gas-plasma source with a hot filament in a hollow cathode [18].

This article reports on the formation of overstoichiometric $TiN_{x>1}$ titanium nitride films by magnetron sputtering i.e., on the formation of films prepared by a *nonequilibrium deposition process* running at an atomic level. A principle of sputtering of $TMN_{x>1}$ overstoichiometric nitride films are briefly described. Interrelationships between the stoichiometry x, mechanical and electrical properties of TiN_x films are investigated in detail.

8.2. Principle of sputtering of $TMN_{x>1}$ nitride films

The principle of formation of overstoichiometric $TMN_{x>1}$ and $TMN_{x=2}$ dinitride films by magnetron sputtering is based on two non-equilibrium processes simultaneously running at atomic level: (1) the heating of the sputtered material to high temperatures first at the substrate and later at the growing film in areas where sputtered atoms and bombarding ions arrive with no or low substrate heating and (2) the pressing of heated areas at high pressures p_{HA}. This can be achieved by a high energy $\mathcal{E}$ delivered to the growing film by bombarding ions with energy $\mathcal{E}_{bi}$ controlled by the negative substrate bias U_s and/or by considering fast neutral atoms sputtered from the target and arriving at the substrate with energy $\mathcal{E}_{fn}$ of several electron-volts controlled by the sputtering gas presser p. Both energies $\mathcal{E}_{bi}$ and/or $\mathcal{E}_{fn}$ are sufficient to heat areas of incident ions or atoms to very high temperatures T, easily exceeding 2500 K, and simultaneously to press these areas at a high-pressure p_{HA} of about $300\mathcal{E}^{1/2}$ GPa, where the energy $\mathcal{E}$ is in electro-volt [10]. The main problem in the formation of overstoichiometric $TMN_{x>1}$ and $TMN_{x=2}$ dinitride films by magnetron sputtering is to increase the number n_N of nitrogen atoms in the magnetron discharge to achieve a high ratio n_N/n_{TM} > 1 which enables the formation of films with the stoichiometry x > 1 and x =2, respectively; here n_{TM} is the number of TM atoms in the sputtered film.

8.3. Experimental

The $TiN_{x>1}$ films were reactively sputtered by a pulsed hybrid dual magnetron (HDM) in a mixture N_2 + Ar. The HDM consists of two different magnetrons M_1 and M_2 with a closed magnetic field B. The magnetron M1 is magnetron with a very low sputtering of its target and the magnetron M2 is a standard, well sputtering magnetron. The low sputtering of the magnetron M1 is achieved by extraction of the central magnet from the magnetron M1. By control of the powers P_{M1} and P_{M2} delivered into the magnetron M1 and the magnetron M2, respectively, it is possible to increase ion bombardment of growing film by increasing the ion flux i_s while keeping the film deposition rate a_D constant, and in this way to sputter overstoichiometric TiN_x films with the stoichiometry x = N/Ti > 1. The increase in is at constant a_D is achieved by increasing the power P_{M1} delivered into the magnetron M1 and keeping the power P_{M2} delivered into the magnetron M2 constant. More details are given in Ref. [10].

The $TiN_{x>1}$ films were reactively sputtered in an N_2 +Ar mixture by pulsed HDM powered by a pulse power supply AE Pinnacle Plus + 5/5 kW (Advanced Energy, Inc.) and operated in a synchronous pulse mode at the repetition frequency $f_r = 1/T$ = 20 kHz and duty cycle τ/T = 0.99 onto Si (100) substrates in a deposition chamber evacuated to a base pressure $p_0 = 1 \times 10^{-3}$ Pa. A small amount of Ar of about 20% was added to N_2 gas to start the magnetron discharge at low values of sputtering gas. The elemental composition of the $TiN_{x>1}$ films on the Si substrate was analyzed in a scanning electron microscope (SU-70, Hitachi) operated at a primary electron energy of 15 keV using energy dispersive spectroscopy (EDS, UltraDry, Thermo Scientific) and wave dispersive spectroscopy (WDS, Magnaray, Thermo Scientific). The pure metal standard was used for the determination of Ti concentration. The nitrogen concentration was calculated as the difference to 100% wt. using a combined WDS and EDS analysis, since there is an inevitable peak overlap of Ti and N x-Ray peaks. The data were measured in the depth of about 600 nm under the film surface with an accuracy of ±10%.

8.4. Results and discussion

As an example, properties of two sputtered overstoichiometric $TiN_{x>1}$ films are reported in detail. Deposition parameters, elemental composition, mechanical properties, macrostress σ and electrical resistivity ρ of these $TiN_{x>1}$ films are summarized in Table 8.1.

From Table 8.1 we can observe the following

- The overstoichiometric $TiN_{x=2.3}$ can be sputtered by pulsed HDM at a low total pressure p_T = 0.17 Pa. This strongly overstoichiometric $TiN_{x=2.3}$ film is created thanks to a high energy $\mathcal{E}_{bi}$ = 8.2 MJ/cm^3 delivered to it by bombarding ions and developing a very high-pressure p_{HA}= 1340 GPa in place of their incidence [10]. The energy was calculated from the formula $\mathcal{E}_{bi} = U_s \times i_s/a_D$; here, Us and Is are the substrate bias and substrate ion current density, respectively [20]. This experiment demonstrates that the formation of $TiN_{x=2}$ dinitride films by magnetron sputtering is possible.
- The decrease of the total gas pressure p_T from 0.30 to 0.17 Pa and mainly the increase of the powers P_{M1} and P_{M2}in the magnetron M1 and M2, respectively, increasing an ionization of N_2 gas results not only in an increase of the stoichiometry x = N/Ti of the TiN_x film but also in a decrease of its hardness H, elastic recovery W_e and H/E^* ratio.
- The overstoichiometric $TiN_{x=2.3}$ film exhibits high hardness H = 16 GPa, high elastic recovery W_e = 69 % and high ratio H/E^* = 0.1.
- Both overstoichiometric films, $TiN_{x=1.4}$ and $TiN_{x=2.3}$, are well conductive and exhibit a low electrical resistivity $\rho \approx 1.5 \times 10^{-4}$ Ωcm.

Table 8.1 Deposition parameters, elemental composition, mechanical properties, macrostress σ and electrical resistivity ρ of two overstoichiometric $TiN_{x>1}$ films sputtered by pulsed HDM at T_s = 450°C, U_s = -20 V, i_s = 4.5 mA/cm², a_D = 6.6 nm/min, $\mathcal{E}_{bi}$ = 8.2 MJ/cm³, d_{s-t} = 80 mm and $p_T = p_{N2} + p_{Ar} \approx p_{N2}$ as a function of p_T.

Film No.	p_T [Pa]	P_{M1} [W]	P_{M2} [W]	h [nm]	N [at. %]	Ti [at. %]	x N/Ti	H [GPa]	E^* [GPa]	W_e [%]	H/E^*	σ [GPa]	ρ [Ω cm]
1	0.30	460	300	1000	58.5	41.5	1.4	25.5	190	84	0.13	-1.6	1.3×10^{-4}
2	0.17	528	380	1400	70	30	2.3	16	163	69	0.10	-1.7	1.6×10^{-4}

The structure of these overstoichiometric $TiN_{x>1}$ films, characterized by XRD diffraction, is displayed in Fig. 8.1. From this figure, it is seen that both films, $TiN_{x=1.4}$ and $TiN_{x=2.3}$, sputtered at T_s = 450°C and U_s = -20V are polycrystalline and their crystallinity improves with decreasing sputtering gas pressure p_T and increasing sputtering power. The decrease in sputtering gas pressure results in two effects: (1) the decrease in collisions between ions and neutral atoms in the substrate sheath with the sheath voltage $U_{sh} = U_p - U_s$ and thereby the increase in the energy $\mathcal{E}_i$ of incident ions and (2) the bombardment of the growing film by fast neutral atoms, which deliver further additional energy $\mathcal{E}_{fn}$ to $\mathcal{E}_{bi}$ into the growing film; here, U_p is the plasma potential. Both the increase in $\mathcal{E}_i$ and the energy $\mathcal{E}_{bi}$ contribute to the improvement of the film crystallinity.

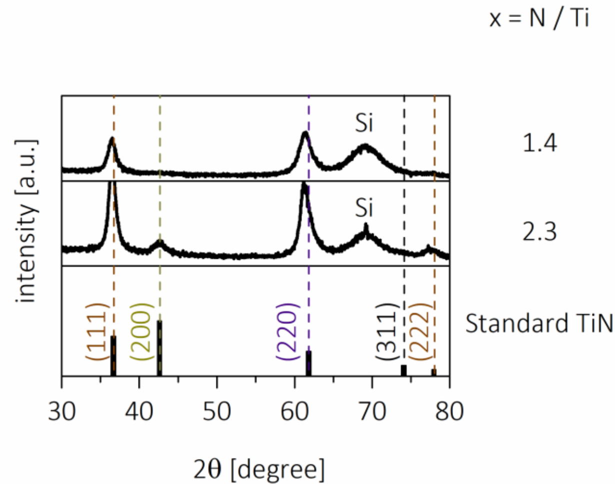

Figure 8.1 XRD patterns of the overstoichiometric $TiN_{x>1}$ films with stoichiometry x = 1.4 and 2.3.

The microstructure of the overstoichiometric $TiN_{x>1}$ films with x = 1.4 and 2.3 characterized by SEM is displayed in Fig. 8.2. The microstructure of the $TiN_{x=1.4}$ is non-columnar. On the other hand, the microstructure of $TiN_{2.3}$ film exhibits a dense, voids-free columnar microstructure. Despite this difference in microstructure both overstoichiometric $TiN_{x>1}$ films exhibit an enhanced resistance to cracking. It is due to their high ratio $H/E^* \geq 0.1$ and high elastic recovery $W_e > 60\%$; more details on an enhanced resistance to cracking of films with a dense, voids-free columnar microstructure is given in the reference [19].

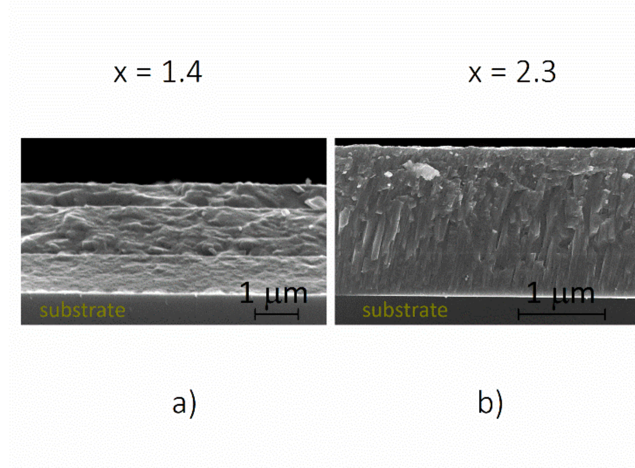

Figure 8.2 SEM images of a cross-section of overstoichiometric $TiN_{x>1}$ films with moderately and strongly enhanced stoichiometry x = N/Ti: (a) the moderately overstoichiometric $TiN_{x=1.4}$ film and (b) the strongly overstoichiometric $TiN_{x=2.3}$ film.

The stoichiometry x of the TiN_x film strongly influences also its color, see Fig. 8.3. The stoichiometric $TiN_{x=1}$ film is golden yellow. On the other hand, a strongly overstoichiometric $TiN_{x=2.3}$ film is brown.

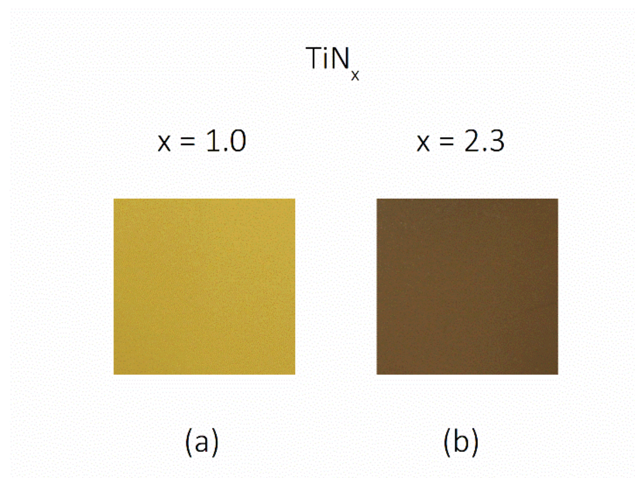

Figure 8.3 Color of TiN_x films with two different values of stoichiometry x. (a) The stoichiometric $TiN_{x=1}$ film with golden like color and (b) the strongly overstoichiometric $TiN_{x=2.3}$ film with brown color.

8.5. *Conclusions*

Main results of a reported investigation of strongly overstoichiometric $TiN_{x>1}$ films can be briefly summarized as follows

1. The strongly overstoichiometric $TiN_{x>1}$ films and TiN_2 dinitride films can be created by a pulsed magnetron if sputtering of its Ti target is reduced and the nitrogen gas is strongly ionized. This sputter deposition process can be realized by a hybrid dual magnetron or in a sputtering system equipped with a standard magnetron and a low-pressure source of strongly ionized nitrogen gas, for instance, a low-pressure arc [18].
2. The $TiN_{x=2.3}$ film with high values of the hardness H = 16 GPa, ratio H/E^* = 0.1, W_e = 70%, dense, voids-free microstructure and low compressive macrostress σ = -1.7 GPa were sputtered by the hybrid dual magnetron at extremely high energy $\mathcal{E}_{bi}$= 8 MJ/cm^3 delivered to growing film by bombarding ions.
3. The high value of $\mathcal{E}_{bi}$ is a necessary condition for the creation of strongly overstoichiometric $TiN_{x>1}$ films because it develops a very high-pressure $p_{HA} \approx$ 1340 GPa in place of incidence of arriving ions [10].
4. Overstoichiometric $TiN_{x>1}$ films are highly flexible films exhibit an enhanced resistance to cracking.
5. The $TiN_{x=2.3}$ film is brown compared with golden stoichiometric $TiN_{x=1}$ film and is well electrically conductive (ρ = 1.7 × 10^{-4} Ωcm).

Acknowledgments

This project was supported in part by the project No. LO 1506 of the Czech Ministry of Education, Youth and Sports under the Program NPU I.

References

[1] E.Horwath-Bordon, R.Riedel, A.Zerr, P.F.McMillan, G.Auffermann, Y.Prots, W.Bronger, R.Kniep, P.Kroll: High-pressure chemistry of nitride-based materials, Critical Review, Chemical Society Reviews, Chem. Soc. Rev. 35 (2006) 987.

[2] S.Aydin, Y.O.Ciftci, A.Tatar: Superhard transition metal tetranitrides: XN_4 (X = Re, Os, W), J.Mater.Res. 27 (13) (2012) 1705.

[3] H.Yan, M.Zhang, Q.Wei, P.Cuo: Theoretical study on tetragonal transition metal dinitrides from first principle calculations, Journal of Alloys and Compounds 581 (2013) 508.

[4] V.S.Bhadram, D.Y.Kim, T.A. Strobel: High-pressure synthesis and characterization of incompressible titanium pernitrides, Chemistry of materials (2016), doi: 10.1021/asc.chemmater.6b00042.

[5] S.Yu, B.Huang, X.Jia, Q.Zeng, A.R.Oganov, L.Zhang, G.Frapper: Exploring the real ground-state structures of molybdenum dinitride, The Journal of Physical Chemistry, Accepted manuscript, doi: 10.1021/acs.jpcc.6b00665.

[6] M.Zhang, K.Cheng, H.Yan, Q.Wei, B.Zheng: Electronic bonding analyses and mechanical strengths of incompressible tetragonal transition metal dinitrides TMN_2 (TM = Ti, Zr, and Hf), Scientific Reports, Nature Communication 6 (2016) 36911.

[7] S.Yu, Q.Zeng, A.R.Oganov, G.Frapper, L.Zhang: Phase stability, chemical bonding and mechanical properties of titanium nitrides: a first-principles study, Phys. Chem. Chem. Phys. 17 (2017) 11763.

[8] S.Yu, Q.Zeng, A.R.Oganov, G.Frapper, B.Huang, H.Niu, L.Zhang: First-principles study of Zr-N crystalline phases: phase stability, electronic and mechanical properties, RSC Advances 7 (2017) 4697.

[9] D.Edstrom, D.G.Sangiovanni, L.Hultman, I.Petrov, J.E.Greene, V.Chirita: Effect of incident N atom kinetic energy on TiN/TiN(001) film growth dynamics: A molecular dynamics investigation, J. Appl. Phys. 121 (2017) 025302.

[10] J.Musil, S.Kos, M.Jaros, R.Cerstvy, S.Haviar, S.Zenkin, Z.Ciperova: Overstoichiometric $TMN_{x>1}$ trasition metal nitride coatings, Jpn. J. Appl. Phys. (2018), submitted for publication March 14, 2018 and presented at the 10th International Symposium on Advanced Plasma Science and its Applications for Nitrides and Nanomaterials/11th International Conference on Plasma Nanotechnology and Science (ISPlasma 2018/IC-PLANTS 2018), March 4-8, 2018, Meijo University, Nagoya, Japan, Oral presentation No. 06B01O.

[11] A.F.Young, J.A.Montoya, C.Sanloup, M.Lazzeri, E.Gregoryanz, S.Scandolo: Interstitial dinitrogen makes PtN_2 an insulating hard solid, Phys. Rev. B: Condens. Matter. Phys. 73 (2006) 153102.

[12] Z.T.Y.Liu, D.Gall,S.V.Khare: Electronic and bonding analysis of hardness in pyrite-type transition-metal pernitrides, Phys .Rev. B: Condens. Matter Mater. Phys. 90 (2014) 134102.

[13] M.Wessel, R.Dronskowski: Nature of N-N bonding within high-pressure nobel-metal pernitrides and the prediction of lanthanum pernitride, J.A. Chem. Soc. 132 (2010) 2421.

[14] E.Gregoryanz, C.Sanloup, M.Somayazulu, J.Bardo, G.Fiquet, H.K.Mao, R.J.Hemley: Synthesis and characterization of a binary noble metal nitride, Nat. Mater. 3 (2004) 294.

[15] J.C.Crowhurt, A.F.Goncharov, B.Sadigh, C.L.Evans, P.G.Morrall, J.L.Fereira, A.J.Nelson: Synthesis and characterization of the nitrides of platinum and iridium, Science 311 (2006) 1275.

[16] A.F.Young, C.Sanloup, E.Gregoryanz, S.Scandolo, R.J.Hemley, H.K.Mao: Synthesis of novel transition metal nitrides IrN_2 and OsN_2, Phys. Rev. Lett. 96 (2006) 155501.

[17] J.C.Crowhurt, A.F.Goncharov, B.Sadigh, J.M.Zaug, D.Aberg, Y.Meng, V.B.Prakapenka: Synthesis of nitrides of iridium and palladium, J. Mater. Res. 23 (2008) 183.

[18] O.V.Krysina, N.N.Koval, I.V.Lopatin, V.V.Shugurov, S.S.Kowalsky: Generation of low-pressure arcs synthesis of nitride coatings, Journal of Physics: Conference Series 669 (2016) 012032.

[19] J.Musil, M.Jaroš, R.Čerstvý, S.Haviar: Evolution of microstructure and macrostress in sputtered hard Ti(Al,V)N films with increasing energy delivered during their growth by bombarding ions, J. Vac. Sci. Technol. A 35(2) (2017) 020601.

[20] J. Musil: Hard nanocomposite coatings: Thermal stability, oxidation resistance and toughness, Surf. Coat. Technol. 207 (2012) 50.

9. Main obtained results

This Ph.D. thesis is dedicated to the preparation and characterization of the multifunctional metal nitride thin films. The obtained results can be briefly summarized as follows:

1. *The energy $\mathcal{E}$*, which is a result of the combination of many parameters used in the deposition of the film, *is a key parameter* determining its final physical and functional properties. The validity of this statement was demonstrated on the evolution of the texture, microstructure, mechanical properties, resistance to cracking and macrostress of the Ti(Al,V)N nitride films with increasing energy $\mathcal{E}$ delivered in them during their growth. It was found that:
    a) The energy $\mathcal{E}$ delivered in the growing film at high sputtering gas pressures ($p \geq 1$ Pa) is dominated by bombarding ions ($\mathcal{E} \approx \mathcal{E}_{bi}$). On the other hand, the energy $\mathcal{E}$ supplied to the growing film at low sputtering gas pressures ($p < 1$ Pa) can be delivered either by the bombarding ions and/or fast neutrals $\mathcal{E}_{fn}$ ($\mathcal{E} \approx \mathcal{E}_{bi} + \mathcal{E}_{fn}$).
    b) The texture of the Ti(Al,V)N nitride films varies from the TiN(200) crystallographic orientation to the TiN(220) one with increasing energy $\mathcal{E}$.
    c) The hardness H, effective Young's modulus E^*, elastic recovery W_e, H/E^* ratio and compressive macrostress ($\sigma < 0$) in the Ti(Al,V)N nitride films increase with increasing energy $\mathcal{E}$.
    d) The columnar microstructure of the film varies from a columnar microstructure to a dense, voids-free microstructure with increasing energy $\mathcal{E}$.
    e) The films with the columnar microstructure and highly packed columns exhibit the compressive macrostress ($\sigma < 0$). It means that the line $\sigma = f(p) = 0$ is not the borderline between the zone *1* and the zone *T* in the Thornton's Structural Zone model (SZM) as it is reported so far but it lies inside the zone *1*.
    f) The compressive macrostress ($\sigma < 0$) in the film generated during its growth can be decreased during its growth by an electron bombardment realized either by the pulsed substrate bias U_{sp} with alternating negative and positive pulses or by the pulsed sputtering of the film at high repetition frequencies of pulses f_r.

2. The values of the plasma U_p and floating U_{fl} potential in magnetron discharges (i) strongly differ when a single magnetron or a dual magnetron is used, and (ii) strongly depends on the electrical connection of the power supply to the dual magnetron. Different values of the U_p and U_{fl} result in a great difference in the energy $\mathcal{E}$ delivered into the growing film, and therefore in different properties of sputter deposited films. The pulsed dual magnetron operating in an asynchronous regime ensures full reproducibility of the plasma and floating potential in generated discharge.

3. The strongly over-stoichiometric $TiN_{x\approx 2}$ films can be deposited by magnetron sputtering if (i) intensive dissociation and ionization of nitrogen gas, and (ii) reduction of sputtered Ti target atom are achieved. The high value of the energy of bombarding ions $\mathcal{E}_{bi} > 8$ MJ/cm^3 is the necessary condition for the creation of strongly over-stoichiometric $TiN_{x\approx 2}$ films.

List of publications of the author

Papers in international journals:

1. **M. Jaroš**, J. Musil, R. Čerstvý, S. Haviar: *"Effect of energy on structure, microstructure and mechanical properties of hard Ti(Al,V)N_x films prepared by magnetron sputtering"*
   Surf. Coat. Technol. 332 (2017) 190 – 197.
2. J. Musil, **M. Jaroš**: *"Plasma and floating potentials in magnetron discharges"*
   J. Vac. Sci. Technol. A. 35 (2017) 060605.
3. J. Musil, **M. Jaroš**, R. Čerstvý, S. Haviar: *"Evolution of microstructure and macrostress in sputtered hard Ti(Al,V)N films with increasing energy delivered during their growth by bombarding ions"*
   J. Vac. Sci. Technol. A. 35 (2017) 020601.
4. J. Musil, **M. Jaroš**, Š. Kos, R. Čerstvý, S. Haviar: "*Hard TiN_2 dinitride films prepared by magnetron sputtering*"
   J. Vac. Sci. Technol. A. 36 (2018) 040602.
5. **M. Jaroš**, J. Musil, R. Čerstvý, S. Haviar: "*Effect of energy on macrostress in Ti(Al,V)N films prepared by magnetron sputtering*"
   Vacuum 158 (2018) 52-59.
6. J. Musil, Š. Kos, **M. Jaroš**, R. Čerstvý, S. Haviar, S. Zenkin, Z. Čiperová: "*Overstoichiometric $TMN_{x>1}$ transition metal nitride coatings*"
   Jap. J. Appl. Phys. (2018), accepted for publication.
7. **M. Jaroš**, J. Musil, S. Haviar: "*Interrelationships among macrostress, microstructure and mechanical behavior of sputtered hard Ti(Al,V)N films*"
   Material Letters 235 (2019) 92.

Participation at international conferences

Oral presentation at international conferences

1. **M. Jaroš**, J. Musil, R. Čerstvý, S. Haviar
   L.6.6 "*Macrostress control in flexible Ti(Al,V)N films*"
   European material research society (E-MRS 2018) Spring Meeting
   18. – 22.6, 2018, Strasbourg, France
2. **M. Jaroš**, J. Musil
   TR3 "*Plasma and floating potentials in magnetron discharges*"
   16th International Conference on Reactive Sputter Deposition (RSD 2017)
   4.–6. 12. 2017, Plzeň, Czech Republic

3. **M. Jaroš**, J. Musil, R. Čerstvý, S. Haviar
   C1-O-TUE-AM2 "*Stress reduction in hard Ti(Al,V)N films resistant to cracking by energy delivered during their growth*"
   European Congress and Exhibition on Advanced Materials and Processes (EUROMAT2017)
   17.–22. 9. 2017, Thessaloniki, Greece

4. **M. Jaroš**, J. Musil, R. Čerstvý, S. Haviar
   F2-1-5 "*Effect of energy on structure, microstructure and enhanced resistance to cracking of hard sputter deposited Ti(Ni)N_x and Ti(Al,V)N_x films*"
   44th International Conference on Metallurgical Coatings and Thin Films (ICMCTF 2017)
   24.–28. 4. 2017, San Diego, USA

5. **M. Jaroš**, J. Musil, R. Čerstvý, S. Haviar
   "*Flexible hard Ti-based nitride films with enhanced resistance to cracking*"
   27th Symposium on Plasma Physics and Technology (SPPT 2016)
   20. - 23. 6. 2016, Prague, Czech Republic

6. **M. Jaroš**, J. Musil, R. Čerstvý, S. Haviar
   MN11 "*Effect of energy on texture and enhanced resistance to cracking of sputter deposited Ti(Ni)N_x and Ti(Al,V)N_x films*"
   4th International Workshop and the 3rd International Mini-Workshop on Solution Plasma and Molecular Technologies (SPM-4 and Mini SPM-3)
   7. - 11. 6. 2016, Plzeň, Czech Republic

7. **M. Jaroš**, J. Musil, R. Čerstvý, S. Haviar
   O7.4-028 "*Effect of energy on texture and enhanced resistance to cracking of sputter deposited Ti(Ni)N_x and Ti(Al,V)N_x films*"
   4th Magnetron, Ion processing and Arc Technologies European Conference and 14th International Symposium on Reactive Sputter Deposition (MIATEC and RSD)
   8. - 11. 12. 2015, Paris, France

Poster presentation at international conferences

1. **M. Jaroš**, J. Musil, R. Čerstvý, S. Haviar
   "*Role of energy delivered to sputtered Ti(Al,V)N films on its physical and mechanical properties*"
   15th International Conference on Reactive Sputter Deposition 2016 (RSD2016)
   1. - 2. 12. 2016 Ghent, Belgium

2. **M. Jaroš**, J. Musil, R. Čerstvý, S. Haviar
   PO2071 "*Flexible hard Ti-based nitrides films with enhanced resistance to cracking*"
   15th International Conference on Plasma Surface Engineering (PSE 2016)
   12. - 16. 9. 2016 Garmisch-Partenkirchen, Germany

Abstract

The Ph.D. thesis is dedicated to reactive magnetron sputtering of flexible hard coatings, and it is divided into 9 main chapters.

Chapter 1 is introduction focusing on the energy $\mathcal{E}$ delivered into the coating during the deposition, as the main parameter which controls the property of the deposited coating. The control of the energy $\mathcal{E}$ is outlined.

Chapter 2 shows the main aims of the Ph.D. thesis. Chapters 3 – 8 shows the results of the thesis in the form of already published articles.

Chapter 3 reports on the effect of the energy $\mathcal{E}_{bi}$, delivered to the sputtered Ti(Al,V)N coating by bombarding ions, on its microstructure, macrostress, mechanical properties, and resistance to cracking. It was shown that (1) the increase of the energy $\mathcal{E}_{bi}$ makes it possible to convert (i) the film microstructure from columnar to dense, non-columnar, (ii) the macrostress from tensile to compressive (iii) the brittle hard coatings to the flexible hard coatings. (2) The flexible hard Ti(Al,V)N coatings with high ratio $H/E^* > 0.1$, high $W_e > 60\%$ and $\sigma < 0$ can be formed not only in the Transition Zone *T* but also in Zone *1* in which the films exhibit a columnar microstructure. (3) The line corresponding to the films with zero macrostress lies in Zone *1* corresponding to the columnar microstructure.

Chapter 4 reports on the effect of the energy $\mathcal{E} = \mathcal{E}_{bi} + \mathcal{E}_{fn}$ of bombarding ions $\mathcal{E}_{bi}$ and/or fast neutrals $\mathcal{E}_{fn}$ on its physical and mechanical properties, and resistance to cracking. It was shown that (1) The energy $\mathcal{E}$ is a key parameter controlling the properties of sputtered Ti(Al,V)N coatings. (2) The structure of coatings varies from TiN(200) to TiN(220) with increasing energy $\mathcal{E}$. (3) The coatings with $H/E^* \geq 0.1$, $W_e \geq 60\%$ and dense microstructure exhibit an enhanced resistance to cracking and are produced when a sufficient energy $\mathcal{E}$ is delivered to the growing coating. (4) The energy $\mathcal{E}_{fn}$ makes it possible to sputter crystalline coatings on dielectric substrates held on a floating potential.

Chapter 5 reports on the plasma U_p and floating U_{fl} potentials in magnetron discharges. It is shown that (1) the differences in U_p and U_{fl} result in strongly different properties of the coatings sputtered by single and dual magnetrons at the same power delivered to the magnetron discharge. (2) In the DC single and dual magnetron discharges, the U_p and U_{fl} depend on the electric conductivity of the surface of the grounded deposition chamber. (3) The pulsed dual magnetron sputtering system enables to sputter coatings with fully reproducible properties.

Chapter 6 reports on the effect of the energy $\mathcal{E}$ delivered into the growing Ti(Al,V)N coatings on its macrostress, microstructure, mechanical properties and resistance to cracking. It is shown that (1) the compressive macrostress can be reduced either by the pulsed bipolar substrate voltage U_{sp} or the electron and ion bombardment during overshoots in the pulsed magnetron sputtering. (2) For formation of flexible coatings, the high compressive macrostress is not needed when coatings exhibit high ratio and non-columnar microstructure.

Chapter 7 reports on the influence of a compressive macrostress in the Ti(Al,V)N coatings on their mechanical properties, structure, microstructure, and resistance to cracking. The macrostress is controlled by the energy $\mathcal{E}_{bi}$. It is shown that (1) the compressive macrostress increases the hardness *H* and the ratio H/E^* of the coatings. (2) The coatings exhibit a dense non-columnar microstructure when the energy $\mathcal{E}_{bi} \geq 3$ MJ/cm^3. (3) The enhanced resistance to cracking of the coatings is controlled by its mechanical properties, microstructure, and macrostress σ.

Chapter 8 reports on the formation of TiN_2 dinitride coatings. For the first time, a possibility to form the TiN_2 dinitride coatings by magnetron sputtering has been demonstrated. The principle of the formation of TiN_2 coatings is briefly described. Mechanical properties of sputtered coatings were investigated in detail.

Chapter 9 contains the main obtained results of the Ph.D. thesis.

Resumé

Disertační práce je zaměřena na reaktivní magnetronové naprašování tvrdých flexibilních povlaků a je rozdělena na 9 hlavních kapitol.

Kapitola 1 je úvod se zaměřením na energii $\mathcal{E}$ dodanou do povlaků během depozice jako hlavního parametru, který ovlivňuje vlastnosti deponovaných povlaků. Dále jsou zmíněny možnosti kontroly energie $\mathcal{E}$.

Kapitola 2 ukazuje hlavní cíle disertační práce. Kapitoly 3 – 8 ukazují výsledky práce ve formě již publikovaných článků.

Kapitola 3 pojednává o vývoji mikrostruktury a vnitřního pnutí u tvrdých Ti(Al,V)N nitridových povlaků připravených magnetronovou depozicí v závislosti na energii iontového bombardu $\mathcal{E}_{bi}$ dodané během jejich růstu. Bylo zjištěno, že: (1) Navýšení energie $\mathcal{E}_{bi}$ dodané do povlaků umožní: (i) přeměnu sloupcovité mikrostruktury na zhuštěnou, (ii) změnu tahového pnutí na pnutí tlakové, (iii) přechodu od křehkých povlaků s nízkým poměrem $H/E^* < 0.1$ a nízkou elastickou vratností $W_e < 60$ % k ohebným materiálům s vysokým poměrem $H/E^* > 0.1$ a vysokou elastickou vratností $W_e > 60$ %. (2) Tlakové vnitřní pnutí se u ohebných povlaků může vytvářet v Zóně *T* i v Zóně *1*. (3) Linie korespondující s nulovým stresem ($\sigma = 0$) leží v Zóně *1* (povlaky se sloupcovitou strukturou).

Kapitola 4 pojednává o efektu energie bombardujících iontů ($\mathcal{E}_{bi}$) a rychlých neutrálů ($\mathcal{E}_{fn}$) dodané do Ti(Al,V)N nitridových povlaků během depozice na jejich strukturu, mikrostrukturu, mechanické vlastnosti a odolnost proti vzniku trhlin. Bylo prokázáno, že: (1) energie $\mathcal{E} = \mathcal{E}_{bi} + \mathcal{E}_{fn}$ dodaná do povlaků během jejich růstu je klíčový parametr rozhodující o vlastnostech povlaků. (2) Struktura povlaků se mění z TiN(200) na TiN(220) se zvětšující se energií $\mathcal{E}$. (3) Povlaky vykazující $H/E^* > 0.1$, $W_e > 60$ % a zhuštěnou strukturu také vykazují zvýšenou odolnost proti vzniku trhlin. (4) Pomocí energie rychlých neutrálů $\mathcal{E}_{fn}$ je možné připravit flexibilní povlaky na nevodivém podkladu.

Kapitola 5 pojednává o rozdílu mezi plazmovým U_p a plovoucím U_{fl} potenciálem během magnetronového výboje. Je ukázáno, že: (1) rozdíly v U_p a U_{fl} vyústí v rozdílné vlastnosti připravovaných povlaků v závislosti na tom, zda povlaky byly připravovány pomocí jednoduchého či duálního magnetronu, (2) v případě výboje vytvářeného stejnosměrným proudem je velikost U_p a U_{fl} silně závislá na vodivosti uzemněné depoziční komory a (3) pulzní duální magnetronový systém umožňuje vytvářet povlaky s reprodukovatelnými vlastnostmi.

Kapitola 6 pojednává o efektu energie $\mathcal{E}$ dodané do Ti(Al,V)N povlaků na jejich tlakové pnutí, mikrostrukturu, mechanické vlastnosti a odolnost proti vzniku trhlin. Je ukázáno, že: (1) tlakové pnutí může být redukováno pomocí pulzního bipolárního napětí U_{sp} na substrátu, nebo pomocí pulzního kladného napětí na magnetronech. (2) Vykazují-li vrstvy vysoký poměr H/E^* a zhuštěnou strukturu, pak vysoké tlakové pnutí není nutná podmínka pro vytváření povlaků se zvýšenou odolností proti vzniku trhlin.

Kapitola 7 shrnuje vliv tlakového pnutí u Ti(Al,V)N nitridových povlaků na mechanické vlastnosti, mikrostrukturu a odolnost proti vzniku trhlin. Tlakové pnutí bylo kontrolováno energií $\mathcal{E}_{bi}$ dopadajících iontů do vrstev během jejich růstu. Je ukázáno, že: (1) tlakové pnutí zvyšuje tvrdost *H* a poměr H/E^*. (2) Povlaky s hustou mikrostrukturou a se zvýšenou odolností proti vzniku trhlin jsou deponovány při $\mathcal{E}_{bi} > 3$ MJ/cm^3. (3) Odolnost proti vzniku trhlin Ti(Al,V)N povlaků je kontrolována jejich mechanickými vlastnostmi, mikrostrukturou a tlakovým pnutím.

Kapitola 8 pojednává o formaci tvrdých TiN_2 nitridových povlaků. Poprvé byla demonstrována možnost vytvoření TiN_2 povlaků pomocí magnetronové depozice. Jsou popsány podmínky, za kterých dochází k formování povlaků TiN_2. Mechanické vlastnosti deponovaných povlaků jsou detailně diskutovány.

Kapitola 9 je věnována hlavním dosaženým výsledkům.

CrossMark
click for updates

LETTERS

Evolution of microstructure and macrostress in sputtered hard Ti(Al,V)N films with increasing energy delivered during their growth by bombarding ions

Jindřich Musil,[a] Martin Jaroš, Radomír Čerstvý, and Stanislav Haviar
Department of Physics and NTIS–European Centre of Excellence, University of West Bohemia, Univerzitní 8, CZ-306 14 Plzeň, Czech Republic

(Received 10 September 2016; accepted 1 November 2016; published 15 November 2016)

This letter reports on the effect of the energy $\mathcal{E}_{bi}$, delivered to the sputtered Ti(Al,V)N film by bombarding ions, on its microstructure, macrostress σ, mechanical properties, and resistance to cracking. The films were deposited by reactive magnetron sputtering. Interrelationships between these parameters were investigated in detail. It was shown that (1) the increase of the energy $\mathcal{E}_{bi}$ makes it possible to convert (1) the film microstructure from columnar to dense, noncolumnar, (2) the macrostress σ from tensile ($\sigma > 0$) to compressive ($\sigma < 0$), (3) the brittle hard film with low ratio $H/E^* < 0.1$ and low elastic recovery $W_e < 60\%$ to the flexible hard film with high ratio $H/E^* \geq 0.1$ and high elastic recovery $W_e \geq 60\%$, (2) the flexible hard Ti(Al,V)N films with high ratio $H/E^* \geq 0.1$, high elastic recovery $W_e \geq 60\%$, and compressive macrostress can be formed not only in the transition zone (zone T in which the films exhibit a dense, voids-free microstructure) of the Thornton's structural zone model (SZM) but also in zone 1 in which the films exhibit a columnar microstructure and (3) the line corresponding to the films with zero macrostress ($\sigma = 0$) in the SZM lies in zone 1 corresponding to the columnar microstructure; here, H is the film hardness and $E^* = E(1 - \nu^2)$ is the effective Young's modulus, E is the Young's modulus, and ν is the Poisson's ratio. © *2016 American Vacuum Society*. [http://dx.doi.org/10.1116/1.4967935]

I. INTRODUCTION

Recently, the hard nanocomposite films with enhanced hardness and unique properties, for instance, the films with high temperature stability and oxidation resistance considerably higher than 1000 °C, high erosion resistance, high electrical conductivity, high optical transparency, etc., have been developed.[1–35] The detailed investigation of correlations between the physical and mechanical properties of these films has shown that it is also possible to create the flexible films which are simultaneously hard and resistant to cracking.[36–44] Such films exhibit a high ratio of the hardness H and the effective Young's modulus E^* ($H/E^* \geq 0.1$), high elastic recovery $W_e \geq 60\%$, compressive macrostress ($\sigma < 0$), and a dense voids-free microstructure; here, $E^* = E/(1 - \nu^2)$, E is the Young's modulus and ν is the Poisson's ratio.[28,45,46] These properties of flexible hard films can be achieved by optimization of the deposition parameters used in sputtering. In this article, it is demonstrated that these parameters are well controlled by the energy $\mathcal{E}_{bi}$ delivered to the growing film by bombarding ions. It is shown that the Ti(Al,V)N films exhibit (1) a columnar microstructure and low resistance to cracking when sputtered at low energy $\mathcal{E}_{bi}$ and (2) a dense, voids-free microstructure and an enhanced resistance to cracking when sputtered at high energy $\mathcal{E}_{bi}$. In the simplest case of a collisionless, fully ionized plasma, the energy $\mathcal{E}_{bi}$ can be expressed in the following form:[28,45–47]

$$\mathcal{E}_{bi}[J/cm^3] = (U_s - U_p)\, i_s/a_D \approx (U_s i_s)/a_D. \quad (1)$$

Equation (1) clearly shows two important facts. The energy $\mathcal{E}_{bi}$ delivered to the growing film by bombarding ions (1) can be easily calculated from measured deposition parameters (U_s, i_s) and the film deposition rate $a_D = h/t_d$ calculated from the measured film thickness h and the deposition time t_d and (2) strongly depends not only on U_s and i_s but also on a_D. The second fact is of extraordinary importance in (1) the reactive sputtering of compounds and (2) the high-rate sputtering of films because the energy $\mathcal{E}_{bi}$ delivered to the growing film deceases with increasing a_D.

The main aim of this letter is to report on results of the detailed investigation of the correlations between the microstructure, structure, macrostress σ, and resistance against cracking of the Ti(Al,V)N film sputtered as a function of the energy $\mathcal{E}_{bi}$ delivered to it by bombarding ions during its growth.

II. EXPERIMENT

The $Ti(Al,V)N_x$ films were sputter deposited in a mixture of $Ar + N_2$ sputtering gases using a DC dual magnetron with closed magnetic field equipped with a TiAlV (6 at. % Al; 4 at. % V) alloy target of diameter ∅ = 50 mm. Magnetrons

[a]Electronic mail: musil@kfy.zcu.cz

RIGHTSLINK

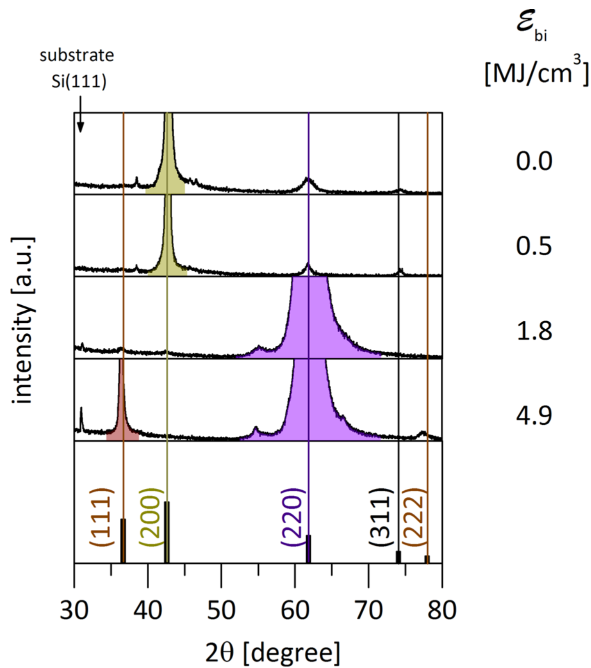

FIG. 1. (Color online) Evolution of XRD patterns of Ti(Al,V)N films with increasing energy $\mathcal{E}_{bi}$ delivered to them during their growth by bombarding ions. Deposition parameters: $I_d = 0.5$ A, $T_s = 500$ °C, $W_t \approx 10$ W/cm^2, $pN_2 = 0.8$ Pa, $p_T = p_{Ar} + pN_2 = 1$ Pa, and U_s ranging from 0 to −100 V. Physical and mechanical properties of these films are given in Table I.

were tilted to the normal of the substrate surface at the angle of 20°. The films were sputtered on Si(111) and Mo substrates at the discharge current $I_d = 0.5$ A, target power density $W_t = I_d U_d/S \approx 10$ W/cm^2, substrate temperature $T_s = 500$ °C, substrate bias U_s ranging from 0 to −100 V, substrate-to-target distance $d_{s\text{-}t} = 60$ mm, partial pressure of nitrogen $p_{N2} = 0.8$ Pa, and total pressure of sputtering gas $p_T = p_{Ar} + p_{N2} = 1$ Pa; here U_d is discharge voltage and S is the area of the target. The Ti(Al,V)N_x films sputtered under these conditions are crystalline and almost stoichiometric $x = N/(Ti + Al + V) \approx 1$ (see Fig. 1).

The film thickness h and the macrostress σ were measured by a DEKTAK 8 Stylus Profiler, Veeco. The film structure was characterized by an XRD spectrometer PANalytical X'Pert PRO in the Bragg-Brentano configuration using CuKα radiation ($\lambda = 0.154187$ nm). The mechanical properties were determined from load versus displacement curves measured by a Fisherscope H 100VP with a Vickers diamond indenter at load L = 20 mN at d/h < 0.1; here, d is the diamond impression in the film at L = 20 mN. The resistance of the Ti(Al,V)N film to cracking was assessed by the indentation test in which the diamond indenter was impressed in the film at high load L = 1 N; for more details, see Ref. 46.

III. RESULTS AND DISCUSSION

The interrelationships between the mechanical properties (H, E^*, W_e, and H/E^*) of the Ti(Al,V)N film, its macrostress

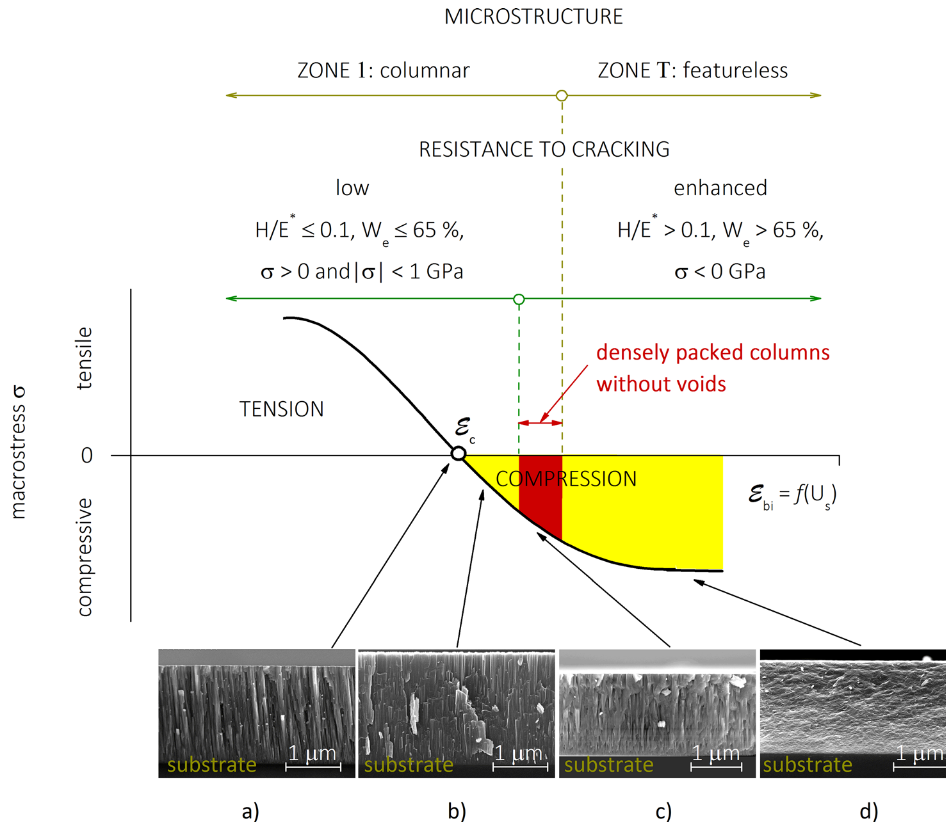

FIG. 2. (Color online) Schematic illustration of the interrelationships between the microstructure, mechanical properties, macrostress σ of the Ti(Al,V)N film, its resistance to cracking, and the energy $\mathcal{E}_{bi}$ delivered to the growing film by bombarding ions in the DC reactive magnetron sputtering. (a) The film no. 1, (b) the film no. 2, (c) the film no. 3, and (d) the film no. 4 (see Table I).

RIGHTSLINK

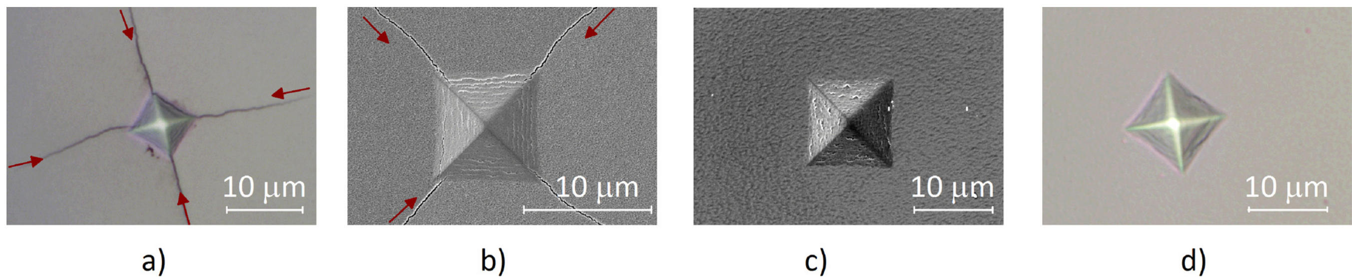

FIG. 3. (Color online) Evolution of the microstructure, the surface morphology with the diamond indenter impression at load L = 1 N and the macrostress σ of the Ti(Al,V)N film with increasing energy $\mathcal{E}_{bi}$. (a) $\mathcal{E}_{bi} = 0$ MJ/cm^3, $\sigma = 0$ GPa, (b) $\mathcal{E}_{bi} = 0.5$ MJ/cm^3, $\sigma = -0.4$ GPa, (c) $\mathcal{E}_{bi} = 1.8$ MJ/cm^3, $\sigma = -2.5$ GPa, and (d) $\mathcal{E}_{bi} = 4.9$ MJ/cm^3, $\sigma = -5.5$ GPa.

σ, microstructure, resistance to cracking, and the energy $\mathcal{E}_{bi}$ delivered to the growing film by bombarding ions were investigated in detail. These interrelationships are schematically illustrated in Fig. 2. Figure 2 displays the evolution of the microstructure, mechanical properties, and the TEM cross-sectional images of the Ti(Al,V)N film with increasing energy $\mathcal{E}_{bi}$. Figure 3 displays the evolution of the surface morphology of the Ti(Al,V)N films after the indentation at high load L = 1 N with increasing energy $\mathcal{E}_{bi}$. Figure 4 shows the transition of the films with a columnar microstructure to the films with a dense, voids-free microstructure with increasing energy $\mathcal{E}_{bi}$. The physical and mechanical properties of these films are given in Table I.

Main conclusions which can be drawn from Figs. 2 and 3 and Table I are the following:

(1) The density of the Ti(Al,V)N film microstructure and the macrostress σ both increase with increasing energy $\mathcal{E}_{bi}$. The microstructure gradually changes from columnar with voids [Fig. 2(a)] to a dense, voids-free microstructure without columns [Fig. 2(d)]. The increase of the energy $\mathcal{E}_{bi}$ results in an increased mobility of the condensing atoms at the surface of the growing film, the microstructure densification and a transition from films with a columnar microstructure to films with a dense, voids-free microstructure.

(2) The Ti(Al,V)N films with a columnar microstructure can exhibit not only tensile macrostress ($\sigma > 0$) but also compressive macrostress ($\sigma < 0$). The compressive macrostress arises when the columns are in a strong contact.

(3) The Ti(Al,V)N films with a columnar microstructure and a weak contact between columns (the low compressive macrostress $|\sigma| \to 0$), however, exhibit low resistance to cracking, see the cracks on the photo in Fig. 3(b). Responsible for the cracking of this films are: (1) the columnar microstructure, (2) the low ratio $H/E^* < 0.1$, (3) the low compressive macrostress $|\sigma| \le 0.5$ GPa and (4) the low elastic recovery $W_e \approx 60\%$ (see Table I).

(4) The Ti(Al,V)N films with a dense microstructure {the very densely packed columns [Fig. 2(c)] and the featureless microstructure without columns corresponding to zone T of the Thornton's structural zone model

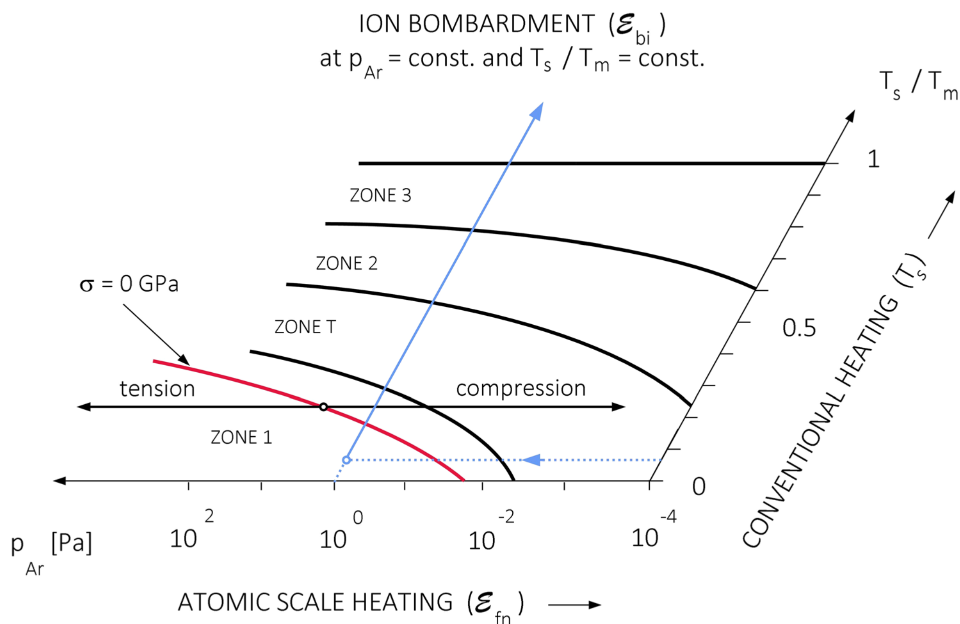

FIG. 4. (Color online) Schematic illustration of two dimensional (2D) Thornton's SZM showing that the line corresponding to the films with zero macrostress ($\sigma = 0$) lies in zone 1. $\mathcal{E}_{fn}$ and $\mathcal{E}_{bi}$ denote the energy delivered to the growing film by fast neutral particles, i.e., by bombarding and condensing fast atoms, and bombarding ions, respectively.

RIGHTSLINK Copyright Clearance Center

TABLE I. Physical and mechanical properties of $Ti(Al,V)N_x$ films sputtered by the DC magnetron at $I_d = 0.5$ A, $W_t \approx 10$ W/cm^2, $T_s = 500$ °C, $d_{s\text{-}t} = 60$ mm, $pN_2 = 0.8$ Pa, and $p_T = 1$ Pa as a function of the substrate bias U_s.

Film no.	$\mathcal{E}_{bi}$ (MJ/cm^3)	U_s (V)	i_s (mA/cm^2)	a_D (nm/min)	h (nm)	H (GPa)	E^* (GPa)	W_e (%)	H/E^*	σ (GPa)	Microstructure
1	0	0	0	12.8	1700	25.2	260	64	0.097	≈0.0	Columnar with voids
2	0.5	−20	0.7	16.7	2000	24.7	268	62	0.092	−0.4	Columnar with voids
3	1.8	−50	0.9	16.2	2100	32.6	275	76	0.119	−2.5	Columnar, voids-free
4	4.9	−100	1.1	13.7	1400	30.1	240	79	0.125	−5.5	Dense, voids-free

(SZM)[48,49] [Fig. 2(d)]} exhibit enhanced resistance to cracking. These films are characterized by (1) a dense voids-free microstructure, (2) the high ratio $H/E^* > 0.1$, (3) the high compressive macrostress $|\sigma| \geq 0.5$ GPa, and (4) the high elastic recovery $W_e \geq 70\%$.

(5) The highest energy of 4.9 MJ/cm^3 cannot be considered as the optimal energy because the Ti(Al,V)N film sputtered at $\mathcal{E}_{bi} = 4.9$ MJ/cm^3 already exhibits too high compressive macrostress $\sigma = -5.5$ GPa, which may result in the film delamination from the substrate when the film is too thick. The films with high ratio $H/E^* > 0.1$, high elastic recovery $W_e > 60\%$, a dense, voids-free microstructure, and a lower compressive macrostress ($\sigma = -2.5$ GPa) are good flexible, hard films with enhanced resistance to cracking.

In Fig. 2, $\mathcal{E}_c$ denotes the critical energy $\mathcal{E}_{bi}$ at which the sputtered films exhibit zero macrostress ($\sigma = 0$). The critical energy $\mathcal{E}_c$ depends on the elemental composition of the film and the ratio T_s/T_m; here, T_s is the substrate temperature and T_m is the melting temperature of the film's material.[28,45] The films sputtered at low energies ($\mathcal{E}_{bi} < \mathcal{E}_c$) exhibit tensile stress ($\sigma > 0$) and the films sputtered at high energies ($\mathcal{E}_{bi} > \mathcal{E}_c$) exhibit compressive stress ($\sigma < 0$). Our experiments show that the line $\sigma = f(p_{Ar})$ corresponding to the films with zero macrostress ($\sigma = 0$) in the Thornton's SZM (Refs. 48 and 49) lies in zone 1, see the curve in Fig. 4. It means that the films with a columnar structure can exhibit also compressive stress ($\sigma < 0$). In the case when the value of the compressive macrostress ($\sigma < 0$) is low, the film with a columnar microstructure easily cracks. This fact was confirmed also in the paper of Pei *et al.*[50] in which the cracking of the TiC/a-C:H films with a columnar microstructure sputtered at a quite high negative substrate bias $U_s = -100$ V is reported. In the case when the value of the compressive macrostress is sufficiently high the films with a columnar microstructure exhibit strongly enhanced resistance to cracking. The blue straight line in Fig. 4 shows the evolution of the film microstructure from columnar to dense, voids-free with increasing ion bombardment ($\mathcal{E}_{bi}$) at constant values of Ar pressure p_{Ar} and T_s/T_m ratio.

IV. CONCLUSIONS

In summary we can conclude that (1) the flexible hard Ti(Al,V)N films with enhanced resistance to cracking can be formed when the energy $\mathcal{E}_{bi}$ delivered to them during their growth is greater than the critical energy $\mathcal{E}_c$; (2) the critical energy $\mathcal{E}_c$ depends on the elemental composition of the film and the ratio T_s/T_m; (3) the flexible hard Ti(Al,V)N films exhibit high ratio $H/E^* \geq 0.1$, high elastic recovery $W_e > 70\%$, compressive macrostress ($\sigma < 0$), and dense, voids-free microstructure; (4) the flexible hard films with columnar voids-free microstructure can be also formed when these films exhibit the compressive macrostress ($\sigma < 0$); (5) the formation of flexible hard Ti(Al,V)N films can be efficiently controlled by the energy $\mathcal{E}_{bi}$ delivered to them during their growth by bombarding ions; and (6) the line $\sigma = f(p)$ corresponding to the films with zero macrostress ($\sigma = 0$) lies in zone 1 of the Thornton's SZM in which films with columnar microstructure are created. All these conclusions are of general validity and were confirmed already in nine different material coating systems.[36–44] Obtained results deepen the present state of the knowledge in the field and represent a huge application potential.

ACKNOWLEDGMENT

This work was supported by the Czech Science Foundation under Project No. GA16-18183S.

[1] H. Gleiter, Prog. Mater. Sci. **33**, 223 (1989).
[2] S. Veprek and S. Reiprich, Thin Solid Films **268**, 64 (1995).
[3] H. Gleiter, Nanostruct. Mater. **6**, 3 (1996).
[4] S. Yip, Nature **391**, 532 (1998).
[5] A. A. Voevodin and J. S. Zabinski, Diamond Relat. Mater. **7**, 463 (1998).
[6] J. Musil, Surf. Coat. Technol. **125**, 322 (2000).
[7] H. Gleiter, Acta Mater. **48**, 1 (2000).
[8] A. Leyland and A. Matthews, Wear **246**, 1 (2000).
[9] L. Hultman, Vacuum **57**, 1 (2000).
[10] R. Hauert and J. Patscheider, Adv. Eng. Mater. **2**, 247 (2000).
[11] S. Veprek, *Handbook of Ceramic Hard Materials*, edited by R. Riedel (Wiley-VCH, Weinheim, 2000), pp. 104–139.
[12] H. Gleiter, Scr. Mater. **44**, 1161 (2001).
[13] R. A. Andrievskii, Russ. Chem. Rev. **71**, 853 (2002).
[14] J. Patscheider, MRS Bull. **28**, 180 (2003).
[15] S. Zhang, D. Sun, Y. Fu, and H. Du, Surf. Coat. Technol. **167**, 113 (2003).
[16] R. A. Andrievski, Russ. Chem. Rev. **74**, 1061 (2005).
[17] S. Zhang, D. Sun, Y. Fu, and H. Du, Surf. Coat. Technol. **198**, 2 (2005).
[18] J. Musil, *Nanostructured Coatings*, edited by J. T. M. De Hosson and A. Cavaleiro (Springer Science + Business Media, LCC, New York, 2006), pp. 407–463.
[19] L. Hultman and C. Mitterer, *Nanostructured Coatings*, edited by J. T. M. De Hosson and A. Cavaleiro (Springer Science + Business Media, LCC, New York, 2006), pp. 464–510.
[20] P. H. Mayrhofer, C. Mitterer, and L. Hultman, Prog. Mater. Sci. **51**, 1032 (2006).
[21] C. Lu, Y. W. Mai, and Y. G. Shen, J. Mater. Sci. **41**, 937 (2006).
[22] C. S. Sandu, F. Medjani, and R. Sanjines, Rev. Adv. Mater. Sci. **15**, 173 (2007), available at http://www.ipme.ru/e-journals/RAMS/no_31507/sandu.pdf.
[23] J. Musil and M. Jirout, Surf. Coat. Technol. **201**, 5148 (2007).
[24] A. Raveh, I. Zukerman, R. Shneck, R. Avni, and I. Fried, Surf. Coat. Technol. **201**, 6136 (2007).

RIGHTSLINK

[25]Y. H. Lu and Y. G. Shen, Appl. Phys. Lett. **90**, 221913 (2007).
[26]S. Zhang, H. L. Wang, S. E. Ong, D. Sun, and X. L. Bui, Plasma Processes Polym. **4**, 219 (2007).
[27]J. Musil, J. Vlček, and P. Zeman, Adv. Appl. Ceram. **107**, 148 (2008).
[28]J. Musil, Surf. Coat. Technol. **207**, 50 (2012).
[29]S. Veprek, J. Vac. Sci. Technol., A **31**, 050822 (2013).
[30]J. Musil, P. Zeman, and P. Baroch, *Comprehensive Materials Processing*, edited by D. Cameron (Elsevier, Amsterdam, 2014), pp. 325–353.
[31]J. Kohout *et al*., Surf. Coat. Technol. **257**, 301 (2014).
[32]P. Zeman, Š. Zuzjaková, P. Mareš, R. Čerstvý, M. Zhang, J. Jiang, E. I. Meletis, and J. Vlček, Ceram. Int. **42**, 4853 (2016).
[33]J. Vlček, A. Belosludtsev, J. Rezek, J. Houška, J. Čapek, R. Čerstvý, and S. Haviar, Surf. Coat. Technol. **290**, 58 (2016).
[34]H. Frager, B. M. Howe, G. Greczynski, J. Jensen, A. B. Mei, J. Lu, L. Hultman, J. E. Greene, and I. Petrov, J. Vac. Sci. Technol., A **33**, 05E103 (2015).
[35]S. Ali, B. Paul, R. Magnusson, G. Greczynski, E. Broitman, B. Jonson, P. Eklund, and J. Birch, Vacuum **131**, 1 (2016).
[36]J. Musil, J. Sklenka, and R. Čerstvý, Surf. Coat. Technol. **206**, 2105 (2012).
[37]J. Musil, R. Jílek, M. Meissner, T. Tolg, and R. Čerstvý, Surf. Coat. Technol. **206**, 4230 (2012).
[38]J. Musil, R. Jílek, and R. Čerstvý, J. Mater. Sci. Eng. A **4**, 27 (2014).
[39]J. Musil, J. Blažek, K. Fajfrlík, and R. Čerstvý, Surf. Coat. Technol. **264**, 114 (2015).
[40]J. Musil, M. Zítek, K. Fajfrlík, and R. Čerstvý, J. Vac. Sci. Technol., A **34**, 021508 (2016).
[41]J. Musil, J. Sklenka, and R. Čerstvý, Appl. Surf. Sci. **370**, 306 (2016).
[42]J. Musil, S. Zenkin, S. Kos, R. Čerstvý, and S. Haviar, Vacuum **131**, 34 (2016).
[43]J. Musil, D. Javdošňák, R. Čerstvý, S. Haviar, G. Remnev, and V. Uglov, Vacuum **133**, 43 (2016).
[44]J. Musil, G. Remnev, L. Legostaev, V. Uglov, A. Lebedynskiy, A. Lauk, J. Procházka, S. Haviar, and E. Smolyanskiy, "Flexible hard Al-Si-N films for high temperature operation," Surf. Coat. Technol. (unpublished).
[45]J. Musil, RSC Adv. **5**, 60482 (2015).
[46]J. Musil, *Thin Films and Coatings: Toughening and Toughening Characterization*, edited by S. Zhang (CRC, Boca Raton, FL, 2015), pp. 377–463.
[47]J. Musil, J. Šícha, D. Heřman, and R. Čerstvý, J. Vac. Sci. Technol., A **25**, 666 (2007).
[48]J. A. Thornton, Annu. Rev. Mater. Sci. **7**, 239 (1977).
[49]J. A. Thornton, Metal. Finish. **77**, 660 (1979).
[50]Y. T. Pei, D. Galvan, and J. Th. M. De Hosson, Acta Mater. **53**, 4505 (2005).

RIGHTSLINK

Surface & Coatings Technology 332 (2017) 190–197

Contents lists available at ScienceDirect

Surface & Coatings Technology

journal homepage: www.elsevier.com/locate/surfcoat

Effect of energy on structure, microstructure and mechanical properties of hard Ti(Al,V)N_x films prepared by magnetron sputtering

M. Jaroš *, J. Musil, R. Čerstvý, S. Haviar

Department of Physics and NTIS – European Centre of Excellence, University of West Bohemia, Univerzitní 8, CZ 306 14, Plzeň, Czech Republic

ARTICLE INFO

Article history:
Received 24 March 2017
Revised 2 June 2017
Accepted in revised form 3 June 2017
Available online 8 September 2017

Keywords:
Ti(Al,V)N_x films
Structure
Microstructure
Mechanical properties
Energy
Magnetron sputtering

ABSTRACT

The article reports on the effect of the energy delivered into the growing film by bombarding ions $\mathscr{E}_{bi}$ and/or fast neutrals $\mathscr{E}_{fn}$ on its structure, microstructure and mechanical properties, and resistance to cracking. The effect of the total delivered energy $\mathscr{E} = \mathscr{E}_{bi} + \mathscr{E}_{fn}$ on the film properties is demonstrated on the Ti(Al,V)N_x films deposited by reactive magnetron sputtering. The films were sputtered onto Si(111) and Mo substrates in a mixture Ar + N_2 gases by a dual magnetron with closed magnetic field and equipped with TiAlV (6 at.% Al, 4 at.% V) alloy targets. It was shown that (1) The energy $\mathscr{E}$ is a key parameter controlling the physical and mechanical properties, and the resistance to cracking of sputtered Ti(Al,V)N_x films, (2) The structure of Ti(Al,V)N_x films varies from TiN(200) to TiN(220) with increasing energy $\mathscr{E}$, (3) The Ti(Al,V)N_x films with high ratio $H/E^* \geq 0.1$, high elastic recovery $W_e \geq 60\%$ and dense voids-free microstructure exhibit an enhanced resistance to cracking and can be produced only in the case when a sufficient energy $\mathscr{E}$ is delivered into the growing film either by bombarding ions or by bombarding fast neutrals and (4) The energy $\mathscr{E}_{fn}$ makes it possible to sputter crystalline films onto dielectric substrates held at a floating potential $U_s = U_{fl}$.

© 2017 Elsevier B.V. All rights reserved.

1. Introduction

It is well known that properties of thin films are determined by their elemental and phase composition (crystalline phase, amorphous phase or mixture of crystalline and amorphous phase), structure (size of grains and their crystallographic orientation), and microstructure (porous/columnar, dense/voids-free). Up to now, the properties of the thin film have been controlled by different deposition parameters, such as the power P of the magnetron discharge, the film thickness h, the substrate temperature T_s, the substrate bias U_s, the substrate ion current density i_s, the flux of ions ν_i incident on the substrate, the deposition rate a_D of the film, the substrate-to-target distance d_{s-t}, the partial pressure of the argon p_{Ar} the reactive gas p_{RG} and the total pressure $p_T = p_{Ar} + p_{RG}$ of sputtering gas mixture, etc., used in its formation. There are a huge number of papers devoted to the investigation of the relationships between the deposition parameters of the film and its structure [1–12], microstructure [8–26], phase and elemental composition [2–5,15–20], macrostress [4–9,18–22], physical and functional properties [1–28]. A set (combination) of many deposition parameters must be always selected in sputtering of the film. The problem in this approach is the fact that a correct combination of the deposition parameters necessary to form the film with prescribed properties is unknown. Different combinations of deposition parameters result in different energy $\mathscr{E}$ delivered into the growing film, which is difficult to predict. It means that the main parameter which really controls the film properties is the energy $\mathscr{E}$ and thereby the correlations between the properties of the film and the energy $\mathscr{E}$ are of a key importance [29–39]. Therefore, an opposite approach in the development of new films should be used. At first, correlations between the film properties and the energy $\mathscr{E}$ should be found. Then, based on this knowledge the necessary deposition parameters which ensure the formation of the films with prescribed properties should be determined.

In the simplest case of a collision-less, fully ionized plasma the energy $\mathscr{E}_{bi}$ can be expressed in the following form [33,39].

$$E_{bi}[J/cm^3] = (U_p - U_s) i_s / a_D \text{ at } U_p > U_s \quad (1)$$

Here, U_p is the plasma potential, U_s is the substrate bias, i_s is the substrate ion current density and a_D is the deposition rate of film. Under the assumption that $|U_p| \ll |U_s|$, which is well fulfilled in many experiments, Eq. (1) can be simplified into the following simple form.

$$E_{bi}[J/cm^3] \approx (|U_s| i_s) / a_D \quad (2)$$

Eq. (2) clearly shows two important facts. The energy $\mathscr{E}_{bi}$ delivered into the growing film by bombarding ions (1) can be easily calculated from the measured deposition parameters (U_s, i_s) and the film deposition rate $a_D = h/t_d$ calculated from the measured film thickness h and the deposition time t_d and (2) strongly depends not only on U_s and i_s

* Corresponding author.
E-mail address: jarosm@kfy.zcu.cz (M. Jaroš).

http://dx.doi.org/10.1016/j.surfcoat.2017.06.074
0257-8972/© 2017 Elsevier B.V. All rights reserved.

Nomenclature

H	hardness
E^*	effective Young's modulus
W_e	elastic recovery
f_r	repetition frequency
τ	duty cycle
I_{da}	discharge current averaged over the period
I_d	DC discharge current
W_t	target power density
$d_{S\text{-}T}$	target-to-substrate distance
T_S	substrate temperature
U_d	DC discharge voltage
U_{dp}	discharge voltage in the pulse
U_S	substrate voltage
U_P	plasma potential
U_{fl}	floating potential
i_S	substrate current density
p_T	total pressure
p_{N2}	partial pressure of nitrogen
p_{Ar}	partial pressure of argon
L	indenter load
h	film thickness
r	radius of the fixed cylinder

but also on a_D. The second fact is of an extraordinary importance in (i) the reactive sputtering of compounds and (ii) the high-rate sputtering of films because the energy $\mathscr{E}_{bi}$ delivered into the growing film deceases with increasing a_D.

This article investigates the effect of the energy $\mathscr{E} = \mathscr{E}_{bi} + \mathscr{E}_{fn}$ delivered into the growing Ti(Al,V)N_x film on the preferred crystallographic orientation (texture) of its grains, microstructure, physical and mechanical properties, and resistance to cracking in detail. A great attention is devoted also to (i) the control of the structure and microstructure of the film by the energy $\mathscr{E}$ delivered into the film during its growth in the DC and pulsed magnetron discharges, (ii) the energy $\mathscr{E}$ delivered into the film held at different substrate biases U_s and (iii) the energy $\mathscr{E}$ delivered into the film by fast neutrals.

2. Experimental

The Ti(Al,V)N_x thin films were sputter deposited in a mixture of Ar + N_2 sputtering gases using a dual magnetron with closed magnetic field equipped with TiAlV (6 at.% Al, 4 at.% V) alloy targets of diameter $\varnothing = 50$ mm. The targets were attached to the cathode bodies of the dual magnetron using pure Ti fixing rings. The magnetrons were powered by an Advanced Energy Pinnacle Plus + 5/5 kW power supply operated either in DC or pulse mode. The magnetrons were tilted to the vertical axis at the angle 20°; for more details see Ref. [40]. The Ti(Al,V)N_x films were deposited onto Si(111) and Mo substrates at low power density $W_t = I_d\, U_d / S \leq 20$ W/cm^2. The Si plates 20 × 20 × 0.52 mm^3 were used for the X-ray diffraction and the Si strips 30 × 5 × 0.64 mm^3 were used for the measurement of the film macrostress. The Mo substrates (80 × 15 × 0.20 mm^3) were used for the assessment of the film resistance to cracking in bending. A pre-deposition etching of the substrates was performed in the pulsed discharge (burning between the substrate and the shutter) at the voltage $U_{et} = 400$ V, current $I_{et} = 0.5$ A, repetition frequency $f_{et} = 100$ kHz, $\tau = 0.5$, substrate temperature $T_s = 500$ °C and substrate-to-target distance $d_{s\text{-}t} = 60$ mm in argon at pressure $p_{Ar} = 1$ Pa for 5 min; the index "et" denotes the ion etching. A pre-deposition cleaning of the magnetron targets was performed in DC mode of sputtering with a closed target at the magnetron voltage $U_d = 400$ V and current $I_d = 0.5$ A, target power density $W_d = 10$ W/cm^2 in argon at pressure $p_{Ar} = 1$ Pa for 3 min. The film thickness h was measured by a stylus profilometer DEKTAK 8. The macrostress σ was evaluated from the bending of Si plate using the Stoney's formula [41]. The film structure was characterized using an XRD diffractomer PANalytical X Pert PRO in the Bragg-Brentano configuration with CuKα radiation. The elemental composition of the Ti(Al,V)N_x films on the Si substrate was analyzed in a scanning electron microscope (SU-70, Hitachi) operated at a primary electron energy of 15 keV using energy dispersive spectroscopy (EDS, UltraDry, Thermo Scientific) and wave dispersive spectroscopy (WDS, Magnaray, Thermo Scientific). Pure metal standards were used for the determination of Ti, Al and V concentrations. The nitrogen concentration was calculated as the difference to 100% wt using a combined WDS (Ti, V) and EDS (Al) analysis, since there is an inevitable peak overlap of Ti and N X-Ray peaks. Mechanical properties of sputtered films were determined from load vs. displacement curves measured by a microhardness tester Fisherscope H100 with Vickers diamond indenter at a load of 20 mN. The resistance of the Ti(Al,V)N_x films to cracking was determined using the indentation test at high loads L ranging from 0.25 to 1 N determining the critical load L_{cr} when cracks in the film occur and by the bending test. The Mo strip coated with the sputtered film was bent around a fixed cylinder of different radius r. By decreasing of the radius r a strain induced in the film was increased. The critical strain ε_{cr} at which cracks in the film occur was measured. The critical strain ε_{cr} was calculated from the following formula [39].

$$\varepsilon_{cr} \approx h_{Mo}/2r \tag{3}$$

Here, h_{Mo} is the thickness of the Mo strip.

3. Results and discussion

From Eq. (2) follows that the same value of the energy $\mathscr{E}_{bi}$ can be obtained either at high values of U_s and low values of i_s or at low values of U_s and high values of i_s and in both cases at the same value of a_D. Main factor affecting the films deposition rate a_D is the power delivered into the magnetron discharge and the substrate-to-target distance. Different combinations of U_s and i_s are discussed in Sections 3.1.1 and 3.1.2. The energy $\mathscr{E}_{fn}$ delivered into the film by fast neutrals controlled by the total sputtering gas pressure p_T is discussed in Section 3.2. The main results of this article are summarized in Section 3.3.

3.1. Energy delivered by bombarding ions

3.1.1. Energy $\mathscr{E}_{bi}$ controlled by the substrate bias U_s

The evolution of the structure and mechanical properties of the Ti(Al,V)N_x film sputtered in DC magnetron discharge with increasing energy $\mathscr{E}_{bi}$, delivered into the growing film by bombarding ions, and controlled by the substrate bias U_s are displayed in Figs. 1 and 2. From Fig. 1 it is seen that the preferred crystallographic orientation of the Ti(Al,V)N_x films strongly depends on the value of the energy $\mathscr{E}_{bi}$. The Ti(Al,V)N_x films with the dominant TiN(200) reflection are sputtered at low values of energy $\mathscr{E}_{bi} \leq 1.1$ MJ/cm^3. The intensity of the TiN(200) reflection decreases with increasing $\mathscr{E}_{bi}$. The dominant TiN(220) reflection occurs at $\mathscr{E}_{bi} = 1.6$ MJ/cm^3 and coexists with the TiN(200) reflection. The TiN(200) reflection is almost fully converted to TiN(111) and TiN(220) reflections approximately at $\mathscr{E}_{bi} = 2.4$ MJ/cm^3. The Ti(Al,V)N_x films sputtered at higher energies $\mathscr{E}_{bi} \geq 2.4$ MJ/cm^3 are composed of TiN(220) and TiN(111) grains.

The stoichiometry x = N/(Ti + Al + V) of the Ti(Al,V)N_x films increases with increasing energy $\mathscr{E}_{bi}$ from x = 1.04 at $\mathscr{E}_{bi} = 0.1$ MJ/cm^3 to x = 1.17 at $\mathscr{E}_{bi} = 4.8$ MJ/cm^3, see Table 1, where also their main physical and mechanical properties are given. From Table 1 it is seen that while the substrate ion current density i_s increases, the deposition rate a_D of the film decreases with increasing negative substrate bias

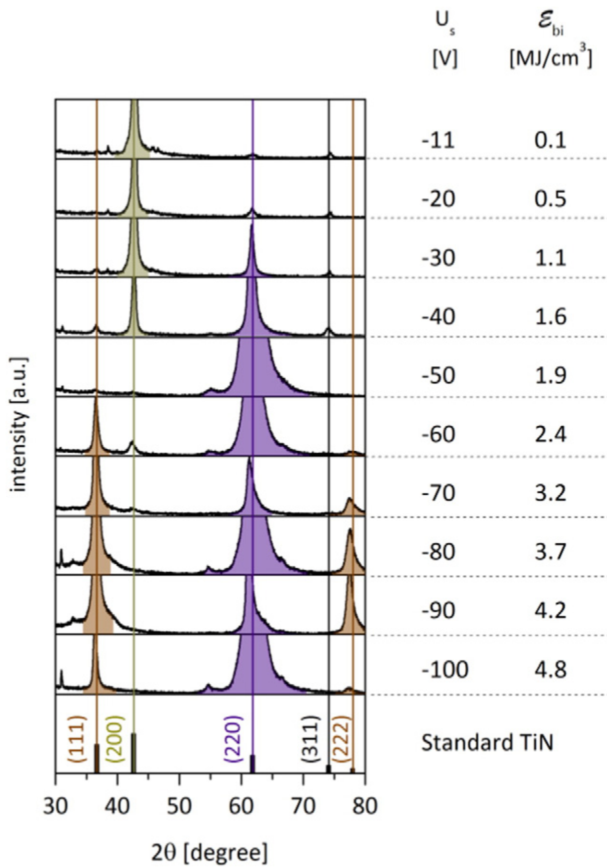

Fig. 1. XRD patterns from $Ti(Al,V)N_x$ films DC sputtered on Si(111) substrate at $I_d = 0.5$ A, $W_t \approx 10$ W/cm^2, $T_s = 500$ °C, $d_{s\text{-}t} = 60$ mm, $p_T = p_{Ar} + p_{N2} = 0.2 + 0.8 = 1$ Pa as a function of $\mathscr{E}_{bi}$, which itself here is a function of negative substrate bias U_s.

U_s. It is the reason why the energy $\mathscr{E}_{bi}$ increases with increasing negative substrate bias U_s. The hardness H increases with increasing $\mathscr{E}_{bi}$ from 22 GPa at $\mathscr{E}_{bi} = 0.1$ MJ/cm^3 to 32 GPa at $\mathscr{E}_{bi} = 1.9$ MJ/cm^3 and then slightly decreases to 30 GPa at $\mathscr{E}_{bi} = 4.8$ MJ/cm^3. The effective Young's modulus E^* also increases with increasing $\mathscr{E}_{bi}$ from 262 GPa at $\mathscr{E}_{bi} = 0.1$ MJ/cm^3 to 275 GPa at $\mathscr{E}_{bi} = 1.9$ MJ/cm^3 but then decreases more strongly, compared with the hardness H, to 240 GPa at $\mathscr{E}_{bi} = 4.8$ MJ/cm^3. The $Ti(Al,V)N_x$ films sputtered at $\mathscr{E}_{bi} \geq 1.7$ MJ/cm^3 exhibit a high ratio $H/E^* > 0.1$ and a high elastic recovery $W_e > 70\%$ and thereby also an enhanced resistance to cracking; for more details see Refs. [42–50].

The evolution of the mechanical properties of the $Ti(Al,V)N_x$ films sputtered in DC magnetron discharge with increasing energy $\mathscr{E}_{bi}$ is displayed in Fig. 2 and Table 1. From Fig. 2 and Table 1 the following can be concluded:

1. The energy $\mathscr{E}_{bi}$ delivered into the growing film increases with increasing negative substrate bias U_s at constant values of (i) the low discharge current $I_d = 0.5$ A and (ii) the high partial pressure of nitrogen $p_{N2} = 0.8$ Pa.
2. The $Ti(Al,V)N_x$ films sputtered at low energies $\mathscr{E}_{bi} \leq 1.7$ MJ/cm^3 exhibit ratio $H/E^* \leq 0.1$, elastic recovery $W_e \leq 70\%$ and a strong TiN (200) texture. These films sputtered at low substrate biases $|U_s| \leq 40$ V are brittle and easily crack.
3. The $Ti(Al,V)N_x$ films sputtered at high substrate biases $|U_s| \geq 50$ V and therefore high energies $\mathscr{E}_{bi} > 1.7$ MJ/cm^3 exhibit high ratio $H/E^* > 0.1$, high elastic recovery $W_e > 70\%$ and no TiN (200) texture. These films exhibit an enhanced resistance to cracking.
4. The $Ti(Al,V)N_x$ films sputtered at the highest energies $\mathscr{E}_{bi} \geq 3.7$ MJ/cm^3 exhibit the highest resistance to cracking.
5. The absence or small amount of the TiN(200) grains in a $Ti(Al,V)N_x$ film can be used as an indicator that the film has enhanced mechanical properties.
6. The compressive macrostress ($\sigma < 0$) generated in sputtered $Ti(Al,V)N_x$ films strongly increases with increasing substrate bias U_s up to -5.5 GPa at $U_s = -100$ V.

The high compressive macrostress σ in the sputtered $Ti(Al,V)N_x$ film strongly decreases its adhesion to the substrate and very often the film delaminates from it. Therefore, the energy $\mathscr{E}_{bi}$ necessary to form flexible hard films with enhanced resistance to cracking needs to be delivered into the growing film at lower negative substrate biases U_s.

3.1.2. Energy $\mathscr{E}_{bi}$ controlled by the substrate ion current density i_s

In this section properties of the $Ti(Al,V)N_x$ films sputtered at a low substrate bias $U_s = -40$ V in a DC and pulsed magnetron discharges are reported. The evolution of the structure and mechanical properties of the $Ti(Al,V)N_x$ film with increasing energy $\mathscr{E}_{bi}$, delivered into the growing film by bombarding ions and controlled by the substrate ion current density i_s are displayed in Figs. 3 and 4, respectively. The substrate ion current density i_s extracted to the substrate from the DC magnetron discharge was increased by increasing the discharge current I_d, i.e. by intensification of the magnetron discharge, which results in the

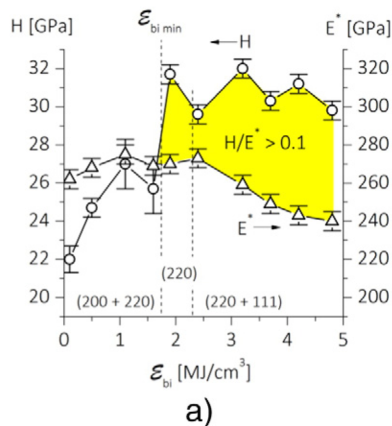

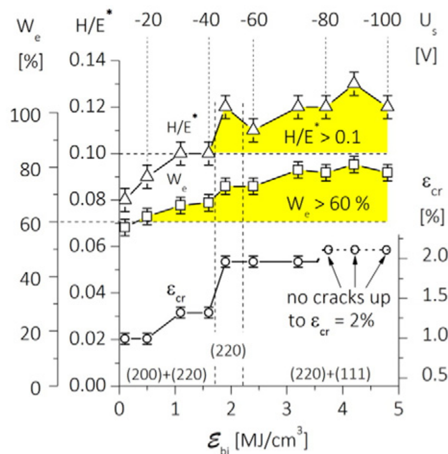

Fig. 2. The evolution of (a) hardness H, effective Young's modulus E^* and TiN texture and (b) elastic recovery W_e, H/E^* ratio, critical strain e_{cr} to failure and TiN texture of the sputtered $Ti(Al,V)N_x$ films as a function of the energy $\mathscr{E}_{bi}$ as which itself here is a function of negative substrate bias U_s.

Table 1
Physical and mechanical properties of Ti(Al,V)N_x films sputtered by DC dual magnetron at $I_d = 0.5$ A, $W_t = (U_d I_d/S) = 10$ W/cm^2, $T_s = 500$°C, $d_{s\text{-}t} = 60$ mm and $p_T = p_{Ar} + p_{N2} = 0.2 + 0.8 = 1$ Pa on Si(111) controlled by the substrate bias U_s; here x = N/(Ti + Al + V) is the film stoichiometry and S is the area of the sputtered target.

U_s [V]	i_s [mA/cm^2]	$\mathscr{E}_{bi}$ [MJ/cm^3]	x	h [nm]	a_D [nm/min]	H [GPa]	E^* [GPa]	W_e [%]	H/E^*	σ [GPa]	Cracks in: Bending ε_{cr} [%]	Cracks in: Indentation L_{cr} [N]
−11	0.24	0.1	1.04	2200	18.3	22	262	58	0.08	−0.4	1.0	0.25
−20	0.74	0.5	1.04	2000	16.7	25	268	62	0.09	−0.4	1.0	0.25
−30	0.93	1.1	0.99	1900	14.6	27	275	66	0.10	−1.0	1.3	0.25
−40	0.96	1.6	1.03	2000	14.3	26	269	67	0.10	−2.4	1.3	0.25
−50	0.91	1.9	1.07	1900	14.6	32	275	76	0.12	−3.1	2.0	>1
−60	0.96	2.4	1.05	2000	14.3	30	273	73	0.11	−1.5	2.0	>1
−70	1.01	3.2	1.11	1600	13.3	32	259	79	0.12	−2.9	2.0	>1
−80	1.04	3.7	1.15	1600	13.3	30	249	78	0.12	−1.9	>2.0	>1
−90	1.07	4.2	1.10	1500	13.6	31	243	81	0.13	−4.0	>2.0	>1
−100	1.10	4.8	1.17	1400	13.7	30	240	78	0.12	−5.5	>2.0	>1

creation of a dense plasma. Higher values of the substrate ion current I_s at $U_s = -40$ V can be extracted from a dense plasma only. However, the increase of the current I_d also results in the increase of the film deposition rate a_D and thereby also in the simultaneous decrease of the energy $\mathscr{E}_{bi}$ delivered to the film during its growth by bombarding ions, see Table 2. In order to increase the ion current density i_s the DC magnetron discharge was replaced by the pulsed bipolar dual magnetron discharge. Higher value of the ion current density i_s was extracted from denser plasma at low substrate biases $U_s \leq |20\text{ V}|$. At low substrate biases $U_s \leq |20\text{ V}|$ the plasma potential U_p increased to +23 V due to the positive value of the magnetron voltage during the pulse-off time. The positive plasma potential of +23 V and the negative substrate bias of −20 V results in the sheath potential $U_{sh} = |43\text{ V}|$, from which the energy $\mathscr{E}_{bi}$ is calculated using Eq. (1). From denser plasma higher ion currents I_s to the substrate were extracted and higher ion current density $i_s \geq 1.7$ mA/cm^2 were achieved. Therefore, the Ti(Al,V)N_x films deposited in the pulsed discharge generated by the pulsed bipolar dual magnetron exhibit high ratio H/$E^* \geq 0.12$, high elastic recovery $W_e \geq 73\%$ and are characterized by a strong TiN(220) texture, see Fig. 3. These films are slightly over-stoichiometric and their stoichiometry x = N/(Ti + Al + V) ranges from 1.00 to 1.09, see Table 2. The evolution of mechanical properties of these films with increasing energy $\mathscr{E}_{bi}$ is displayed in Fig. 4.

From Figs. 3 and 4 and Table 2 the following can be concluded:

1. The energy $\mathscr{E}_{bi}$ delivered into the growing film prepared in the DC magnetron discharge decreases with increasing discharge current I_d due to increasing of the film deposition rate a_D. All films are formed at low energy $\mathscr{E}_{bi} < 1.7$ MJ/cm^3. They are polycrystalline, almost stoichiometric (x = N/(Ti + Al + V) ≈ 1) and exhibit strong TiN(200) texture and columnar microstructure which is responsible for a low

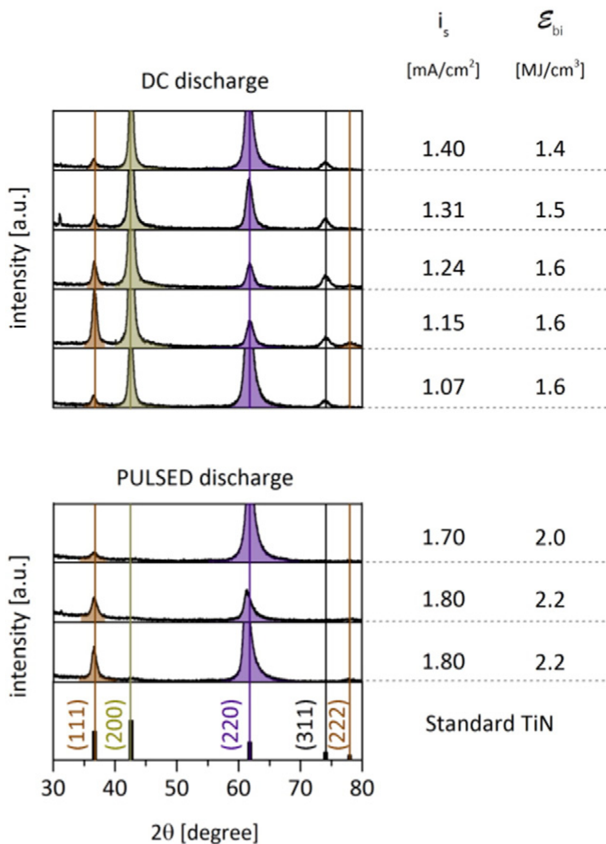

Fig. 3. XRD patterns from Ti(Al,V)N_x films on the Si(111) substrate sputtered at $T_s = 500$ °C, $d_{s\text{-}t} = 60$ mm, $p_T = 1$ Pa, $p_{N2} = 0.8$ Pa using (i) DC deposition at $W_t \leq 16.5$ W/cm^2, $U_s = -40$V, (ii) pulse deposition at $f_r = 100$ kHz, τ = 0.5, $W_t = 16.3$ W/cm^2, $U_s = -20$V as a function $\mathscr{E}_{bi}$ controlled by substrate ion current density.

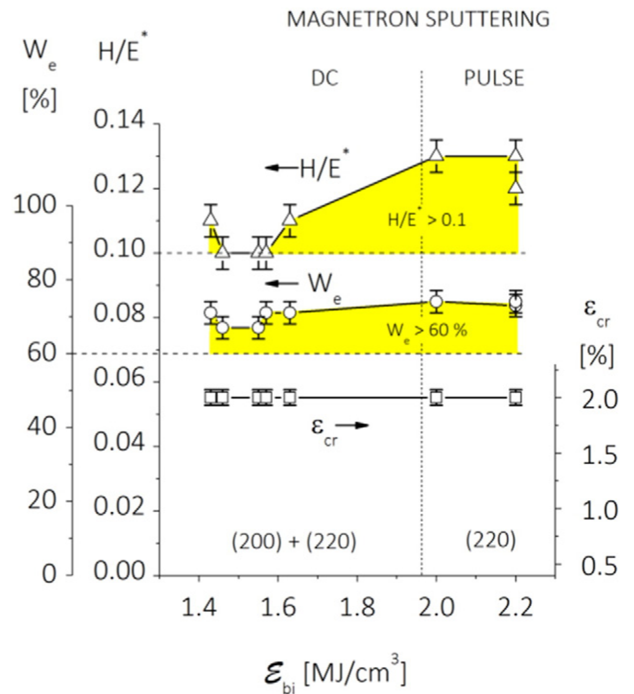

Fig. 4. H/E* ratio, elastic recovery W_e, and critical strain ε_{cr} in Ti(Al,V)N_x films reactively sputtered onto Si(111) and Mo substrate in (i) the DC discharge at W_t ranging from 11.4 to 16.5 W/cm^2, U_s = -40V, and (ii) the pulsed bipolar dual magnetron discharge at W_t = 16.3 W/cm^2, U_s = -15 and -20 V, f_r = 100 kHz, and T_s = 500 °C, $d_{s\text{-}t}$ = 60 mm, $p_T = p_{Ar} + p_{N2} = 0.2 + 0.8 = 1$ Pa as a function of $\mathscr{E}_{bi}$ as which itself here is a function of substrate ion current density i_s.

Table 2
Physical and mechanical properties of $Ti(Al,V)N_x$ films sputtered on the Si(111) and Mo substrates at $d_{S-T} = 60$ mm, $T_s = 500$ °C, $p_T = p_{Ar} + p_{N2} = 0.2 + 0.8 = 1$ Pa by (i) DC dual magnetron discharge at $U_s = -40$ V, $U_p \approx +3$ V, (ii) pulsed bipolar dual magnetron discharge at $f_r = 100$ kHz, $\tau = 0.5$, $I_{da} = 1.6$ V, $U_p \approx +23$ V. The substrate ion current density is was controlled by the discharge current I_d.

DC dual magnetron deposition												Cracks in	
I_d	W_t	i_s	$\mathscr{E}_{bi}$	x	h	a_D	H	E^*	W_e	H/E^*	σ	Bending ε_{cr}	Indentation L_{cr}
[A]	[W/cm²]	[mA/cm²]	[MJ/cm³]		[nm]	[nm/min]	[GPa]	[GPa]	[%]		[GPa]	[%]	[N]
0.55	11.4	1.07	1.6	1.03	1900	15.8	29.0	272	71	0.11	−1.8	2.0	0.25
0.60	12.6	1.15	1.6	1.09	2000	17.5	28.1	274	70	0.10	−1.4	2.0	0.25
0.65	13.8	1.24	1.6	1.02	2100	19.1	26.7	272	67	0.10	−1.3	2.0	0.25
0.70	15.2	1.31	1.5	1.05	2200	21.6	26.9	278	67	0.10	−1.4	2.0	0.25
0.75	16.5	1.40	1.4	1.05	2200	23.4	29.9	283	71	0.11	−1.8	2.0	0.25
Pulsed dual bipolar magnetron deposition													
U_s	W_t	i_s	$\mathscr{E}_{bi}$	x	h	a_D	H	E^*	W_e	H/E^*	σ	ε_{cr}	L_{cr}
[V]	[W/cm²]	[mA/cm²]	[MJ/cm³]		[nm]	[nm/min]	[GPa]	[GPa]	[%]		[GPa]	[%]	[N]
−15	16.3	1.7	2.0	1.09	1.0	20.0	24.0	190	74	0.13	−1.7	2.0	1
−20	16.3	1.8	2.2	1.03	1.3	21.7	24.3	194	73	0.13	−1.4	2.0	>1
−20	16.3	1.8	2.2	1.00	2.5	21.7	28.5	235	74	0.12	−1.4	2.0	>1

resistance to cracking despite quite high ratio $H/E^* \approx 0.1$ and high elastic recovery $W_e > 60\%$.

2. All $Ti(Al,V)N_x$ films prepared in the pulsed bipolar dual magnetron discharge are deposited at high ion current density $i_s \geq 1.7$ mA/cm². They are also polycrystalline and almost stoichiometric ($x = N/(Ti + Al + V) \approx 1$) but exhibit no TiN(200) texture, high ratio $H/E^* \geq 0.12$ and high elastic recovery $W_e > 60\%$. These films exhibit an enhanced resistance to cracking in the indentation test ($L_{cr} \geq 1$ N) but a lower resistance to cracking in the bending test.
3. This experiment also confirms the conclusion already given in the Section 3.1.1 that the polycrystalline $Ti(Al,V)N_x$ films with the TiN(200) texture are brittle, i.e. they exhibit a low resistance to cracking. On the contrary the films with the TiN(220) texture are strong and tough, and exhibit the an enhanced resistance to cracking, see Table 2.
4. The thick (1000 to 2000 nm) $Ti(Al,V)N_x$ films sputtered at low negative substrate biases $|U_s| \leq 40$ V and energies $\mathscr{E}_{bi}$ ranging from 1.6 to 2.2 MJ/cm³ exhibit low compressive macrostresses ($|\sigma| \leq 2$ GPa).

3.2. Energy $\mathscr{E}_{fn}$ delivered by fast neutrals and controlled by the total sputtering gas pressure p_T

The energy $\mathscr{E}$ can be delivered into the growing film not only by bombarding ions ($\mathscr{E}_{bi}$) but also by bombarding fast neutrals ($\mathscr{E}_{fn}$) at low sputtering gas pressures $p_T = p_{Ar} + p_{N2} < 1$ Pa. This fact is demonstrated by sputtering of the $Ti(Al,V)N_x$ films held at the floating potential ($U_s = U_{fl}$) as a function of the total sputtering gas pressure p_T. The $Ti(Al,V)N_x$ films were sputtered by pulsed dual magnetron operated in a bipolar mode at the repetition frequency of pulses $f_r = 200$ kHz, $\tau = 0.5$, $I_{dp} = 1.2$ A, $U_{da} \approx 220$ V, $U_s = U_{fl}$, $T_s = 500$°C, $d_{s-t} = 60$ mm, $p_{N2}/p_T = 0.8$. As the substrates are held at the floating potential $U_s = U_{fl}$ both the substrate ion current density i_s and the energy $\mathscr{E}_{bi}$ are very low, almost zero. It means that in this case the energy $\mathscr{E}$ is delivered into the growing film mainly by fast neutrals, i.e. $\mathscr{E} \approx \mathscr{E}_{fn}$. The energy of fast neutrals $\mathscr{E}_{fn}$ increases with decreasing p_T due to the prolongation of the mean free path λ and therefore a reduction of collisions between atoms. It means that a lower energy $\mathscr{E}_{fn}$ is delivered into the growing film at higher pressures p_T compared with $\mathscr{E}_{fn}$ delivered into it at lower pressures p_T. The evolution of the structure of the $Ti(Al,V)N_x$ films sputtered under these conditions is displayed in Fig. 5. These films are crystalline and slightly over-stoichiometric ($x = N / (Ti + Al + V) \approx$ from 1.06 to 1.25. Physical and mechanical properties of sputtered $Ti(Al,V)N_x$ films are summarized in Table 3.

This experiment demonstrates the indirect but clear effect of the energy $\mathscr{E}_{fn}$ on the physical and mechanical properties of $Ti(Al,V)N_x$ films sputtered between low (0.4 Pa) and high (1 Pa) total sputtering gas pressure p_T and partial pressure of nitrogen $p_{N2} = 0.8\ p_T$ on substrate held at floating potential ($U_s = U_{fl}$). From Fig. 5 and Table 3 the following can be concluded:

1. The structure of $Ti(Al,V)N_x$ films varies from the dominant TiN(200) to the dominant TiN(220) texture with decreasing total sputtering gas pressure p_T. It is indirect evidence that the energy $\mathscr{E}_{fn}$ increases with decreasing p_T as expected.
2. The ratio H/E^*, elastic recovery W_e and compressive macrostress ($\sigma < 0$) increase with decreasing p_T. Also these facts indicate that the energy $\mathscr{E}_{fn}$ increases with decreasing p_T.
3. The $Ti(Al,V)N_x$ films are over-stoichiometric ($x = [N/(Ti + Al + V)] \geq 1$) films and their stoichiometry × increases with decreasing p_T probably due to the domination of nitrogen N absorption on the

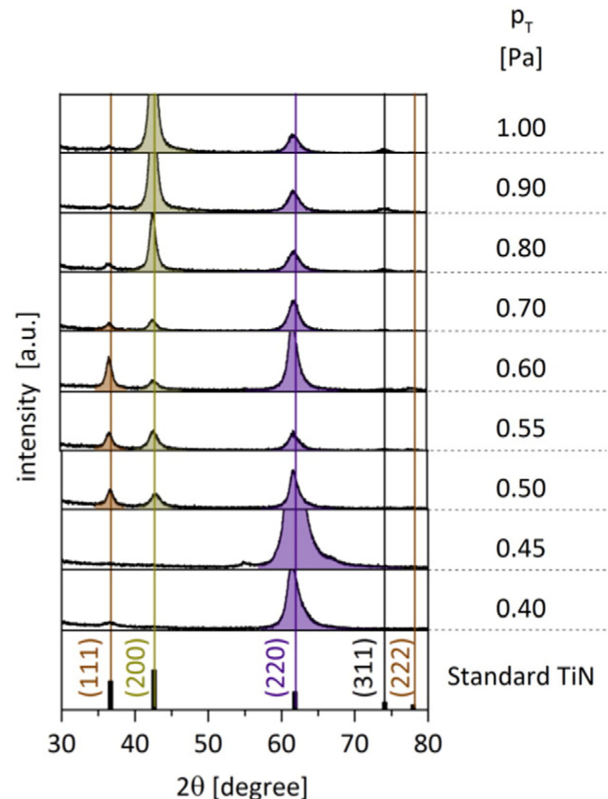

Fig. 5. Evolution of XRD patterns from $Ti(Al,V)N_x$ film sputtered by pulsed bipolar dual magnetron on Si(111) substrate at $f_r = 200$ kHz, $I_{dp} = 1.2$ A, $W_t \approx 13$ W/cm², $U_s = U_{fl}$, $T_s = 500$ °C, $d_{s-t} = 60$ mm with decreasing total sputtering gas pressure p_T.

Table 3
Physical and mechanical properties of $Ti(Al,V)N_x$ films sputtered by pulsed bipolar dual magnetron at $f_r = 200$ kHz, $I_{dp} = 1.2$ A, $W_t = 13$ W/cm^2, $U_s = U_{fl}$, $T_s = 500$ °C, $d_{s\text{-}t} = 60$ mm, $p_{N2} = 0.8$ Pa on Si(111) and Mo substrate controlled by the magnetron sputtering gas pressure $p_T = p_{Ar} + p_{N2}$; $W_t = (U_d I_d/S)$, S is the area of sputtered target and $x = N/(Ti + Al + V)$ is the film stoichiometry.

p_T	h	x	a_D	H	E^*	W_e	H/E^*	σ	Cracks in	
[Pa]	[nm]		[nm/min]	[GPa]	[GPa]	[%]		[GPa]	Bending ε_{cr} [%]	Indentation at L_{cr} [N]
0.40	800		6.7	21.8	173	75	0.13	−2.0	> 2.0	0.5*
0.45	1100	1.23	7.3	31.0	225	82	0.14	−2.2	2.0	0.5*
0.50	1300	1.24	8.3	25.5	209	76	0.12	−1.7	2.0	>1
0.55	1400	1.25	8.7	25.4	214	75	0.12	−1.9	2.0	>1
0.60	1800	1.17	12.0	27.6	238	75	0.12	−1.4	2.0	>1
0.70	1600	1.11	11.4	24.9	245	70	0.10	−1.3	1.3	>1
0.80	2000	1.06	15.3	18.1	179	63	0.10	−0.7	1.0	0.25
0.90	1800	1.10	15.0	23.2	237	68	0.10	−0.6	1.0	0.25
1.00	1900	1.10	15.8	23.8	240	68	0.10	−0.6	1.3	0.25

*The indentation load L_{cr} is low due to delamination of the film from the substrate not due to the film cracking.

film surface over its resputtering from the film surface when the film deposition rate a_D decreases with decreasing p_T.

4. The microstructure of the $Ti(Al,V)N_x$ films converts from columnar to dense, voids-free non-columnar microstructure with decreasing p_T, see Fig. 6.
5. The resistance of $Ti(Al,V)N_x$ films against cracking improves with decreasing p_T, see Table 3.

All these findings show that the energy $\mathcal{E}_{fn}$ can fully substitute the energy $\mathcal{E}_{bi}$ in the formation of flexible hard coatings. This fact opens a new way to form flexible hard nanocrystalline films on electrically insulating substrates.

In summary, it can be concluded that the microstructure of the films deposited onto the substrate held at the floating potential $U_s = U_{fl}$ can be densified by the bombardment of the fast neutrals when the film is sputtered at low values of the sputtering gas pressure $p_T < 0.7$ Pa. Moreover, it is possible to sputter defect-free electrically insulating films because there is no accumulation of charge on the surface of the growing film. These are the main advantages of the sputtering of the films held at the floating potential $U_s = U_{fl}$ at low sputtering gas pressures ($p_T <$ 0.7 Pa).

3.3. Interrelationships between energies $\mathcal{E}_{bi}$ and $\mathcal{E}_{fn}$, preferred crystallographic orientation and resistance to cracking of $Ti(Al,V)N_x$ films

Main results of our investigation are summarized in Fig. 7. This figure clearly illustrates main interrelationships between the $\mathcal{E}_{bi}$ controlled by ion bombardment (U_s, i_s) and the energy of fast neutrals $\mathcal{E}_{fn}$ controlled by the total pressure of sputtering gas p_T, the preferred orientation and the resistance to cracking of the $Ti(Al,V)N_x$ film. The low and enhanced resistance to cracking is characterized by the diamond indenter load L_{cr} at which the tested film cracks, see Fig. 8. In Fig. 8 the morphology of two Ti(Al,V)N films after loading by the diamond indenter at the same high load L = 1 N are compared: (a) the brittle hard Ti(Al,V)N film with low $H/E^* = 0.9$, low $W_e = 58\%$ sputtered at low energy $\mathcal{E}_{bi} = 0.5$ MJ/cm^3 and (b) the flexible hard Ti(Al,V)N film with high $H/E^* = 0.12$, high $W_e = 78\%$ sputtered at high energy $\mathcal{E}_{bi} = 4.8$ MJ/cm^3. This figure clearly shows that while the brittle hard film sputtered at low energy cracks, the flexible hard film exhibit no cracks under the same load L = 1 N.

Three main conclusions shown in Fig. 7 are:

1. The $Ti(Al,V)N_x$ films sputtered at low energies $\mathcal{E}_{bi} < 1.7$ MJ/cm^3 or under low bombardment by fast neutrals $\mathcal{E}_{fn}$ at high sputtering gas pressures $p_T > 0.7$ Pa containing TiN(200) grains exhibit columnar microstructure and low resistance to cracking.
2. The $Ti(Al,V)N_x$ films sputtered at high energies $\mathcal{E}_{bi} \geq 1.7$ MJ/cm^3 or under high bombardment by fast neutrals $\mathcal{E}_{fn}$ at low sputtering gas pressures $p_T \leq 0.7$ Pa containing no or low amount of TiN(200) grains exhibit dense, voids-free non-columnar microstructure and enhanced resistance to cracking.
3. The energy $\mathcal{E}_{bi}$ delivered to the growing film can be fully substituted by the energy of fast neutrals $\mathcal{E}_{fn}$ in formation of the film with the same properties.

4. Conclusions

The article reports on a detailed investigation of the interrelationships between the energy $\mathcal{E}_{bi}$ and $\mathcal{E}_{fn}$ delivered to the $Ti(Al,V)N_x$ film by bombarding ions and fast neutrals, respectively, and its structure,

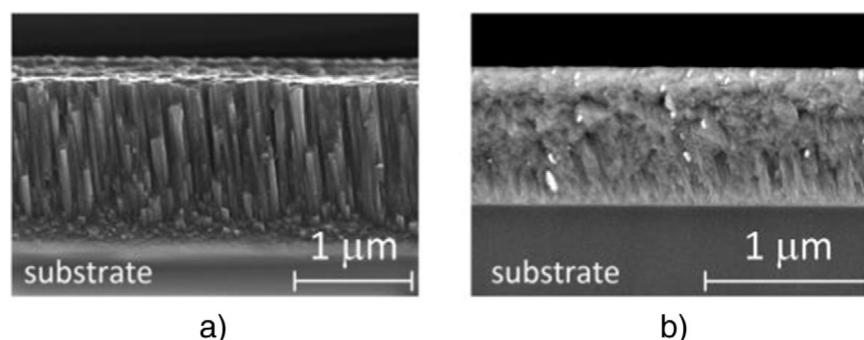

Fig. 6. SEM images of the microstructure of $Ti(Al,V)N_x$ film sputtered by pulsed bipolar dual magnetron on Si(111) substrate at $f_r = 200$ kHz, $I_d = 1.2$ A, $W_t \approx 13$ W/cm^2, $U_s = U_{fl}$, $T_s = 500$ °C, $d_{s\text{-}t} = 60$ mm, $p_{N2} = 0.8$ Pa and (a) $p_T = 1$ Pa and (b) $p_T = 0.4$ Pa.

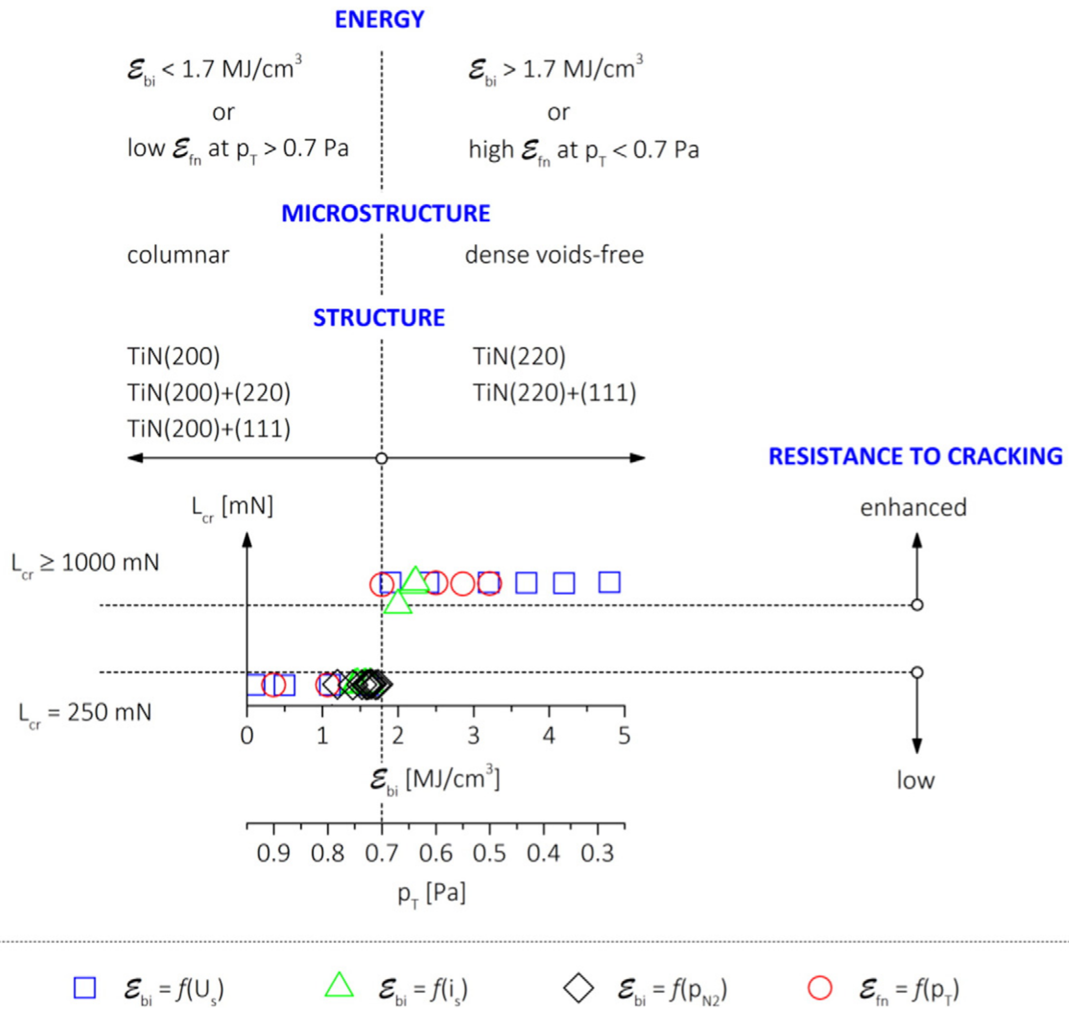

Fig. 7. Schematic illustration of interrelationships between the energy $\mathcal{E}_{bi}$ and $\mathcal{E}_{fn}$, and the structure, microstructure and resistance to cracking of the $Ti(Al,V)N_x$ film.

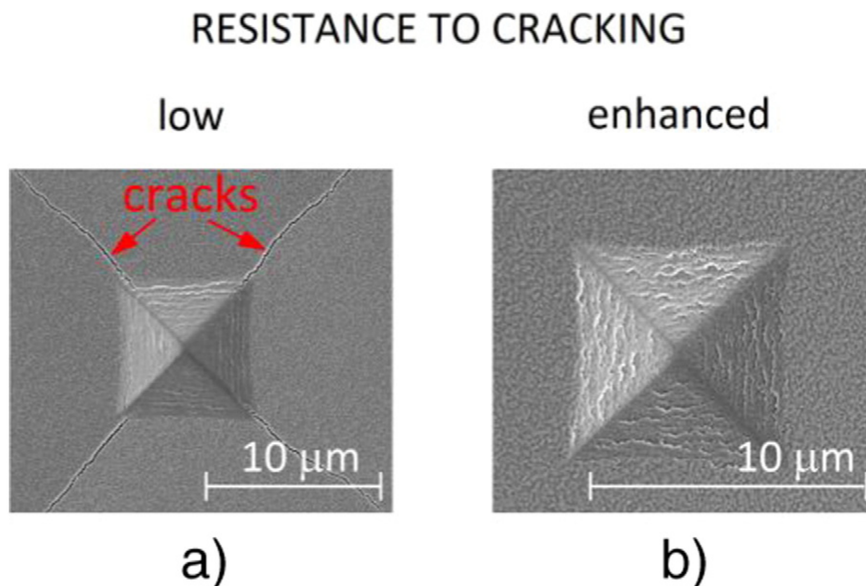

Fig. 8. Comparison of the surface morphology of (a) brittle hard $Ti(Al,V)N_x$ films sputtered at low energy $\mathcal{E}_{bi} = 0.5$ MJ/cm^3 exhibiting stoichiometry x = 1.04 and (b) flexible hard $Ti(Al,V)N_x$ film sputtered at high energy $\mathcal{E}_{bi} = 4.8$ MJ/cm^3 exhibiting stoichiometry x = 1.17.

microstructure, mechanical properties, and resistance to cracking. Main conclusions of this study can be summarized as follows

1. The texture of the Ti(Al,V)N_x films varies from TiN(200) to TiN(220) with increasing energy $\mathscr{E}_{bi}$ or $\mathscr{E}_{fn}$.
2. The Ti(Al,V)N_x films sputtered at low energies $\mathscr{E}_{bi}$ < 1.7 MJ/cm^3 and high sputtering gas pressures p_T > 0.7 Pa are characterized by the TiN(200) reflection and low resistance to cracking. On the other hand, the Ti(Al,V)N_x films sputtered at high energies $\mathscr{E}_{bi}$ ≥ 1.7 MJ/cm^3 and low pressures p_T < 0.7 Pa exhibit no TiN(200) reflection but an enhanced resistance to cracking. It indicates that the absence of the TiN (200) reflection in the XRD pattern can be used as an indicator that the Ti(Al,V)N_x film with enhanced resistance to cracking is formed.
3. The Ti(Al,V)N_x films with high ratio $H/E^* \geq 0.1$, high elastic recovery W_e ≥ 60%, dense, voids-free non-columnar microstructure and compressive macrostress ($\sigma < 0$) exhibit an enhanced resistance to cracking.
4. In sputtering of the Ti(Al,V)N_x films with enhanced resistance to cracking the energy $\mathscr{E}_{bi}$ can be fully substituted by the energy $\mathscr{E}_{fn}$. This finding is of a general validity. Moreover, the use of the energy $\mathscr{E}_{fn}$ in deposition of films makes it possible to sputter nanocrystalline and crystalline films onto electrically insulating substrates without their heating and arcing on their surfaces.
5. The energy $\mathscr{E}$ is a key parameter controlling physical and mechanical properties of sputtered films including their resistance to cracking and enabling their production in a reproducible way.

Acknowledgments

This work was supported by the project LO1506 of the Czech Ministry of Education, Youth and Sports under the program NPU I.

References

[1] H.S. Barshilia, A. Jain, K.S. Rajam, Structure, hardness and thermal stability of nanolayered TiN/CrN multilayer coatings, Vacuum 72 (2003) 241–248.
[2] J. Musil, H. Zeman, J. Kasl, Relationship between structure and mechanical properties in hard Al-Si-Cu-N films prepared by magnetron sputtering, Thin Solid Films 413 (2002) 121–130.
[3] S. Carvalho, L. Rebouta, A. Cavaleiro, L.A. Rocha, J. Comes, E. Alves, Microstructure and mechanical properties of nanocomposite (Ti,Si,Al)N coatings, Thin Solid Films 398-399 (2001) 391–396.
[4] C.H. Lai, M.H. Tsai, S.J. Lin, J.W. Yeh, Influence of substrate temperature and mechanical properties of multi-element (AlCrTaTiZr)N coatings, Surf. Coat. Technol. 201 (2007) 6993–6998.
[5] L. Karlsson, L. Hultman, M.P. Johansson, J.-E. Sundgren, H. Ljungcrantz, Growth, microstructure, and mechanical properties of arc evaporated TiC1-xN1-x 0 (≤ × ≤1) films, Surf. Coat. Technol. 126 (2000) 1–14.
[6] J. Patscheider, T. Zehnder, M. Diserens, Structure-performance relations in nanocomposite coatings, Surf. Coat. Technol. 146 (2001) 201–208.
[7] J.H. Huang, Z.E. Tsai, G.P. Yu, Mechanical properties and corrosion resistance of nanocrystalline ZrNxOy coatings on AISL 304 stainless steel by ion plating, Surf. Coat. Technol. 202 (2008) 4992–5000.
[8] J. Almer, M. Oden, G. Hakansson, Microstructure, stress and mechanical properties of arc-evaporated Cr-C-N coatings, Thin Solid Films 385 (2001) 190–197.
[9] P. Jedrzejowski, J.E. Klemberg-Sapieha, L. Martinu, Relationship between the mechanical properties and the microstructure of nanocomposite TiN/SiN1.3 coatings prepared by low temperature PECVD, Thin Solid Films 426 (2003) 150–159.
[10] T. Mae, M. Nose, M. Zhou, T. Nagae, K. Shimamura, The effect of Si addition on the structure and mechanical properties of ZrN thin films deposited by an rf reactive sputtering method, Surf. Coat. Technol. 142-144 (2001) 954–958.
[11] J. Soldán, J. Neidhardt, B. Satory, R. Kaindl, R. Cerstvy, P.H. Mayrhofer, R. Tessadri, P. Polcik, M. Lechthaler, C. Mitterer, Structure-property relations of arc-evaporated Al-Cr-Si-N coatings, Surf. Coat. Technol. 202 (2008) 3555–3562.
[12] H. Watanabe, Y. Sato, C. Nie, A. Ando, S. Ohtani, N. Iwamoto, The mechanical properties and microstructure of Ti-Si-N nanocomposite films by ion plating, Surf. Coat. Technol. 169-170 (2003) 452–455.
[13] M. Audronis, A. Leyland, P.J. Kelly, A. Matthews, The effect of pulsed magnetron sputtering on the structure and mechanical properties of CrB2 coatings, Surf. Coat. Technol. 201 (2006) 3970–3976.
[14] W.J. Meng, R.C. Tittsworth, L.E. Rehn, Mechanical properties and microstructure of TiC/amorphous hydrocarbon nanocomposite coatings, Thin Solid Films 377-376 (2000) 222–232.
[15] J. Ding, Y. Meng, S. Wen, Mechanical properties and fracture toughness of multilayer hard coatings using nanoindentation, Thin Solid Films 371 (2000) 178–182.
[16] J. Lin, B. Mishra, J.J. Moore, W.D. Sproul, Microstructure, mechanical and tribological properties of Cr1-xAlxN films deposited by pulsed-closed field unbalanced magnetron sputtering (P-CFUBMS), Surf. Coat. Technol. 201 (2006) 4329–4334.
[17] K. Polychronopoulou, C. Rebholtz, M.A. Baker, L. Theodorou, N.G. Demas, S.J. Hinder, A.A. Polycarpou, C.C. Doumanidis, K. Bobel, Nanostructure, mechanical and tribological properties of reactive magnetron sputtered TiCx coatings, Diamond Relat. Mater. 17 (2008) 2054-2061.
[18] Y.T. Pei, D. Galvan, J.Th.M. De Hosson, Nanostructure and properties of TiC/a-C:H composite coatings, Acta Mater. 53 (2005) 4505–4521.
[19] J. Soldán, J. Musil, Structure and mechanical properties of DC magnetron sputtered TiC/Cu films, Vacuum 81 (2006) 531–538.
[20] M. Oden, J. Almer, G. Hakansson, M. Olsson, Microstructure-property relationships in arc-evaporated Cr-N coatings, Thin Solid Films 377-376 (2000) 407–412.
[21] A. Pelisson, M. Parlinska-Wojtan, H.J. Hug, J. Patscheider, Microstructure and mechanical properties of Al-Si-N transparent hard coatings deposited by magnetron sputtering, Surf. Coat. Technol. 202 (2007) 884–889.
[22] F. Lapostolle, A. Billard, J. von Stebut, Structure/mechanical properties relationship of titanium-oxygen coatings reactively sputter – deposited, Surf. Coat. Technol. 135 (2000) 1–7.
[23] J.A. Thornton, (i) Recent developments in sputtering – magnetron sputtering, Metal Finishing 77 (5) (1979) 83–87(ii) High rate thick films growth, Ann. Rev. Mater. Sci. 7 (1979) 239–260.
[24] J. Musil, V. Poulek, V. Valvoda, R. Kužel Jr., H.A. Jehn, M.E. Baumgartner, Relation of deposition conditions of Ti-N films prepared by dc magnetron sputtering to their microstructure and macrostress, Surf.Coat.Technol. 60 (1993) 484–488.
[25] B.A. Movchan, A.V. Demchishin, Study of the structure and properties of thick vacuum condensates of nickel, titanium, tungsten, aluminum oxide and zirconium oxide, Phys. Met. Metallogr. 28 (1969) 83–90.
[26] P. Pokorný, J. Musil, P. Fitl, M. Novotný, J. Lančok, J. Bulíř, Contamination of magnetron sputtered metallic films by oxygen from residual atmosphere in deposition chamber, Plasma Processes Polym. 12 (2015) 416–421.
[27] J. Musil, H. Zeman, F. Kunc, H. Poláková, Relationships between hardness, Young's modulus and elastic recovery in hard nanocomposite coatings, Surf. Coat.Technol. 154 (2002) 304–313.
[28] J. Musil, Sputtering systems with enhanced ionization for ion plating of hard wear resistant coatings, Proc. of the 1st Meeting on the Ion Engineering Society of Japan (IESJ-92), Tokyo, Japan 1992, pp. 295–304.
[29] H. Poláková, J. Musil, J. Vlček, J. Alaart, C. Mitterer, Structure-hardness relations in sputtered Ti-Al-V-N films, Thin Solid Films 444 (2003) 189–198.
[30] J. Musil, H. Poláková, J. Šůna, J. Vlček, Effect of ion bombardment on properties of hard reactively sputtered single-phase films, Surf.Coat.Technol. 177-178 (2004) 289–298.
[31] J. Musil, J. Šůna, The role of energy in formation of sputtered nanocomposite films, Mater. Sci. Forum 502 (2005) 291–296.
[32] J. Musil, J. Šícha, D. Heřman, R. Čerstvý, Role of energy in low-temperature high-rate formation of hydrophilic TiO_2 thin films using pulsed magnetron sputtering, J. Vac. Sci. Technol. A 25 (4) (2007) 666–674.
[33] J. Musil, Flexible hard nanocomposite coatings, RSC Adv. 5 (2015) 60482–60495.
[34] J. Musil, J. Vlček, P. Baroch, Magnetron discharges for thin films plasma processing, Chapter 3, in: Y. Pauleau (Ed.), Materials Surface Processing by Directed Energy Techniques, Elsevier Science Publisher B.V., Oxford, UK 2006, pp. 67–106.
[35] J. Musil, Physical and mechanical properties of hard nanocomposite films prepared by reactive magnetron sputtering, Chapter 10, in: J.T.M. De Hosson, A. Cavaleiro (Eds.), Nanostructured Coatings, Springer Science + Business Media, LCC, New York 2006, pp. 407–463.
[36] J. Musil, Low-pressure magnetron sputtering, Vacuum 50 (3–4) (1998) 363–372.
[37] J. Musil, Hard and superhard nanocomposite coatings, Surf.Coat.Technol. 125 (2000) 322–330.
[38] J. Musil, Hard nanocomposite coatings: thermal stability, oxidation resistance and toughness, Surf. Coat. Technol. 207 (2012) 50–65.
[39] J. Musil, Advanced hard nanocomposite coatings with enhanced toughness and resistance to cracking, Chapter 7, in: S. Zhang (Ed.), Thin Films and Coatings: Toughening and Toughening Characterization, CRC Press, USA 2015, pp. 377–463.
[40] J. Musil, P. Baroch, Discharge in dual magnetron sputtering system, IEEE Trans. Plasma Sci. 33 (20) (2005) 338–339.
[41] G.G. Stoney, The transition of metallic films deposited by electrolysis, Proc. R. Soc. London, Ser. A82 (1909) 172–175.
[42] J. Musil, J. Sklenka, R. Čerstvý, Transparent Zr-Al-O oxide coatings with enhanced resistance to cracking, Surf. Coat. Technol. 206 (2012) 2105–2109.
[43] J. Musil, R. Jílek, M. Meissner, T. Tolg, R. Čerstvý, Two-phase single layer Al-O-N nanocomposite films with enhanced resistance to cracking, Surf.Coat.Technol. 206 (2012) 4230–4234.
[44] J. Musil, R. Jílek, R. Čerstvý, Flexible Ti-Ni-N thin films prepared by magnetron sputtering, J. Mater. Sci. Technol. A 4 (2) (2014) 27–33.
[45] J. Musil, J. Blažek, K. Fajfrlík, R. Čerstvý, Flexible antibacterial Al-Cu-N films, Surf. Coat. Technol. 264 (2015) 114–120.
[46] J. Musil, M. Zítek, K. Fajfrlík, R. Čerstvý, Flexible antibacterial Zr-Cu-N thin films resistant to cracking, J. Vac Sci. Technol. A 34 (2016) 021508–1to −7.
[47] J. Musil, J. Sklenka, R. Čerstvý, Protection of brittle film against cracking, Appl. Surf. Sci. 370 (306) (2016) 306–311.
[48] J. Musil, S. Zenkin, S. Kos, R. Čerstvý, S. Haviar, Flexible hydrophobic ZrN nitride films, Vacuum 131 (2016) (2016) 34–38.
[49] J. Musil, D. Javdošňák, R. Čerstvý, S. Haviar, G. Remnev, V. Uglov, Effect of energy on formation of flexible Al-Si-N films prepared by magnetron sputtering, Vacuum 133 (2016) 43–45.
[50] J. Musil, G. Remnev, L. Legostaev, V. Uglov, A. Lebedynskiy, A. Lauk, J. Procházka, S. Haviar, E.Smolyanskiy: flexible hard Al-Si-N films for high temperature operation, Surf. Coat. Technol. 307 (2016) 1112–1118.

CrossMark

Plasma and floating potentials in magnetron discharges

Jindřich Musil[a)] and Martin Jaroš
Department of Physics and NTIS Centre of Excellence, Faculty of Applied Sciences, University of West Bohemia, Univerzitní 8, CZ - 306 14 Plzeň, Czech Republic

(Received 26 June 2017; accepted 31 August 2017; published 19 September 2017)

This letter reports on great differences in values of the plasma U_p and floating U_{fl} potentials in sputtering discharges generated by single and dual magnetrons. It is shown that (i) the differences in U_p and U_{fl} result in strongly different properties of films sputtered by single and dual magnetrons at the same power delivered to the magnetron discharge, (ii) in the direct current single and dual magnetron discharges, the values of U_p and U_{fl} strongly depend on the electric conductivity of the surface of the grounded deposition chamber, and (iii) a pulsed dual magnetron with a closed magnetic B field is the only one sputtering system, which enables us to sputter the films with fully reproducible properties. © *2017 American Vacuum Society*. [http://dx.doi.org/10.1116/1.4992054]

I. INTRODUCTION

It is well known that the energy $\mathcal{E}_{bi}$ delivered into a sputtered film by bombarding ions decides on its physical and mechanical properties such as its structure, microstructure, hardness H, effective Young's modulus E^*, elastic recovery W_e, ratio H/E^*, and macrostress σ. In the simplest case of 100% ionized and collisionless discharge, the energy $\mathcal{E}_{bi}$ is determined by the following formula:[1,2]

$$\mathcal{E}_{bi}(MJ/cm^3) = (U_p - U_s)\, i_s/a_D. \qquad (1)$$

Here, U_p is the plasma potential, U_s is the substrate bias, i_s is the substrate ion current density, and a_D is the deposition rate of the film. Equation (1) shows that the effect of U_p on E_{bi} can be very small in the case when $|U_p| \ll |U_s|$, but U_p can strongly influence $\mathcal{E}_{bi}$ in the case when $|U_p| \approx |U_s|$. The plasma potential U_p strongly depends on the deposition parameters used in magnetron sputtering, the mode (type) of the magnetron operation [the direct current (DC), pulsed, high-power pulsed magnetron sputtering],[3–9] the geometrical arrangement of the sputtering device,[10] the target power density $W_t = U_d I_d/S$,[11] the sputtering gas pressure p,[6,11] and the state of the surface of the deposition chamber (electrically conductive, semiconducting, and electrically insulating); here, U_d and I_d are the voltage and current of the magnetron discharge and S is the area of the sputtered target. These facts are the main reason why the properties of films sputtered under the same deposition conditions can strongly differ and in many cases cannot be formed in a reproducible way. No investigation of this problem was performed so far. Up to now, main attention was focused on the measurement of the degree of ionization of sputtering gas, electron and ion energy distribution functions[12] and species generated in the magnetron discharges in reactive sputtering and in the presence of different kinds of inert and reactive sputtering gases and their mixtures.

This article shows great differences in the values of the plasma potential U_p and the floating potential U_{fl} in the magnetron discharge generated by (1) the DC single and DC dual magnetron and (2) the pulsed dual magnetron operating at the same deposition conditions. Besides, it is shown that the electric conductivity of the surface of walls of the deposition chamber strongly influences U_p and U_{fl} in reactive magnetron sputtering of films. The way how U_p and U_{fl} changes can be fully eliminated is shown.

II. EXPERIMENT

The plasma potential U_p and the floating potential U_{fl} in the magnetron discharge were measured in a cylindrical deposition chamber (diameter Ø = 600 mm and height h = 600 mm) equipped successively with three sputtering systems: (1) DC single magnetron, (2) DC dual magnetron, and (3) pulsed dual magnetron, see Fig. 1. All magnetrons were the same and were equipped with Ti (6Al 4V) alloy targets made of a VT6 titanium alloy containing 6 at. % Al and 4 at. % V. Both DC and pulsed dual magnetron systems have a closed magnetic field B between magnetrons, see Figs. 1(b) and 1(c). The sputtering discharges were generated at the same power $P_{DC} = P_{1DC} + P_{2DC} = P_{1p} + P_{2p} = 500$ W and the same sputtering gas pressure $p = p_{Ar} + p_{N_2} = 0.2 + 0.8 = 1$ Pa; here, indexes 1DC and 2DC and 1p and 2p denote the powers delivered to magnetrons 1 and 2 by two DC power supplies (Advanced Energy Pinnacle Plus+ 5/5 kW operated in a DC mode) and by a pulsed power supply (Advanced Energy Pinnacle Plus+ 5/5 kW operated in the bipolar mode with asynchronous pulses), respectively, see Fig. 2; p_{Ar} and p_{N_2} are partial pressures of argon and nitrogen, respectively. More details on the discharge of the dual magnetron with closed and open (mirror) magnetic fields B are given in Ref. 13.

The voltage on magnetron 1 and magnetron 2 in the DC dual magnetron system and in the pulsed dual magnetron system is shown in Fig. 2. Figure 2(b) shows that during pulse-off time, the magnetron voltage is slightly positive. It enables us to remove the positive charge accumulated on the target when electrically insulating films are sputtered, to avoid arcing on the target surface, and to form defect free films.[14] The Ti(Al,V)N films were reactively sputtered on Si(100) substrates placed at the substrate temperature of $T_s = 500\,°C$, the substrate-to-target distance of $d_{s\text{-}t} = 60$ mm, and the total sputtering gas pressure of $p_T = p_{Ar} + p_{N_2} = 0.2$ Pa + 0.8

[a)]Electronic mail: musil@kfy.zcu.cz

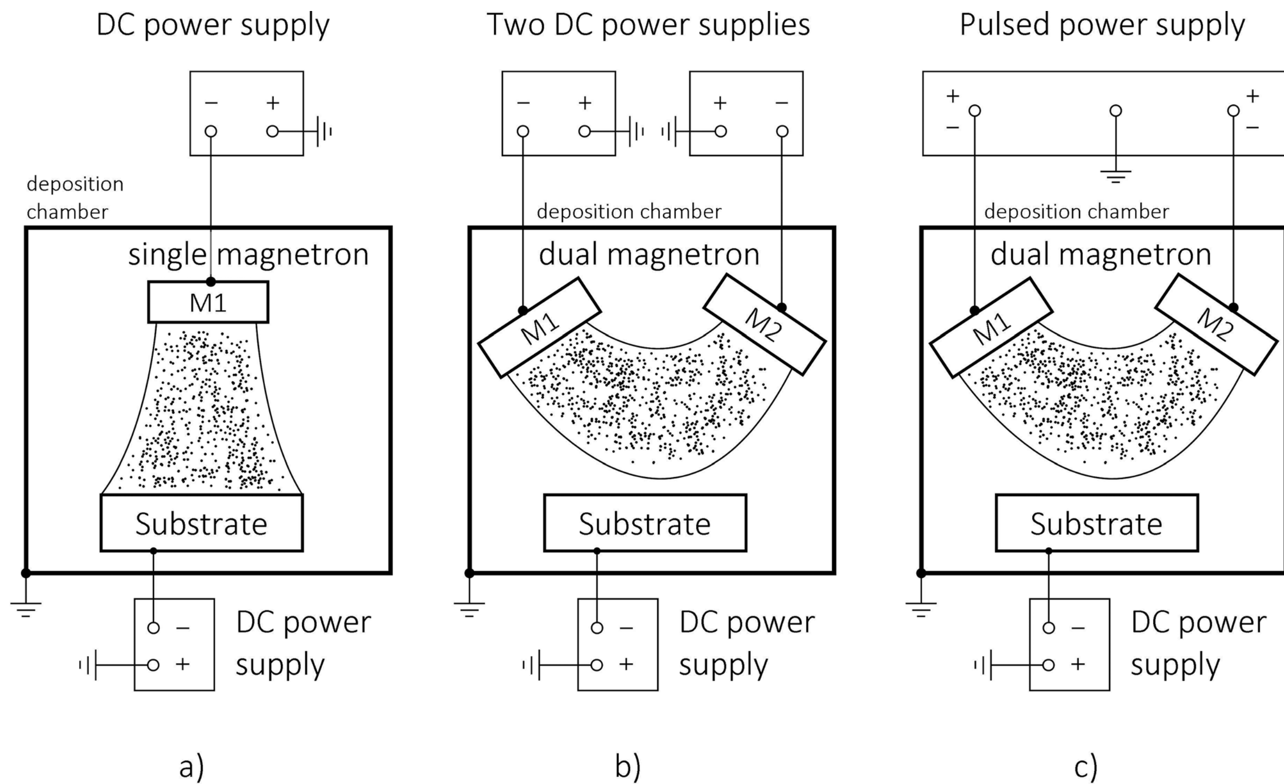

FIG. 1. Schematic illustration of the discharge generated by (a) DC single magnetron, (b) DC dual magnetron, and (c) pulsed dual magnetron and the electrical connection of power supplies.

Pa = 1 Pa; here, p_{Ar} and p_{N_2} are the partial pressure of argon and nitrogen, respectively. All measurements of the plasma potential U_p and the floating potential U_{fl} were carried out in the discharge generated at an unheated substrate. The change in the electrical conductivity of the surface of the deposition chamber from electrically conductive to nonconductive (electrically insulating) was made by a pulsed reactive sputtering of TiO_2 films from the Ti(Al,V) targets of the dual magnetron at the total pressure of $p_T = p_{Ar} + p_{O_2} = 0.5 + 0.5 = 1$ Pa and the pulsed averaged power of $P_{da} = 1000$ W.

III. RESULTS AND DISCUSSION

In this section, two problems were investigated in detail: (1) Differences in the plasma potential U_p and the floating potential U_{fl} in the DC and pulsed magnetron discharges and (2) The elimination of the effect of the electrical conductivity of the surface of the deposition chamber on the properties of sputtered films and the finding of the magnetron sputtering system which enables us to sputter films with fully reproducible properties.

The plasma potential U_p and the floating potential U_{fl} were determined from Volt-Ampere (V-A) characteristics measured at the substrate. Our experiments show that the V-A characteristics at the substrate measured in the discharge generated by the DC single magnetron [Fig. 1(a)] and by the DC dual magnetron [Fig. 1(b)] are identical. Therefore, the V-A characteristics measured at the substrate immersed in the DC dual magnetron discharge and in the Pulsed bipolar dual magnetron discharge are only compared, see Fig. 3.

Figure 3 shows strong differences in the values of U_p and U_s in the DC and Pulsed bipolar dual magnetron discharges generated at the same power P = 500 W. The main results of this experiment are as follows:

(1) The single magnetrons [Fig. 1(a)] and the dual magnetrons with a closed magnetic field [Fig. 1(b)] powered by the DC power always have the ground outside the magnetron discharge, i.e., outside the chamber walls. In contrast, the pulsed dual magnetrons with a closed magnetic field operated with asynchronous pulses [Fig. 1(c)] have the ground inside the magnetron discharge.
(2) In discharges of the DC single and DC dual magnetrons, the floating potential U_{fl} is negative. Therefore, the films sputtered in discharges generated by the DC single and dual magnetrons are bombarded by electrons at negative substrate biases $|U_s| < |U_{fl}|$. In contrast, the films sputtered in discharges generated by the pulsed dual magnetrons with a closed B field are bombarded by ions at positive substrate biases if $U_{fl} \geq U_s \geq 0$. It is the main reason why the properties of the films sputtered under the same deposition conditions on the grounded substrate by the DC and pulsed dual magnetrons strongly differ, see Fig. 3 and Table I.

Figure 4 displays XRD patterns of the Ti(Al,V)N films reactively sputtered on the grounded substrate ($U_s = 0$) by the DC and Pulsed bipolar dual magnetron at the same deposition conditions: $W_{t\ DC} = 12.8\ W/cm^2$, $W_{tp} = 25.6\ W/cm^2$, $T_s = 500\,°C$, $d_{s\text{-}t} = 60$ mm, and $p_T = p_{Ar} + p_{N_2} = 0.2 + 0.8 = 1$ Pa; here,

FIG. 2. (Color online) Schematic illustration of the voltage on magnetron 1 and magnetron 2 at (a) DC dual magnetron and (b) pulsed bipolar dual magnetron operated with asynchronous pulses.

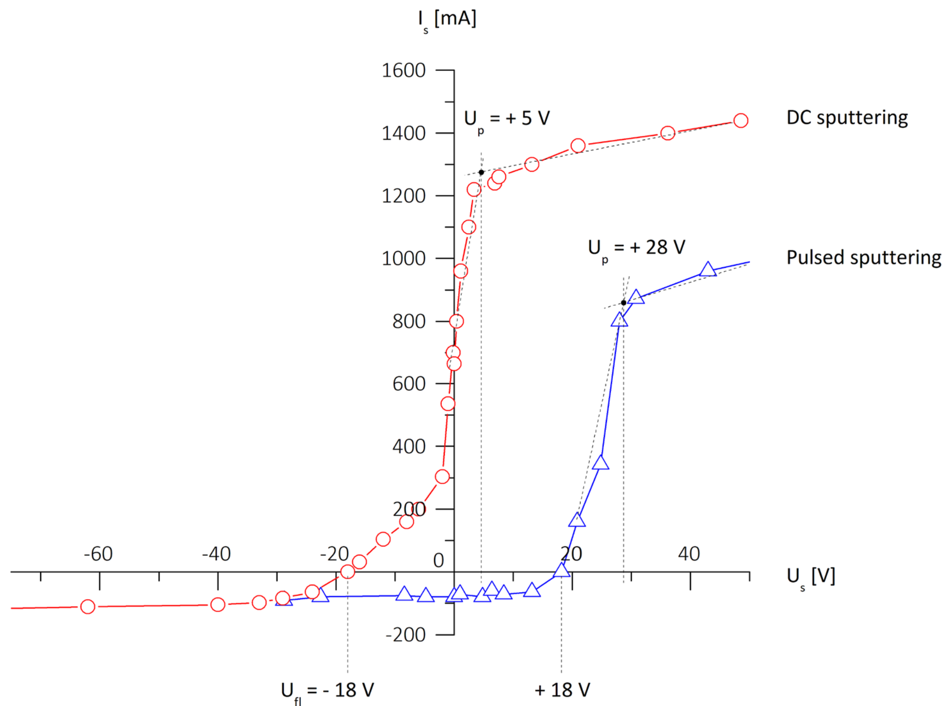

FIG. 3. (Color online) V-A characteristics measured on the substrate immersed in the dual magnetron discharge powered by (a) DC power $P_{1DC} = P_{2DC} = 250$ W and (b) Pulsed power with asynchronous pulses with $P_{1p} = P_{2p} = 500$ W, repetition frequency $f_r = 1/T = 100$ kHz, and duty cycle $\tau/T = 0.5$; here, indexes 1 DC and 2 DC and 1p and 2p denote the powers delivered to magnetrons 1 and 2 by the two DC power supplies and the pulsed power supply, respectively.

TABLE I. Properties of Ti(Al,V)N films sputtered on the grounded substrate ($U_s = 0$) by DC and Pulsed bipolar dual magnetron at the same deposition conditions: $W_{t\,DC} = W_{tp} = 12.8\,W/cm^2$, $T_s = 500\,°C$, $d_{s\text{-}t} = 60\,mm$ and $p_T = p_{Ar} + p_{N_2} = 0.2 + 0.8 = 1\,Pa$ at different energies $\mathcal{E}_{bi}$ and $\mathcal{E}_{el}$.

Sputtering	U_s (V)	I_s	i_s (mA/cm^2)	$\mathcal{E}_{bi}$ (MJ/cm^3)	$\mathcal{E}_{el}$ (MJ/cm^3)	h (nm)	a_D (nm/min)	H (GPa)	E^* (GPa)	W_e (%)	H/E^*	σ (GPa)
DC	0	Electrons	10.60	—	3.4	1700	18.9	16.1	195	58	0.08	0.3
Pulsed	0	ions	1.12	1	—	1400	15.6	23.5	224	67	0.10	−1.2

$W_{t\,DC}$ and $W_{t\,p}$ are the target power density of one magnetron in the DC dual magnetron and in the pulsed bipolar dual magnetron, respectively. The structures of both films strongly differ. While the DC sputtered film is polycrystalline, the pulsed sputtered film exhibits a strong TiN (111) structure. These strong changes in the film structure also result in strong differences in the mechanical properties of the films sputtered by the DC and pulsed dual magnetron, respectively, see Table I. The film deposited by DC dual magnetron sputtering exhibits lower values of hardness H, elastic recovery W_e, and low ratio $H/E^* \leq 0.1$ compared to the film deposited by pulsed dual magnetron sputtering. Moreover, the pulsed sputtered film exhibits an enhanced resistance to cracking due to the high ratio $H/E^* = 0.1$.[2,15] This experiment clearly shows how important it is to know the floating U_{fl} and plasma U_p on the substrate and inside magnetron discharge, respectively, during deposition of the film. Also, it is worthwhile to note that the deposition rate a_D of the Ti(Al,V)N film sputtered by DC and Pulsed bipolar dual magnetron at the same deposition conditions, i.e., at $W_{t\,DC} \approx W_{tp} = 12.8\,W/cm^2$, $T_s = 500\,°C$, $d_{s\text{-}t} = 60\,mm$, and $p_T = p_{Ar} + p_{N_2} = 0.2 + 0.8 = 1\,Pa$, is approximately the same.

A. Elimination of the effect of chamber walls on the properties of sputtered films

The place of the ground of the electrical connection of power supplies used for the generation of the magnetron discharge—outside discharge (the chamber walls) or inside discharge (the sputtered target of the magnetron)—strongly influences V-A characteristics on the substrate, see Fig. 5. When the ground is outside discharge, the V-A characteristics depend on the electrical conductivity of the chamber walls, see Fig. 5(a). The negative floating potential U_{fl} on the substrate increases with the decreasing electrical conductivity of the chamber walls. This change in U_{fl} is caused by the wall contamination by (1) oxygen and nitrogen during opening of the deposition chamber to air for the deloading of coated parts (samples) and its loading by noncoated ones and particularly (2) condensing of different reactive species created during the reactive magnetron sputtering of films. The increase in negative floating potential U_{fl} is connected with a secondary electron yield of the surface of chamber walls increasing with the decrease in its electrical conductivity. The contamination of the surface of the grounded deposition chamber is the main reason why the sputtering of the films with fully reproducible properties is a very serious problem.

This problem can be fully avoided in the case when the ground is inside the magnetron discharge, see Fig. 5(b). In this case, the V-A characteristics do not depend on the electric conductivity of the surface of chamber walls. This means that the Pulsed sputtering by the dual magnetron with a closed B field is the best sputtering system enabling deposition of films with fully reproducible properties.

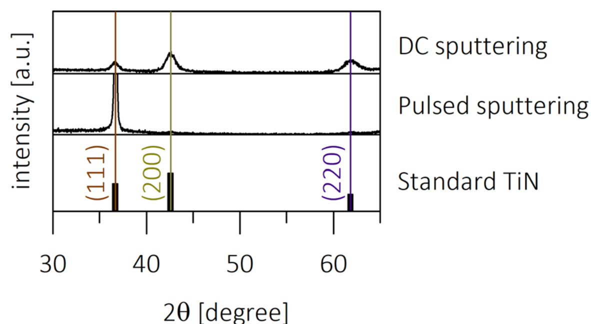

FIG. 4. (Color online) XRD patterns of the Ti(Al,V)N films sputtered on the grounded substrate ($U_s = 0$) by DC and pulsed dual magnetrons powered at the same deposition conditions: $W_{t\,DC} \approx W_{tp} = 12.8\,W/cm^2$, $T_s = 500\,°C$, $d_{s\text{-}t} = 60\,mm$, and $p_T = p_{Ar} + p_{N_2} = 0.2 + 0.8 = 1\,Pa$.

IV. CONCLUSIONS

The results of the reported investigation are very important for both the deepening of the present state of knowledge in the field of reactive magnetron sputtering of thin films and the design of new advanced sputtering systems which enable us to sputter the films with fully reproducible properties. Main results can be summarized as follows:

(1) The properties of the films sputtered by the single and dual magnetrons at the same power P delivered to the magnetron discharge and other constant deposition conditions (U_s, T_s, $d_{s\text{-}t}$, and p) differ due to different values of the plasma potential U_p and the floating potential U_{fl}, which results in a different energy $\mathcal{E}_{bi} = (U_p - U_s)\,i_s/a_D$ delivered to the growing film by bombarding ions.
(2) The values of U_p and U_s strongly depend on the electrical connection of the power supply of the magnetron. For the single and DC dual magnetron, the ground is outside discharge. In contrast, for the pulsed dual magnetron with a closed magnetic field, the ground is inside the discharge.
(3) The properties of the films sputtered on the grounded substrate by the single and DC dual magnetrons at the

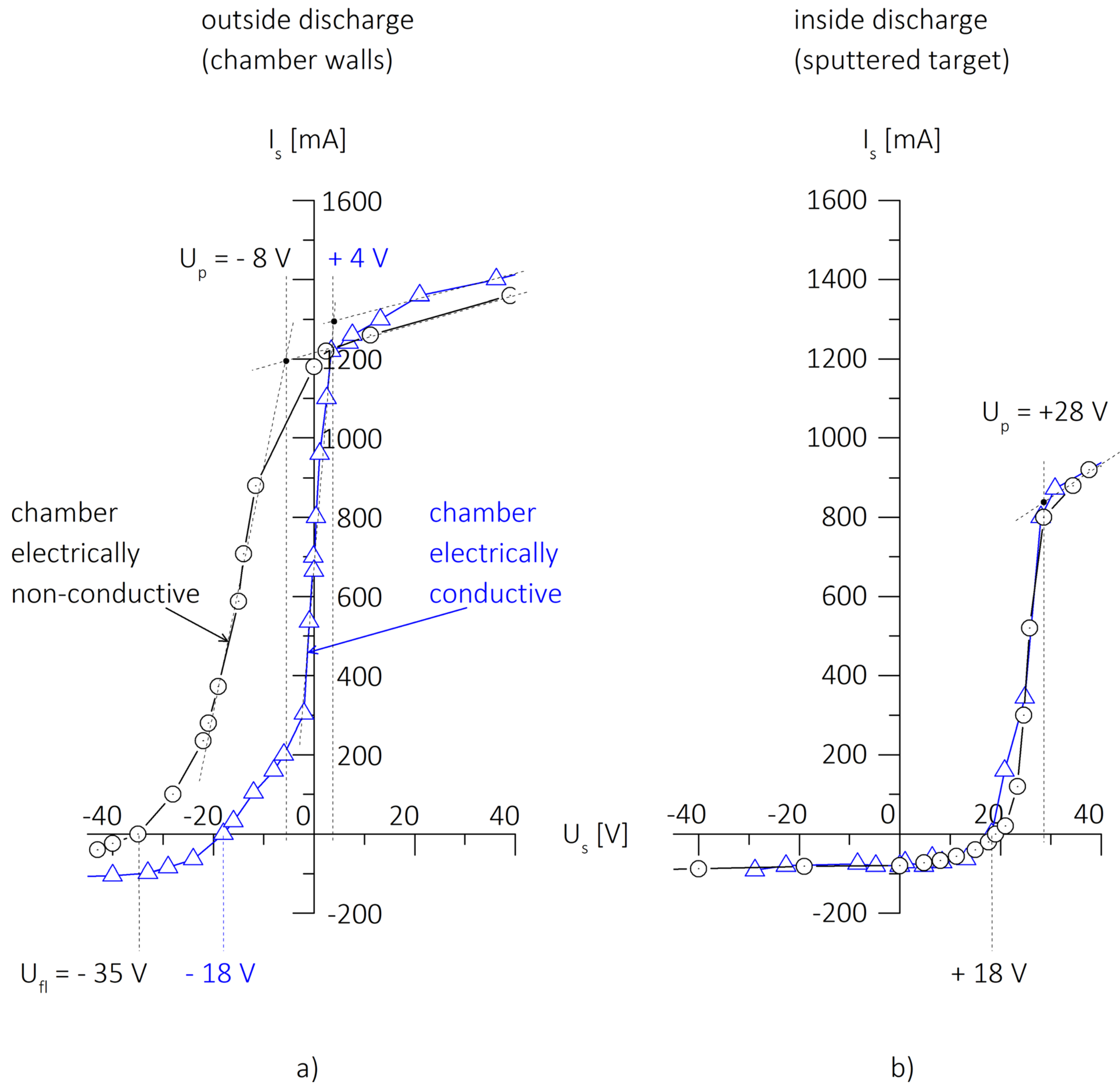

FIG. 5. (Color online) V-A characteristics measured on the substrate immersed in the dual magnetron discharge powered by (a) DC power and (b) pulsed power with asynchronous pulses in the deposition chamber whose walls are electrically conductive (triangles) and nonconductive (circles).

same power P and other constant deposition conditions strongly differ from those sputtered by the pulsed dual magnetrons with a closed magnetic field. It is due to the fact that while in the single and DC dual magnetron discharge, electrons flow on the grounded substrate, in the pulsed dual magnetron with a closed magnetic field, ions flow on the grounded substrate. It results in a great difference in the energy $\mathcal{E}$ delivered to the growing film.

(4) In discharges of the single magnetrons and the DC dual magnetrons powered by two grounded power supplies, the values of U_p and U_s depend on the state of the surface of the chamber walls (electrically conductive or nonconductive) and the formation of reactively sputtered films is very difficult. On the other hand, in pulsed discharges of the dual magnetrons with a closed magnetic field in which the ground is inserted inside the discharge, the values of U_p and U_{fl} do not depend on the state of deposition chamber walls. This means that the pulsed dual magnetron ensures a long-term reactive sputtering of the films with fully reproducible properties without any effect of varying contamination of the deposition chamber walls.

ACKNOWLEDGMENTS

This work was supported by the Project No. LO1506 of the Czech Ministry of Education, Youth and Sports under

the program NPU I. The authors thank R. Čerstvý for the measurement of XRD patterns of the Ti(Al,V)N films.

[1]J. Musil, J. Šícha, D. Heřman, and R. Čerstvý, J. Vac. Sci. Technol., A **25**, 666 (2007).
[2]J. Musil, Surf. Coat. Technol. **207**, 50 (2012).
[3]J. W. Bradley, H. Bäcker, P. J. Kelly, and R. D. Arnell, Surf. Coat. Technol. **135**, 221 (2001).
[4]C. Muratore, J. J. Moore, and J. A. Rees, Surf. Coat. Technol. **163**, 12 (2003).
[5]H. Bäcker, P. S. Henderson, J. W. Bradley, and P. J. Kelly, Surf. Coat. Technol. **174**, 909 (2003).
[6]J. Vlček, A. D. Pajdarová, and J. Musil, Contrib. Plasma Phys. **44**, 426 (2004).
[7]F. Richter, Th. Welyel, Th. Dunger, and H. Kupfer, Surf. Coat. Technol. **188**, 384 (2004).
[8]A. Mishra, P. J. Kelly, and J. W. Bradley, Plasma Sources Sci. Technol. **19**, 045014 (2010).
[9]B. B. Sahu, J. G. Han, J. B. Kim, M. Kumar, S. Jin, and M. Hori, Plasma Processes Polym. **13**, 134 (2016).
[10]J. W. Bradley, H. Bäcker, P. J. Kelly, and R. D. Arnell, Surf. Coat. Technol. **142**, 337 (2001).
[11]L. Sirghi, T. Aoki, and Y. Hatanaka, Surf. Coat. Technol. **187**, 358 (2004).
[12]A. D. Pajdarová, J. Vlček, P. Kudláček, and J. Lukáš, Plasma Sources Sci. Technol. **18**, 025008 (2009).
[13]J. Musil and P. Baroch, IEEE Trans. Plasma Sci. **33**, 338 (2005).
[14]W. D. Sproul, D. J. Christie, and D. C. Carter, Thin Solid Films **491**, 1 (2005).
[15]J. Musil, RSC Adv. **5**, 60482 (2015).

Vacuum 158 (2018) 52–59

Contents lists available at ScienceDirect

Vacuum

journal homepage: www.elsevier.com/locate/vacuum

Effect of energy on macrostress in Ti(Al,V)N films prepared by magnetron sputtering

M. Jaroš*, J. Musil, R. Čerstvý, S. Haviar

Department of Physics and NTIS – European Centre of Excellence, University of West Bohemia, Univerzitní 8, CZ-306 14, Plzeň, Czech Republic

ARTICLE INFO

Keywords:
Ti(Al,V)N films
Energy
Mechanical properties
Macrostress
Film cracking
Magnetron sputtering

ABSTRACT

The article reports on the effect of the energy $\mathscr{E}$ delivered into the growing film on its macrostress, microstructure, mechanical properties and resistance to cracking of Ti(Al,V)N films. The Ti(Al,V)N films were deposited on Si(111) and Mo substrates by magnetron sputtering in a mixture Ar + N_2 gases using a dual magnetron with closed magnetic field and equipped with TiAlV (6 at.% Al, 4 at.% V) alloy targets. It is shown that the compressive macrostress σ in sputtered films can be reduced either by the pulsed bipolar bias voltage U_{sp} with alternating negative and positive pulses or the electron and ion bombardment during overshoots in the pulsed magnetron sputtering. All sputtered films with high ratio $H/E^* \geq 0.1$, compressive macrostress ($\sigma < 0$), and non-columnar microstructure exhibit an enhanced resistance to cracking; here H is the hardness and E^* is the effective Young's modulus. The high compressive macrostress in the film is not the necessary condition for the formation of the films with an enhanced resistance to cracking.

1. Introduction

There is a huge number of papers devoted to the investigation of relationships between the deposition parameters of the film and its structure [1–12], microstructure [8–26], phase and elemental composition [2–5,15–20], macrostress [4–9,18–25], physical and functional properties [1–31]. Despite these facts, it is very difficult to sputter in different deposition chambers with different magnetrons, and different power supplies (DC, pulsed) the films with reproducible properties. It is due to the fact that different combinations of deposition parameters, different magnetrons (single, dual, etc.) and different arrangement of substrate holders (stationary, rotating) result in different energies $\mathscr{E}$ delivered into the growing film. It means that the main parameter controlling the properties of the film is the energy $\mathscr{E}$ [32–42]. Therefore, the knowledge of correlations between the energy $\mathscr{E}$ and the film properties is very important.

In deposition of films using an ion plating process, i.e. in the case when the substrate on which the film is deposited is held on a negative substrate bias U_s, the most important is the energy $\mathscr{E}_{bi}$ delivered to the film during its growth by bombarded ions. In the simplest case of a collision-less, fully ionized plasma the energy $\mathscr{E}_{bi}$ can be expressed in the following form [42].

$$\mathscr{E}_{bi}\ [J/cm^3] = |U_p - U_s| \times i_s/a_D \quad (1)$$

Here, U_p is the plasma potential, U_s is the substrate bias, i_s is the substrate ion current density and a_D is the deposition rate of the film. Under the assumption that $|U_p| \ll |U_s|$, which is well fulfilled in many experiments, Eq. (1) can be simplified in the following simple form

$$\mathscr{E}_{bi}\ [J/cm^3] \approx (|U_s| i_s)/a_D \quad (2)$$

Eq. (2) shows that the energy $\mathscr{E}_{bi}$ delivered to the growing film by bombarding ions can be easily calculated from measured deposition parameters (U_s, i_s) and the film deposition rate $a_D = h/t_d$ calculated from the measured film thickness h and the deposition time t_d.

Recently, it was demonstrated that, the Ti(Al,V)N films with enhanced resistance to cracking are created at high energies $\mathscr{E}_{bi} > 1.7\ MJ/cm^3$ [43]. However, the intensive ion bombardment generates high compressive stresses (up to -3 GPa to −5 GPa) in sputtered films [44]. Such films easily delaminate from the substrate and crack. Therefore, it is necessary to decrease the compressive macrostress σ but simultaneously to deliver to the film sufficiently high energy $\mathscr{E}_{bi}$ necessary to sputter the film with dense, non-columnar microstructure exhibiting no delamination from substrate and an enhanced resistance resistance to cracking.

The solution of this quite difficult task is the subject of this article. It is shown that the films with an enhanced resistance to cracking and a low compressive macrostress $|\sigma| \leq 1$ GPa can be formed in the case

* Corresponding author.
E-mail address: jarosm@kfy.zcu.cz (M. Jaroš).

https://doi.org/10.1016/j.vacuum.2018.09.038
Received 4 April 2018; Received in revised form 7 August 2018; Accepted 17 September 2018
Available online 18 September 2018
0042-207X/ © 2018 Published by Elsevier Ltd.

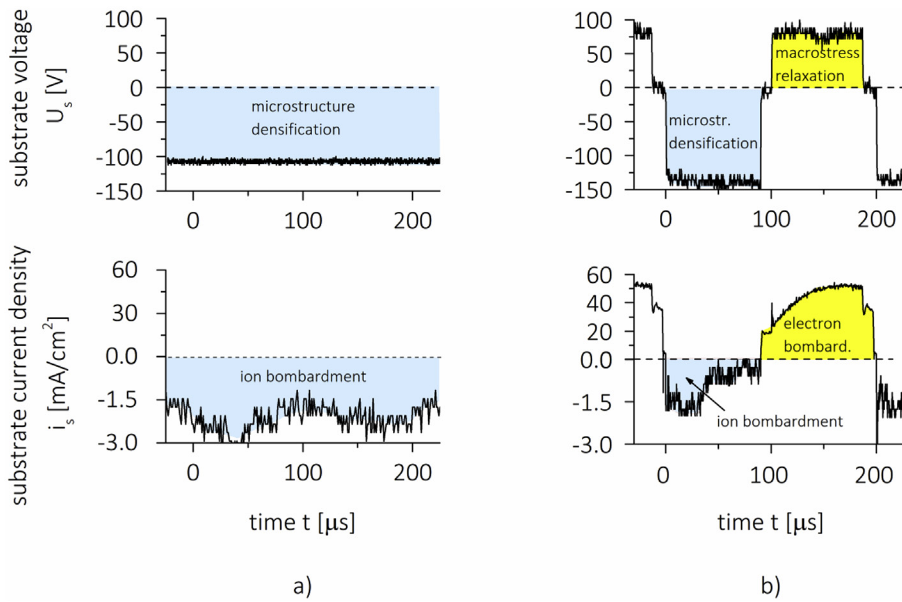

Fig. 1. Comparison of DC and pulsed substrate bias used in deposition of Ti(Al,V)N films by DC dual magnetron discharge generated at $I_d = 1$ A, $T_s = 500\,°C$, $d_{s\text{-}t} = 60$ mm, $p_T = p_{Ar} + p_{N2} = 0.8 + 0.2 = 1$ Pa. (a) Continuous ion bombardment and (b) alternating ion/electron bombardment of the growing Ti(Al,V)N film by ions and electrons produced by DC bias (U_s = - 100 V) and pulsed bias (U_{sp} = - 130/+70 V, f_r = 5 kHz), respectively. Here, U_{sp} is the pulsed substrate bias U_{sp} and i_{sp} is the pulsed substrate current density.

Table 1
Physical and mechanical properties and compressive macrostress ($\sigma < 0$) in the Ti(Al,V)N films sputtered by DC dual magnetron operated at I_d = 1 A, T_s = 500 °C, $d_{s\text{-}t}$ = 60 mm, $p_T = p_{Ar} + p_{N2}$ = 0.2 + 0.8 = 1 Pa on the substrate held at (i) DC substrate bias voltage $U_{s\,DC}$ and (ii) pulsed substrate bias voltage U_{sp} with repetition frequency of pulses f_r = 5 kHz. The bending test was performed on the films sputtered on the Mo strip and the indentation test on the films sputtered on the Si substrates.

bias voltage	f_r [kHz]	U_{sp} [V]	i_s [mA/cm^2]	h [nm]	a_D [nm/min]	τ_e/τ_i	$\mathscr{E}_{bip}$ [MJ/cm^3]	σ [GPa]	H [GPa]	E* [GPa]	W_e [%]	H/E*	ε_{cr} [%]	L_{cr} [N]	structure	texture
DC	0	−40	1.0	2100	36.0	0	1.6	−1.7	28.4	282	70	0.10	–	0.25	crystaline	(200)+(220)
DC	0	−100	1.8	1100	37.5	0	3.7	−4.0	30.7	220	81	0.14	> 2.0	> 1	crystaline	(220)
pulsed	5	−100/+70	0.9	1000	33.0	1.3	1.6	−0.8	19.1	175	68	0.11	1.3	0.75	XRA	

$\mathscr{E}_{bip}$ is the average energy of ions during the negative pulse of pulsed substrate bias U_{sp}, and XRA is X-ray amorphous.

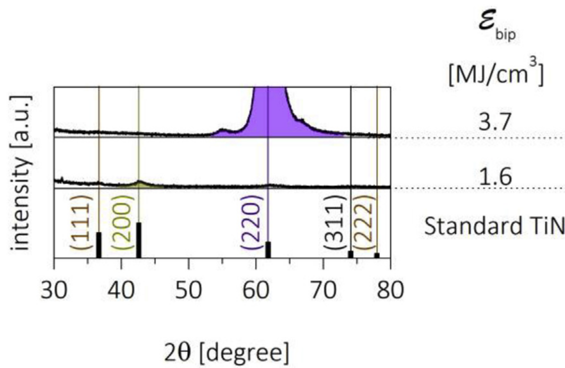

Fig. 2. Comparison of the structure of the Ti(Al,V)N film sputter deposited at (i) DC substrate bias $U_{s\,DC}$ = −100 V and a high energy $\mathscr{E}_{bi}$ = 3.7 MJ/cm^3 and (ii) the pulsed substrate bias U_{sp} and a low energy $\mathscr{E}_{bip}$ = 1.6 MJ/cm^3.

when σ generated in sputtered film is relaxed by bombardment of electrons during its growth. Two methods are described in detail: (1) the DC sputtering with pulsed bipolar bias with alternating negative and positive pulses and (2) the pulsed sputtering with electron bombardment of the film during overshoots at the end of each pulse. Both methods efficiently reduce the compressive macrosrostress ($\sigma < 0$) in sputtered films. It was demonstrated in sputtering of the Ti(Al,V)N nitride films.

2. Experimental

The Ti(Al,V)N nitride films were reactively sputter deposited on Si (111) and Mo substrates at substrate temperature T_s = 500 °C and substrate-to-target distance $d_{s\text{-}t}$ = 60 mm by a dual magnetron with closed magnetic field equipped with TiAlV (6 at.% Al, 4 at.% V) alloy targets of diameter ∅ = 50 mm in a mixture of Ar + N2 sputtering gases. The magnetrons were tilted at angle 20° to the vertical axis [45] and supplied by an Advanced Energy Pinnacle Plus+ 5/5 kW power supply operated either in the DC or pulse mode. The Ti(Al,V)N films deposited by a dual magnetron powered by DC power were sputtered at I_d = 1 A results in $W_t = I_d U_d/S \approx 16$ W/cm^2, and the substrate held either at constant negative bias U_s or at pulsed bipolar positive/negative bias. The Ti(Al,V)N films deposited by a dual magnetron powered by pulsed power were sputtered at the repetition frequency of pulses f_r ranging from 100 kHz to 350 kHz, τ/T = 0.5 and I_d ranging from 1.6 to 2 A resulting in the target power density $W_t = I_{dp} U_{dp}/S < 16$ W/cm^2 and the substrate bias held at the floating potential U_{fl} or at the constant negative bias; here I_{dp} and U_{dp} is the discharge current and voltage during pulse-on time, respectively, and S is the total area of the sputtered target. All Ti(Al,V)N_x films were sputtered in the nitrogen-rich atmosphere at p_{N2}/p_T = 0.8. The films sputtered under these conditions were almost stoichiometric (x = N/(Ti + Al + V) ≈ 1) and their stoichiometry x varied in a very narrow range from 0.98 to 1.09 only. The Si plates (20 × 20 × 0.64 mm^3) were used for of X-ray diffraction patterns and the Si strips (30 × 5 × 0.64 mm^3) were used for the measurement of the macrostress σ in the sputtered films. The Mo substrates (80 × 15 × 0.20 mm^3) coated by sputtered films were used for the assessment of the film resistance to cracking in bending. A pre-

Table 2
Physical and mechanical properties and compressive macrostress ($\sigma < 0$) in the Ti(Al,V)N films sputtered by DC dual magnetron operated at I_d = 1 A, T_s = 500 °C, d_{s-t} = 60 mm, $p_T = p_{Ar} + p_{N2}$ = 0.2 + 0.8 = 1 Pa on the substrate held at pulsed bipolar substrate bias U_{sp} with two repetition frequencies f_r of alternating negative and positive pulses. The bending test was performed on the films sputtered on the Mo strip and the indentation test on the films sputtered on the Si substrates.

f_r	U_{sp}	h	i_{sp}	a_D	τ_e/τ_i	$\mathscr{E}_{bip}$	σ	H	E*	W_e	H/E*	ε_{cr}	L_{cr}	texture
[kHz]	[V]	[nm]	[mA/cm²]	[nm/min]		[MJ/cm³]	[GPa]	[GPa]	[GPa]	[%]		[%]	[N]	
High electron bombardment														
25	−130/+110	1500	1.3	45.0	3.2	2.3	−1.7	29.5	260	73	0.11	> 2	> 1	(220)
25	−130/+110	2600	1.3	45.0	3.2	2.4	−1.9	28	270	70	0.10	> 2	> 1	(220)
Low electron bombardment														
5	−130/+70	1300	1.3	33.0	1.3	3.1	−2.1	28.2	211	79	0.13	delam	> 1	(220)
5	−130/+70	2100	1.3	31.0	1.3	3.3	−2.4	33.5	246	82	0.14	delam	> 1	(220)

$\mathscr{E}_{bip}$ is the average energy of ions during the negative pulse of pulsed substrate bias U_{sp}.
"delam" denotes that the films delaminates from Mo strips during bending.

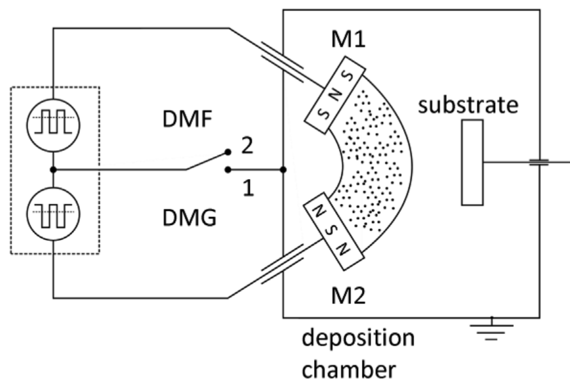

Fig. 3. Schematic illustration of the asymmetric bipolar Advanced Energy Pinnacle Plus+ 5 kW pulsed power supply (PSU). The abbreviations DMG and DMF denote that the PSU symmetry point is grounded (the position 1) and floating, i.e. disconnected from the grounded deposition chamber, (the position 2).

deposition etching of substrates was performed in the pulsed discharge (generated between the substrate and the shutter) at the voltage U = 400 V, current I = 0.5 A, repetition frequency f_r = 100 kHz, τ/T = 0.5, substrate temperature T_s = 500 °C and shutter-to-target distance d_{s-t} = 60 mm in argon at pressure p_{Ar} = 1 Pa for 5 min. A pre-deposition cleaning of the magnetron targets was performed in DC mode of sputtering at the magnetron voltage U_d = 400 V and current I_d = 0.5 A, target power density $W_t \approx 10\ \mathrm{W/cm^2}$ in argon at pressure p_{Ar} = 1 Pa for 3 min.

The film thickness h was measured by a stylus profilometer DEKTAK 8. The macrostress σ was evaluated from the bending of Si plate using the Stoney's formula [46]. The film structure was characterized by X-ray diffraction using an XRD diffractometer PANalytical X Pert PRO in the Bragg-Brentano configuration with CuKα radiation. The elemental composition of the Ti(Al,V)N films deposited on Si substrates was analyzed by a scanning electron microscope (SU-70, Hitachi) operated at a primary electron energy of 15 keV using both the energy dispersive spectroscopy (EDS, UltraDry, Thermo Scientific) and the wave dispersive spectroscopy (WDS, Magnaray, Thermo Scientific). Pure metal standards for the determination of Ti, Al and V concentrations in the film were used. The nitrogen concentration was calculated as the difference to 100 wt %. The Ti(Al,V)$N_{x\approx1}$ films exhibit stochiometry x = N/(Ti + Al + V) ranging from 0.98 to 1.09. Mechanical properties of sputtered films were determined from load vs. displacement curves measured by a microhardness tester Fisherscope H100 with Vickers diamond indenter at a load of 20 mN. The resistance of the Ti(Al,V)N films to cracking was determined by (i) the indentation test at high loads L_{cr} (critical load when cracks occur) ranging from 0.25 to 1 N and (ii) the bending test; more details are given in Refs. [42,47,48]. The Mo strip coated with the sputtered film was bent around a fixed cylinder of different radius r. The strain induced in the film by bending was increased by decreasing of the radius r of fixed cylinder. The critical strain ε_{cr} at which cracks in the film occur was measured. The critical strain ε_{cr} was calculated from the following formula [42].

$$\varepsilon_{cr} \approx h_{Mo}/2r \tag{3}$$

Here, h_{Mo} is the thickness of the Mo strip.

3. Results and discussion

In this section two ways of sputtering of the low-stress Ti(Al,V)N films with enhanced resistance to cracking are described in detail. Both methods of a reduction of the macrostress σ in sputtered films are based on an electron heating of the film material during its growth controlled by the energy $\mathscr{E}_{bi}$ delivered into the growing film by bombarding ions. This section consists of three subsections: (1) The macrostress reduction controlled by pulsed bipolar substrate bias U_{sp}, (2) The macrostress reduction controlled by overshoots in pulsed sputtering and (3) Correlations between the energy $\mathscr{E}_{bi}$, the macrostress σ in film, its microstructure and resistance to cracking.

3.1. *Macrostress reduction by pulsed bipolar substrate bias U_{ps}*

The principle of a reduction of the macrostress σ in the sputtered film at a pulsed substrate bias U_{sp} is based on alternating of the ion and the electron bombardment of film during its growth, see Fig. 1. The alternating ion and electron bombardment of the growing film is realized by alternating negative and positive pulses. The microstructure of growing film is densified during the negative pulse of the substrate bias U_{sp} by ion bombardment. Simultaneously, the compressive macrostress ($\sigma < 0$) is generated in the film and its magnitude increases with increasing voltage of the negative pulse. On the other hand, the macrostress σ, generated in the film during the ion bombardment, is relaxed by the electron current which thermally anneals the growing film during the positive pulse of the pulsed substrate bias U_{sp}. It means that the films sputtered at DC substrate bias $U_{s\ DC}$ will always exhibit a higher compressive macrostress ($\sigma < 0$) compared with the films sputtered at a pulsed bipolar substrate bias U_{sp}.

The relaxing of the compressive macrostress ($\sigma < 0$) in sputtered film by the electron bombardment was confirmed by sputtering of the Ti(Al,V)N films under the same deposition conditions at DC and pulsed bipolar bias. Results of this experiment are summarized in Table 1. From Table 1 the following important issues can be drawn.

1. The film sputter deposited at DC negative bias U_s, i.e. at the ion bombardment of the growing film only, exhibits the high compressive macrostress (σ = - 4 GPa) compared with the film sputter deposited at the pulsed bias U_{sp} with alternating negative and positive pulses (σ = - 0.8 GPa).

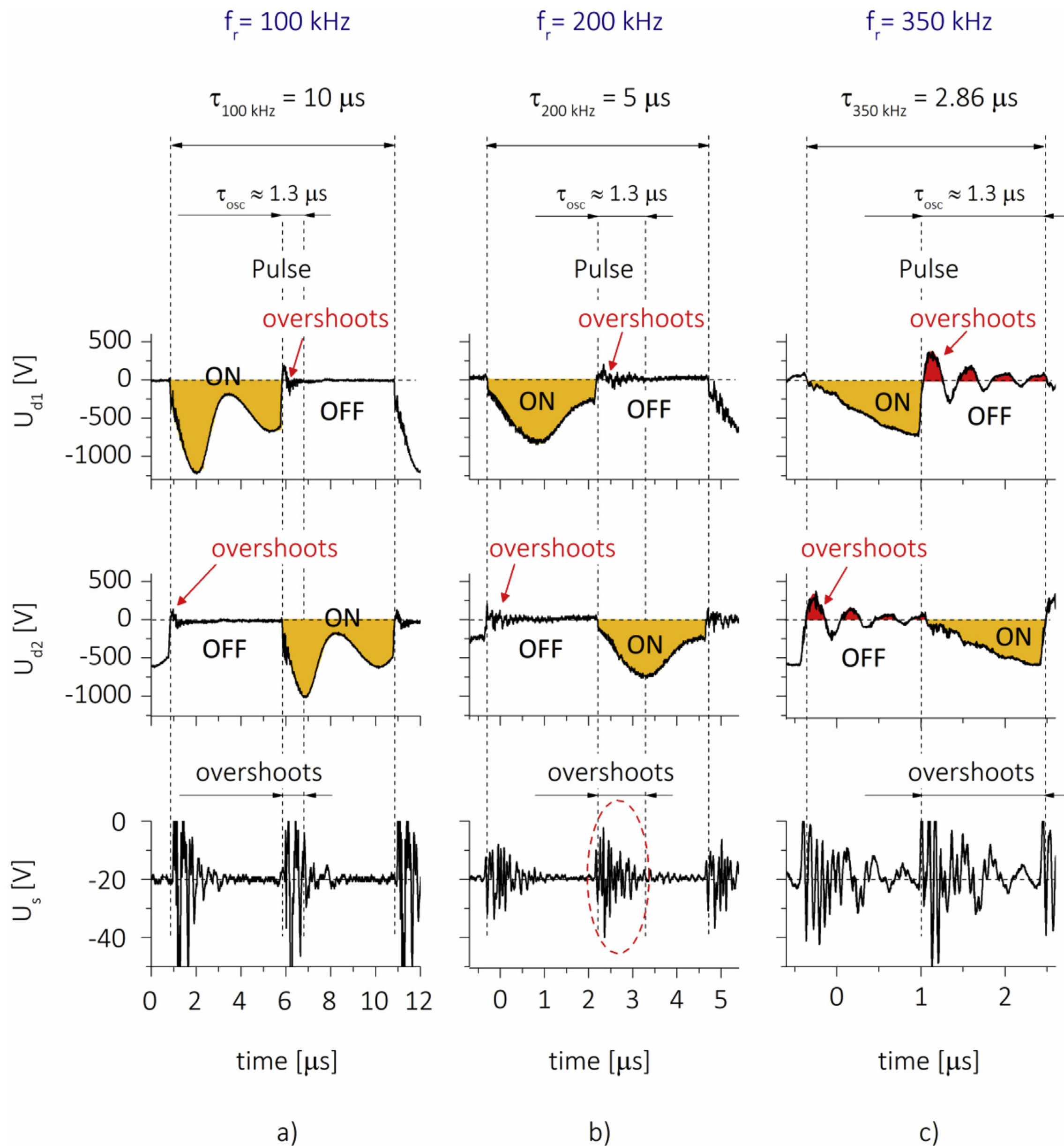

Fig. 4. Time waveforms of the voltage U_{d1} and U_{d2} on the magnetron 1 and the magnetron 2, respectively, of the dual magnetron (DMG) operated in pulsed bipolar mode at $I_d = I_{d1} + I_{d2} = 1.6$ A, $T_s = 500$ °C, $d_{s-t} = 60$ mm, $p_T = p_{Ar} + p_{N2} = 0.2 + 0.8 = 1$ Pa and three repetition frequencies (a) 100 kHz, (b) 200 kHz and (c) 350 kHz, and the DC substrate bias $U_{s\ DC} = -20$ V.

Table 3
Physical and mechanical properties of the Ti(Al,V)N films sputtered by pulsed dual magnetron at $W_d = 12$ W/cm^2, $T_s = 500$ °C, $d_{s-t} = 60$ mm, $p_T = p_{Ar} + p_{N2} = 0.2 + 0.8 = 1$ Pa, floating potential $U_s = U_{fl}$ at two repetition frequencies $f_r = 200$ kHz and 350 kHz.

f_r	h	a_D	E_{bi}	σ	H	E*	W_e	H/E*	ε_{cr}	L_{cr}	micostructure
[kHz]	[nm]	[nm/min]	[MJ/cm^3]	[GPa]	[GPa]	[GPa]	[%]		[%]	[N]	
200	1900	15.8	–	−0.6	23.8	240	68	0.10	1.3	0.25	columnar
350	1300	4.6	–	−2.4	21.4	173	76	0.12	> 2	> 1	dense

2. The energy $\mathscr{E}_{bi}$ delivered to the film growing at pulsed bipolar bias U_{sp} is lower (1.6 MJ/cm^3) than the energy delivered to the film growing at DC bias $U_{s\ DC}$ (3.7 MJ/cm^3). This is a reason why the film sputter deposited at a pulsed bias U_{sp} exhibits the X-ray amorphous structure and the film sputter deposited at DC bias $U_{s\ DC}$ is the crystalline with a dominant TiN (220) texture, see Fig. 2.
3. The electron bombardment of the growing film, however, results not only in the strong decrease of the compressive macrostress σ but also in decrease of its hardness H, elastic recovery W_e, H/E* ratio and the low resistance to cracking, see Table 1.

The electron bombardment of the growing film is the reason why the macrostress σ generated in the film sputter deposited at the pulsed substrate bias U_{sp} with alternating negative and positive pulses is

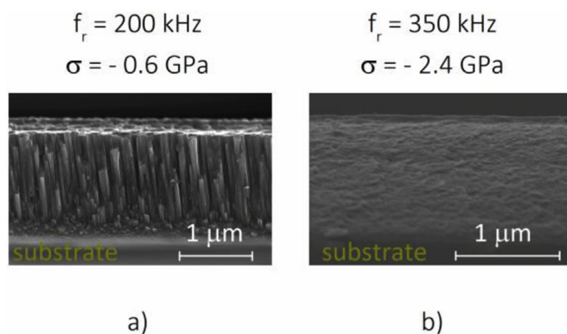

Fig. 5. Microstructure of the Ti(Al,V)N films with (a) low and (b) high compressive macrostress ($\sigma < 0$) sputtered on Si(111) substrates by pulsed DM at two repetition frequencies $f_r = 200$ kHz and $f_r = 350$ kHz, respectively, and $W_d = 12$ W/cm^2, $U_s = U_{fl}$, $T_s = 500$ °C, $d_{s-t} = 60$ mm, $p_T = p_{Ar} + p_{N2} = 0.2 + 0.8 = 1$ Pa.

considerably lower than that in the film sputter deposited at the DC negative substrate bias voltage U_s. The length of the negative pulse τ_i and the length of positive pulse τ_e can be different. It means that the efficiency of a relaxing of macrostress σ in the film can be controlled by the ratio τ_e/τ_i. The possibility to control the macrostress σ in sputtered films by the ratio τ_e/τ_i was also demonstrated in sputtering the Ti(Al,V)N films at pulsed bipolar substrate bias U_{sp}. Results of this experiment are summarized in Table 2.

Table 2 shows the properties of the Ti(Al,V)N films sputtered at pulsed substrate bias U_s with two repetition frequencies f_r of alternating negative and positive pulses of different lengths and the same value of the negative substrate voltage $U_{sp} = -130$ V and two values of the positive substrate voltage ($f_r = 5$ kHz with $U_s = -130/+70$ V, $\tau_e/\tau_i = 1.3$ (low electron bombardment), and $f_r = 25$ kHz with $U_s = -130/+130$ V, $\tau_e/\tau_i = 3.2$ (high electron bombardment)); here τ_e and τ_i is the length of positive and negative pulse, respectively. This selection of parameters of the pulsed bipolar bias U_{sp} makes it possible to investigate the effect of the electron bombardment on mechanical properties of the film, its macrostress σ and resistance to cracking. From Table 2 it is seen that (1) the Ti(Al,V)N film sputtered under high electron bombardment ($U_{sp+} = +110$ V) and the ion energy $\mathscr{E}_{bi} = 2.4$ MJ/cm^3 exhibit high hardness $H = 28$ GPa, high ratio $H/E^* = 0.10$, high elastic recovery $W_e = 70\%$, low compressive macrostress $\sigma = -1.9$ GPa and enhanced resistance to cracking ($\varepsilon_{cr} > 2$ and $L_{cr} > 1$ N) and (2) the Ti(Al,V)N film sputtered under lower electron bombardment ($U_{sp+} = +70$ V) and the higher ion energy $\mathscr{E}_{bi} = 3.1$ MJ/cm^3 exhibit higher values H, H/E*, W_e, $|\sigma| > 2$ GPa and also an enhanced resistance to cracking in compression ($L_{cr} > 1$ N) but this film already delaminates from Mo strip due too high compressive macrostress $|\sigma| > 2$ GPa. This experiment clearly demonstrates that properties of the sputtered film can be well controlled by an optimized bombardment with ions and electrons during its growth.

3.2. Macrostress reduction by overshoots in pulsed sputtering

The control of the energy of bombarding ions $\mathscr{E}_{bi}$ by the pulsed sputtering of the film is based on the utilization of strong discharge oscillations connected with transient pulse phenomena after the pulse off. Experiments demonstrating this fact were performed in the pulsed dual magnetron (DM) discharge. The DM was supplied by the pulse asymmetric bipolar Advanced Energy Pinnacle Plus+ 5 kW power supply unit (PSU) with the reverse positive pulse (10% of the negative voltage). Each magnetron is alternatively sputtered (pulse-on) or discharged (pulse-off) with the repetition frequency $f_r = 1/T_r$. The schematic illustration of the PSU supplying the DM composed of two independent asymmetric bipolar units is shown in Fig. 3. The PSU symmetry point can be either floating (the DM is floating PSU – DMF) or connected to the grounded chamber (the DM is grounded PSU – DMG). In our experiment the PSU - DMG was used.

The oscillations generated in the pulsed bipolar DM discharge are illustrated in Fig. 4. This figure shows the time evolution of the voltage U_{d1} on the magnetron 1 (M1) and U_{d2} on the magnetron 2 (M2) of the dual magnetron with a closed magnetic field B [45]. The pulsed bipolar DM discharge was generated at three repetition frequencies (a) 100 kHz, (b) 200 kHz and (c) 350 kHz. The oscillations superposed on the DC substrate bias U_{sp} are clearly seen.

The principle of the control of the macrostress σ in the growing film during pulsed sputtering is based on the control of the ion bombardment of the film during its growth. Splashes of oscillations (called as the packets or the overshoots) superposed on the substrate potential U_s play a key role in the control of the film macrostress σ, see Fig. 4. These splashes are generated after the switching off of pulses. Therefore, the magnitude of σ in the sputtered film depends on the total number of splashes N_{spls} generated during the whole time of the film deposition. The number N_{spls} of splashes increases with increasing repetition frequency f_r of pulses. Fig. 4 shows that (1) the magnetron voltage U_d sinusoidally changes during the pulse-on time τ_{on}, (2) the length of sinusoid decreases with increasing f_r from $\sim T$ at $f_r = 100$ kHz to $\sim T_r/4$ at $f_r \approx 350$ kHz, and (3) the splashes of oscillations, strongly attenuating with increasing time, are created not only on the voltage waveform of the discharge voltage $U_d(t)$ but also on the waveform of the DC negative substrate bias $U_{s\ DC}$; the splashes of oscillations are denoted by dotted ellipses in Fig. 4b, (4) the duration of the splashes of oscillations is $\tau_{osc} \approx 1.3$ μs is practically constant and does not depend on the repetition frequency of pulses f_r and (5) the number of splashes of oscillations N_{spls} increases with increasing f_r.

During oscillations of the substrate bias U_{sp} the growing film is exposed to a strong ion bombardment. It is due to a strong increase of U_{sp} during negative half periods of oscillations. This strong ion bombardment results in increase of macrostress σ generated in the film. Therefore, a reduction of the macrostress σ in the sputtered film can be achieved by a reduction of the number N_{spls} of splashes of the oscillations. It can be achieved by decreasing of the repetition frequency f_r of sputtering pulses. This fact was confirmed experimentally by sputtering of the Ti(Al,V)N films on the Si(111) substrates held on the floating potential $U_s = U_{fl}$ under the same deposition conditions at two repetition frequencies of pulses $f_r = 200$ kHz and 350 kHz. The film sputter deposited at $f_r = 200$ kHz, i.e. under a lower ion bombardment, exhibits not only the low macrostress (σ = - 0.6 GPa) as expected but also the columnar microstructure because the ion bombardment was already weak and insufficient to create the film with dense voids-free microstructure, see Table 3 and Fig. 5. More information about overshoots and its effect on plasma and coating properties can be found in Refs. [49–57].

This experiment shows that a pulsed magnetron sputtering is an efficient way which allow to control the macrostress σ of the film held even at a floating potential $U_s = U_{fl}$ a and its microstructure by selection of repetition frequency of pulses. This finding is of a great application potential, particularly for sputtering of dielectric films or deposition of films on dielectric substrates, for instance, on glass, etc. Both, the films with porous columnar microstructure or flexible hard protective films with dense, voids-free microstructure can be created on substrates held at a floating potential $U_s = U_{fl}$.

3.3. Control of macostress in films sputtered at high repetition frequencies of pulses

Fig. 6 shows V-A discharge characteristics of a pulsed magnetron discharge used for sputtering of the Ti(Al,V)N films at $f_r = 350$ kHz and different values of the DC substrate bias $U_{s\ DC}$ ranging from negative (−60 V) to positive (+40 V) including grounded and floating substrates, i.e. $U_{s\ DC} = 0$ and $U_{s\ DC} = U_{fl}$ ranging from +15 to ∼ +150 V. From Fig. 6a it is seen that the main source of the ion energy $\mathscr{E}_{bi}$ during

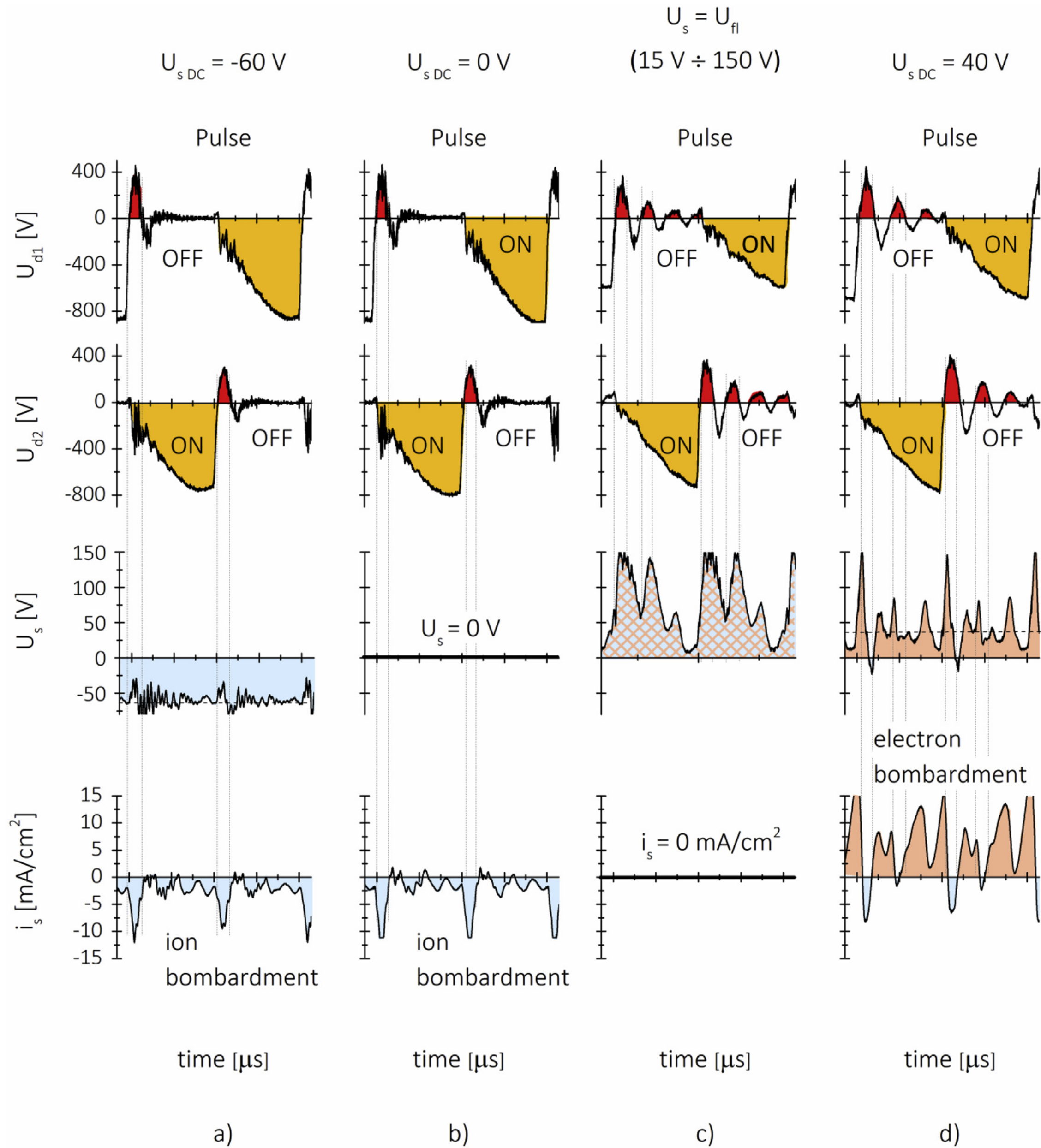

Fig. 6. Time evolution of voltage U_{d1} and U_{d2} on the magnetron M1 and M2 of dual magnetron, voltage U_s on the substrate and current density on the substrate in pulsed dual magnetron discharge generated at W_d = 12 W/cm^2, T_s = 500 °C, $d_{s\text{-}t}$ = 60 mm, $p_T = p_{Ar} + p_{N2}$ = 0.2 + 0.8 = 1 Pa, f_r = 350 kHz and the substrate biased at a) $U_{s\ DC}$ = −60 V, b) grounded U_s = 0 V, c) floating $U_s = U_{fl}$ = 15–150 V and d) $U_{s\ DC}$ = +40 V.

Table 4
Mechanical properties, compressive macrostress (σ < 0) and resistance to cracking of the Ti(Al,V)N films sputtered by pulsed DC dual magnetron, operated in bipolar mode at I_d = 2 A, i_s ranging from 2.2 to 2.4 mA/cm^2 T_s = 500 °C, $d_{s\text{-}t}$ = 60 mm, $p_T = p_{Ar} + p_{N2}$ = 0.2 + 0.8 = 1 Pa and f_r = 350 kHz on Si(111) substrates, as a function of negative DC substrate bias $U_{s\ DC}$.

$U_{s\ DC}$	h	a_D	$\mathscr{E}_{bi}$	σ	H	E*	W_e	H/E*	ε_{cr}	L_{cr}	TiN
[V]	[nm]	[nm/min]	[MJ/cm^3]	[GPa]	[GPa]	[GPa]	[%]		[%]	[N]	structure
−60	1100	18.0	7.5	−0.3	8.3	141	40	0.06	2	0.25	220
−80	1000	16.7	11.1	−0.2	10.4	139	49	0.07	2	0.25	220
−100	800	13.3	17.7	−0.4	9.4	143	44	0.07	2	0.25	220
−100	1000	11.1	21.2	−0.4	9.7	142	46	0.07	2	0.25	220

the film deposition are positive half-periods of overshoot oscillations when the sheat voltage is positive, i.e. $U_{sh} \approx U_{dp} - U_s > 0$ and superposed on the negative DC substrate voltage $U_{s\ DC} < 0$. All films sputtered at $U_{s\ DC} < 0$ and f_r = 350 kHz exhibit similar properties, see Table 4. On the other hand, the compressive macrostress (σ < 0) generated in these films by bombarding ions is relaxed to low values σ ≈ −0.3 GPa by bombarding electrons during negative half-periods of the oscillations when the substrate current density $I_s \approx 0$ and the sheat

voltage is negative, i.e. $U_{sh} = U_{dp} - U_s < 0$. This decrease of compressive macrostress results in a decrease of the hardness to H ≈ 9 GPa. From Fig. 6b and c it is seen that also films sputtered at grounded, floating and positively biased substrates are bombarded by ions. This fact is demonstrated by positive peaks of the sheat voltage corresponding to positive half-periods of overshoot oscillations. In the case of a floating substrate potential (Fig. 6c) the ion bombardment cannot be measured since fluxes of electrons and ions incident on the substrate are the same and the substrate current $I_s = 0\,mA/cm^2$. On the contrary, at a positive substrate bias the electron bombardment of sputtered film dominates over an ion bombardment, see Fig. 6d.

Physical and mechanical properties of Ti(Al,V)N_x films sputtered by pulsed dual magnetron at $f_r = 350$ kHz at different values of negative DC substrate bias $U_{s\ DC}$ were investigated in detail, see Table 4. The energy $\mathscr{E}_{bi}$ increases and the film deposition rate a_D decreases with increasing negative $U_{s\ DC}$. On the other hand, values of H, E*, H/E* ratio, W_e and σ are low of about 10 GPa, 140 GPa, 0.07, 45% and −0.3 GPa, respectively. These films are brittle and easily crack. For more detail see Ref. [47].

4. Conclusions

The article reports on a detailed investigation of the effect of the energy $\mathscr{E}_{bi}$ delivered into the Ti(Al,V)N film by bombarding ions on its macrostress, microstructure, mechanical properties and resistance to cracking. Main conclusions of this study can be summarized as follows:

1. The compressive macrostress σ in sputter deposited Ti(Al,V)N films can be reduced by (i) the pulsed bipolar bias voltage U_{sp} with alternating negative and positive pulses and/or (ii) the alternating ion and electron bombardment of the growing film during overshoots generated in a pulsed magnetron sputtering discharge.
2. The Ti(Al,V)N films with enhanced resistance to cracking are formed only in the case when the energy $\mathscr{E}$ delivered during their growth is sufficiently high ($\mathscr{E}_{bi} > 1.7\,MJ/cm^3$). These films exhibit (i) a dense, voids-free microstructure, (ii) a high ratio H/E* ≥ 0.1, (iii) a high elastic recovery $W_e \geq 60\%$ and (iv) an enhanced resistance to cracking.
3. A reduction of compressive macrostress (σ < 0) down to about σ ≈ - 0.4 GPa results in a reduction of the film hardness and its resistance to cracking.
4. Our investigations clearly demonstrate the compressive macrostress (σ < 0) generated in the sputtered film can be effectively controlled by alternating ion and electron bombardment already during its growth.

Acknowledgements

This work was supported by the project LO1506 of the Czech Ministry of Education, Youth and Sports under the program NPU I.

References

[1] F. Lapostolle, A. Billard, J. von Stebut, Structure/mechanical properties relationship of titanium-oxygen coatings reactively sputter – deposited, Surf. Coating. Technol. 135 (2000) 1–7.
[2] L. Karlsson, L. Hultman, M.P. Johansson, J.-E. Sundgren, H. Ljungcrantz, Growth, microstructure, and mechanical properties of arc evaporated $TiC_{1-x}N_{1-x}$ (0 ≤ x ≤ 1) films, Surf. Coating. Technol. 126 (2000) 1–14.
[3] J. Ding, Y. Meng, S. Wen, Mechanical properties and fracture toughness of multilayer hard coatings using nanoindentation, Thin Solid Films 371 (2000) 178–182.
[4] W.J. Meng, R.C. Tittsworth, L.E. Rehn, Mechanical properties and microstructure of TiC/amorphous hydrocarbon nanocomposite coatings, Thin Solid Films 377–376 (2000) 222–232.
[5] M. Oden, J. Almer, G. Hakansson, M. Olsson, Microstructure-property relationships in arc-evaporated Cr-N coatings, Thin Solid Films 377–376 (2000) 407–412.
[6] J. Patscheider, T. Zehnder, M. Diserens, Structure-performance relations in nanocomposite coatings, Surf. Coating. Technol. 146 (2001) 201–208.
[7] T. Mae, M. Nose, M. Zhou, T. Nagae, K. Shimamura, The effect of Si addition on the structure and mechanical properties of ZrN thin films deposited by an rf reactive sputtering method, Surf. Coating. Technol. 142–144 (2001) 954–958.
[8] S. Carvalho, L. Rebouta, A. Cavaleiro, L.A. Rocha, J. Comes, E. Alves, Microstructure and mechanical properties of nanocomposite (Ti,Si,Al)N coatings, Thin Solid Films 398–399 (2001) 391–396.
[9] J. Almer, M. Oden, G. Hakansson, Microstructure, stress and mechanical properties of arc-evaporated Cr-C-N coatings, Thin Solid Films 385 (2001) 190–197.
[10] J. Musil, H. Zeman, F. Kunc, H. Poláková, Relationships between hardness, Young's modulus and elastic recovery in hard nanocomposite coatings, Surf. Coat.Technol. 154 (2002) 304–313.
[11] J. Musil, H. Zeman, J. Kasl, Relationship between structure and mechanical properties in hard Al-Si-Cu-N films prepared by magnetron sputtering, Thin Solid Films 413 (2002) 121–130.
[12] H. Watanabe, Y. Sato, C. Nie, A. Ando, S. Ohtani, N. Iwamoto, The mechanical properties and microstructure of Ti-Si-N nanocomposite films by ion plating, Surf. Coating. Technol. 169–170 (2003) 452–455.
[13] H.S. Barshilia, A. Jain, K.S. Rajam, Structure, hardness and thermal stability of nanolayered TiN/CrN multilayer coatings, Vacuum 72 (2003) 241–248.
[14] P. Jedrzejowski, J.E. Klemberg-Sapieha, L. Martinu, Relationship between the mechanical properties and the microstructure of nanocomposite $TiN/SiN_{1.3}$ coatings prepared by low temperature PECVD, Thin Solid Films 426 (2003) 150–159.
[15] Y.T. Pei, D. Galvan, J.ThM. De Hosson, Nanostructure and properties of TiC/a-C:H composite coatings, Acta Mater. 53 (2005) 4505–4521.
[16] J. Soldán, J. Musil, Structure and mechanical properties of DC magnetron sputtered TiC/Cu films, Vacuum 81 (2006) 531–538.
[17] J. Lin, B. Mishra, J.J. Moore, W.D. Sproul, Microstructure, mechanical and tribological properties of Cr1-xAlxN films deposited by pulsed-closed field unbalanced magnetron sputtering (P-CFUBMS), Surf. Coating. Technol. 201 (2006) 4329–4334.
[18] M. Audronis, A. Leyland, P.J. Kelly, A. Matthews, The effect of pulsed magnetron sputtering on the structure and mechanical properties of CrB2 coatings, Surf. Coating. Technol. 201 (2006) 3970–3976.
[19] C.H. Lai, M.H. Tsai, S.J. Lin, J.W. Yeh, Influence of substrate temperature and mechanical properties of multi-element (AlCrTaTiZr)N coatings, Surf. Coating. Technol. 201 (2007) 6993–6998.
[20] N.J.M. Carvalho, E. Yoestbergen, B.J. Kooi, J.ThM. De Hooson, Stress analysis and microstructure of PVD monolayer TiN and multilayer TiN/(Ti,Al)N coatings, Thin Solid Films 429 (2003) 179.
[21] G. Liu, Y. Yang, B. Huang, X. Luo, S. Ouzang, G. Zhao, N. Jin, P. li, Effects of substrate tempriture on the structure, residual stress and nanohardness of Ti6Al4V films prepared by magnetron sputtering, Appl. Surf. Sci. 370 (2016) 53.
[22] J. Kohout, E. Bousser, T. Schmitt, R. Vernhes, O. Zabeida, J. Klemberg-Sapieha, L. Martinu, Stable reactive deposition of amorphous Al2O3 films with low residual stress and enhanced toughness using pulsed dc magnetron sputtering with very low duty cycle, Vacuum 124 (2016) 96.
[23] A. Pelisson, M. Parlinska-Wojtan, H.J. Hug, J. Patscheider, Microstructure and mechanical properties of Al-Si-N transparent hard coatings deposited by magnetron sputtering, Surf. Coating. Technol. 202 (2007) 884–889.
[24] J. Soldán, J. Neidhardt, B. Satory, R. Kaindl, R. Cerstvy, P.H. Mayrhofer, R. Tessadri, P. Polcik, M. Lechthaler, C. Mitterer, Structure-property relations of arc-evaporated Al-Cr-Si-N coatings, Surf. Coating. Technol. 202 (2008) 3555–3562.
[25] K. Polychronopoulou, C. Rebholtz, M.a. Baker, L. Theodorou, N.G. Demas, S.J. Hinder, A.A. Polycarpou, C.C. Doumanidis, K. Bobel, Nanostructure, mechanical and tribological properties of reactive magnetron sputtered TiCx coatings, Diam. Relat. Mater. 17 (2008) 2054–2061.
[26] J.H. Huang, Z.E. Tsai, G.P. Yu, Mechanical properties and corrosion resistance of nanocrystalline ZrNxOy coatings on AlSL 304 stainless steel by ion plating, Surf. Coating. Technol. 202 (2008) 4992–5000.
[27] J. Musil, Sputtering systems with enhanced ionization for ion plating of hard wear resistant coatings, Proc. Of the 1st Meeting on the Ion Engineering Society of Japan (IESJ-92), Tokyo, Japan, 1992, pp. 295–304.
[28] H. Poláková, J. Musil, J. Vlček, J. Alaart, C. Mitterer, Structure- hardness relations in sputtered Ti-Al-V-N films, Thin Solid Films 444 (2003) 189–198.
[29] J. Musil, H. Poláková, J. Šůna, J. Vlček, Effect of ion bombardment on properties of hard reactively sputtered single-phase films, Surf.Coat.Technol. 177–178 (2004) 289–298.
[30] J. Musil, J. Šůna, The role of energy in formation of sputtered nanocomposite films, Mater. Sci. Forum 502 (2005) 291–296.
[31] J. Musil, J. Šícha, D. Heřman, R. Čerstvý, Role of energy in low-temperature high-rate formation of hydrophilic TiO2 thin films using pulsed magnetron sputtering, J. Vac. Sci. Technol., A 25 (4) (2007) 666–674.
[32] J. Musil, Flexible hard nanocomposite coatings, RSC Adv. 5 (2015) 60482–60495.
[33] J. Musil, J. Vlček, P. Baroch, Magnetron discharges for thin films plasma processing, in: Y. Pauleau (Ed.), Chapter 3 in „Materials Surface Processing by Directed Energy Techniques, Elsevier Science Publisher B.V., Oxford, UK, 2006, pp. 67–106.
[34] (a) J.A. Thornton, Recent developments in sputtering – magnetron sputtering, Met. Finish. 77 (5) (1979) 83–87;
(b) J.A. Thornton, High rate thick films growth, Annu. Rev. Mater. Sci. 7 (1977) 239–260.
[35] J. Musil, J.T.M. DeHosson, A. Cavaleiro (Eds.), Physical and Mechanical Properties of Hard Nanocomposite Films Prepared by Reactive Magnetron Sputtering, Chapter 10 in Nanostructured Coatings, Springer Science + Business Media, LCC, New York, 2006, pp. 407–463.
[36] J. Musil, V. Poulek, V. Valvoda, R. Kužel Jr., H.A. Jehn, M.E. Baumgartner, Relation of deposition conditions of Ti-N films prepared by dc magnetron sputtering to their microstructure and macrostress, Surf.Coat.Technol. 60 (1993) 484–488.
[37] B.A. Movchan, A.V. Demchishin, Study of the structure and properties of thick

vacuum condensates of nickel, titanium, tungsten, aluminum oxide and zirconium oxide, Phys. Met. Metallogr. 28 (1969) 83–90.

[38] P. Pokorný, J. Musil, P. Fitl, M. Novotný, J. Lančok, J. Bulíř, Contamination of magnetron sputtered metallic films by oxygen from residual atmosphere in deposition chamber, Plasma Process. Polym. 12 (2015) 416–421.

[39] J. Musil, Low-pressure magnetron sputtering, Vacuum 50 (3–4) (1998) 363–372.

[40] J. Musil, Hard and superhard nanocomposite coatings, Surf.Coat.Technol. 125 (2000) 322–330.

[41] J. Musil, Hard nanocomposite coatings: thermal stability, oxidation resistance and toughness, Surf.Coat.Technol. 207 (2012) 50–65.

[42] J. Musil, Advanced hard nanocomposite coatings with enhanced toughness and resistance to cracking, in: S. Zhang (Ed.), Chapter 7 in Thin Films and Coatings: Toughening and Toughening Characterization, CRC Press, USA, 2015, pp. 377–463.

[43] M. Jaroš, J. Musil, R. Čerstvý, S. Haviar, Effect of energy on physical and mechanical properties of hard Ti(Al,V)Nx films prepared by magnetron sputtering, Surf.Coat.Technol. 332 (2017) 190–197.

[44] J. Musil, M. Jaroš, R. Čerstvý, S. Haviar, Evolution of microstructure and macrostress in sputtered hard Ti(Al,V)N films with increasing energy delivered during their growth by bombarding ions, J. Vac. Sci. Technol. 35 (2017) 020601.

[45] J. Musil, P. Baroch, Discharge in dual magnetron sputtering system, IEEE Trans. Plasma Sci. 33 (20) (2005) 338–339.

[46] G.G. Stoney, The transition of metallic films deposited by electrolysis, Proc. R. Soc. London, Ser. A82 (1909) 172–175.

[47] J. Musil, J. Sklenka, R. Čerstvý, Transparent Zr-Al-O oxide coatings with enhanced resistance to cracking, Surf. Coating. Technol. 206 (2012) 2105–2109.

[48] J. Musil, J. Sklenka, R. Čerstvý, Protection of brittle film against cracking, Appl. Surf. Sci. 370 (306) (2016) 306–311.

[49] J. Šícha, O. Novák, J. Vlček, P. Kudláček, Ion flux characteristics in pulsed dual magnetron discharge used for deposition of photoactive TiO2 films, Plasma Process. Polym. 8 (2011) 191–198.

[50] J.W. Bradley, H. Bäcker, P.J. Kelly, R.D. Arnell, Space and time resolved Langmuir probe measurements in a 100 kHz pulsed rectangular magnetron system, Surf. Coating. Technol. 142 (2001) 337–341.

[51] J. Vlček, A.D. Pajdarová, J. Musil, Pulsed dc magnetron discharges and their utilization on plasma surface engieneering, Contrib. Plasma Phys. 44 (2004) 426–436.

[52] R.D. Armell, P.J. Kelly, J.W. Bradley, Recent developments in pulsed magnetron sputtering, Surf. Coating. Technol. 188 (2004) 158–163.

[53] C. Muratore, J.J. Moore, J.A. Rees, Electrostatic quadrupole plasma mass spectrometer and Langmuir probe measurements of mid-frequency pulsed DC magnetron discharges, Surf. Coating. Technol. 163 (2003) 12–18.

[54] F. Richter, Th Welyel, Th Dunger, H. Kupfer, time-resolved characterization of pulsed magnetron discharges using Langmuir probes, Surf. Coating. Technol. 188 (2004) 384–391.

[55] H. Bäcker, P.S. Henderson, J.W. Bradley, P.J. Kelly, Time-resolved investigation of plasma parametres during deposition of Ti and TiO2 thin films, Surf. Coating. Technol. 174 (2003) 909–913.

[56] J. Lin, J.J. Moore, B. Mishra, W.D. Sproul, J.A. Rees, Examination of the phenomena in pulsed-closed field unbalanced magnetron sputtering (P-CFUBMS) of Cr-Al-N thin films, Surf. Coating. Technol. 201 (2007) 4640–4652.

[57] J.M. Anton, B. Mishra, J.J. Moore, J.A. Rees, W.D. Sproul, Investigation of processing parameters for pulsed closed unbalanced magnetron co-sputtered TiC-C thin films, Surf. Coating. Technol. 201 (2006) 4131–4135.

Materials Letters 235 (2019) 92–96

Contents lists available at ScienceDirect

Materials Letters

journal homepage: www.elsevier.com/locate/mlblue

Interrelationships among macrostress, microstructure and mechanical behavior of sputtered hard Ti(Al,V)N films

M. Jaroš, J. Musil *, S. Haviar

Department of Physics and NTIS Centre of Excellence, Faculty of Applied Sciences, University of West Bohemia, Univerzitní 22, CZ-306 14 Plzeň, Czech Republic

ARTICLE INFO

Article history:
Received 4 July 2018
Received in revised form 13 September 2018
Accepted 30 September 2018
Available online 2 October 2018

Keywords:
Ti(Al, V)N films
Hardness
Macrostress
Energy
Microstructure
Structure
Mechanical properties
Resistance to cracking

ABSTRACT

The article reports on the influence of a compressive macrostress σ in the Ti(Al,V)N films on their mechanical properties, structure, microstructure, and resistance to cracking. The macrostress σ is controlled by the energy $\mathcal{E}_{bi}$ delivered into the growing film by bombarding ions. The Ti(Al,V)N films were sputtered by a dual magnetron with closed magnetic field. It is shown that (1) the compressive macrostress (σ < 0) increases the hardness H of the film and the ratio H/E*, (2) the films exhibits a dense, voids-free, non-columnar microstructure in the case when the energy $\mathcal{E}_{bi} \geq 3$ MJ/cm^3, (3) the enhanced resistance to cracking of the films is controlled by its mechanical properties, microstructure and macrostress σ; here E* is the effective Young's modulus.

© 2018 Elsevier B.V. All rights reserved.

1. Introduction

A macrostress σ generated in the film prepared by an ion plating sputtering strongly influences its hardness H and structure and thereby its physical and functional properties. The stabilization of the β-Ta [1] or the c-Zr_3N_4 phase in the film [2], the superconductivity of film [3], the Curie temperature of film [4], a change of the preferred orientation of film [5–7], and the lifetime of the cutting tools coated by protective hard coatings [8–10] can be given as examples. However, so far, there is little information about the influence of σ on the hardness H of film and its resistance to cracking [11–13].

2. Experimental

The Ti(Al,V)N thin films were sputter deposited using a dual magnetron with closed magnetic field equipped with TiAlV (6 at.% Al, 4 at.% V) alloy targets (∅ = 50 mm) in a mixture of 20% Ar + 80% N_2 sputtering gases at the total pressure $p_T = p_{Ar} + p_{N2}$ ranging from 0.4 to 1.0 Pa. The magnetrons were powered by an Advanced Energy Pinnacle Plus + 5/5 kW power supply operated either in the DC or the pulse mode at a low power density in the pulse of $W_{t\ DC} = W_{tp} \leq 25$ W/cm^2; here $W_{t\ DC}$ and W_{tp} is the target power density in the DC discharge and during the pulse-on in the pulsed discharge. For a more detailed description of deposition conditions see Ref. [14–18]. The Ti(Al,V)N films were deposited onto Si(1 1 1) substrates.

The film thickness was measured by a stylus profilometer DEKTAK 8. The macrostress σ was evaluated from the bending of the Si plate using the Stoney's formula [19]. The elemental composition of the Ti(Al,V)N films on the Si substrate was analyzed in a scanning electron microscope (SU-70, Hitachi) operated at a primary electron energy of 15 keV using energy dispersive spectroscopy (EDS, UltraDry, Thermo Scientific) and wave dispersive spectroscopy (WDS, Magnaray, Thermo Scientific). Mechanical properties of sputtered films were determined from load vs. displacement curves measured by a microhardness tester Fisherscope H100 with Vickers diamond indenter at a load of 20 mN. The resistance of the Ti(Al,V)N films to cracking was assessed by a critical load L_{cr} at which cracks in the film occurred.

3. Results and discussion

It is well known that the hardness H, structure, microstructure of the sputtered film and the macrostress σ generated in it during its growth depend on many deposition parameters. It means that

* Corresponding author.
E-mail addresses: jarosm@kfy.zcu.cz (M. Jaroš), musil@kfy.zcu.cz (J. Musil).

https://doi.org/10.1016/j.matlet.2018.09.173
0167-577X/© 2018 Elsevier B.V. All rights reserved.

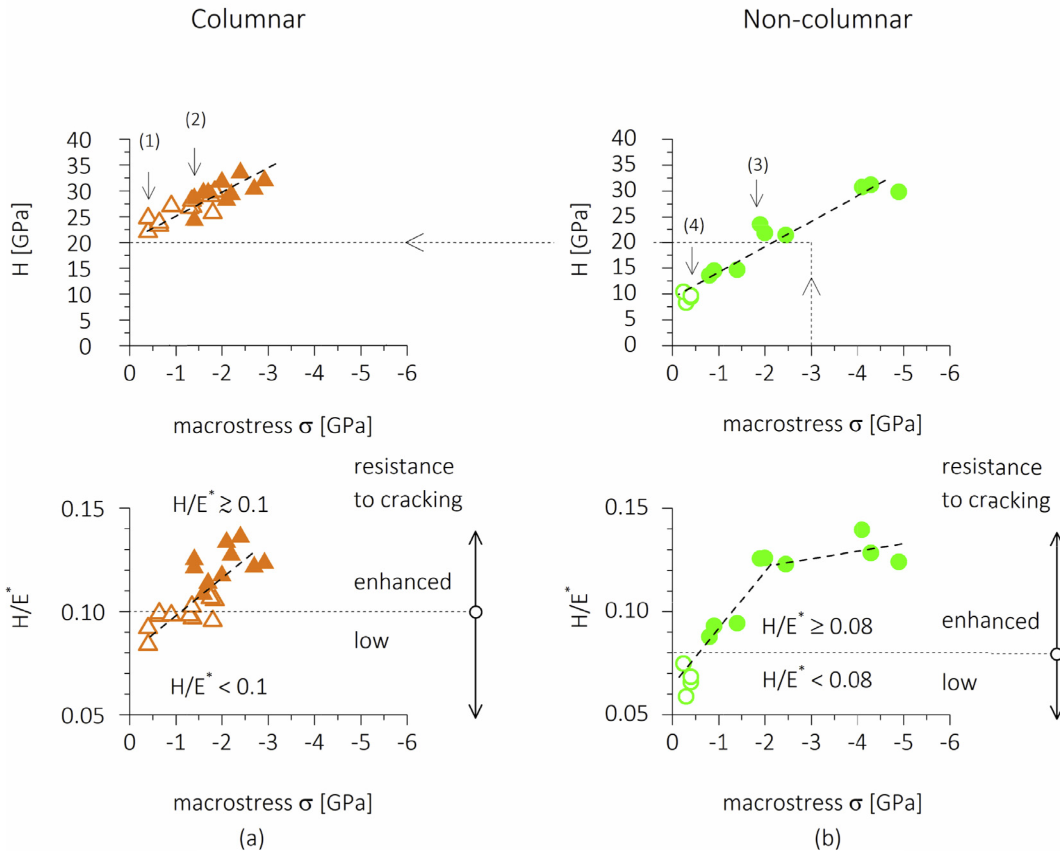

Fig. 1. The hardness H and H/E* ratio of the Ti(Al,V)N film with columnar and non-columnar microstructure as a function of compressive macrostress σ < 0. The open and full symbols denote films with low and enhanced resistance to cracking, respectively.

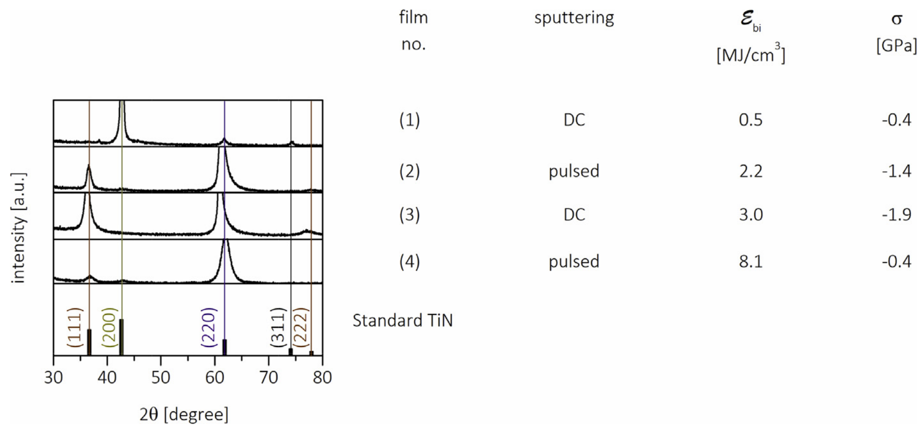

Fig. 2. XRD patterns of the Ti(Al,V)N films with columnar microstructure (the films No. 1 and 2) and with non-columnar microstructure (the films No. 3 and 4). The films with numbers 1, 2, 3, 4 are given in Fig. 1 and their physical and mechanical properties in Table 1.

the interrelationship between the deposition parameters of the film and its properties is a multi-parameters function

$$\text{Film properties} = f(U_d, I_d, W_t, T_s, U_s, i_s, \nu_i, \nu_{ca}, d_{s-t}, h, a_D, p_0, p_{Ar}, p_{RG}, p_T, \text{etc.}) \quad (1)$$

Here U_d is the voltage of the magnetron discharge, I_d is the current of the magnetron discharge, W_t is the target power density, T_s is the substrate temperature, U_s is the substrate bias, i_s is the substrate ion current density, ν_i is the flux of the bombarding ions, ν_{ca} is the flux of the condensing atoms, $d_{s\text{-}t}$ is the substrate-to-target distance, a_D is the deposition rate of the coating, p_0 is the base pressure in the deposition chamber before the admission of the sputtering gas, p_{Ar} is the partial pressure of argon, p_{RG} is the partial pressure of a reactive gas, $p_T = p_{Ar} + p_{RG}$ is the total pressure of the sputtering gas.

This fact significantly complicates the search correct interrelations among H, σ, structure and microstructure of the sputtered film and its resistance to cracking because every deposition param-

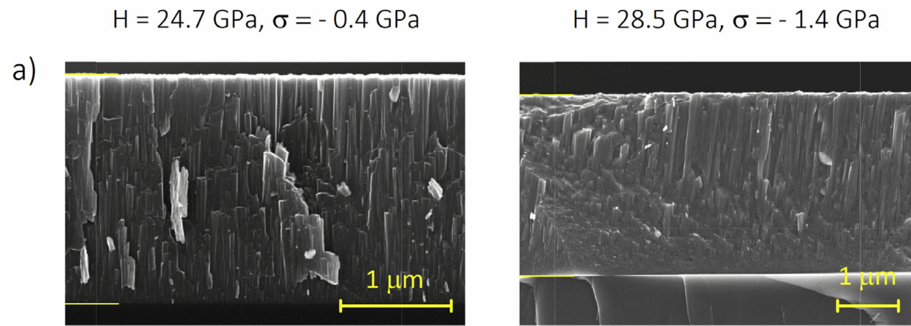

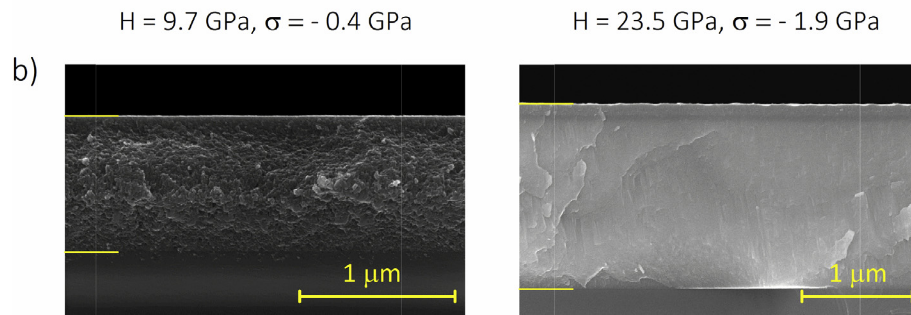

Fig. 3. SEM images of cross-section of the Ti(Al,V)N films with columnar microstructure (the films No. 1 and 2) and with non-columnar microstructure (the films No. 3 and 4). The films with numbers 1, 2, 3, 4 are given in Fig. 1 and their physical and mechanical properties in Table 1.

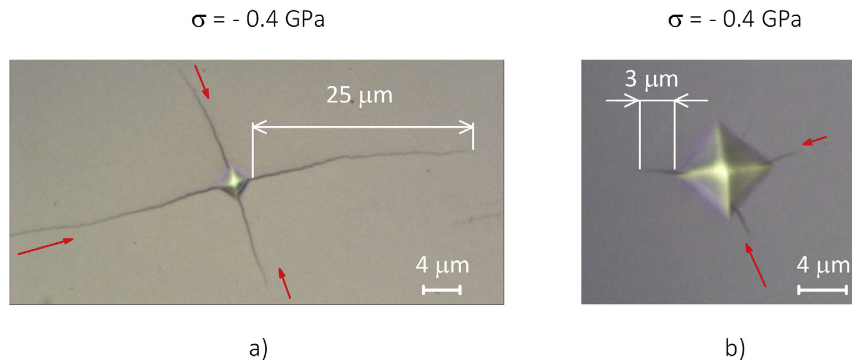

Fig. 4. LOM image of surface morphology of Ti(Al,V)N films after the indentation test. Measured Ti(Al,V)N films exhibit compressive macrostress $\sigma = -0.4$ GPa and (a) columnar microstructure (the film No. 1) or (b) non-columnar microstructure (the film No. 4), respectively. Indentation test was carried out for the load (a) L = 0.25 N or (b) L = 0.75 N, respectively.

Table 1
Physical and mechanical properties of four Ti(Al,V)N films denoted in Fig. 1 as films No. 1, 2, 3, and 4. The data of the film No. 2 are from Ref. [17].

Film No.	Sputtering process	h [nm]	U_s [V]	i_s [mA/cm^2]	a_D [nm/min]	$\mathcal{E}_{bi}$ [MJ/cm^3]	σ [GPa]	H [GPa]	E* [GPa]	H/E*	W_e [%]	L_{cr} [N]	Microstructure
1	DC	2000	−20	0.7	17	0.5	−0.4	24.7	268	0.07	62	0.25	comulnar – voids
2	pulsed/100 kHz	2500	−20	1.8	22	2.2	−1.4	28.5	235	0.12	73	>1	comulnar – dense
3	DC	1200	−20	1.9	15	3	−1.9	23.5	187	0.13	80	>1	non-columnar
4	pulsed/350 kHz	1000	−100*	1.5	11	8.1	−0.4	9.7	142	0.07	46	0.25	non-columnar

* Pulsed discharge with strong overshoots.

eter has a different effect on these properties of the sputtered film. It is due to the fact that at each combination of deposition parameters a different energy $\mathcal{E}$ is delivered into the growing coating. In this case, it is impossible to sputter the film with fully reproducible properties. Therefore, the film properties must be expressed as a function of one parameter only, i.e. as a function of the energy $\mathcal{E}$

$$\text{Film properties} = f(\mathcal{E}) \quad (2)$$

The energy $\mathcal{E}$ is the key parameter which controls properties of the sputtered film and enables its formation with fully reproducible properties. This is the reason why the interrelations among H, σ, structure and microstructure of the sputtered film and its resistance to cracking are compared based on the energy $\mathcal{E}$. In our experiments the energy is delivered into the sputtered Ti(Al,V)N films by bombarding ions, i.e. $\mathcal{E} = \mathcal{E}_{bi}$. The energy $\mathcal{E}_{bi}$ is calculated from the measured values of the substrate bias U_s, substrate ion current density i_s and the film deposition rate a_D from the formula [20]

$$\mathcal{E}_{bi} = U_s \times i_s / a_D \quad (3)$$

Interrelationships among the hardness H, H/E^* ratio, microstructure, structure, and compressive macrostress σ in the Ti(Al,V)N film and its resistance to cracking are displayed in Figs. 1–4. The evolution of H and H/E^* of the Ti(Al,V)N film with columnar microstructure and dense non-columnar microstructure as a function of compressive macrostress σ is displayed in Fig. 1. Fig. 1a shows that the H and H/E^* ratio of the Ti(Al,V)N film with columnar microstructure increase from 22 to 31 GPa and 0.08 to 0.13, respectively, with increasing σ from −0.4 to −3 GPa. The Ti(Al,V)N films with dense, non-columnar microstructure also exhibit the same behavior. H and H/E^* ratio increase from 8 to 30 GPa and 0.06 to 0.14, respectively, with increasing σ from −0.4 to −5.5 GPa but with a smaller increase of H/E^*at σ ranging from −2 to −5.5 GPa than that in films with smaller compressive macrostress $|\sigma| < 2$ GPa.

Main results displayed in Fig. 1 can be briefly summarized as follows

1. The magnitude of the hardness H of the films with low compressive macrostress $|\sigma| < 3$ GPa strongly depend on their microstructure. Films with columnar microstructure exhibit higher H compared with the films with non-columnar microstructure. This difference is due to different values of $\mathcal{E}_{bi}$ used in sputtering and relaxing of σ by an electron heating of the growing film during overshoots in pulsed sputtering, see Table 1 and Ref. [17].
2. The hardness H of the film is a complex function of two competing parameters – the energy $\mathcal{E}_{bi}$ and enhancement or relaxing σ – which strongly influence its growth process and thus its structure, microstructure, and mechanical properties, particularly its H/E^* ratio and elastic recovery W_e, see Figs. 2 and 3 and Table 1. This is a reason why, for instance, the films with approx. same H exhibit different microstructure (compare the films No. 1 and No. 3) or the films with a low compressive macrostress exhibit different H, H/E, W_e, structure and microstructure (compare the films No. 1 and No. 4).

The energy $\mathcal{E}_{bi}$ strongly influences also the preferred orientation of the sputtered Ti(Al,V)N films, see Fig. 2. In this figure, the effect of $\mathcal{E}_{bi}$ on the structure of Ti(Al,V)N films deposited by DC and pulsed sputtering is illustrated. The films with numbers 1, 2, 3, 4 are given in Fig. 1 and their physical and mechanical properties in Table 1.

The microstructure of the Ti(Al,V)N film depends on the energy $\mathcal{E}_{bi}$ delivered into the growing film by bombarding ions. The energy $\mathcal{E}_{bi}$ is calculated from the measured values of the substrate bias U_s, the substrate ion current density i_s and the film deposition rate a_D from the formula $\mathcal{E}_{bi} = U_s \times i_s/a_D$; more details are given in Ref. [20]. The films sputtered at low energies $\mathcal{E}_{bi} < 3$ MJ/cm^3 have a columnar microstructure, see Fig. 3a. On the contrary, the films sputtered at high energies $\mathcal{E}_{bi} \geq 3$ MJ/cm^3 have a non-columnar microstructure, see Fig. 3b. It is worthwhile to note that also the films with dense, voids-free non-columnar can be soft if the compressive macrostress generated under high ion bombardment at a high $\mathcal{E}_{bi}$ is simultaneously relaxed by a sufficiently high electron heating using the pulsed sputtering with overshoots or the pulsed substrate bias U_{sp} with alternating polarity of pulses [17], see the film No. 4 in Table 1.

The macrostress σ and the microstructure of the sputtered film strongly influence also its resistance to cracking [19]. The effect of the microstructure of the Ti(Al,V)N film with a low compressive macrostress $\sigma = -0.4$ GPa on its resistance to cracking is illustrated in Fig. 4. The resistance of the film to cracking was assessed by the indentation test in which the diamond indenter was impressed into the film surface under a high load L at which the film cracks [20]. Longer cracks mean a weaker resistance to cracking. On the other hand, shorter cracks mean an enhanced resistance to cracking.

The surface morphology of the Ti(Al,V)N film with columnar and non-columnar microstructure after indentation test at L = 0.25 N and L = 0.75 N is displayed in Fig. 4a and b, respectively. From this figure, it is seen that the film with columnar microstructure exhibits a low resistance to cracking. On the other hand, the film with non-columnar microstructure with shorter cracks even at a higher load L exhibits an enhanced resistance to cracking. This experiment clearly shows that the film microstructure is a key parameter which decides on its resistance to cracking as shown in Ref. [14,15,20].

4. Conclusions

Main results of this investigation can be briefly summarized as follows

1. The hardness H of the film increases with increasing compressive macrostress σ.
2. The hardness H of the film is a complex function of two competing parameters: the energy $\mathcal{E}_{bi}$ and macrostress. Both parameters $\mathcal{E}_{bi}$ and σ influence the growth process of the film and thereby also its structure, microstructure, and mechanical properties.
3. The compressive residual macrostress σ leads to an apparent increase in hardness H and fracture resistance of sputtered films.
4. The macrostress σ generated in the film during its growth can be simultaneously relaxed by the electron heating using either a pulsed sputtering with overshoots or a pulsed bias with pulses of alternating polarity. This way a different combination of mechanical properties of the film and its microstructure and macrostress σ can be achieved.
5. Hard films with high ratio $H/E^* > 0.1$, high elastic recovery $W_e > 60\%$, dense, voids-free microstructure and compressive macrostress $\sigma < 0$ exhibit an enhanced resistance to cracking.
6. The energy $\mathcal{E}_{bi}$ is a key parameter which makes it possible to create the films with prescribed properties in the fully reproducible way.

Acknowledgment

This work was supported by the project LO1506 of the Czech Ministry of Education, Youth and Sports under program NPU I.

References

[1] K. Kondo, M. Nakabayashi, K. Kawakami, T. Chijimatsu, M. Nakaishi, M. Yamada, M. Yamabe, K. Sugishima, Stress stabilization of βtantalum and its crystal structure, J. Vac. Sci. Technol. A 11 (1993) 3067.
[2] M. Chhowalla, H.E. Unalan, Thin films of hard cubic Zr3N4 stabilized by stress, Nat. Mater. 4 (2005) 317–322.
[3] Y. Han, W.Y. Li, L.X. Cao, X.Y. Wang, B. Xu, B.R. Zhao, Y.Q. Guo, J.L. Yang, Superconductivity in iron telluride thin films under tensile stress, PRL 104 (2010) 017003.
[4] G.A. Rossetti Jr., L.E. Cross, K. Kushida, Stress induced shift of the Curie point in epitaxial PbTiO3 thin films, Appl. Phys. Lett. 59 (1991) 2524.
[5] A.R. Shetty, A. Karimi, Texture change through film thickness and off-axis accommodation of (0 0 2) planes, Appl. Surf. Sci. 258 (2011) 1630–1638.
[6] J.P. Zhao, Z.Y. Chen, X. Wang, Y.H. Yu, S.Q. Yang, T.S. Shi, X.H. Liu, The influence of ion energy on the structure of TiN films during filtered arc deposition, Nucl. Instrum. Methods Phys. Res. B 135 (1998) 388–391.
[7] G. Abadias, Stress and preferred orientation in nitride-based PVD coatings, Surf. Coat. Technol. 202 (2008) 2223–2235.
[8] G. Skordaris, K.D. Bouzakis, T. Kotsanis, P. Charalampous, E. Bouzakis, B. Breidenstein, B. Bergmann, B. Denkena, Effect of PVD film's residual stresses on their mechanical properties, brittleness, adhesion and cutting performance of coated tools, CIRP J. Manuf. Sci. Technol. 18 (2017) 145–151.
[9] W. Tillmann, T. Sprute, F. Hoffmann, Y. Chang, C. Tsai, Influence of bias voltage on residual stresses and tribological properties of TiAlVN-coatings at elevated temperatures, Surf. Coat. Technol. 231 (2013) 122–125.
[10] O. Gonzalo, V.G. Navas, B. Coto, I. Bengoetxea, U.R. de Gopegi, M. Etxaniz, Influence of the coating residual stresses on the tool wear, Procedia Eng. 19 (2011) 106–111.
[11] J. Musil, Hard and superhard nanocomposite coatings, Surf. Coat. Technol. 125 (2000) 322–330.
[12] S. Kataria, S.K. Srivastava, G. Praveen Kumar, Siju Srinivas, D.V. Jakeer Khan, Sridhar Rao, Harish C. Barshilia, Nanocrystalline TiN coatings with improved toughness deposited by pulsing the nitrogen flow rate, Surf. Coat. Technol. 206 (2012) 4279–4286.
[13] H. Poláková, J. Musil, J. Vlček, J. Allaart, C. Mitterer, Structure-hardness relations in sputtered Ti–Al–V–N films, Thin Solid Films 444 (2003) 189–198.
[14] J. Musil, Hard nanocomposite coatings: thermal stability, oxidation resistance and toughness, Surf. Coat. Technol. 207 (2012) 50–65.
[15] J. Musil, Flexible hard nanocomposite coatings, RSC Adv. 5 (2015) 60482–60495.
[16] M. Jaroš, J. Musil, R. Čerstvý, S. Haviar, Effect of energy on physical and mechanical properties of hard Ti(Al, V)Nx films prepared by magnetron sputtering, Surf. Coat. Technol. 332 (2017) 190–197.
[17] M. Jaroš, J. Musil, R. Čerstvý, S. Haviar, Effect of energy on macrostress in Ti(Al, V)N films prepared by magnetron sputtering, under revision in journal Vacuum (2018).
[18] J. Musil, Š. Kos, M. Jaroš, R. Čerstvý, S. Haviar, S. Zenkin, Z. Čiperová, Overstoichiometric TMNx > 1 transition metal nitride coatings, Jap. J. Appl. Phys. (2018), submitted for publication.
[19] G.G. Stoney, The transition of metallic films deposited by electrolysis, Proc. R. Soc. London, Ser. A82 (1909) 172–175.
[20] J. Musil, Advanced hard nanocomposite coatings with enhanced toughness and resistance to cracking, CRC Press, USA, 2015, pp. 377–463.

Hard TiN_2 dinitride films prepared by magnetron sputtering

Jindřich Musil,[a] Martin Jaroš, Šimon Kos, Radomír Čerstvý, and Stanislav Haviar
Department of Physics and NTIS Centre of Excellence, Faculty of Applied Sciences, University of West Bohemia, Univerzitní 22, CZ-306 14 Plzeň, Czech Republic

(Received 3 May 2018; accepted 11 June 2018; published 28 June 2018)

This letter reports on the formation of hard TiN_2 dinitride films prepared by magnetron sputtering. TiN_2 films were reactively sputtered in an $Ar + N_2$ gas mixture using a pulsed dual magnetron with a closed magnetic field B. The principle of the formation of TiN_2 films by magnetron sputtering is briefly described. The stoichiometry $x = N/Ti$ of the TiN_x films was controlled by deposition parameters, and its maximum value of $x = 2.3$ was achieved. For the first time, a possibility to form the TiN_2 dinitride films by magnetron sputtering has been demonstrated. The mechanical properties of sputtered films were investigated in detail. *Published by the AVS.*
https://doi.org/10.1116/1.5038555

I. INTRODUCTION

Recently, a great attention has been devoted to the formation of nitrogen-rich $TMN_{x>1}$ transition metal nitrides with the stoichiometry $x = N/TM$ ranging from 1 to 2 (Refs. 1 and 3–10) and also with $x = 4$.[2] Theoretical studies of these materials based on *ab initio* calculations show that these novel overstoichiometric nitrides should exhibit extraordinary properties such as superhardness, high electrical conductivity, and optical transparency, which originate from metal-nitrogen charge transfer, the nature of the N–N bonds, and the mixture of ionic and covalent N–N bonds.[11–14] It was reported that bulk titanium dinitrides were successfully synthesized under high pressure and high temperature (HPHT synthesis), i.e., using *an equilibrium process*.[1,4,14–17] For instance, the TiN_2 ultraincompressible dinitride material with bulk modulus 360–385 GPa was synthesized from the titanium nitride flakes and N_2 gas compressed to 73 GPa and heated to 2400 K in a laser-heated diamond anvil cell.[4] Recently, it was reported that titanium dinitrides were prepared also in the form of $TiN_{x=2}$ films at low pressures of about 0.3 Pa by simultaneous action of a Ti evaporation by an arc evaporator and a strong ionization of N_2 gas in a gas-plasma source with a hot filament in a hollow cathode.[18]

This article reports on the formation of overstoichiometric $TiN_{x>1}$ titanium nitride films by magnetron sputtering, i.e., the formation of films prepared by a *nonequilibrium deposition process* running at an atomic level. The principle of sputtering of $TMN_{x>1}$ overstoichiometric nitride films is briefly described. Interrelationships among the stoichiometry x, the mechanical and electrical properties of TiN_x films are investigated in detail.

II. PRINCIPLE OF SPUTTERING OF $TMN_{X>1}$ NITRIDE FILMS

The principle of formation of overstoichiometric $TMN_{x>1}$ and $TMN_{x=2}$ dinitride films by magnetron sputtering is based on two nonequilibrium processes simultaneously running at an atomic level: (1) the heating of the sputtered material to high temperatures first at the substrate and later at the growing film in areas where sputtered atoms and bombarding ions arrive with no or low substrate heating and (2) the pressing of the heated areas at high pressures p. This can be achieved by a high energy $\mathcal{E}$ delivered into the growing film by bombarding ions with energy $\mathcal{E}_{bi}$ controlled by the negative substrate bias U_s and/or by condensing fast neutral atoms sputtered from the target and arriving at the substrate with energy $\mathcal{E}_{fn}$ of several electron-volt controlled by the sputtering gas pressure p. Both energies $\mathcal{E}_{bi}$ and/or $\mathcal{E}_{fn}$ are sufficient to heat areas of incident ions or atoms to very high temperatures T, easily exceeding 2500 K, and simultaneously to press these areas at a high pressure p of about $300\mathcal{E}^{1/2}$ GPa, where the energy $\mathcal{E}$ is in electron-volt.[10] The main problem in the formation of overstoichiometric $TMN_{x>1}$ and $TMN_{x=2}$ dinitride films by magnetron sputtering is to increase the number n_N of nitrogen atoms in the magnetron discharge to achieve a high ratio $n_N/n_{TM} > 1$, which enables the formation of films with the stoichiometry $x > 1$ and $x = 2$, respectively; here, n_{TM} is the number of TM atoms in the sputtered film.

III. EXPERIMENT

The $TiN_{x>1}$ films were reactively sputtered by a pulsed hybrid dual magnetron (HDM) in an $N_2 + Ar$ mixture. The HDM consists of two different magnetrons M1 and M2 with a closed magnetic field B. The magnetron M1 is a magnetron with a very low sputtering of its target, and the magnetron M2 is a standard, well sputtering magnetron. The low sputtering of the magnetron M1 was achieved by extraction of the central magnet from the magnetron M1. By the control of the powers P_{M1} and P_{M2} delivered into the magnetrons M1 and M2, respectively, it is possible to increase the ion bombardment of the growing film by increasing the ion flux i_s while keeping the film deposition rate a_D constant, and in this way to sputter overstoichiometric TiN_x films with the stoichiometry $x = N/Ti > 1$. The increase in i_s at constant a_D is achieved by increasing the power P_{M1} delivered into the magnetron M1 and keeping the power P_{M2} delivered into the magnetron M2 constant. More details are given in Ref. 10.

[a]Electronic mail: musil@kfy.zcu.cz

TABLE I. Deposition parameters, elemental composition, mechanical properties, macrostress σ, and electrical resistivity ρ of two overstoichiometric $TiN_{x>1}$ films sputtered by pulsed HDM at $T_s = 450\,°C$, $U_s = -20\,V$, $i_s = 4.5\,mA/cm^2$, $a_D = 6.6\,nm/min$, $\mathcal{E}_{bi} = 8.2\,MJ/cm^3$, $d_{s\text{-}t} = 80\,mm$, and $p_T = p_{N_2} + p_{Ar} \approx p_{N_2}$ as a function of p_T. h is the film thickness.

Film No.	p_T (Pa)	P_{M1} (W)	P_{M2} (W)	h (nm)	N (at. %)	Ti (at. %)	x N/Ti	H (GPa)	E* (GPa)	We (%)	H/E*	σ (GPa)	ρ (Ωcm)
1	0.30	460	300	1000	58.5	41.5	1.4	25.5	190	84	0.13	−1.6	1.3×10^{-4}
2	0.17	528	380	1400	70	30	2.3	16	163	69	0.10	−1.7	1.6×10^{-4}

IV. RESULTS AND DISCUSSION

As an example, properties of two sputtered overstoichiometric $TiN_{x>1}$ films are reported in detail. The $TiN_{x>1}$ films were reactively sputtered in an N_2 + Ar mixture by pulsed HDM powered by a pulsed power supply AE Pinnacle Plus + 5/5 kW (Advanced Energy, Inc.) and operated in a synchronous pulse mode at the repetition frequency $f_r = 1/T = 20\,kHz$ and duty cycle $\tau/T = 0.99$ onto Si (100) substrates in a deposition chamber evacuated to a base pressure $p_0 = 1 \times 10^{-3}\,Pa$. A small amount of Ar of about 20% was added to the N_2 gas to start the magnetron discharge at low pressures of sputtering gas. The elemental composition of the $TiN_{x>1}$ films on the Si substrate was analyzed with a scanning electron microscope (SU-70, Hitachi) operated at a primary electron energy of 15 keV using an energy dispersive spectrometer (EDS, UltraDry, Thermo Scientific) and a wave dispersive spectrometer (WDS, Magnaray, Thermo Scientific). Pure metal standards were used for the determination of Ti concentration. The nitrogen concentration was calculated as the difference to 100 wt. % using a combined WDS and EDS analysis due to overlapping of Ti and N x-ray peaks. The data were measured in the depth of about 600 nm under the film surface with an accuracy of ±10%. Deposition parameters, elemental composition, mechanical properties, macrostress σ, and electrical resistivity ρ of these $TiN_{x>1}$ films are summarized in Table I.

From Table I we can observe the following

(1) The overstoichiometric $TiN_{x=2.3}$ can be sputtered by pulsed HDM at a low total pressure $p_T = 0.17$ Pa. This strongly overstoichiometric $TiN_{x=2.3}$ film is created thanks to a high energy $\mathcal{E}_{bi} = 8.2\,MJ/cm^3$ delivered into it by bombarding ions and developing a very high pressure p = 1340 GPa in place of their incidence.[10] The energy $\mathcal{E}_{bi}$ was calculated from the formula $\mathcal{E}_{bi} = (U_s.i_s)/a_D$; here, U_s and i_s are the substrate bias and the substrate ion current density, respectively.[20] This experiment demonstrates that the formation of $TiN_{x=2}$ dintride films by magnetron sputtering is possible.

(2) The decrease in the total gas pressure p_T from 0.30 to 0.17 Pa and mainly the increase in the powers P_{M1} and P_{M2} in the magnetron M1 and M2, respectively, increasing the ionization of the N_2 gas results not only in an increase in the stoichiometry x = N/Ti of the TiN_x film but also in a decrease in its hardness H, elastic recovery W_e, and H/E* ratio.

(3) The overstoichiometric $TiN_{x=2.3}$ film still exhibits high hardness H = 16 GPa, high elastic recovery $W_e = 69\%$, and high ratio $H/E^* = 0.1$.

(4) Both overstoichiometric films, $TiN_{x=1.4}$ and $TiN_{x=2.3}$, are well conductive and exhibit a low electrical resistivity $\rho \approx 1.5 \times 10^{-4}\,\Omega cm$.

The structure of these overstoichiometric $TiN_{x>1}$ films, characterized by XRD diffraction, is displayed in Fig. 1. From this figure, it is seen that both films, $TiN_{x=1.4}$ and $TiN_{x=2.3}$, sputtered at $T_s = 450\,°C$ and $U_s = -20\,V$ are polycrystalline, and their crystallinity improves with decreasing sputtering gas pressure p_T and increasing sputtering power. The decrease in sputtering gas pressure results in two effects: (1) the decrease in collisions between ions and neutral atoms in the substrate sheath with the sheath voltage $U_{sh} = U_p - U_s$ and thereby the increase in the energy $\mathcal{E}_i$ of incident ions and (2) the bombardment of the growing film by fast neutral

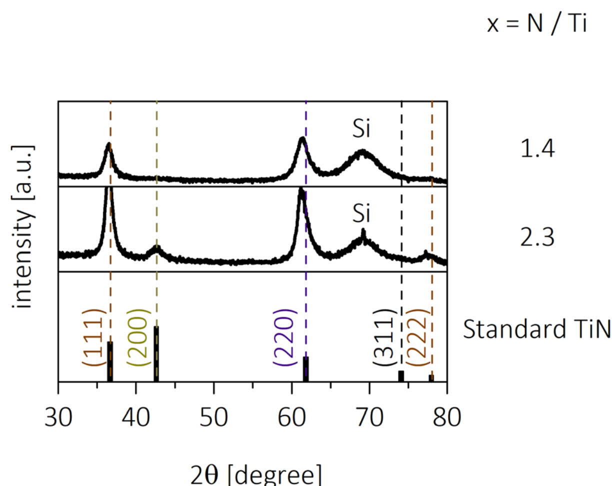

FIG. 1. (Color online) XRD patterns of the overstoichiometric $TiN_{x>1}$ films with stoichiometry x = 1.4 and 2.3.

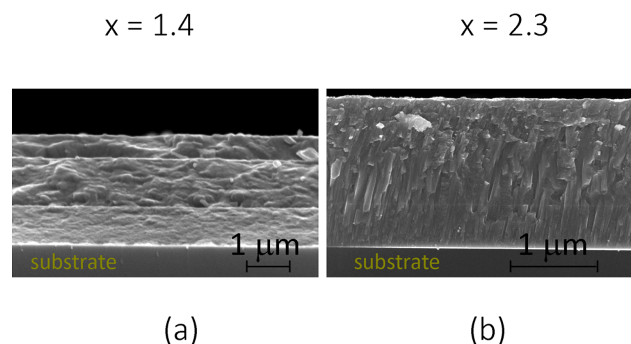

FIG. 2. (Color online) SEM images of cross-section of overstoichiometric $TiN_{x>1}$ films with moderately and strongly enhanced stoichiometry x = N/Ti: (a) the moderately overstoichiometric $TiN_{x=1.4}$ film and (b) the strongly overstoichiometric $TiN_{x=2.3}$ film.

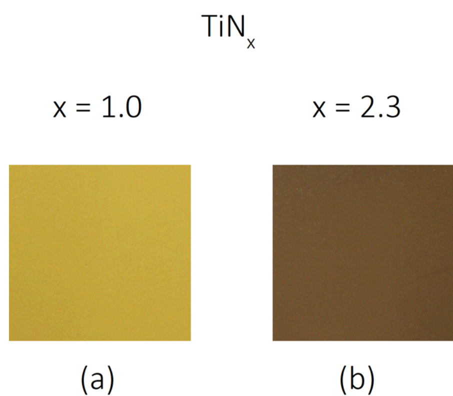

FIG. 3. (Color online) Color of TiN_x films with two different values of stoichiometry x. (a) The stoichiometric $TiN_{x=1}$ film with goldenlike color and (b) the strongly overstoichiometric $TiN_{x=2.3}$ film with brown color.

atoms, which deliver further additional energy $\mathcal{E}_{fn}$ to $\mathcal{E}_{bi}$ into the growing film; here, U_p is the plasma potential. Both the increase in $\mathcal{E}_i$ and the energy $\mathcal{E}_{bi}$ contribute to the improvement of the film crystallinity.

The microstructure of the overstoichiometric $TiN_{x>1}$ films with x = 1.4 and 2.3 characterized by SEM is displayed in Fig. 2. The microstructure of $TiN_{x=1.4}$ is noncolumnar. On the other hand, the microstructure of the $TiN_{2.3}$ film exhibits a dense, void-free columnar microstructure. Despite this difference in the microstructure, both overstoichiometric $TiN_{x>1}$ films exhibit an enhanced resistance to cracking. It is due to their high ratio $H/E^* \geq 0.1$ and high elastic recovery $W_e > 60\%$; more details on an enhanced resistance to cracking of films with a dense, void-free columnar microstructure are given in Ref. 19.

The stoichiometry x of the TiN_x film strongly influences also its color (see Fig. 3). The stoichiometric $TiN_{x=1}$ film is golden yellow. On the other hand, a strongly overstoichiometric $TiN_{x=2.3}$ film is brown.

V. CONCLUSIONS

Main results of the reported investigation of strongly overstoichiometric $TiN_{x>1}$ films can be briefly summarized as follows:

(1) The strongly overstoichiometric $TiN_{x>1}$ films and TiN_2 dinitride films can be created by a pulsed magnetron if sputtering of its Ti target is reduced, and the nitrogen gas is strongly ionized. This sputter deposition process can be realized by a hybrid dual magnetron or in a sputtering system equipped with a standard magnetron and a low-pressure source of strongly ionized nitrogen gas, for instance, a low-pressure arc.[18]
(2) The $TiN_{x=2.3}$ film with high values of the hardness H = 16 GPa, ratio $H/E^* = 0.1$, $W_e = 70\%$, dense, void-free microstructure, and low compressive macrostress $\sigma = -1.7$ GPa was sputtered by the hybrid dual magnetron at extremely high energy $\mathcal{E}_{bi} = 8$ MJ/cm^3 delivered into the growing film by bombarding ions.
(3) The high value of E_{bi} is a necessary condition for the creation of strongly overstoichiometric $TiN_{x>1}$ films because it gives rise to a very high pressure $p \approx 1340$ GPa in the place of incidence of arriving ions.[10]
(4) Overstoichiometric $TiN_{x>1}$ films are highly flexible films and exhibit an enhanced resistance to cracking.
(5) The $TiN_{x=2.3}$ film is brown compared with golden stoichiometric $TiN_{x=1}$ film and is well electrically conductive ($\rho = 1.7 \times 10^{-4}$ Ω cm).

ACKNOWLEDGMENT

This work was supported in part by the Project No. LO 1506 of the Czech Ministry of Education, Youth and Sports under the Program NPU I.

[1]E. Horwath-Bordon, R. Riedel, A. Zerr, P. F. McMillan, G. Auffermann, Y. Prots, W. Bronger, R. Kniep, and P. Kroll, Chem. Soc. Rev. **35**, 987 (2006).
[2]S. Aydin, Y. O. Ciftci, and A. Tatar, J. Mater. Res. **27**, 1705 (2012).
[3]H. Yan, M. Zhang, Q. Wei, and P. Cuo, J. Alloys Compd. **581**, 508 (2013).
[4]V. S. Bhadram, D. Y. Kim, and T. A. Strobel, Chem. Mater. **28**, 1616 (2016).
[5]S. Yu, B. Huang, X. Jia, Q. Zeng, A. R. Oganov, L. Zhang, and G. Frapper, J. Phys. Chem. C **120**, 11060 (2016).
[6]M. Zhang, K. Cheng, H. Yan, Q. Wei, and B. Zheng, Sci. Rep. **6**, 36911 (2016).
[7]S. Yu, Q. Zeng, A. R. Oganov, G. Frapper, and L. Zhang, Phys. Chem. Chem. Phys. **17**, 11763 (2015).
[8]S. Yu, Q. Zeng, A. R. Oganov, G. Frapper, B. Huang, H. Niu, and L. Zhang, RSC Adv. **7**, 4697 (2017).
[9]D. Edstrom, D. G. Sangiovanni, L. Hultman, I. Petrov, J. E. Greene, and V. Chirita, J. Appl. Phys. **121**, 025302 (2017).
[10]J. Musil, Š. Kos, M. Jaroš, R. Čerstvý, S. Haviar, S. Zenkin, and Z. Čiperová, "Overstoichiometric $TMN_{x>1}$ transition metal nitride coatings," oral presentation at the *10th International Symposium on Advanced Plasma Science and its Applications for Nitrides and Nanomaterials/11th International Conference on Plasma Nanotechnology and Science (ISPlasma 2018/IC-PLANTS 2018)*, Meijo University, Nagoya, Japan, 4–8 March 2018, No. 06B01O [Jpn. J. Appl. Phys. (submitted)].
[11]A. F. Young, J. A. Montoya, C. Sanloup, M. Lazzeri, E. Gregoryanz, and S. Scandolo, Phys. Rev. B **73**, 153102 (2006).
[12]Z. T. Y. Liu, D. Gall, and S. V. Khare, Phys. Rev. B **90**, 134102 (2014).
[13]M. Wessel and R. Dronskowski, J. Am. Chem. Soc. **132**, 2421 (2010).
[14]E. Gregoryanz, C. Sanloup, M. Somayazulu, J. Bardo, G. Fiquet, H. K. Mao, and R. J. Hemley, Nat. Mater. **3**, 294 (2004).
[15]J. C. Crowhurt, A. F. Goncharov, B. Sadigh, C. L. Evans, P. G. Morrall, J. L. Fereira, and A. J. Nelson, Science **311**, 1275 (2006).
[16]A. F. Young, C. Sanloup, E. Gregoryanz, S. Scandolo, R. J. Hemley, and H. K. Mao, Phys. Rev. Lett. **96**, 155501 (2006).
[17]J. C. Crowhurt, A. F. Goncharov, B. Sadigh, J. M. Zaug, D. Aberg, Y. Meng, and V. B. Prakapenka, J. Mater. Res. **23**, 183 (2008).
[18]O. V. Krysina, N. N. Koval, I. V. Lopatin, V. V. Shugurov, and S. S. Kowalsky, J. Phys.: Conf. Ser. **669**, 012032 (2016).
[19]J. Musil, M. Jaroš, R. Čerstvý, and S. Haviar, J. Vac. Sci. Technol., A **35**, 020601 (2017).
[20]J. Musil, Surf. Coat. Technol. **207**, 50 (2012).